Stable hydrogen isotope ratios in the clay fraction of soil

Zur Erlangung des akademischen Grades eines

DOKTORS DER NATURWISSENSCHAFTEN (Dr. rer. nat.)

von der KIT-Fakultät für

Bauingenieur-, Geo- und Umweltwissenschaften des

Karlsruher Instituts für Technologie (KIT)

genehmigte

DISSERTATION

von

Stefan Merseburger

Tag der mündlichen Prüfung: 14.12.2022

Referent: Prof. Dr. Wolfgang Wilcke

Korreferentin: Prof. Dr. Yvonne Oelmann

Karlsruhe (2022)

Abstract

The study of the natural abundance of stable isotopes of hydrogen (H) in organic matter has contributed new insights to ecology, forensic sciences, and paleoclimatology. Previous studies have shown that the $^2H/^1H$ isotope ratio (δ^2H) of nonexchangeable H (δ^2H_n) of bulk soil and demineralized soil organic matter is related to the δ^2H value of local precipitation. Up to now, methodological difficulties with the removal of exchangeable H in the soil clay fraction have complicated the establishment of a similar relationship between the δ^2H_n values of soil clay fractions and the δ^2H value of local precipitation.

The overall goal of my work is to determine the δ^2H_n values of soil clay fractions by separating exchangeable and nonexchangeable H with steam equilibration and investigate their drivers. For this purpose, (1) I adapted the steam equilibration method previously used for bulk soil and demineralized soil organic matter to determine δ^2H_n values. This was required to test the influence of the classical separation method for clay fractions, including the removal of dithionite-soluble iron, organic matter, carbonates and salts, on the δ^2H_n values of clay minerals. Subsequently, (2) I investigated whether there is a global correlation between the δ^2H values of local precipitation and the δ^2H_n values of clay fractions. The steam equilibration approach requires the equilibrium fractionation factor between the H of the steam and the exchangeable H of the sample ($\alpha_{ex\text{-}w}$), which is unknown. Therefore, (3) I developed an experimental method to determine sample-specific $\alpha_{ex\text{-}w}$ values.

I used the clay minerals kaolinite, illite, montmorillonite, and vermiculite and topsoil samples from 24 locations on five continents. All samples underwent a separation of the clay fraction. The δ^2H_n values were determined by steam equilibration and Pyrolysis-Elemental Analyzer-Isotope Ratio Mass Spectrometry. Moreover, the topsoil samples were chemically characterized including H, C_{org}, N, Na, Mg, Al, K, Ca, Fe and Fe_d concentrations and the potential cation-exchange capacity.

The classic clay separation method did not significantly change the δ^2H_n values of five different clay minerals. The δ^2H_n values of the clay fractions from various regions of the world ranged from -167 ± 1 ‰ for a northern Siberian sample to -44 ± 4 ‰ in western Kenia for $\alpha_{ex\text{-}w} = 1$ and from -191 ± 3 to -81 ± 4 ‰ for $\alpha_{ex\text{-}w} = 1.08$. The δ^2H values of local annual precipitation correlated significantly with the δ^2H_n values of the clay fractions ($r = 0.88$ for $\alpha_{ex\text{-}w} = 1$ and 0.65 for $\alpha_{ex\text{-}w} = 1.08$, $p < 0.001$). A multiple regression model including hillslope as a possible measure of allochthonous clay accumulation in addition to the δ^2H values of seasonal precipitation explained 86 % and 89 % of the observed variation in δ^2H values of the clay fractions for $\alpha_{ex\text{-}w} = 1$ and 1.08, respectively. The $\alpha_{ex\text{-}w}$ values of seven clay minerals ranged from 1.071 to 1.140 and of 19 topsoil clay fractions from 0.885 to 1.216. The $\alpha_{ex\text{-}w}$ determination method did not work for kaolinite, likely because of its small exchangeable H concentration. The $\alpha_{ex\text{-}w}$ value of the topsoil clay fractions correlated with the soil clay content ($r = 0.63$, $p = 0.004$), local mean annual temperature ($r = 0.68$, $p = 0.001$) and the δ^2H values of local precipitation ($r = 0.72$, $p < 0.001$) mainly reflecting the different clay mineralogy under different climatic weathering regimes.

My results demonstrate that the δ^2H_n values of the bulk topsoil can be described as a mixture of isotopically heavier soil organic matter H and isotopically lighter clay fraction H. The δ^2H_n values of clay fractions in soil are driven by the δ^2H values of local precipitation, independent of the assigned $\alpha_{ex\text{-}w}$ value, but are influenced by the dominant clay mineral type. When climate-affected mineralogy is taken into account, unknown soil samples can be assigned to the globally varying δ^2H precipitation signal. The proposed $\alpha_{ex\text{-}w}$ determination method can be used to reduce the uncertainty of steam equilibration for determining the δ^2H_n values of hygroscopic samples.

Zusammenfassung

Die Untersuchung der natürlichen Häufigkeit von stabilen Isotopen des Wasserstoffs (H) in organischen Substanzen hat neue Erkenntnisse für die ökologische Forschung, die forensischen Wissenschaften und die Paläoklimatologie hervorgebracht. Frühere Studien haben gezeigt, dass das $^{2}H/^{1}H$-Isotopenverhältnis ($\delta^{2}H$) von nicht-austauschbarem H ($\delta^{2}H_{n}$) des Bodens und der demineralisierten organischen Bodensubstanz mit dem $\delta^{2}H$-Wert des lokalen Niederschlags in Zusammenhang steht. Bisher haben methodische Schwierigkeiten bei der Entfernung von austauschbarem H in der Tonfraktion des Bodens die Untersuchung einer ähnlichen Beziehung zwischen den $\delta^{2}H_{n}$-Werten der Tonfraktionen des Bodens und dem $\delta^{2}H$-Wert des lokalen Niederschlags erschwert.

Das übergeordnete Ziel meiner Arbeit besteht darin, die $\delta^{2}H_{n}$-Werte von Tonfraktionen im Boden durch die Trennung von austauschbarem und nicht-austauschbarem H mittels Dampfäquilibrierung zu bestimmen und deren Einflussfaktoren zu untersuchen. Zu diesem Zweck habe ich (1) die Dampfäquilibrierungsmethode angepasst. Dies war erforderlich, um den Einfluss der klassischen Behandlung zur Separation von Tonfraktionen, einschließlich der Entfernung von dithionitlöslichem Eisen, organischer Substanz, Karbonaten und Salzen, auf die $\delta^{2}H_{n}$-Werte von Tonmineralen zu testen. Anschließend habe ich (2) untersucht, ob es eine globale Korrelation zwischen den $\delta^{2}H$-Werten des lokalen Niederschlags und den $\delta^{2}H_{n}$-Werten von Oberbodentonfraktionen gibt. Der Ansatz der Dampfäquilibrierung erfordert den Gleichgewichtsfraktionsfaktor zwischen dem H des Dampfes und dem austauschbaren H der Probe ($\alpha_{ex\text{-}w}$), der nicht bekannt ist. Daher habe ich (3) eine experimentelle Methode zur Bestimmung der probenspezifischen $\alpha_{ex\text{-}w}$-Werte entwickelt.

Ich verwendete die Tonminerale Kaolinit, Illit, Montmorillonit und Vermiculit sowie Oberbodenproben von 24 Standorten auf fünf Kontinenten. Bei allen Proben wurden die Tonfraktionen separiert. Die $\delta^{2}H_{n}$-Werte wurden mittels Dampfäquilibrierung und Pyrolyse-Elementaranalysator-Isotopenverhältnis-Massenspektrometrie bestimmt. Darüber hinaus wurden die Oberbodenproben chemisch charakterisiert, einschließlich der Konzentrationen von H, C_{org}, N, Na, Mg, Al, K, Ca, Fe und Fe_{d} sowie der potenziellen Kationenaustauschkapazität.

Die klassische Tonseparierung veränderte die $\delta^{2}H_{n}$-Werte von fünf verschiedenen Tonmineralien nicht wesentlich. Die $\delta^{2}H_{n}$-Werte der Tonfraktionen aus verschiedenen Regionen der Welt reichten von -167±1‰ für eine nordsibirische Probe bis -44±4‰ in Westkenia für $\alpha_{ex\text{-}w}$=1 und von -191±3 bis -81±4‰ für $\alpha_{ex\text{-}w}$=1,08. Die $\delta^{2}H$-Werte des lokalen Jahresniederschlags korrelierten signifikant mit den $\delta^{2}H_{n}$-Werten der Tonfraktionen ($r=0{,}88$ für $\alpha_{ex\text{-}w}$=1 und 0,65 für $\alpha_{ex\text{-}w}$=1,08, $p<0{,}001$). Ein multiples Regressionsmodell, das zusätzlich zu den $\delta^{2}H$-Werten des saisonalen Niederschlags auch die Hangneigung als mögliches Maß für die allochthone Tonakkumulation einbezog, erklärte 86% und 89% der beobachteten Variation der $\delta^{2}H$-Werte der Tonfraktionen für $\alpha_{ex\text{-}w}$=1 bzw. 1,08. Die $\alpha_{ex\text{-}w}$-Werte von sieben Tonmineralen reichten von 1,071 bis 1,140 und von 19 Oberbodentonfraktionen von 0,885 bis 1,216. Die $\alpha_{ex\text{-}w}$-Bestimmungsmethode funktionierte nicht für Kaolinit, wahrscheinlich wegen seines geringen austauschbarem H-Gehalts. Der $\alpha_{ex\text{-}w}$-Wert der Oberbodentonfraktionen korrelierte mit dem Tongehalt des Bodens ($r=0{,}63$, $p=0{,}004$), der lokalen Jahresmitteltemperatur ($r=0{,}68$, $p=0{,}001$) und den $\delta^{2}H$-Werten des lokalen Niederschlags ($r=0{,}72$, $p<0{,}001$), was die unterschiedliche Tonmineralogie unter verschiedenen klimatischen Verwitterungsregimen widerspiegelt.

Meine Ergebnisse zeigen, dass die $\delta^{2}H_{n}$-Werte des Oberbodens als eine Mischung aus isotopisch schwereren H der organischen Bodensubstanz und isotopisch leichteren H der Tonfraktionen beschrieben werden können. Die $\delta^{2}H_{n}$-Werte der Tonfraktionen im Boden werden von den $\delta^{2}H$-Werten der lokalen Niederschläge beeinflusst. Wenn die klimatisch beeinflusste Mineralogie berücksichtigt wird, können unbekannte Bodenproben dem global variierenden $\delta^{2}H$ Niederschlagswerten zugeordnet werden. Die vorgeschlagene $\alpha_{ex\text{-}w}$-Bestimmungsmethode kann verwendet werden, um die Unsicherheit der Dampfäquilibrierung zur Bestimmung der $\delta^{2}H_{n}$-Werte von hygroskopischen Proben zu verringern.

Content

List of tables

List of figures

List of abbreviations

^2H	Deuterium
AWI-TD1	Deuterium depleted water from the Alfred-Wegener-Institute
BCR-2	Basalt, Columbia River, reference material distributed by USGS
CEC	Cation-exchange capacity
CF-IRMS	Continous flow isotope ratio mass spectrometer
CI	Confidence intervall
C_{org}	Organic carbon
DCB	Dithionite-citrate-bicarbonate method of Mehra and Jackson (1958)
DFG	Deutsche Forschungsgemeinschaft
DOI	Digital Object Identifier
e.g.	For example, from Latin *exempli gratia*
EC	Electrical conductivity
Eq.	Equation
FAO	Food and Agricultural Organization of the United Nations
Fe_d	Dithionite-soluble iron
GISP	Greenland Ice Sheet Precipitation (water)
GNIP	Global Network of Isotopes in Precipitation
HTC	High temperature convertion (pyrolysis)
i.e.	That is, from Latin *id est*
IAEA	International Atomic Energy Agency
IAEA-604	Water reference enriched in δ^2H distributed by the International Atomic Energy Agency
IAEA-CH7	Polyethylene reference material of the International Atomic Energy Agency
ICP-MS	Inductively-coupled plasma mass spectrometry
ICP-OES	Inductively-coupled plasma atomic emission spectroscopy
ID	Inner diameter
IMt-2	Illite distributed by the Clay Mineral Society (USA)
IRMS	Isotope ratio mass spectrometer
IUSS	International Union of Soil Sciences
KGa-2	Kaolinite distributed by the Clay Mineral Society (USA)
MAP	Mean annual precipitation
MAT	Mean annual temperature

n.a.	Not available or not applicable
n.d.	Not determined
OIPC	Online Isotopes in Precipitation Calculator (OIPC, version 3.1; Bowen, 2022; Bowen & Revenaugh, 2003)
p.a.	*Pro analysi* quality
PE	Polyethylene
PET	Annual average potential evapotranspiration for a reference crop
PTFE	Polytetrafluoroethylene
RSD	Relative standard deviations
SCa-3	Mg-rich montmorillonite distributed by the Clay Mineral Society (USA)
SD	Standard deviation
SE	Standard error
SLAP	Standard Light Antarctic Precipitation (Water)
SOM	Soil organic matter
SWy-3	Na-saturated montmorillonite distributed by the Clay Mineral Society (USA)
TFM	PTFE modified with perfluorpropylvinylether
USGS	United States Geological Survey
VSMOW	Vienna Standard Mean Ocean Water
WMO	World Meteorological Organization
WRB	World Reference Base for Soil Resources
χ_e	Proportion of isotopically exchangeable hydrogen
$\alpha_{ex\text{-}w}$	Equilibrium fractionation factor between exchangeable H of the sample and steam H
$\delta^{18}O$	Stable oxygen isotope ratio
$\delta^{2}H$	Stable hydrogen isotope ratio
$\delta^{2}H_{ex}$	Stable isotope ratio of exchangeable hydrogen
$\delta^{2}H_{n}$	Stable isotope ratio of nonexchangeable hydrogen
$\delta^{2}H_{p}$	Stable hydrogen isotope ratio of precipitation

Acknowledgments

I want to thank Prof. Dr. Yvonne Oelmann and Prof. Dr. Wolfgang Wilcke for the initial project idea and for their trust in my ability to conduct this exciting research project and for their scientific guidance. I thank Prof. Dr. Wolfgang Wilcke for supervision and his steady professional support of my research.

I thank Dr. Marc Ruppenthal for providing the starting point with his dissertation including a comprehensive set of samples and data from Argentina. I thank Pablo Álvarez, Dr. Benjamin Bandowe, Nuria Basdediós, Bastian Bayer, Dr. Simon Blotevogel, Dr. Melanie Brunn, Tobias Fabian, Dr. Eva Koller-France, Arnim Kessler, Martin Kull, Dr. Soni Lama, Lukas Lorenz, Dr. Sophia Leimer, Dr. Ledesma, José, Nadine Gill, Esthela Gonzalez and Dr. Tobias Wirsing for a friendly working environment, advice and support as well as helpful and stimulating discussions. Furthermore, I would like to thank the helpful colleagues from neighboring laboratories who provided me with equipment or spontaneously helped me out repeatedly with liquid nitrogen, especially Gesine Preuß for her support and exchange in questions of isotope analysis. I thank Nadja Werling and Prof. Dr. Katja Emmerich for advice and supplementary measurements. I thank Dr. Heiko Moossen for sharing the experience on hydrogen isotope analysis of the MPG BGC-IsoLab and the DTTG and their members for their helpful clay mineralogy workshop.

I thank Nadine Gill and Martin Kull for assistance in the laboratory work, Andre Velescu for support with the ICP-MS and ICP-OES measurements, Prof. Dr. Harro Meijer for a working example of the memory correction algorithm and Dr. Sophia Leimer for support with the R implementation, Dr. Maria Hörhold for contributing the deuterium-depleted water (‘AWI-TD1’) and PD Dr. Stefan Dultz for contributing the vermiculite. I thank all providers of soil samples: Prof. Dr. Lars Kutzbach and Dr. Christian Knoblauch (RU-PS2), Prof. Dr. Christian Siewert (RU-17, RU-S20), Dr. Suzanne Robin Jacobs and Sadadi Ojoatre (KE-20, KE-38, KE-44), Dr. Tobias Wirsing (DE-KA1, DE-KA2), Dr. Benjamin Bandowe (UZ-K1), Andre Velescu and Tobias Fabian (EC-BOM, EC-CAJ, EC-SF1). I am grateful for funding of my work through a grant from the German Science Foundation (DFG, Wi1601/25-1) awarded to Prof. Dr. Wolfgang Wilcke and to the Karlsruhe House of Young Scientists for supplementary funding in the later stage of my PhD study.

Last but not the least, I want to thank my family and friends, especially Birte for staying at my side with constant patience and understanding as well as Paula and Merle for being there.

1 Summarizing overview

1.1 Introduction

The global water cycle distributes hydrogen isotopes unevenly. Since the 1960s, the Global Network of Isotopes in Precipitation surveys this distribution (IAEA/WMO, 2022), and many studies have modeled the long-term distribution of hydrogen isotopes on earth (Araguás-Araguás et al., 2000; Bowen & Revenaugh, 2003; Dansgaard, 1964; Jouzel et al., 1987; Terzer-Wassmuth et al., 2021). The local precipitation signal is reflected by the stable H isotope ratios of the nonexchangeable pool of hydrogen (δ^2H_n) in organic matter (Bowen, Chesson, et al., 2005; Ruppenthal et al., 2015; Wassenaar & Hobson, 1998; Werner et al., 2016). By determining their δ^2H_n, many organic substances like collagen, keratin, cellulose or microbial tissue can be traced to their origin in the hydrogen isoscape of precipitation (West et al., 2010). When complex hygroscopic materials like soil and clay minerals are studied, the measurement of the δ^2H values can be influenced by unwanted exchange of H with ambient atmospheric water vapor during sample preparation. The quickly exchanging H can blur the stable H isotope signal of the nonexchangeable H pool (Bauer & Vennemann, 2014; Gilg et al., 2004; Kanik et al., 2022; VanDeVelde & Bowen, 2013). Steam equilibration avoids this problem by a controlled H exchange, permitting to determine stable isotope ratios of structural H in clay minerals and soil clay fractions, which cannot easily be exchanged with water (δ^2H_n values) and reflect that of ambient soil water at the time of mineral formation (Gilg & Sheppard, 1996; Lawrence & Taylor, 1972; Savin & Epstein, 1970a). The δ^2H_n values of structural H in minerals might bear geographic information similar to those of soil organic matter (SOM; Ruppenthal et al., 2015). This is attributed to the fact that the H-isotopic composition of soil water is related to that of local precipitation and is influenced by evapotranspiration in the soil-plant system, both of which vary with location (Bowen, 2022; Sprenger et al., 2016).

To reliably determine δ^2H_n values of structural H in clay minerals requires the removal of the influence of exchangeable H. The exchangeable H in clay minerals comprises adsorbed and interlayer water, which quickly equilibrates with ambient water and thus does not bear a stable isotopic signal (Bauer & Vennemann, 2014). The current state-of-the-art methods for continuous flow isotope ratio mass spectrometry (CF-IRMS) remove the exchangeable H at varying temperatures ranging between 100 °C and 250 °C in vacuum (Bauer & Vennemann, 2014; Gilg et al., 2004; VanDeVelde &

Bowen, 2013). Because different clay minerals require different temperatures for the removal of exchangeable H (Gilg et al., 2004), the currently applied methods cannot guarantee to always remove the entire exchangeable H pool in clay minerals or clay fractions. Another methodological challenge originates from the fact that after vacuum drying, a hygroscopic sample quickly attracts atmospheric water. This reintroduces exchangeable H, which must be prevented (Bauer & Vennemann, 2014; Bowen, Chesson, et al., 2005; VanDeVelde & Bowen, 2013).

An alternative to the vacuum extraction methods is provided by steam equilibration. After equilibrating the same clay mineral or fraction sample with several waters of different H-isotopic composition (δ^2H_w), a mass balance calculation allows for the quantification of the contribution of exchangeable H to the total H pool (χ_e) and of the δ^2H_n values, but requires the knowledge of the equilibrium fractionation factor ($\alpha_{ex\text{-}w}$) between exchangeable H of the sample and equilibration water (Schimmelmann, 1991). However, such methods have up to now mostly been applied to determine nonexchangeable H in organic matter (Bowen, Chesson, et al., 2005; Epstein et al., 1976; Hobson et al., 2012; Kelly et al., 2009; Qi & Coplen, 2011; Ruppenthal et al., 2013, 2015; Schimmelmann, 1991; Schimmelmann et al., 2020; Soto et al., 2017; Wassenaar & Hobson, 2000, 2003) and bulk soil (Ruppenthal et al., 2010). The only study I know of, in which steam equilibration was applied to a clay mineral is that of Hsieh and Yapp (1999), who determined the δ^2H_n value of halloysite. However, steam equilibration was not further developed to a standard method for clay minerals (Gilg et al., 2004) or soil clay fractions.

To measure the δ^2H value of nonexchangeable H in soil clay fractions requires the separation of this fraction. To reach a full dispersion of the soil particles, Fe oxides, carbonates and SOM must be removed, using chemicals that might attack hydroxyl groups and thus have an effect on the δ^2H_n values of clay fractions. The removal of iron oxides by the dithionite-citrate-bicarbonate (DCB) method of Mehra and Jackson (1958) and carbonates by acetic acid was shown to not affect the δ^2H values of hydrous minerals (Gilg et al., 2004). The commonly used removal method for SOM by oxidation with hydrogen peroxide (H_2O_2) can change δ^2H values of some clay minerals, e.g., montmorillonite (Hyeong & Capuano, 2000). Similarly, the alternative treatment with disodium peroxodisulphate ($Na_2O_8S_2$) showed a strong positive shift of the δ^2H values after the treatment of a montmorillonite sample (Menegatti et al., 1999). However,

Hyeong and Capuano (2000) and Menegatti et al. (1999) did not test the possibility that the apparent change in δ^2H values after treatment with H_2O_2 or $Na_2O_8S_2$ was related with an unaccounted remoistening of the hygroscopic samples. I suggest that remoistening must be ruled out, before these two chemicals are defined as inappropriate for the purpose of determining δ^2H_n values of soil clay fractions. Moreover, both SOM oxidation methods may not remove SOM exhaustively so that the measured δ^2H_n values of clay fractions need to be corrected for the δ^2H_n values of the remaining SOM.

Ruppenthal et al. (2010) found a correlation between the δ^2H values of local mean annual precipitation and the δ^2H_n values of a global set of bulk soil samples, which was less close than that with the δ^2H_n values of demineralized SOM (Ruppenthal, 2014; Ruppenthal et al., 2015). This finding suggested that the δ^2H_n values of mineral components of the soil had generally a less close relationship with the δ^2H values of precipitation than SOM or that different minerals showed different relationships resulting in scatter introduced by different mineral compositions. In addition, different ratios of the concentrations of C-bonded, nonexchangeable organic H to those of mineral-bound nonexchangeable H could also have contributed to the less close relationship. In soils which are frozen for a longer time chemical weathering and thus clay mineral formation might be largely restricted to the nonfrozen period, because mineral formation depends on temperature and the availability of liquid water (Folkoff & Meentemeyer, 1985; Maher, 2010, 2011; Richards & Kump, 2003). Below the freezing point, chemical weathering occurs at a slow rate (P. W. Borden et al., 2010; Chuvilin et al., 1998; Lessovaia et al., 2021). Thus, when assessing the relationship between δ^2H values of precipitation and δ^2H_n values of soil clay fractions including periglacial soils, the seasonal δ^2H values of precipitation could be more important than the annual ones.

For samples with a high proportion of exchangeable H, δ^2H_n values calculated based on steam equilibration respond sensitively to variations in the $\alpha_{ex\text{-}w}$ value, because the $\alpha_{ex\text{-}w}$ value influences both slope and intercept of the regression line of δ^2H_t values of the studied sample on δ^2H_w values (Eq. 1.1; Feng et al., 1993; Hsieh & Yapp, 1999; Ruppenthal et al., 2010; Sessions & Hayes, 2005; Wassenaar & Hobson, 2000). Thus, the measurement of accurate δ^2H_n values by steam equilibration requires the knowledge of a sample-specific $\alpha_{ex\text{-}w}$ value, particularly if the sample consists of an unknown mixture of different minerals. To the best of my knowledge, there is no established method to

determine $\alpha_{ex\text{-}w}$ for complex mixtures of compounds commonly occurring in soil and plants in the temperature range used for steam equilibration (ca. 110-130°C). However, some studies determined $\alpha_{ex\text{-}w}$ for cellulose by reducing the exchangeable H fraction via addition of nitro groups (Chesson et al., 2009; Feng et al., 1993; Filot et al., 2006; Grinsted & Wilson, 1979; Schimmelmann, 1991). From the intersection of the two resulting regression lines of the δ^2H value of total H on those of the waters used for steam equilibration for the original cellulose and the nitrated cellulose, respectively, Schimmelmann (1991) calculated an $\alpha_{ex\text{-}w}$ value of 1.08. This $\alpha_{ex\text{-}w}$ value has been widely used to determine δ^2H_n values of various organic compounds, plants, SOM and bulk soil by steam equilibration (Hobson et al., 1999; Ruppenthal et al., 2010, 2013, 2015; Sauer et al., 2009; Schimmelmann et al., 1999; Soto et al., 2017; Wassenaar & Hobson, 2000, 2003). Other studies that applied an equilibration method to organic materials and clay minerals neglected equilibrium fractionation between exchangeable H in the studied material and ambient water vapor-H thus assuming an $\alpha_{ex\text{-}w}$ value of 1 (Bowen, Chesson, et al., 2005; Chesson et al., 2009; Hsieh & Yapp, 1999; Qi & Coplen, 2011). Based on the same principle of a reduction of the exchangeable H pool, but using for hygroscopic samples substantially different drying conditions after identical steam equilibration, the determination of $\alpha_{ex\text{-}w}$ values should be possible.

The inclusion of clay and mica reference materials used in several studies that applied conventional δ^2H analysis with vacuum drying (Bauer & Vennemann, 2014; Fagan, 2001; Kanik et al., 2022; Menegatti et al., 1999; Qi et al., 2017; VanDeVelde & Bowen, 2013) allows for the comparison of the reported δ^2H values with my nonexchangeable δ^2H values obtained by steam equilibration. Differences between both methods is expected to be noticeable, because a hygroscopic sample quickly attracts atmospheric water after vacuum drying and thus reintroducing exchangeable H, which has been found to be problematic in previous studies (Bauer & Vennemann, 2014; Bowen et al., 2005; VanDeVelde & Bowen, 2013).

The following research questions were addressed in my thesis:

1) Is it possible to determine the nonexchangeable hydrogen isotope ratios (δ^2H_n values) of clay fractions? This requires that (a) I can adapt a steam equilibration method for clay minerals and soil clay fractions. Furthermore, (b) the traditional treatment of soil samples (with the extraction of iron oxides, the removal of

carbonates and SOM and the separation of the clay fraction) must not alter the isotopic composition of the nonexchangeable H pool of clay minerals (**Chapter 2**).

2) How do the modeled δ^2H values of local precipitation (δ^2H_p) relate with the δ^2H_n values of soil clay fractions (**Chapter 3**)?
3) Can the manipulation of the exchangeable H pool size (χ_e) via differently intensive drying be used to determine sample-specific $\alpha_{ex\text{-}w}$ values for individual clay minerals and soil clay fractions? Moreover, I tested the hypothesis that the $\alpha_{ex\text{-}w}$ and thus δ^2H_n values of soil clay fractions are influenced by their climate-driven mineralogical composition (**Chapter 4**).
4) Are the nonexchangeable δ^2H values of clay minerals comparable with conventional δ^2H measurements when similar drying of clay minerals is used (**Chapter 1**)?

1.2 Material and methods

1.2.1 Samples

I used kaolinite (KGa-2), dioctahedral illite (IMt-2), Na-saturated montmorillonite (SWy-3) and Mg-rich trioctahedral montmorillonite (SCa-3) distributed by the Clay Mineral Society (Chantilly, VA, USA) and a trioctahedral vermiculite (contributed by Stefan Dultz, Hannover, Germany) as clay mineral reference materials (Table 2.1) (**Chapters 2, 4**). SCa-3 and IMt-2 were delivered as brittle rock chips with a macroscopically visible heterogeneity in grain sizes and colors. SWy-3 and KGa-2 were delivered as fine-grained powders. The standards are described by the baseline studies of the Clay Minerals Society Source Clays (D. Borden & Giese, 2001; Chipera & Bish, 2001; A. U. Dogan et al., 2006; M. Dogan et al., 2007; Guggenheim & Van Groos, 2001; Kogel & Lewis, 2001; Mermut et al., 2001) and by Hower and Mowatt (1966) for IMt-2. The trioctahedral vermiculite was characterized by Dultz et al. (2005), Bors et al. (1997) and Steudel et al. (2008; 2009). Furthermore, I included USGS57 biotite and USGS58 muscovite described by Qi et al. (2017) (**Chapters 2**, **4**) and microcrystalline cellulose (A17730 Alfa Aesar, Ward Hill, MA, USA) (**Chapter 4**).

I used 30 (**Chapter 3**) and 22 (**Chapter 4**) topsoil samples from nine countries on five continents that cover a wide range of topographical elevations and latitudes and thus modeled δ^2H values of local precipitation (Table 3.1 and Figure 3.1). All samples

were taken from the upper mineral horizon, mostly from the first 10 cm, and stored dark and dry for 1–28 years.

1.2.2 Clay separation

I sieved air-dried A-horizon samples to < 2 mm when necessary and gently ground the clay standards IMt-2 and SCa-3 with a hand mortar to this size.

The following treatment steps and their sequence were chosen according to recommendations of Gilg et al. (2004) and VanDeVelde and Bowen (2013). I treated the clay mineral standards and the topsoil samples during the clay separation process in the same manner, using the residual sediment of each step for the subsequent step, respectively (Figure 2.1) (**Chapters 2–4**).

I used the clay separation, steam equilibration and isotope ratio mass spectrometry (IRMS) methods (**Chapters 2–4**) that are described in detail in **Chapter 2**. In short, after sieving the air-dry soil to < 2 mm I removed Fe oxides with the dithionite-citrate-buffer (DCB) method of Mehra and Jackson (1958). To remove carbonates, I used a Na-acetate acetic acid buffer adjusted to pH 4.8. To remove organic matter, I added H_2O_2 in a water bath at 50 °C. After each sample treatment, I removed water-soluble salts by washing with deionized water and measured electrical conductivity (EC). Washing was repeated until the EC of the supernatants had reached < 400 µS/cm. I determined the grain sizes by pipet analysis according to DIN ISO 11277 (2002), but instead of a dispersion agent I used water with a pH of ~ 7.5. In this water, I separated the grain sizes by a repeated sedimentation in 2-L cylinders. Clay fractions were precipitated with $MgCl_2$. A H_2O_2 treatment of the precipitate reduced the organic matter concentration in the clay fractions further. After final washings until the EC of the supernatant had reached < 100 µS/cm, the clay fractions were dried at 60 °C and pulverized. This comparatively fast separation leaves residues of the clay in the silt separates, which I named therefore '≤silt'.

The entire clay separation procedure took 10 to 12 weeks and up to 12 samples could be simultaneously processed (**Chapters 2, 3**). The procedure was repeated three times for all samples in separate batches to yield three independent replicates of all clay fractions (**Chapter 2**). After the treatment, the interlayers of all swellable clay minerals should be mostly Na saturated.

The 30 samples were distributed among four treatment batches (**Chapter 3**; two additional batches to the two batches also used for **Chapter 2**). As quality check, I included sample SK-Oso in each treatment batch, which resulted in relative standard deviations (RSD) of 2 % for each particle-size fraction and the concentrations of pedogenic Fe oxides. The RSD of the C concentration amounted to 6 %, those of N and H to 4 % and that of the potential cation-exchange capacity (CEC) to 5 %. As a measure for the spatial heterogeneity of soils with the same modeled δ^2H values of rainfall, I analyzed three samples from northern, central and southern Argentina (AR-2, AR-10, AR-19) in triplicate (-A, -B and -C), collected in the field with approximately 100 m distance from each other (Ruppenthal et al., 2015, Table 3.1). The triplicates were treated in separate batches (**Chapter 3**). I measured all treatment batches in independent equilibrations and IRMS sequences (**Chapter 3**).

1.2.3 Chemical sample properties

The C concentrations were measured with an Elemental Analyzer (Flash 2000 HTC, Thermo Fisher, Waltham, MA, USA and EuroVector 3000, EuroVector, Pavia, Italy) (**Chapters 2–4**).

The pH was determined with a glass electrode (SenTix® 81 on ph 3310, WTW, Weilheim, Germany) in a deionized water suspension at a soil:water ratio of 1:2.5 (v/v) (**Chapters 2–4**).

The potential cation-exchange capacity (CEC) of the clay fractions was determined with the Cu(II)-triethylentetramine method (Ammann et al., 2005; Meier & Kahr, 1999), using additionally a phosphate puffer (pH = 7.0) and 24 h shaking time (Stanjek & Künkel, 2016; Steudel et al., 2009). The potential CEC was referred to oven-dry soil (24 h at 105 °C) (**Chapters 2–4**).

To determine the elemental concentration of Na, Mg, Al, K, Ca and Fe (**Chapter 3**), I weighed 0.1 g of the clay fractions in pressure vessels, added 2 mL HNO_3 (69 % suprapur), 0.5 mL H_2O_2 (30 %, suprapur) and 1.5 mL HF (48 %, suprapur). The samples were digested in a microwave oven (MARS XPress, CEM, Matthews, NC, USA). After cooling, I added of 10 mL 5% H_3BO_3 to mask residual HF in the microwave oven. Afterwards, the solutions were transferred into a volumetric flask and made up to 50 mL with ultrapure water. An aliquot of 100 µL was diluted with 1% HNO_3 solution to 10 mL for the ICP-MS (Agilent 7900, Santa Clara, CA, USA) and ICP-OES (Agilent 5100)

measurements. The accuracy of concentration measurements was checked by repeated analysis of the reference materials BCR-2 (Basalt, Columbia River, USGS, Denver, CO, USA) in each digestion batch (n = 2). The recovery of BCR-2 deviated less than 10 % from the certified elemental value for the investigated elements, and was therefore accepted. The relative standard deviation (RSD) of BCR-2 was 4 % for Na, 1 % for Mg, Al, K and Ca and 3 % for Fe (**Chapter 3**).

1.2.4 Steam equilibration

I modified the equilibration device of Ruppenthal et al. (Figure 2.2). I replaced the liquid nitrogen trap by a membrane pump to remove water vapor, which could corrode the rotary vane pump and I added a glove bag, which was filled with argon to allow for a fast gas-tight sealing of the tin capsules without contact to ambient air. In comparison to the method of Ruppenthal et al. (2013), I prolonged the pre- and post-equilibration drying phase during permanent evacuation, which requires a stainless steel tubing inside the oven (**Chapters 2–4**).

Figure 1.1: The steam equilibration apparatus.

The optimum equilibration time was determined experimentally for two soil samples (DE-KA2, SK-Oso, Figure 2.3) and the clay reference materials following a suggestion of Wassenaar and Hobson (2000). After evacuating the stainless-steel vessel

(~ 10 L) for two hours inside a fan-assisted heating oven at 120 °C, I injected 4 mL of equilibration water with a δ^2H value of 335 ‰ through a high temperature septum. Within 0.25, 1, 4, 16 and 64 h (**Chapter 2**) at the same temperature, hydrogen from the steam equilibrated with the exchangeable H fraction of the samples. This was followed by 15 min of vacuum drying with a diaphragm pump and 45 min with a rotary vane pump, both at 120 °C, further followed by a 2-h cooling phase at room temperature under continuous evacuation (≤ 1 Pa), which I called "medium" drying intensity (**Chapters 2–4**). I transferred the vacuum chamber into a glove bag and flushed twice with dried Ar for a moisture-free atmosphere. To depressurize the vessel to ambient air pressure, I flooded the vessel with dried Ar at ~1.3 bar. While the Ar continuously flowed into the vessel, I opened the vessel and directly closed the tin capsules with a filed and extended concretor's nippler inside the vessel. This was done in a way that the tin of the smooth-walled capsules was not cut-off but compressed to a gas-tight seal (Qi et al., 2010) applying the same force for all capsules. The procedure was necessary to avoid even the slightest contact of the sample with ambient air moisture, which is a prerequisite for the correct determination of the H concentrations and δ^2H values (**Chapter 4**).

For further equilibrations, I chose an equilibration time of 16 h (Figure 2.3) (**Chapters 2–4**). I placed a maximum of 80 samples each with an analyte mass of 1–2 mg (2–3.5 mg for biotite and muscovite) in the equilibration vessel. To test whether there was an effect of remoistening of the samples after the different drying procedures on their δ^2H_t values, I included untreated SCa-3 montmorillonite considered as particularly hygroscopic in each equilibration batch. I closed the tin capsules with SCa-3 montmorillonite in triplicate before and again in triplicate after all other samples and found on average only a small difference of 2.2 ± standard deviation (SD) 2.0 ‰, because of diffusing moisture during the sealing process of the samples at the end of the equilibration. For quality control, I included KGa-2 and blanks in triplicates in each equilibration batch (**Chapters 2–4**).

I used two to four waters with known δ^2H values (AWI-TD1: -266 ‰, Laboratory water: -58 ‰, medium deuterium-enriched water: 137 ‰, highly deuterium-enriched water: 334 ‰) to replace all exchangeable H in the sample with the H of the equilibration water and to calculate the contribution of exchangeable H and the δ^2H_n value. I produced the two deuterium-enriched waters by mixing ^2H_2O and ultrapure

water (Faghihi et al., 2015). The treatment batches one and two were equilibrated with two isotopically different waters and the third batch with four waters (**Chapter 2**). For **Chapter 3**, I used three and for **Chapter 4** four isotopically different waters.

In addition to the medium drying intensity (**Chapters 2–4**), I realized a weaker and a stronger drying intensity (**Chapter 4**). For the weaker drying intensity, the temperature was maintained at 120 °C after the 16-h equilibration and the stainless-steel vessel was evacuated with the diaphragm pump for 1 h. Then, the vessel was cooled down for 2 h at room temperature outside of the oven, while evacuating with the diaphragm pump to a final pressure of 150 to 300 Pa. For the stronger drying intensity, the temperature was maintained at 120 °C after the 16-h equilibration and the stainless-steel vessel was evacuated with the diaphragm pump for 15 min and additionally with the rotary vane pump for another 45 min. After this drying phase, I assumed that the equilibration was terminated. Then, the temperature was raised to 200 °C for 2 h, followed by cooling for 3 h at room temperature outside the oven, evacuating continuously with the rotary vane pump to a final vacuum < 1 Pa (Figure 4.1).

1.2.5 Hydrogen isotope ratio measurement

The concentrations of H and δ^2H values were determined with an Elemental Analyzer-Isotope Ratio Mass Spectrometer (Flash 2000 HTC-Delta V Advantage, Thermo Fisher, Waltham, MA, USA). The samples were pyrolyzed in the chromium-filled Al_2O_3 reactor at 1250 °C. I used the setup "A1" described in Gehre et al. (2017), but adapted it for a smaller inner diameter (7 mm) of the inner tube with a 40 mm octagonal graphite crucible. In combination with 2 x 5 mm smooth wall tin capsules, long sequences of up to 130–150 capsules were possible. For normalization of the measured δ^2H values of each carousel run, I used three international laboratory standards (VSMOW, SLAP and IAEA-604). Additionally, I used GISP to test for correct normalization and fractionation by halogen release from chrome (Gehre et al., 2015). I purchased all international laboratory standards from USGS (Reston Stable Isotope Lab, Reston, VA, USA) packed in silver capsules (25 µL). I used polyethylene powder as an internal laboratory standard for sample bracketing and IAEA-CH7 for quality control at the beginning and end of each sequence. I did not notice any problems concerning drift or residual nonlinearity of the EA-IRMS system. I corrected small memory effects with the help of a pool-wise memory correction algorithm using one or two pools (Guidotti et al., 2013). Over the duration of

the experimental period from 24th June 2019 to 21st May 2021 the PE-powder was measured with a mean δ^2H value of -70.0 ± 1.5 ‰ (n = 771), GISP with -188.9 ± 1.7 ‰ (n = 121) and IAEA-CH7 with -100.4 ± 1.7 ‰ (n = 182). The values were indistinguishable from the certified or recommended values.

1.2.6 Data evaluation

Statistical analyses and the correction of isotope data were conducted with the free software environment R (R Core Team, 2022; Wickham et al., 2019). I normalized all stable H isotope ratios to the VSMOW-SLAP scale (Paul et al., 2007), which I extended with IAEA-604 to 799.9‰ (when $\delta^2H_w > 0$ in **Chapter 2** and always in **Chapters 3, 4**), and expressed them in ‰ relative to Vienna Standard Mean Ocean Water (VSMOW). All errors are given as 1 standard deviation (SD).

To determine reliable δ^2H_n values, I removed samples that came into contact with atmospheric humidity after the equilibration. I detected such samples by (a) visual inspection for holes and (b) the absence of an Ar peak after the H_2 peak in the Elemental Analyzer chromatogram. Steam equilibrations of the same sample with isotopically different waters need to result in the same contribution of exchangeable H to the total H concentration (same χ_e). Moreover, (c) I removed individual H isotope measurements as outliers, when both, the H concentration and the residual of the equilibrium line, were 0.5 times outside the interquartile range of all other equilibrations of the same sample (**Chapters 2–4**).

I used the regression equation (Eq. 1.1) of the known δ^2H_w on the measured δ^2H_t values to determine δ^2H_n values and the contribution of the exchangeable to the total H concentration (χ_e) (Feng et al., 1993; Filot et al., 2006; Ruppenthal et al., 2010, 2013, 2015; Sauer et al., 2009).

$$\delta^2H_t = \chi_e\, \alpha_{ex-w}\, \delta^2H_w + (1-\chi_e)\delta^2H_n + 1000\, \chi_e(\alpha_{ex-w} - 1) \qquad (Eq.\ 1.1)$$

In **Chapter 2**, I assumed that there is no equilibrium fractionation between the exchangeable H in the clay minerals and soil clay fractions and the steam (i.e., $\alpha_{ex\text{-}w} = 1$) (Bowen, Chesson, et al., 2005; Chesson et al., 2009; Hsieh & Yapp, 1999; Qi & Coplen, 2011). The fractionation factor $\alpha_{ex\text{-}w}$ is a temperature-dependent material constant, which is difficult to determine. Therefore, it is common practice to use the value of 1.08 for $\alpha_{ex\text{-}w}$, which had been determined for cellulose by (Schimmelmann, 1991) for organic materials (Qi & Coplen, 2011; Ruppenthal et al., 2010, 2013, 2015; Sauer et al., 2009;

Soto et al., 2017; Wassenaar & Hobson, 2000, 2003). While for some clay minerals, several fractionation factors are available for the equilibrium fractionation of nonexchangeable H between mineral and ambient water at the time of mineral formation (Gilg & Sheppard, 1996; Liu & Epstein, 1984; Méheut et al., 2010; O'Neil & Kharaka, 1976; Savin & Epstein, 1970b), I am not aware of any reported fractionation factor between exchangeable H in clay minerals and steam-H at 120 °C.

The slope is the product of χ_e and $\alpha_{ex\text{-}w}$ and the intercept is $(1-\chi_e)\delta^2H_n + 1000\,\chi_e(\alpha_{ex-w} - 1)$. Assuming $\alpha_{ex\text{-}w} = 1$ and using δ^2H_t from the regression line for $\delta^2H_w = 0$, Equation 1.1 is rearranged to calculate δ^2H_n (Eq. 1. 2).

$$\delta^2H_n = \frac{intercept}{1-slope} \qquad (Eq.\ 1.2)$$

Using Gaussian error propagation for Eq. 1.2, I estimated the standard deviation of the δ^2H_n values with Eq. 1.3, neglecting covariance of slope and intercept.

$$SD = \sqrt{\left(\frac{1}{1-slope} * SD_{intercept}\right)^2 + \left(\frac{intercept}{(slope-1)^2} * SD_{slope}\right)^2} \qquad (Eq.\ 1.3)$$

In **Chapter 3**, I combined slope = $\alpha_{ex\text{-}w} \cdot \chi_e$ and δ^2H_t from the regression line for $\delta^2H_w = 0$ to solve Equation 1.1 for δ^2H_n (Eq. 1.4).

$$\delta^2H_n = \frac{\alpha_{ex-w}\ intercept - 1000\ slope\ (\alpha_{ex-w}-1)}{\alpha_{ex-w} - slope} \qquad (Eq.\ 1.4)$$

For Eq. 1.4, I assumed either no fractionation ($\alpha_{ex\text{-}w} = 1$) or $\alpha_{ex\text{-}w} = 1.08$ (Ruppenthal et al., 2010, 2013, 2015; Sauer et al., 2009; Soto et al., 2017; Wassenaar & Hobson, 2000, 2003), which covered the range of $\alpha_{ex\text{-}w}$ values reported in the literature. The standard deviation (SD) of the δ^2H_n values was estimated by using Gaussian error propagation (Section 4.6.2). I recalculated the δ^2H_n values for bulk soil and SOM reported by Ruppenthal et al. (2014; 2015) for a different $\alpha_{ex\text{-}w}$ value with the help of the reported χ_e values.

I calculated the mean annual δ^2H values of local precipitation ($\delta^2H_{p,\,annual}$) for all my study sites with the Online Isotopes in Precipitation Calculator (OIPC, version 3.1; Bowen, 2022; Bowen & Revenaugh, 2003; IAEA/WMO, 2022). To calculate mean seasonal δ^2H_p values ($\delta^2H_{p,\,seasonal}$) representing the volume-weighted mean δ^2H_p value of the months with an average temperature > 0 °C (Bowen, Wassenaar, et al., 2005), I used the δ^2H_p values of the OIPC and temperature and precipitation data of the sampling locations from the years 1970-2000 (Fick & Hijmans, 2017). The 95% confidence interval of the $\delta^2H_{p,\,seasonal}$ values were taken from raster grids (Bowen, Wassenaar, et al., 2005).

To test for normal distribution, I used the Shapiro-Wilk Normality test. If necessary, I transformed the variables to their logarithmic, reciprocal or square root values based on the skewness of the original distribution (Webster, 2001). Linear models were validated by investigating their residuals with the Shapiro-Wilk test for normal distribution and using the Breusch-Pagan test for homoscedasticity. For the multiple regression, I used globally available climatic and topographic variables (Table 3.1). I used principal component analysis (normalized and varimax rotated) to identify statistically independent explanatory variables and only accepted principal components with eigenvalues > 1 (Revelle, 2021). As independent explanatory variables, I used the highest loading variable of each principal component. I implemented stepwise multiple regression analysis with the R packages "StepReg" (Junhui Li et al., 2021), using the corrected Akaike information criterion to choose the 'best' model in a bi-directional model selection process with 0.05 as significance threshold for in- or exclusion of variables. Relative weights were determined with the R package "relaimpo" (Grömping, 2007).

In line with reports from the literature, I did not fully get rid of some remaining organic matter in the clay fractions, particularly at high clay concentrations (Kaiser et al., 2002; Mikutta et al., 2005; von Lützow et al., 2007). Therefore, I corrected the measured δ^2H values of the clay fractions ($\delta^2H_{n,clay}$) with Eq. 1.3. For this purpose, I used an updated regression of the δ^2H_n values of soil organic C concentrations on δ^2H values of the mean annual local precipitation of Ruppenthal et al. (2014; 2015), because the number of worldwide stations contributing to the Online Isotopes in Precipitation Calculator had tripled since 2015 (Bowen, 2022).

$$\delta^2H_{n,inorg.clay} = \frac{\delta^2H_{n,clay} - f_{n,SOM}\,\delta^2H_{n,SOM}}{1 - f_{n,SOM}}, \text{ with } \delta^2H_{n,SOM} = 0.985\,\delta^2H_p - 54.6‰ \quad (Eq.\ 1.5)$$

$\delta^2H_{n,\ inorg.\ clay}$ is the δ^2H_n value corrected for the contribution of SOM and thus the inorganic part of the clay fractions. $f_{n,\ SOM}$ is the contribution of C-bonded H in SOM to the total nonexchangeable H in my soil clay fractions. The C-bonded H from SOM was estimated by assuming 25 g of H per kg of C_{org} (Rice & MacCarthy, 1991), that SOM contains 50% C and that 80% of this H was nonexchangeable (Ruppenthal et al., 2013; Schimmelmann, 1991; Wassenaar & Hobson, 2000). I furthermore assumed that the clay separation procedure did not change the δ^2H_n value of the SOM.

In **Chapter 4**, I determined the $\alpha_{ex\text{-}w}$, by drying the samples after 16-h equilibration differently, the slope (m_i) and intercept (b_i) of the equilibration line can be manipulated

because χ_e is varied ($\chi_{e,1} \neq \chi_{e,2}$). Meanwhile, the $\alpha_{ex\text{-}w}$ and δ^2H_n values remain unchanged, because $\alpha_{ex\text{-}w}$ depends on the equilibration temperature, which is always the same and δ^2H_n values are independent of χ_e.

Assuming that the δ^2H_n values of the different drying procedures are the same and solving Eq. 1.4 in the form of $\delta^2H_{n,1} = \delta^2H_{n,2}$ for $\alpha_{ex\text{-}w}$ yields Eq. 1.6

$$\alpha_{ex-w} = \frac{b_1 m_2 - b_2 m_1 + 1000\,(m_2 - m_1)}{b_1 - b_2 + 1000\,(m_2 - m_1)}, \qquad (Eq.\ 1.6)$$

As a test, I calculated $\alpha_{ex\text{-}w}$ in two other ways with the identical result (Section 4.6.1). I estimated the SD of $\alpha_{ex\text{-}w}$ by applying Gaussian error propagation (Section 4.6.2). A larger difference between the slopes and a smaller scattering around the equilibration lines resulted in a smaller propagated error. I accepted only $\alpha_{ex\text{-}w}$ values with a propagated SD < 0.2. Moreover, I only used pairs of equilibration lines if the stronger drying resulted in a steeper slope than the weaker drying. With the medium-drying equilibration line taken from **Chapters 2 and 3**, when available, resulted in a maximum of three possible equilibration line pairs, and thus three possibilities for deriving $\alpha_{ex\text{-}w}$. I then calculated the arithmetic mean and SD of the $\alpha_{ex\text{-}w}$ values from different combinations of equilibration line pairs (**Chapter 4**).

1.3 Results and Discussion

1.3.1 Testing the δ^2H_n determination of clay fractions (Chapter 2)

In a first step to adapt the steam equilibration method, I determined the optimum equilibration time (Figure 2.3). In my experiment, the δ^2H_t values of the equilibrated samples did not fully reach a plateau after 64 h, but changed little beyond 16 h. A similarly slow increase of the δ^2H_t values with time during vacuum drying at constant temperature were observed for some clay minerals (Faucher & Thomas, 1955; O'Neil & Kharaka, 1976). Likewise, Schimmelmann (2006) reported an asymptotic convergence to a plateau for kerogen-H. Thus, full equilibrium of the clay minerals with the steam occurs only at equilibration times, which are not feasible for routine measurement. Therefore, I decided to run my equilibration for 16 h, because after 16 h the change in the δ^2H_t value was only minor. The linear regression of the δ^2H_t value of my clay minerals and soil clay fractions on the δ^2H values of the equilibration water consistently resulted in coefficients of determination > 0.99. The precision of the δ^2H_n measurements of the three soil clay fractions ranged from ± 0.6 ‰ for Oso to ± 6.9 ‰ for KA-1 (± 1 SD);

the precision of untreated bulk samples of clay minerals ranged from ± 0.9 ‰ for KGa-2 kaolinite to ± 7.5 ‰ for Mg-montmorillionite (all n = 3). I attribute the high precision of the δ^2H_n value of kaolinite and the Oso clay fraction to their high structural H concentration and a corresponding small exchangeable H fraction of total H. The KGa-2 kaolinite had the smallest exchangeable H fraction of total H of all studied clay minerals, and the Oso clay fraction of all studied soil samples. In contrast, the swellable vermiculite and montmorillonites contain less structural H and much more exchangeable H than kaolinite. Consequently, the δ^2H_n measurements of trioctahedral vermiculite showed a higher error.

To evaluate the effect of the clay separation on the δ^2H_n values of clay minerals, I compared δ^2H_n values of the untreated bulk clay mineral samples with the δ^2H_n values of the clay mineral samples, which I carried through the clay separation method. Both δ^2H_n values were similar, except for the trioctahedral vermiculite. The latter was related with the fact that in my treatment, I only collected 1 % of the bulk sample in the clay fraction of the vermiculite, which was not representative for the bulk vermiculite. Therefore, I additionally measured the δ^2H_n values of the '≤silt' and sand fractions of the trioctahedral vermiculite and calculated a mass-weighted mean of the δ^2H_n values of the grain-size fractions. The resulting calculated δ^2H_n value of the bulk vermiculite was similar to that of the untreated sample, illustrating that the clay separation method did not influence the δ^2H_n value of the clay fraction. Because it was not possible to remove the entire SOM from the soil clay fractions, I had to consider the influence of nonexchangeable H in remaining SOM. The maximum residual organic C concentration in the three clay fractions was 35.7 g kg^{-1}. To assess the influence of C-bonded H in organic matter on my δ^2H_n values of the three soil clay fractions, I estimated the nonexchangeable H from organic matter to contributed 15–34 % to the total nonexchangeable H in my three soil clay fractions. Furthermore, my correction of the δ^2H_n values of the soil clay fractions by the contribution of the nonremoved SOM only affected the δ^2H_n value of one of my three soil samples, Oso, more than marginally. In the Oso sample, the corrected δ^2H_n value was shifted by 15 ‰ (**Chapter 2**).

1.3.2 Relationship of the δ^2H values of precipitation with the δ^2H_n values of soil clay fractions (Chapter 3)

The δ^2H_n values of the clay fractions, calculated with Eq. 1.2, ranged from -167 ‰ for north Siberia to -44 ‰ for west Kenia, calculated with $\alpha_{ex\text{-}w} = 1$ and from -191 ‰ for south Argentina (-181 ‰ for north Siberia) to -81 ‰ for west Kenia for $\alpha_{ex\text{-}w} = 1.08$ (Table 3.2). No matter which $\alpha_{ex\text{-}w}$ was used, there was always a significant correlation between the δ^2H values of mean annual and seasonal local precipitation and the δ^2H_n values of the clay fractions (Figure 3.2). As expected, the bulk soil from a climosequence in Argentina (data taken from Ruppenthal, 2014 and recalculated for $\alpha_{ex\text{-}w} = 1$) fell in between demineralized organic matter and clay fractions for both $\alpha_{ex\text{-}w}$ values.

My range of δ^2H_n values of clay fractions for both $\alpha_{ex\text{-}w}$ values is similar to that reported by Lawrence and Taylor (1971) of -30 to -165 ‰ for clay minerals and hydroxides in soils of the USA (Table 3.2). The fact that the δ^2H_n values of the bulk soils of the Argentinean subset of samples could be explained as a mixture of those of demineralized organic matter and the clay fractions illustrated that the nonexchangeable H pool of different soil constituents such as organic matter and clay minerals showed a different equilibrium H isotope fractionation between ambient water and the individual constituents (i.e., different $\alpha_{min\text{-}water}$ values; Figure 3.3). Moreover, I found that the influence of the remaining C_{org} concentrations in the soil clay fractions on their δ^2H_n values can be neglected, because the estimated shift of the C-bonded H on the regression of the δ^2H values of mean annual and seasonal local precipitation on the δ^2H_n values of the clay fractions was minor. Additionally, I found an influence of the assumed preliminary $\alpha_{ex\text{-}w}$ values and the dominant clay mineral type, as assessed via the potential cation-exchange capacity on the results of the regression analysis. Considering other climatic and geomorphological site properties in an additional multiple regression analysis indicated that the consideration of hillslope as explanatory variable increased the explained variance of the δ^2H_n values of the soil clay fractons, which is similar to the finding of Schaub et al. (2009) for $\delta^{18}O$ values of soil clay fractions. Moreover, my results illustrate that the $\alpha_{ex\text{-}w}$ values, particularly of the 2:1 clay minerals, need to be better constrained (**Chapter 3**).

1.3.3 Determination of sample-specific $\alpha_{ex\text{-}w}$ and its variation in soil clay fractions (Chapter 4)

I was able to determine the $\alpha_{ex\text{-}w}$ value for 7 of 10 clay minerals, 19 of 22 topsoil clay fractions, and all 3 other materials (two different micas and cellulose, Table 4.1). The missing data are attributable to the fact that the slopes of the regression lines of the δ^2H_t values of the sample on the δ^2H_w values after the different drying procedures were not sufficiently different to reliably determine the intersection point of the two regression lines in at least one of three considered pairs (weaker-medium, weaker-stronger, and medium-stronger drying). Among the 29 successful $\alpha_{ex\text{-}w}$ determinations, there was a significant difference between the contributions of exchangeable H to total H in the minerals and clay fractions after weaker and stronger drying (paired t-tests, mean 11.2 %, $p < 0.001$), ranging from 1 to 24 %, Table 4.1). The overall mean $\alpha_{ex\text{-}w}$ value was 1.080 ± SD 0.080 (n=29) and thus identical with the $\alpha_{ex\text{-}w}$ value frequently chosen in the literature for bulk soil and organic matter (Ruppenthal et al., 2010). Thus, an $\alpha_{ex\text{-}w}$ value of 1.080 is a suitable first estimate for soil minerals.

The $\alpha_{ex\text{-}w}$ values of the 19 topsoil clay fractions correlated with the soil clay content ($r = 0.63$, $p = 0.04$), local mean annual temperature ($r = 0.68$, $p = 0.01$) and the δ^2H values of local precipitation ($r = 0.72$, $p < 0.001$) mainly reflecting the different clay mineralogy under different climatic weathering regimes. The $\alpha_{ex\text{-}w}$ and δ^2H_n values show different relations with the local precipitation, depending on their grouping based on the CEC_{pot} into 1:1- and 2:1 clay mineral-dominated mixtures. My findings are in line with the fact that the hot-humid inner tropical zone at low latitude (and δ^2H_p values near 0) is usually dominated by 1:1 clay minerals, while the temperate zone at intermediate latitude and δ^2H_p values shows a prevalence of 2:1 clay minerals (FAO, 2009; Ito & Wagai, 2017) (**Chapter 4**).

In **Chapter 3**, I had shown, that the δ^2H values of local annual precipitation ($\delta^2H_{p,\,annual}$) correlated significantly with the δ^2H values of a global set of soil clay fractions for an assumed constant $\alpha_{ex\text{-}w}$ value of 1 or 1.08, respectively (Figure 3.2). Moreover, I showed that the climate-determined mineralogy of the soil clay fraction, which I assessed via the CEC_{pot}, influenced this relationship (Figure 3.5). The latter finding is redrawn in Figure 1.2a for an $\alpha_{ex\text{-}w}$ value of 1 (Figure 1.2c) to allow for a direct comparison. When I now used the sample-specific $\alpha_{ex\text{-}w}$ value to calculate the δ^2H_n values of the soil clay fraction, the relationship between the $\delta^2H_{p,\,annual}$ values and

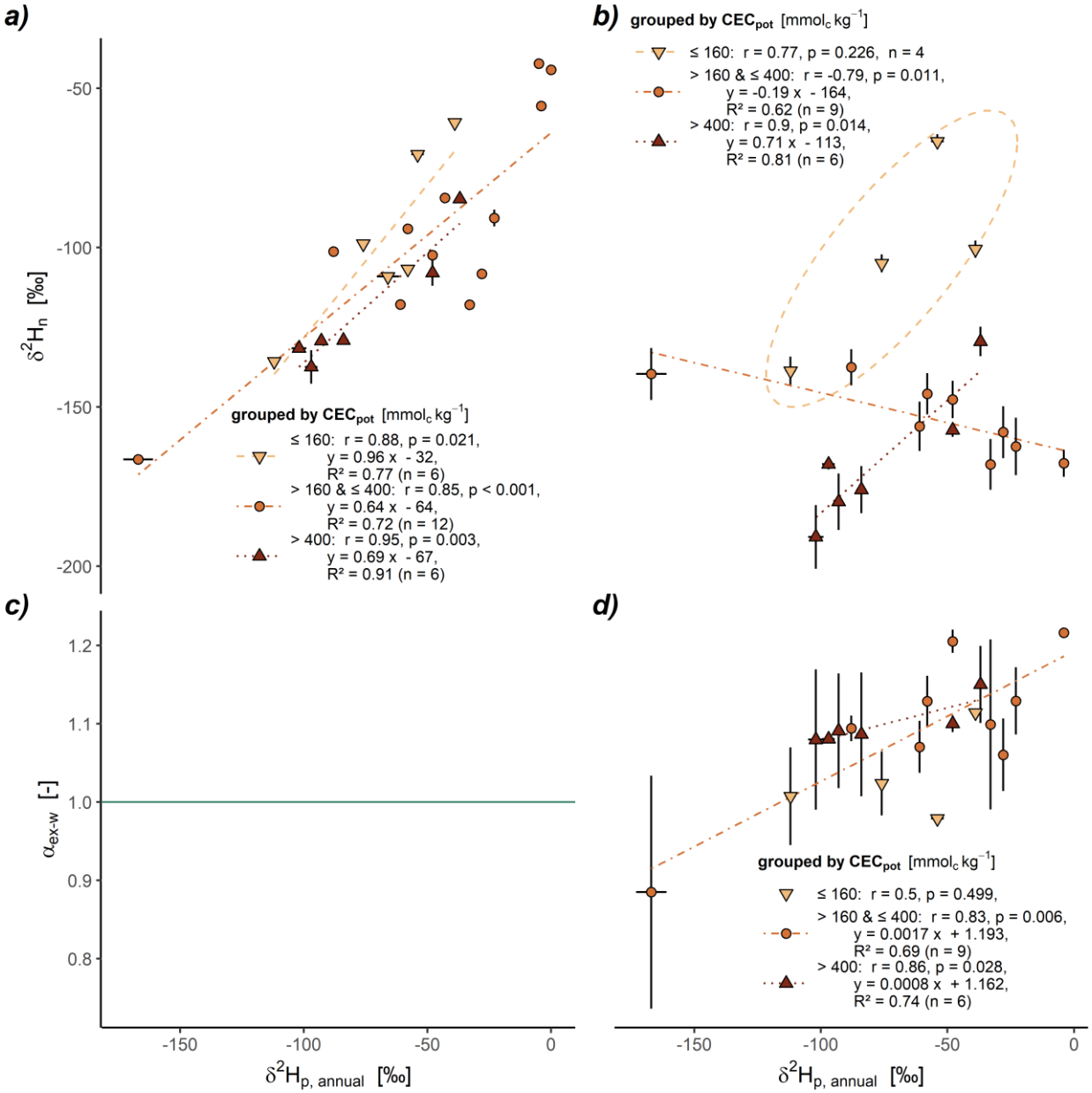

Figure 1.2: Relationships between the δ^2H values of local mean annual precipitation ($\delta^2H_{p,\ annual}$) and the δ^2H_n values of soil clay fractions calculated with $\alpha_{ex\text{-}w}$ = 1 (a) (no equilibrium fractionation) and with a sample-specific $\alpha_{ex\text{-}w}$ value (b) and relationships between the $\delta^2H_{p,\ annual}$ values and a constant $\alpha_{ex\text{-}w}$ value of 1 (c) and sample-specific $\alpha_{ex\text{-}w}$ values (d). The $\delta^2H_{p,\ annual}$ values are from the Online Isotopes in Precipitation Calculator, version 3.1 (Bowen 2022). The filling and symbol shape group clay fractions by the potential cation-exchange capacity (CEC_{pot}). The dashed to dotted lines show linear regression lines only when the correlations are significant or group the samples with a $CEC_{pot} \leq 160$ mmol$_c$ kg^{-1} together (b). The error bars of the δ^2H_p values indicate the 68% confidence interval and might be smaller than the symbol size. The error bars of δ^2H_n values indicate in (a) the SD from field triplicates, available for three sample locations from Argentina; in (b), the SD is derived by Gaussian error propagation.

the δ^2H values of a global set of soil clay fractions disappeared (Figure 1.2b). Instead, the $\delta^2H_{p,\,annual}$ values correlated with the sample-specific $\alpha_{ex\text{-}w}$ values (Figure 1.2d). This finding illustrates that the relationship between the $\delta^2H_{p,\,annual}$ values and the δ^2H_n values of soil clay fractions was strongly influenced by the mineralogical composition of the soil clay fraction. The soil clay fractions with a $CEC_{pot} \leq 160$ $mmol_c$ kg^{-1}, presumably dominated by 1:1 clay minerals which is common in inner tropical soils (FAO, 2009; Ito & Wagai, 2017), showed systematically higher δ^2H_n values and tend to lower $\alpha_{ex\text{-}w}$ values than all other samples, which are presumable richer in 2:1 clay minerals (Figure 1.2b,d).

1.3.4 Comparison of δ^2H_t and δ^2H_n measurements of clay minerals

The current state-of-the-art methods to remove exchangeable H before continuous flow isotope ratio mass spectrometry (CF-IRMS) use varying temperatures ranging from 100 °C to 350 °C (Bauer & Vennemann, 2014; Gilg et al., 2004; Savin & Epstein, 1970a; VanDeVelde & Bowen, 2013; Vitali et al., 2002). The chosen temperature varies with the investigated clay minerals. For smectites, 200 to 250°C was considered to deliver satisfying results (Bauer & Vennemann, 2014; VanDeVelde & Bowen, 2013). However, Marumo et al. (1995) still found an influence of interlayer water at 200 °C for a poorly crystallized smectite accompanied by an initial dehydroxylation at the same temperature.

My own measurements, in which I eliminated the influence of exchangeable H on the δ^2H_n value by steam equilibration, yielded generally isotopically lighter δ^2H_n values for clay minerals than the conventional measurements in which exchangeable H was removed via vacuum extraction at 200 ± 50 °C (Table 1.1). However, the δ^2H_n values of USGS biotite and muscovite were nearly identical irrespective of the used measurement method. I suggest that the latter is attributable to the smallest exchangeable H fraction (χ_e).

Table 1.1: Comparison of conventional δ^2H measurements after pretreatment at 200 ± 50 °C in vacuum with my own δ^2H_n measurements via steam equilibration for clay minerals and mica.

Sample	Conventional δ^2H measurements				This study					
					untreated bulk sample			treated clay fraction		
	Source	Sample treatment		δ^2H analysis method	δ^2H	δ^2H_n	χ_e	$\delta^2H_{n,\alpha=1}$	δ^2H_n	χ_e	$\delta^2H_{n,\alpha=1}$
					‰	‰	%	‰	‰	%	‰
SWy montmorillonite	Menegati et al. (1999)	ultrasonication, CH_2O_2, <2 µm fraction		"dried overnight at 250°C under high vacuum, then heated in a vacuum at T>1100°C to release H_2 and H_2O. Molecular hydrogen was converted to water by reaction with copper oxide"; then Zn-reduction; dual-inlet IRMS	-117	-150±7	22±2	-136±4	-150	10	-131±2
		$Na_2S_2O_8$, ultrasonication, CH_2O_2, <2 µm fraction			-89						
	Fagan (2001)	untreated; 1- 2 µm		2–3 h at 150 °C in vacuo, heated in a vacuum to 1000 °C to release H_2 and H_2O; H_2 converted to water by reaction with CuO; hot uranium reduction; dual-inlet IRMS	-135						
		ultrasonic-cation, Na acetate, H_2O_2, DCB			-117.5						
	Bauer & Vennemann (2014)	untreated		3 h at 200 °C in a vacuum of 2 Pa, rapid single-sample transfer before reduction to H_2 in a glassy carbon-filled EA at 1450 °C; continuous flow IRMS	-135						
		untreated		150 °C until pressure remains at background level; heated to 1500 °C with subsequent CuO oxidization; Zn reduction of trapped water at 500°C; dual-inlet IRMS	-129						
	Kanik et al. (2022)	NaOCl + ultrasonication + saturation with…	K	4 h at 200°C in vaccum oven, transfer to "zero-blank" autosampler within ~1–2.5 min & 4 h He-flush before reduction to H_2 in glassy carbon filled EA at 1450 °C; continuous flow IRMS	-140.0						
			Ca		-130.5						
			Na		-131.5						
SCa-3 montmorillonite	VanDeVelde & Bowen (2013) #	untreated		after 4 h 200°C vacuum degassing, transfer to "zero-blank" autosampler with <5 min laboratory air exposure; glassy carbon-filled EA at 1400 °C; NBS-30 calibrated δ^2H values; continuous flow IRMS	-83	-202±15	54±4	-101±8	n.a.	n.a.	-100±4
IMt illite					-102	-158±4	14±1	-139±2	-141	8	-131±4
USGS biotite	Qi et al. (2017)	untreated		six laboratories analyzed air-dried samples with glassy-carbon- or Cr-filled HTC-EA-continuous flow IRMS and one with heating to >1400°C, subsequent CuO oxidization, reduction of trapped water with Cr at 900 °C, dual-inlet IRMS	-91.5	-94±1	4±1	-95.3±0.9	n.d.	n.d.	n.d.
USGS muscovite					-28.4	-29	2	-30.7±1.4	n.d.	n.d.	n.d.

n.a. – not available, because the result of the treated vermiculite showed an inacceptable SD of $\alpha_{ex\text{-}w}$ above 0.2 and was therefore omitted

n.d. – not determined

δ^2H values were extracted from Figure 3a of VanDeVelde & Bowen (2013)

* Na citrate bicarbonate and Na dithionite treatment

In contrast, I observed large differences between the δ^2H_n values of clay minerals determined in my study and the δ^2H_t measurements of the same material in other studies ($\Delta^2H_{n\text{-}t}$). The $\Delta^2H_{n\text{-}t}$ values increased with increasing size of χ_e. This agrees with findings of Bauer and Vennemann (2014), who observed rehydration by water vapor in the laboratory air which varied with grain size and interlayer cation composition of the clay mineral sample. By limiting the exposure time to laboratory air before CF-IRMS measurement, the results for SWy-1 were closer to my δ^2H_n determination ($\Delta^2H_{n\text{-}t}$ = -15 ‰) and identical with those of Fagan (2001; SWy-1 vs. SWy-3 from the same origin). Kanik et al. (2022) shortened the exposure time to laboratory air prior to CF-IRMS measurement to ~1–2.5 min, additionally using a hot autosampler. Moreover, Kanik et al. (2022) reduced the exchangeable H fraction by K-saturation of SWy-1, which led to a collapse of the interlayer space. This resulted in a $\Delta^2H_{n\text{-}t}$ value of only -10 ‰ thus coming close to my own measurements in which I eliminated the influence of exchangeable H on the δ^2H_n values completely (Table 1.1). The nearly doubled $\Delta^2H_{n\text{-}t}$ for SWy montmorillonite in the study of Kanik et al. (2022) can be explained by an exchangeable H fraction of 22 ± 2 % after 200 °C vacuum drying. Consequently, the large size of of the χ_e of 54 ± 5 % for SCa-3 montmorillonite in the study of VanDeVelde and Bowen (2013) led to substantially different total and nonexchangeable δ^2H values with $\Delta^2H_{n\text{-}t}$ = -119 ‰. Contributing to this, the double charged interlayer cation of the SCa-3 montmorillonite approximately doubles the water uptake at the same partial pressure (Bauer & Vennemann, 2014).

1.4 Error Discussion

I am aware that, despite my best efforts, the data presented may be affected by various sources of uncertainty. The classification of soils in the field and the differentiation of different soil horizons for soil description and sampling was done by experienced pedologists based on the field guides of the German soil classification (KA5) (AG Boden, 2005) and the World Reference Base for Soil Resources (IUSS Working Group WRB, 2015). Nevertheless, a possible bias due to subjective assessment in the field cannot be excluded (**Chapters 2–4**).

The grain size determination and the chemical characterization of the samples in the laboratory was repeated twice in **Chapter 2** exhibiting an acceptable variation of the

resulting values of each sample property (Table 2.5): For the untreated bulk samples the SD of the Fe_d concentrations ranged from 0.0 to 0.7 and for the C_{org} concentrations from 0.01 to 2.2 mg g^{-1} (n = 3). For the grain size determination, the SD of the relative masses ranged for sand from 0.2 to 5.7 %, for silt and clay from 1 to 10 % (n = 2). For the C_{org} concentration of the clay fractions the SD ranged from 0.0 to 3.7 mg g^{-1} (n = 3). The soil clay fractions showed in general a higher SD than the clay mineral samples. In **Chapters 3** and **4**, I treated one soil sample (SK-Oso) in four separate batches, exhibiting a high precision of my measurements (Table 1.2).

Table 1.2: Selected properties of the repeatedly measured sample "SK-Oso" with means and standard deviations (SD).

treatment batch number	Bulk samples				Clay fractions					
	Sand	Silt	Clay	Fe_d	C	N	CEC	δ^2H_n ± SD	χ_e ± SD	H ± SD
	[%]			[mg g^{-1}]			[$mmol_c$ kg^{-1}]	[‰]	[%]	[mg g^{-1}]
1	34.5	50.5	15.0	9.4	36	2.7	120.8	-95.1 ± 1.2	16.9 ± 0.3	10.3 ± 0.2
2	33.6	51.7	14.8	9.3	33.1	2.7	121.2	-101.9 ± 1.2	17.6 ± 0.4	9.8 ± 0.1
3	32.5	52.3	15.1	9.5	37.9	3	122.8	-98.3 ± 1.3	18.7 ± 0.4	10.7 ± 0.3
4	33.3	51.2	15.5	9.7	34.8	2.8	134.3	-99.4 ± 1.7	18.0 ± 0.5	10.5 ± 0.6
Mean	*33.5*	*51.4*	*15.1*	*9.5*	*35.5*	*2.8*	*124.8*	*-98.7*	*17.8*	*10.3*
± SD:	*± 0.8*	*± 0.8*	*± 0.3*	*± 0.2*	*± 2*	*± 0.1*	*± 6.4*	*± 2.8*	*± 0.8*	*± 0.4*

The 3-4 times repeated measurement of the δ^2H_n values in soil clay fractions and clay minerals showed a high precision for the whole procure (clay separation, steam equilibration and EA-IRMS measurement; Table 1.2 and Table 2.3) with SD ranging from ± 0.9 ‰ to ± 7.5 ‰ (**Chapters 1–3**). Nevertheless, a systematic influence of the clay separation treatment cannot be entirely excluded. Gilg et al. (2004) reviewed several steps of the sequential clay separation procedure for δ^2H analyses of clay minerals and suggested a treatment with H_2O_2 as satisfactory for the SOM removal. However, several authors have shown that the SOM removal with H_2O_2 from the clay fraction can be inefficient and is selective with respect to composition and age, which is well known (Eusterhues et al., 2003; Kaiser et al., 2002; Leifeld & Kögel-Knabner, 2001; Mikutta et al., 2005; von Lützow et al., 2007). Unfortunately, the influence of the selective SOM removal by H_2O_2, NaOCl or $Na_2S_2O_8$ on δ^2H_n values of SOM in the clay fraction is unknown. After each soil sample had undergone repeated H_2O_2 treatment steps, none of my clay fractions was completely free of SOM with C_{org} concentrations from 1.0 to 58.9 mg g^{-1}. I estimated the influence of remaining C_{org}-associated H to moderately shift most δ^2H_n values of the samples, up to a maximum of 19 ‰ (**Chapters 2–3**).

Nevertheless, the overall influence of this shift on the relationship between seasonal or annual mean δ^2H precipitation values and the δ^2H_n values of topsoil clay fractions was minor (**Chapter 3**). Another limitation of the clay separation method consists of the fact that a 15-min single-step application of the DCB method removes nearly all hematite but only about 80% of the goethite, and even repeated applications of the DCB method might leave some Fe oxides untouched (Mehra & Jackson, 1958). After a 30-min single-step application, my bulk soil Fe_d concentrations did not correlate with the total Fe concentration of the clay fractions, which I used as surrogate of the concentrations of remaining Fe oxides in the clay fractions ($\rho = 0.07$, $p = 0.74$, $n = 23$), although the total Fe concentrations also includes Si-bound Fe. The results showed that there was no relationship between the total and the residual Fe concentration in the clay fractions, precluding a systematic bias by the DCB step of the clay separation method (**Chapter 3**).

Over the duration of the experimental period of hydrogen isotope measurements from 24th June 2019 to 21st May 2021 a PE-powder was measured with a mean δ^2H value of -70.0 ± 1.5‰ (n = 771) as in-house standard for drift control. I used GISP with -188.9 ± 1.7 ‰ (n = 121) to test for a correct normalization of each IRMS measurement sequence and IAEA-CH7 with -100.4 ± 1.7 ‰ (n = 182) as quality check at the beginning and and of each IRMS sequence (Figure 1.3). The values were indistinguishable from the certified or recommended values.

During δ^2H analysis, the samples were pyrolyzed in the chromium-filled Al_2O_3 reactor at 1250 °C as recommended by Gehre et al. (2017). Compared to a glassy carbon reactor set up the chromium-filled Al_2O_3 reactor is less influenced by high N, S or halogen concentrations, because in the pyrolysis these elements are bound to Cr (Gehre et al., 2015; Nair et al., 2015; Renpenning et al., 2015, 2017). Because a back diffusion of halogens is possible when chromium(III) chloride reacts with molecular hydrogen, which affects δ^2H measurements of water (Gehre et al., 2015), I renewed the reactor filling for each IRMS sequence and used GISP before the measurement of the reference material for normalization to test for a release of halogens from the previously measured soil clay fractions. The GISP values were indistinguishable from the certified values, indicating that no back diffusion of halogens occurred.

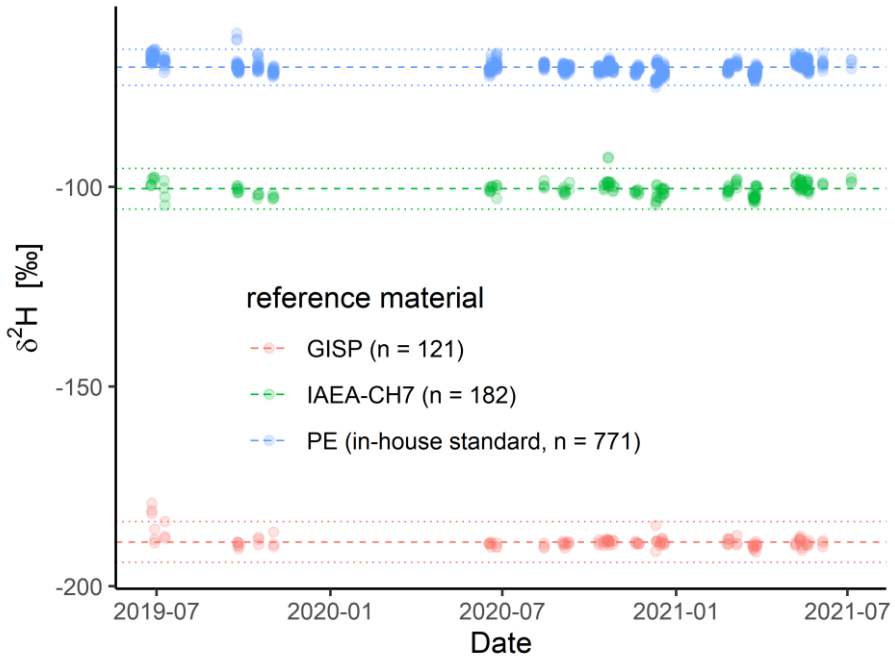

Figure 1.3: All δ^2H measurements of three reference materials over the experimental period. The dashed line is the average and the dotted line is the 3σ standard deviation.

During this study, the uncertainty caused by using an assumed $\alpha_{ex\text{-}w}$ value became obvious. While **Chapter 2** is based on the assumption that the equilibrium fractionation between the steam-H and exchangeable H of the clay sample can be neglected ($\alpha_{ex\text{-}w}$ = 1; Bowen et al., 2005; Chesson et al., 2009; Hsieh & Yapp, 1999; Qi & Coplen, 2011), **Chapter 3** reveals that different assumptions of $\alpha_{ex\text{-}w}$ between 0 and 1.08 result in deviating δ^2H_n values. Independent of the choice of the $\alpha_{ex\text{-}w}$ values, the external precision of my δ^2H_n determinations assessed via three field triplicates was low (SD 2.5 to 5.1 ‰). To overcome the need of an estimated $\alpha_{ex\text{-}w}$ value, I developed a method to determine sample-specific $\alpha_{ex\text{-}w}$ experimentally in **Chapter 4**. Although this method was successful, the determined $\alpha_{ex\text{-}w}$ values showed a considerable uncertainty (SD 0.008 to 0.149, see Table 4.1). The proposed technical improvements to the steam equilibration apparatus (Section 4.6.3) may reduce the latter. Nevertheless, a small amount of residual water-H of the exchangeable pool could have been affected by additional fractionation in the drying phase after equilibration. Our elevated temperatures of 120 and 200 °C are likely associated with only a small difference in the size of this fractionation, since elevated temperatures are associated with higher vibrational energies, minimizing stable isotope fractionation (Bigeleisen, 1965) (**Chapter 4**).

1.5 General Conclusions

The results of my research allow to draw the following conclusions:

1) The steam equilibration method previously used for bulk soils and SOM can be used for precise measurements of δ^2H_n values in clay fractions of soils and clay minerals, provided the contact of the clays with ambient air humidity after equilibration can be entirely avoided. To achieve this, the samples must be handled in a water vapor-free Ar atmosphere. This technique should be universally applicable to other hygroscopic materials. I did not detect a significant effect of the classical clay separation treatment, including removal of Fe oxides and carbonates, reduction of SOM and dispersion of the remaining material, on the δ^2H_n values of clay minerals. However, the incomplete destruction of SOM required a correction of the data, which relied on the unproven assumption that the H_2O_2 treatment did not change the δ^2H_n values of the SOM (**Chapter 2**).

2) Our results confirmed that there is a significant correlation between the δ^2H values of local precipitation and the δ^2H_n values of soil clay fractions at a global scale. However, this relationship is less close than previously observed for soil organic matter. The remaining organic matter in the soil clay influenced the δ^2H_n values of the soil clay fractions little. However, the equilibrium fractionation factor between ambient water-H and exchangeable H in the clay fraction ($\alpha_{ex\text{-}w}$) in the range of 1-1.08 influenced the regression of the δ^2H_n values of soil clay fractions on the δ^2H values of local precipitation but did not change the overall positive relationship. The mineral composition, assessed via the potential cation-exchange capacity, had a strong influence on the regression of the δ^2H_n values of soil clay fractions on the δ^2H values of local precipitation. The inclusion of seasonal local precipitation, hillslope and latitude in a multiple regression model explained up to 89% of the variation in the δ^2H_n values of soil clay fractions. This suggest that only ambient water H during non-frozen periods contributed to the nonexchangeable H of clay fractions in the soil. The hillslope can be interpreted as an indication of the degree to which clay minerals are autochthonous, because the higher the hillslope is, the higher is the erosion risk, while the eroded clay accumulates on flat terrain. The influence of latitude reflected the fact that clay mineral formation is climate-specific, tending to be dominated by

1:1 clay minerals in the inner tropics and of 2:1 clay mineals in the temperate zone (**Chapter 3**).

3) Steam equilibration with at least two distinctly different drying conditions can be used to determine the equilibrium fractionation factor between the H of the steam and the exchangeable H pool of the sample ($\alpha_{ex\text{-}w}$). My approach is universally applicable to all materials that respond sufficiently to the applied drying conditions with a substantial difference in their contribution of exchangeable H to total H. I did not detect a significant effect of the classical clay fracitionation treatment, including removal of Fe oxides and carbonates, reduction of SOM and dispersion of the remaining material, on the $\alpha_{ex\text{-}w}$ values of clay minerals. I found that the $\alpha_{ex\text{-}w}$ values of topsoil clay fractions are influenced by their mineralogical composition as assessed via their cation-exchange capacity. Thus, the previously reported correlations between δ^2H values of local precipitation and δ^2H_n values of clay minerals, soil clay fractions, and bulk soils are not only driven by the equilibrium between ambient water and non-exchangeable mineral-H but also by the mineral-specific $\alpha_{ex\text{-}w}$ values, which vary systematically among different climate zones with different weathering regimes (**Chapter 4**).

4) My δ^2H_n measurements of clay minerals via steam equilibration showed generally isotopically lighter H in the nonexchangeable fraction than the conventional δ^2H measurements using vacuum drying at variable temperature. The shift towards more negative δ^2H_n values after steam equilibration was negligible for mica, which contain little exchangeable H but increased with increasing exchangeable H contributions to total H in increasingly hygroscopic samples (**Chapter 1**).

1.6 Author contributions

Yvonne Oelmann and Wolfgang Wilcke had the initial scientific idea for this PhD thesis, acquired the funding and administrated the project. They also set up the study design (**Chapters 2 and 3**). I gathered all soil samples and related information from various collaborators, archives or collected in one case (DE-KA1) more sample material at the identical sampling location (**Chapters 1–4**). I conducted all laboratory analysis,

evaluated the data, drafted the visualizations and wrote all first manuscript versions (**Chapters 1–4**). In the laboratory, I received technical support from Nadine Gill (washing of samples, weighing for IRMS analysis, EA reactor exchange; **Chapters 1–4**); Martin Kull (CN analysis; **Chapter 3**) and Andre Velescu (ICP-MS and ICP-OES handling; **Chapter 3**). Sadadi Ojoatre contributed three soil samples from Kenya which were particulary important for the spread of the $\delta^2H_{p,\,annual}$ data with a value near 0‰. He furthermore contributed writing-review and editing. Wolfgang Wilcke contributed to the investigation, writing-review & editing and supervised my thesis (**Chapters 1–4**). Yvonne Oelmann and Arnim Kessler contributed to the investigation, writing-review and editing (**Chapters 2–4**).

1.7 References

AG Boden. (2005). *Bodenkundliche Kartieranleitung* (5th ed.). Schweizerbart'sche Vlgsb.

Ammann, L., Bergaya, F., & Lagaly, G. (2005). Determination of the cation exchange capacity of clays with copper complexes revisited. *Clay Minerals*, *40*(4), 441–453. https://doi.org/10.1180/0009855054040182

Araguás-Araguás, L., Froehlich, K., & Rozanski, K. (2000). Deuterium and oxygen-18 isotope composition of precipitation and atmospheric moisture. *Hydrological Processes*, *14*(8), 1341–1355. https://doi.org/10.1002/1099-1085(20000615)14:8<1341::AID-HYP983>3.0.CO;2-Z

Bauer, K. K., & Vennemann, T. W. (2014). Analytical methods for the measurement of hydrogen isotope composition and water content in clay minerals by TC/EA. *Chemical Geology*, *363*, 229–240. https://doi.org/10.1016/j.chemgeo.2013.10.039

Bigeleisen, J. (1965). Chemistry of Isotopes: Isotope chemistry has opened new areas of chemical physics, geochemistry, and molecular biology. *Science*, *147*(3657), 463–471.

Borden, D., & Giese, R. F. (2001). Baseline studies of the clay minerals society source clays: Cation exchange capacity measurements by the ammonia-electrode method. *Clays and Clay Minerals*, *49*(5), 444–445.

Borden, P. W., Ping, C.-L., McCarthy, P. J., & Naidu, S. (2010). Clay mineralogy in arctic tundra Gelisols, northern Alaska. *Soil Science Society of America Journal*, *74*(2), 580–592. https://doi.org/10.2136/sssaj2009.0187

Bors, J., Gorny, A., & Dultz, S. (1997). Iodide, caesium and strontium adsorption by organophilic vermiculite. *Clay Minerals*, *32*(1), 21–28. https://doi.org/10.1180/claymin.1997.032.1.04

Bowen, G. J. (2022). *WaterIsotopes.org*. The Online Isotopes in Precipitation Calculator, Version 3.1. http://wateriso.utah.edu/waterisotopes/pages/data_access/oipc.html

Bowen, G. J., Chesson, L., Nielson, K., Cerling, T. E., & Ehleringer, J. R. (2005). Treatment methods for the determination of δ^2H and $\delta^{18}O$ of hair keratin by continuous-flow isotope-ratio mass spectrometry. *Rapid Communications in Mass Spectrometry*, *19*(17), 2371–2378. https://doi.org/10.1002/rcm.2069

Bowen, G. J., & Revenaugh, J. (2003). Interpolating the isotopic composition of modern meteoric precipitation: Isotopic composition of modern precipitation. *Water Resources Research*, *39*(10), 1299–1312. https://doi.org/10.1029/2003WR002086

Bowen, G. J., Wassenaar, L. I., & Hobson, K. A. (2005). Global application of stable hydrogen and oxygen isotopes to wildlife forensics. *Oecologia*, *143*(3), 337–348. https://doi.org/10.1007/s00442-004-1813-y

Chesson, L. A., Podlesak, D. W., Cerling, T. E., & Ehleringer, J. R. (2009). Evaluating uncertainty in the calculation of non-exchangeable hydrogen fractions within organic materials. *Rapid Communications in Mass Spectrometry*, *23*(9), 1275–1280.

Chipera, S. J., & Bish, D. L. (2001). Baseline Studies of the Clay Minerals Society Source Clays: Powder X-Ray Diffraction Analyses. *Clays and Clay Minerals*, *49*(5), 398–409.

Chuvilin, E. M., Ershov, E. D., & Smirnova, O. G. (1998). Ionic migration in frozen soils and ice. *Proceedings of the 7th International Permafrost Conference, Yellowknife, NWT, 23–27 June 1998*, 167–171.

Dansgaard, W. (1964). Stable isotopes in precipitation. *Tellus*, *16*(4), 436–468.

DIN ISO 11277. (2002). *Bodenbeschaffenheit—Bestimmung der Partikelgrößenverteilung in Mineralböden. Verfahren mittels Siebung und Sedimentation*. Beuth Verlag. https://doi.org/10.31030/9283499

Dogan, A. U., Dogan, M., Onal, M., Sarikaya, Y., Aburub, A., & Wurster, D. E. (2006). Baseline studies of the Clay Minerals Society source clays: Specific surface area by the Brunauer Emmett Teller (BET) method. *Clays and Clay Minerals*, *54*(1), 62–66. https://doi.org/10.1346/CCMN.2006.0540108

Dogan, M., Dogan, A. U., Yesilyurt, F. I., Alaygut, D., Buckner, I., & Wurster, D. E. (2007). Baseline studies of the Clay Minerals Society special clays: Specific surface area by the Brunauer Emmett Teller (BET) method. *Clays and Clay Minerals*, *55*(5), 534–541. https://doi.org/10.1346/CCMN.2007.0550508

Dultz, S., Riebe, B., & Bunnenberg, C. (2005). Temperature effects on iodine adsorption on organo-clay minerals: II. Structural effects. *Applied Clay Science*, *28*(1), 17–30. https://doi.org/10.1016/j.clay.2004.01.005

Epstein, S., Yapp, C. J., & Hall, J. H. (1976). The determination of the D/H ratio of non-exchangeable hydrogen in cellulose extracted from aquatic and land plants. *Earth and Planetary Science Letters*, *30*(2), 241–251. https://doi.org/10.1016/0012-821X(76)90251-X

Eusterhues, K., Rumpel, C., Kleber, M., & Kögel-Knabner, I. (2003). Stabilisation of soil organic matter by interactions with minerals as revealed by mineral dissolution and oxidative degradation. *Organic Geochemistry*, *34*(12), 1591–1600. https://doi.org/10.1016/j.orggeochem.2003.08.007

Fagan, R. (2001). *Oxygen-and hydrogen-isotope study of hydroxyl-group behavior in standard smectite and kaolinite* [PhD Thesis]. Faculty of Graduate Studies, University of Western Ontario.

Faghihi, V., Meijer, H. a. J., & Gröning, M. (2015). A thoroughly validated spreadsheet for calculating isotopic abundances (^{2}H, ^{17}O, ^{18}O) for mixtures of waters with different isotopic compositions. *Rapid Communications in Mass Spectrometry: RCM*, *29*(15), 1351–1356. https://doi.org/10.1002/rcm.7232

FAO. (2009). *Harmonized World Soil Database: Topsoil CEC (clay), Version 1.1*. https://data.apps.fao.org/map/catalog/srv/eng/catalog.search#/metadata/2427214a-42dc-4862-b58a-00b73cbc7a6f

Faucher, J. A., & Thomas, H. C. (1955). Exchange between Heavy Water and Clay Minerals. *The Journal of Physical Chemistry*, *59*(2), 189–191. https://doi.org/10.1021/j150524a026

Feng, X., Krishnamurthy, R. V., & Epstein, S. (1993). Determination of D/H ratios of nonexchangeable hydrogen in cellulose: A method based on the cellulose-water exchange reaction. *Geochimica et Cosmochimica Acta*, *57*(17), 4249–4256. https://doi.org/10.1016/0016-7037(93)90320-V

Fick, S. E., & Hijmans, R. J. (2017). WorldClim 2: New 1-km spatial resolution climate surfaces for global land areas. *International Journal of Climatology*, *37*(12), 4302–4315. https://doi.org/10.1002/joc.5086

Filot, M. S., Leuenberger, M., Pazdur, A., & Boettger, T. (2006). Rapid online equilibration method to determine the D/H ratios of non-exchangeable hydrogen in cellulose. *Rapid Communications in Mass Spectrometry*, *20*(22), 3337–3344. https://doi.org/10.1002/rcm.2743

Folkoff, M. E., & Meentemeyer, V. (1985). Climatic control of the assemblages of secondary clay minerals in the A-horizon of United States soils. *Earth Surface Processes and Landforms*, *10*(6), 621–633. https://doi.org/10.1002/esp.3290100609

Gehre, M., Renpenning, J., Geilmann, H., Qi, H., Coplen, T. B., Kümmel, S., Ivdra, N., Brand, W. A., & Schimmelmann, A. (2017). Optimization of on-line hydrogen stable isotope ratio measurements of halogen- and sulfur-bearing organic compounds using elemental analyzer–chromium/high-temperature conversion isotope ratio mass spectrometry (EA-Cr/HTC-IRMS). *Rapid Communications in Mass Spectrometry*, *31*(6), 475–484. https://doi.org/10.1002/rcm.7810

Gehre, M., Renpenning, J., Gilevska, T., Qi, H., Coplen, T. B., Meijer, H. A., Brand, W. A., & Schimmelmann, A. (2015). On-line hydrogen-isotope measurements of organic samples using elemental chromium: An extension for high temperature elemental-analyzer techniques. *Analytical Chemistry*, *87*(10), 5198–5205.

Gilg, H. A., Girard, J.-P., & Sheppard, S. M. F. (2004). Conventional and Less Conventional Techniques for Hydrogen and Oxygen Isotope Analysis of Clays, Associated Minerals and Pore Waters in Sediments and Soils. In *Handbook of Stable Isotope Analytical Techniques. Volume 1* (pp. 38–61). Elsevier. https://doi.org/10.1016/B978-044451114-0/50004-1

Gilg, H. A., & Sheppard, S. M. F. (1996). Hydrogen isotope fractionation between kaolinite and water revisited. *Geochimica et Cosmochimica Acta*, *60*(3), 529–533. https://doi.org/10.1016/0016-7037(95)00417-3

Grinsted, M. J., & Wilson, A. T. (1979). Hydrogen isotopic chemistry of cellulose and other organic material of geochemical interest. *New Zealand Journal of Science*, *22*(3), 281–287.

Grömping, U. (2007). Relative importance for linear regression in R: The package relaimpo. *Journal of Statistical Software*, *17*, 1–27.

Guggenheim, S., & Van Groos, A. K. (2001). Baseline studies of the clay minerals society source clays: Thermal analysis. *Clays and Clay Minerals*, *49*(5), 433–443.

Guidotti, S., Jansen, H. G., Aerts-Bijma, A. T., Verstappen-Dumoulin, B. M. a. A., van Dijk, G., & Meijer, H. a. J. (2013). Doubly Labelled Water analysis: Preparation, memory correction, calibration and quality assurance for delta δ^2H and $\delta^{18}O$ measurements over four orders of magnitudes. *Rapid Communications in Mass Spectrometry*, *27*(9), 1055–1066. https://doi.org/10.1002/rcm.6540

Hobson, K. A., Atwell, L., & Wassenaar, L. I. (1999). Influence of drinking water and diet on the stable-hydrogen isotope ratios of animal tissues. *Proceedings of the National Academy of Sciences*, *96*(14), 8003–8006.

Hobson, K. A., Soto, D. X., Paulson, D. R., Wassenaar, L. I., & Matthews, J. H. (2012). A dragonfly (δ^2H) isoscape for North America: A new tool for determining natal origins of migratory

aquatic emergent insects. *Methods in Ecology and Evolution*, *3*(4), 766–772. https://doi.org/10.1111/j.2041-210X.2012.00202.x

Hower, J., & Mowatt, T. C. (1966). The mineralogy of illites and mixed-layer illite/montmorillonites. *American Mineralogist*, *51*(5–6), 825–854. https://doi.org/10.1346/CCMN.1999.0470617

Hsieh, J. C., & Yapp, C. J. (1999). Hydrogen-isotope exchange in halloysite: Insight from room-temperature experiments. *Clays and Clay Minerals*, *47*(6), 811–816.

Hyeong, K., & Capuano, R. M. (2000). The effect of organic matter and the H_2O_2 organic-matter-removal method on the δD of smectite-rich samples. *Geochimica et Cosmochimica Acta*, *64*(22), 3829–3837.

IAEA/WMO. (2022). *Global Network of Isotopes in Precipitation. The GNIP Database*. https://nucleus.iaea.org/wiser

Ito, A., & Wagai, R. (2017). Global distribution of clay-size minerals on land surface for biogeochemical and climatological studies. *Scientific Data*, *4*, sdata2017103. https://doi.org/10.1038/sdata.2017.103

IUSS Working Group WRB. (2015). *World Reference Base for Soil Resources 2014, update 2015, International soil classification system for naming soils and creating legends for soil maps. World Soil Resources Reports No. 106*. Food and Agriculture Organization of the United Nations (FAO).

Jouzel, J., Russell, G. L., Suozzo, R. J., Koster, R. D., White, J. W. C., & Broecker, W. S. (1987). Simulations of the HDO and H_2 ^{18}O atmospheric cycles using the NASA GISS general circulation model: The seasonal cycle for present-day conditions. *Journal of Geophysical Research: Atmospheres*, *92*(D12), 14739–14760. https://doi.org/10.1029/JD092iD12p14739

Junhui Li, Xiaohuan Lu, Kun Cheng, & Wenxin Liu. (2021). *StepReg: Stepwise regression analysis* [Manual]. https://CRAN.R-project.org/package=StepReg

Kaiser, K., Eusterhues, K., Rumpel, C., Guggenberger, G., & Kögel-Knabner, I. (2002). Stabilization of organic matter by soil minerals—Investigations of density and particle-size fractions from two acid forest soils. *Journal of Plant Nutrition and Soil Science*, *165*(4), 451–459. https://doi.org/10.1002/1522-2624(200208)165:4<451::AID-JPLN451>3.0.CO;2-B

Kanik, N. J., Longstaffe, F. J., Kuligiewicz, A., & Derkowski, A. (2022). Systematics of smectite hydrogen-isotope composition: Structural hydrogen versus adsorbed water. *Applied Clay Science*, *216*, 106338. https://doi.org/10.1016/j.clay.2021.106338

Kelly, J. F., Bridge, E. S., Fudickar, A. M., & Wassenaar, L. I. (2009). A test of comparative equilibration for determining non-exchangeable stable hydrogen isotope values in complex organic materials. *Rapid Communications in Mass Spectrometry*, *23*(15), 2316–2320. https://doi.org/10.1002/rcm.4150

Kogel, J. E., & Lewis, S. A. (2001). Baseline studies of the clay minerals society source clays: Chemical analysis by inductively coupled plasma-mass spectroscopy (ICP-MS). *Clays and Clay Minerals*, *49*(5), 387–392.

Lawrence, J. R., & Taylor, H. P. (1971). Deuterium and oxygen-18 correlation: Clay minerals and hydroxides in Quaternary soils compared to meteoric waters. *Geochimica et Cosmochimica Acta*, *35*(10), 993–1003. https://doi.org/10.1016/0016-7037(71)90017-2

Lawrence, J. R., & Taylor, H. P. (1972). Hydrogen and oxygen isotope systematics in weathering profiles. *Geochimica et Cosmochimica Acta*, *36*(12), 1377–1393. https://doi.org/10.1016/0016-7037(72)90068-3

Leifeld, J., & Kögel-Knabner, I. (2001). Organic carbon and nitrogen in fine soil fractions after treatment with hydrogen peroxide. *Soil Biology and Biochemistry*, *33*(15), 2155–2158. https://doi.org/10.1016/S0038-0717(01)00127-4

Lessovaia, S. N., Desyatkin, R. V., Okoneshnikova, M. V., & Ivanova, A. Z. (2021). Clay mineralogy of Cryosols formed in an ultra-continental climate of Siberia. *IOP Conference Series: Earth and Environmental Science*, *862*(1), 012070. https://doi.org/10.1088/1755-1315/862/1/012070

Liu, K.-K., & Epstein, S. (1984). The hydrogen isotope fractionation between kaolinite and water. *Chemical Geology*, *46*(4), 335–350. https://doi.org/10.1016/0009-2541(84)90176-1

Maher, K. (2010). The dependence of chemical weathering rates on fluid residence time. *Earth and Planetary Science Letters*, *294*(1), 101–110. https://doi.org/10.1016/j.epsl.2010.03.010

Maher, K. (2011). The role of fluid residence time and topographic scales in determining chemical fluxes from landscapes. *Earth and Planetary Science Letters*, *312*(1), 48–58. https://doi.org/10.1016/j.epsl.2011.09.040

Marumo, K., Longstaffe, F. J., & Matsubaya, O. (1995). Stable isotope geochemistry of clay minerals from fossil and active hydrothermal systems, southwestern Hokkaido, Japan. *Geochimica et Cosmochimica Acta*, *59*(12), 2545–2559. https://doi.org/10.1016/0016-7037(95)00149-2

Méheut, M., Lazzeri, M., Balan, E., & Mauri, F. (2010). First-principles calculation of H/D isotopic fractionation between hydrous minerals and water. *Geochimica et Cosmochimica Acta*, *74*(14), 3874–3882. https://doi.org/10.1016/j.gca.2010.04.020

Mehra, O. P., & Jackson, M. L. (1958). Iron Oxide Removal from Soils and Clays by a Dithionite-Citrate System Buffered with Sodium Bicarbonate. *Clays and Clay Minerals*, *7*(1), 317–327. https://doi.org/10.1346/CCMN.1958.0070122

Meier, L. P., & Kahr, G. (1999). Determination of the Cation Exchange Capacity (CEC) of Clay Minerals Using the Complexes of Copper(II) Ion with Triethylenetetramine and Tetraethylenepentamine. *Clays and Clay Minerals*, *47*(3), 386–388. https://doi.org/10.1346/CCMN.1999.0470315

Menegatti, A. P., Frueh-Green, G. L., & Stille, P. (1999). Removal of organic matter by disodium peroxodisulphate: Effects on mineral structure, chemical composition and physicochemical properties of some clay minerals. *Clay Minerals*, *34*(2), 247–257.

Mermut, A. R., Angel, & Cano, F. (2001). Baseline studies of the clay minerals society source clays: Chemical analyses of major elements. *Clays and Clay Minerals*, 381–386.

Mikutta, R., Kleber, M., Kaiser, K., & Jahn, R. (2005). Review: Organic Matter Removal from Soils using Hydrogen Peroxide, Sodium Hypochlorite, and Disodium Peroxodisulfate. *Soil Science Society of America Journal*, *69*(1), 120–135. https://doi.org/10.2136/sssaj2005.0120

Nair, S., Geilmann, H., Coplen, T. B., Qi, H., Gehre, M., Schimmelmann, A., & Brand, W. A. (2015). Isotopic disproportionation during hydrogen isotopic analysis of nitrogen-bearing organic compounds. *Rapid Communications in Mass Spectrometry*, *29*(9), 878–884. https://doi.org/10.1002/rcm.7174

O'Neil, J. R., & Kharaka, Y. K. (1976). Hydrogen and oxygen isotope exchange reactions between clay minerals and water. *Geochimica et Cosmochimica Acta*, *40*(2), 241–246. https://doi.org/10.1016/0016-7037(76)90181-2

Paul, D., Skrzypek, G., & Fórizs, I. (2007). Normalization of measured stable isotopic compositions to isotope reference scales – a review. *Rapid Communications in Mass Spectrometry*, *21*(18), 3006–3014. https://doi.org/10.1002/rcm.3185

Qi, H., & Coplen, T. B. (2011). Investigation of preparation techniques for δ^2H analysis of keratin materials and a proposed analytical protocol. *Rapid Communications in Mass Spectrometry*, *25*(15), 2209–2222. https://doi.org/10.1002/rcm.5095

Qi, H., Coplen, T. B., Gehre, M., Vennemann, T. W., Brand, W. A., Geilmann, H., Olack, G., Bindeman, I. N., Palandri, J., Huang, L., & Longstaffe, F. J. (2017). New biotite and muscovite isotopic reference materials, USGS57 and USGS58, for δ^2H measurements–A replacement for NBS 30. *Chemical Geology*, *467*, 89–99. https://doi.org/10.1016/j.chemgeo.2017.07.027

Qi, H., Gröning, M., Coplen, T. B., Buck, B., Mroczkowski, S. J., Brand, W. A., Geilmann, H., & Gehre, M. (2010). Novel silver-tubing method for quantitative introduction of water into high-temperature conversion systems for stable hydrogen and oxygen isotopic measurements. *Rapid Communications in Mass Spectrometry*, *24*(13), 1821–1827. https://doi.org/10.1002/rcm.4559

R Core Team. (2022). *R: A language and environment for statistical computing* [Manual]. https://www.R-project.org/

Renpenning, J., Kümmel, S., Hitzfeld, K. L., Schimmelmann, A., & Gehre, M. (2015). Compound-Specific Hydrogen Isotope Analysis of Heteroatom-Bearing Compounds via Gas Chromatography–Chromium-Based High-Temperature Conversion (Cr/HTC)–Isotope Ratio Mass Spectrometry. *Analytical Chemistry*, *87*(18), 9443–9450. https://doi.org/10.1021/acs.analchem.5b02475

Renpenning, J., Schimmelmann, A., & Gehre, M. (2017). Compound-specific hydrogen isotope analysis of fluorine-, chlorine-, bromine- and iodine-bearing organics using gas chromatography–chromium-based high-temperature conversion (Cr/HTC) isotope ratio mass spectrometry. *Rapid Communications in Mass Spectrometry*, *31*(13), 1095–1102. https://doi.org/10.1002/rcm.7872

Revelle, W. (2021). *psych: Procedures for psychological, psychometric, and personality research* [Manual]. https://CRAN.R-project.org/package=psych

Rice, J. A., & MacCarthy, P. (1991). Statistical evaluation of the elemental composition of humic substances. *Organic Geochemistry*, *17*(5), 635–648. https://doi.org/10.1016/0146-6380(91)90006-6

Richards, P. L., & Kump, L. R. (2003). Soil pore-water distributions and the temperature feedback of weathering in soils. *Geochimica et Cosmochimica Acta*, *67*(20), 3803–3815. https://doi.org/10.1016/S0016-7037(03)00270-9

Ruppenthal, M. (2014). *Stable isotope ratios of nonexchangeable hydrogen in bulk organic matter as novel biogeochemical tracer* [PhD Thesis]. University of Tübingen.

Ruppenthal, M., Oelmann, Y., del Valle, H. F., & Wilcke, W. (2015). Stable isotope ratios of nonexchangeable hydrogen in organic matter of soils and plants along a 2100-km climosequence in Argentina: New insights into soil organic matter sources and transformations? *Geochimica et Cosmochimica Acta*, *152*, 54–71. https://doi.org/10.1016/j.gca.2014.12.024

Ruppenthal, M., Oelmann, Y., & Wilcke, W. (2010). Isotope ratios of nonexchangeable hydrogen in soils from different climate zones. *Geoderma*, *155*(3–4), 231–241. https://doi.org/10.1016/j.geoderma.2009.12.005

Ruppenthal, M., Oelmann, Y., & Wilcke, W. (2013). Optimized Demineralization Technique for the Measurement of Stable Isotope Ratios of Nonexchangeable H in Soil Organic Matter. *Environmental Science & Technology*, *47*(2), 949–957. https://doi.org/10.1021/es303448g

Sauer, P. E., Schimmelmann, A., Sessions, A. L., & Topalov, K. (2009). Simplified batch equilibration for D/H determination of non-exchangeable hydrogen in solid organic material. *Rapid Communications in Mass Spectrometry*, *23*(7), 949–956. https://doi.org/10.1002/rcm.3954

Savin, S. M., & Epstein, S. (1970a). The oxygen and hydrogen isotope geochemistry of clay minerals. *Geochimica et Cosmochimica Acta*, *34*(1), 25–42. https://doi.org/10.1016/0016-7037(70)90149-3

Savin, S. M., & Epstein, S. (1970b). The oyxgen and hydrogen isotope geochemistry of ocean sediments and shales. *Geochimica et Cosmochimica Acta*, *34*(1), 43–63. https://doi.org/10.1016/0016-7037(70)90150-X

Schaub, M., Seth, B., & Alewell, C. (2009). Determination of $\delta^{18}O$ in soils: Measuring conditions and a potential application. *Rapid Communications in Mass Spectrometry*, *23*(2), 313–318. https://doi.org/10.1002/rcm.3871

Schimmelmann, A. (1991). Determination of the concentration and stable isotopic composition of nonexchangeable hydrogen in organic matter. *Analytical Chemistry*, *63*(21), 2456–2459. https://doi.org/10.1021/ac00021a013

Schimmelmann, A., Lewan, M. D., & Wintsch, R. P. (1999). D/H isotope ratios of kerogen, bitumen, oil, and water in hydrous pyrolysis of source rocks containing kerogen types I, II, IIS, and III. *Geochimica et Cosmochimica Acta*, *63*(22), 3751–3766. https://doi.org/10.1016/S0016-7037(99)00221-5

Schimmelmann, A., Qi, H., Dunn, P. J. H., Camin, F., Bontempo, L., Potočnik, D., Ogrinc, N., Kelly, S., Carter, J. F., Abrahim, A., Reid, L. T., & Coplen, T. B. (2020). Food Matrix Reference Materials for Hydrogen, Carbon, Nitrogen, Oxygen, and Sulfur Stable Isotope-Ratio Measurements: Collagens, Flours, Honeys, and Vegetable Oils. *Journal of Agricultural and Food Chemistry*, *68*(39), 10852–10864. https://doi.org/10.1021/acs.jafc.0c02610

Schimmelmann, A., Sessions, A. L., & Mastalerz, M. (2006). Hydrogen isotopic (D/H) composition of organic matter during diagenesis and thermal maturation. *Annu. Rev. Earth Planet. Sci.*, *34*, 501–533.

Sessions, A. L., & Hayes, J. M. (2005). Calculation of hydrogen isotopic fractionations in biogeochemical systems. *Geochimica et Cosmochimica Acta*, *69*(3), 593–597. https://doi.org/10.1016/j.gca.2004.08.005

Soto, D. X., Koehler, G., Wassenaar, L. I., & Hobson, K. A. (2017). Re-evaluation of the hydrogen stable isotopic composition of keratin calibration standards for wildlife and forensic science applications. *Rapid Communications in Mass Spectrometry*, *31*(14), 1193–1203. https://doi.org/10.1002/rcm.7893

Sprenger, M., Leistert, H., Gimbel, K., & Weiler, M. (2016). Illuminating hydrological processes at the soil-vegetation-atmosphere interface with water stable isotopes. *Reviews of Geophysics*, *54*(3), 674–704. https://doi.org/10.1002/2015RG000515

Stanjek, H., & Künkel, D. (2016). CEC determination with Cu-triethylenetetramine: Recommendations for improving reproducibility and accuracy. *Clay Minerals*, *51*(1), 1–17. https://doi.org/10.1180/claymin.2016.051.1.01

Steudel, A. (2008). *Selection strategy and modification of layer silicates for technical applications* [Univ.-Verlag Karlsruhe]. https://doi.org/10.5445/IR/1000010008

Steudel, A., Weidler, P. G., Schuhmann, R., & Emmerich, K. (2009). Cation exchange reactions of vermiculite with Cu-triethylenetetramine as affected by mechanical and chemical pretreatment. *Clays and Clay Minerals*, *57*(4), 486–493. Scopus. https://doi.org/10.1346/CCMN.2009.0570409

Terzer-Wassmuth, S., Wassenaar, L. I., Welker, J. M., & Araguás-Araguás, L. J. (2021). Improved high-resolution global and regionalized isoscapes of $\delta^{18}O$, $\delta^{2}H$ and d-excess in precipitation. *Hydrological Processes*, *35*(6), e14254. https://doi.org/10.1002/hyp.14254

VanDeVelde, J. H., & Bowen, G. J. (2013). Effects of chemical pretreatments on the hydrogen isotope composition of 2:1 clay minerals: Clay mineral isotope treatment effects. *Rapid Communications in Mass Spectrometry*, *27*(10), 1143–1148. https://doi.org/10.1002/rcm.6554

Vitali, F., Longstaffe, F. J., McCarthy, P. J., Plint, A. G., & Caldwell, W. G. E. (2002). Stable isotopic investigation of clay minerals and pedogenesis in an interfluve paleosol from the Cenomanian Dunvegan Formation, NE British Columbia, Canada. *Chemical Geology*, *192*(3–4), 269–287. https://doi.org/10.1016/S0009-2541(02)00225-5

von Lützow, M., Kögel-Knabner, I., Ekschmitt, K., Flessa, H., Guggenberger, G., Matzner, E., & Marschner, B. (2007). SOM fractionation methods: Relevance to functional pools and to stabilization mechanisms. *Soil Biology and Biochemistry*, *39*(9), 2183–2207. https://doi.org/10.1016/j.soilbio.2007.03.007

Wassenaar, L. I., & Hobson, K. A. (1998). Natal origins of migratory monarch butterflies at wintering colonies in Mexico: New isotopic evidence. *Proceedings of the National Academy of Sciences*, *95*(26), 15436–15439.

Wassenaar, L. I., & Hobson, K. A. (2000). Improved Method for Determining the Stable-Hydrogen Isotopic Composition (δD) of Complex Organic Materials of Environmental Interest. *Environmental Science & Technology*, *34*(11), 2354–2360. https://doi.org/10.1021/es990804i

Wassenaar, L. I., & Hobson, K. A. (2003). Comparative equilibration and online technique for determination of non-exchangeable hydrogen of keratins for use in animal migration studies. *Isotopes in Environmental and Health Studies*, *39*(3), 211–217. https://doi.org/10.1080/1025601031000096781

Webster, R. (2001). Statistics to support soil research and their presentation: Statistics to support soil research. *European Journal of Soil Science*, *52*(2), 331–340. https://doi.org/10.1046/j.1365-2389.2001.00383.x

Werner, S. J., Hobson, K. A., Wilgenburg, S. L. V., & Fischer, J. W. (2016). Multi-isotopic ($\delta^{2}H$, $\delta^{13}C$, $\delta^{15}N$) tracing of molt origin for red-winged blackbirds associated with agro-ecosystems. *PLOS ONE*, *11*(11), e0165996. https://doi.org/10.1371/journal.pone.0165996

West, J. B., Bowen, G. J., Dawson, T. E., & Tu, K. P. (Eds.). (2010). *Isoscapes*. Springer Netherlands. https://doi.org/10.1007/978-90-481-3354-3

Wickham, H., Averick, M., Bryan, J., Chang, W., McGowan, L. D., François, R., Grolemund, G., Hayes, A., Henry, L., Hester, J., Kuhn, M., Pedersen, T. L., Miller, E., Bache, S. M., Müller, K., Ooms, J., Robinson, D., Seidel, D. P., Spinu, V., … Yutani, H. (2019). Welcome to the tidyverse. *Journal of Open Source Software*, *4*(43), 1686. https://doi.org/10.21105/joss.01686

2 Non-exchangeable stable hydrogen isotope ratios in clay minerals and soil clay fractions: A method test

Stefan Merseburger [1], Arnim Kessler [2], Yvonne Oelmann [2], Wolfgang Wilcke [1*]

[1] Institute of Geography and Geoecology, Karlsruhe Institute of Technology (KIT), Karlsruhe, Germany
[2] Geoecology, University of Tübingen, Tübingen, Germany

Chapter 2 is published in the European Journal of Soil Science, 2022; 73(4), e13289, https://doi.org/10.1111/ejss.13289.

Abstract

Stable hydrogen isotope ratios (δ^2H values) in structural hydroxyl groups of pedogenic clay minerals are inherited from the surrounding water at the time of their formation. Only non-exchangeable H preserves the environmental forensic and paleoclimate information (δ^2H_n value). To measure δ^2H_n values in structural H of clay minerals and soil clay fractions, we adapted a steam equilibration method by accounting for high hygroscopicity. Our δ^2H_n values for USGS57 biotite (-95.3 ± SD 0.9‰) and USGS58 muscovite (-30.7 ± 1.4‰) differed slightly but significantly from the reported δ^2H values (-91.5 ± 2.4‰ and -28.4 ± 1.6‰), because the minerals contained 1.1–4.4% of exchangeable H. The low SD of replicate measurements (n = 3) confirmed a high precision. The clay separation method including destruction of Fe oxides, carbonates and soil organic matter, and dispersion did not significantly change the δ^2H_n values of five different clay minerals. However, we were unable to remove all organic matter from the soil clay fractions resulting in an estimated bias of 1‰ in two samples and 15‰ in the carbon-richest sample. Our results demonstrate that δ^2H_n values of structural H of clay minerals and soil clay fractions can be reliably measured without interference from atmospheric water and the method used to separate the soil clay fraction.

Highlights

- We tested steam equilibration to determine stable isotope ratios of structural H in clay.
- Gas-tight capsule sealing in Ar atmosphere was necessary to avoid remoistening.
- Our steam equilibration method showed a high accuracy and precision.
- The clay separation method did not change stable isotope ratios of structural H in clay.

2.1 Introduction

The stable isotope ratios of structural H in clay minerals and soil clay fractions, which cannot easily be exchanged with water (δ^2H_n values), reflect that of ambient soil water at the time of mineral formation (Gilg & Sheppard, 1996; Lawrence & Taylor, 1972; Savin & Epstein, 1970a). The δ^2H_n values of structural H in minerals might bear

geographic information similar to those of soil organic matter (SOM) (Ruppenthal et al., 2015). This is attributed to the fact that the H-isotopic composition of soil water is related to that of local precipitation and is influenced by evapotranspiration in the soil-plant system, both of which vary with location (Bowen, 2021; Sprenger et al., 2016). Moreover, clay minerals could serve as paleoclimate indicators, because of the partly high geological age. Furthermore, clay minerals are more frequent than the authigenic carbonate minerals that are currently the most commonly used paleoclimate indicators in soils (Cerling, 1984; VanDeVelde & Bowen, 2013).

To reliably determine δ^2H_n values of structural H in clay minerals requires the removal of the influence of exchangeable H. The exchangeable H in clay minerals comprises adsorbed and interlayer water, which quickly equilibrates with ambient water and thus does not bear a stable isotopic signal (Bauer & Vennemann, 2014). The current state-of-the-art methods for continuous flow isotope ratio mass spectrometry (CF-IRMS) remove the exchangeable H at varying temperatures ranging between 100 °C and 250 °C under vacuum (Bauer & Vennemann, 2014; Gilg et al., 2004; VanDeVelde & Bowen, 2013). Because different clay minerals require different temperatures for the removal of exchangeable H (Gilg et al., 2004), the currently applied methods cannot guarantee to always remove the entire exchangeable H pool in clay minerals or clay fractions. Another methodological challenge originates from the fact that after vacuum drying, a hygroscopic sample quickly attracts atmospheric water. This reintroduces exchangeable H, which must be prevented (Bauer & Vennemann, 2014; Bowen et al., 2005; VanDeVelde & Bowen, 2013).

An alternative to vacuum drying methods is provided by steam equilibration. A mass balance calculation after equilibrating the same clay mineral or fraction sample with several waters of different H-isotopic composition allows for the quantification of the contribution of exchangeable H to the total H pool and of the δ^2H_n values (Schimmelmann, 1991). However, such methods have up to now mostly been applied to determine nonexchangeable H in organic matter (Bowen et al., 2005; Epstein et al., 1976; Hobson et al., 2012; Kelly et al., 2009; Qi & Coplen, 2011; Ruppenthal et al., 2013, 2015; Schimmelmann, 1991; Schimmelmann et al., 2020; Soto et al., 2017; Wassenaar & Hobson, 2000, 2003) and bulk soil (Ruppenthal et al., 2010). The only study we know of in which steam equilibration was applied to a clay mineral is that of Hsieh and Yapp (1999), who determined the δ^2H_n value of halloysite. However, steam equilibration was

not further developed to a standard method for clay minerals (Gilg et al., 2004) or soil clay fractions.

To measure the δ^2H value of non-exchangeable H in soil clay fractions requires the separation of this fraction. To reach a full dispersion of the soil particles, Fe oxides, carbonates and SOM must be removed, using chemicals that might attack hydroxyl groups and thus have an effect on the δ^2H_n values of clay fractions. The removal of iron oxides by the dithionite-citrate-bicarbonate (DCB) method of Mehra and Jackson (1958) and carbonates by acetic acid was shown to not affect the δ^2H values of hydrous minerals (Gilg et al., 2004). The commonly used removal method for SOM by oxidation with hydrogen peroxide (H_2O_2) can change δ^2H values of some clay minerals, for example, montmorillonite (Hyeong & Capuano, 2000). Similarly, the alternative treatment with disodium peroxodisulphate ($Na_2O_8S_2$) showed a strong positive shift of the δ^2H values after the treatment of a montmorillonite sample (Menegatti et al., 1999). However, Hyeong and Capuano (2000) and Menegatti et al. (1999) did not test the possibility that the apparent change in δ^2H values after treatment with H_2O_2 or $Na_2O_8S_2$ was related to an unaccounted remoistening of the hygroscopic samples. We suggest that remoistening must be ruled out, before these two chemicals are defined as inappropriate for the purpose of determining δ^2H_n values of soil clay fractions. Moreover, both SOM oxidation methods may not remove organic matter exhaustively so that the measured δ^2H_n values of clay fractions need to be corrected for the δ^2H_n values of the remaining organic matter.

We hypothesised that (a) we can adapt a steam equilibration method, formerly applied to SOM and bulk soil (Ruppenthal et al., 2013) for clay minerals and clay fractions of soils and thereby strictly avoid remoistening of the hygroscopic samples via exchange with atmospheric water. Moreover, we hypothesised that (b) the traditional treatment of soil samples (with the extraction of iron oxides, the removal of carbonates and SOM and the separation of the clay fraction) does not alter the isotopic composition of the non-exchangeable H pool of clay minerals.

2.2 Material and methods

2.2.1 Samples

We used kaolinite (KGa-2), illite (IMt-2), Na-montmorillonite (SWy-3) and Mg-montmorillonite (SCa-3) distributed by the Clay Mineral Society (Chantilly, VA, USA) and a vermiculite (contributed by Stefan Dultz, Hannover, Germany) as clay mineral reference materials (Table 2.1). SCa-3 and IMt-2 were delivered as brittle rock chips with a macroscopically visible heterogeneity in grain sizes and colors. SWy-3 and KGa-2 were delivered as fine-grained powders. The standards are described by the baseline studies of the Clay Minerals Society Source Clays (Borden & Giese, 2001; Chipera & Bish, 2001; A. U. Dogan et al., 2006; M. Dogan et al., 2007; Guggenheim & Van Groos, 2001; Kogel & Lewis, 2001; Mermut et al., 2001) and by Hower and Mowatt (1966) for IMt-2. The vermiculite was characterised by Dultz et al. (2005), Bors et al. (1997) and Steudel et al. (2008; 2009).

Moreover, we used A horizons from the Osobita mountain in Slovakia (Oso, Lobe et al., 1998) and two sites near Karlsruhe (KA-1 and KA-2) in Germany (Table 2.2). We chose these samples because of their high concentrations of clay and SOM. High clay concentrations complicate the removal of SOM (Eusterhues et al., 2005; Kaiser et al., 2002; Mikutta et al., 2005; von Lützow et al., 2007) required for subsequent analysis of the isotope ratio of H in clay. Therefore, the treatment intensity and duration needed to be adjusted to constitute a worst-case test for methodological artefacts.

Table 2.1: Selected properties of the used clay minerals.

Sample	Origin	LOI* [Mass-%]	CEC [$mmol_c\ kg^{-1}$]	Principal cations	Surface area (N_2) [$m^2\ g^{-1}$]	Chemical composition
Kaolinite (KGa-2)	Georgia, USA	12.6	33		23.50	$(Ca_{tr}\ K_{tr})[Al_{3.66}Fe(III)_{.07}Mn_{tr}\ Mg_{tr}\ Ti_{.16}][Si_{4.00}]O_{10}(OH)_8$
Na-mont-morillonite (SWy-3)	Wyoming, USA	10.3 † 0.612 ‡	764	Na^+, Ca^{2+}	31.82	$(Ca_{.12}Na_{.32}K_{.05})[Al_{3.01}Fe(III)_{.41}Mn_{.01}Mg_{.54}Ti_{.02}][Si_{7.98}Al_{.02}]O_{20}(OH)_4$
Mg-mont-morillonite (SCa-3)	California, USA	21.2	~1170 § 1140 §§	Mg^{2+} §§	43.2 – 65.3	$(Mg_{.45}Ca_{.15}Na_{.26}K_{.01})[Al_{2.55}Fe(III)_{.12}Mn_{tr}\ Mg_{1.31}Ti_{.02}][Si_{7.81}Al_{.19}]O_{20}(OH)_4$
Illite (IMt-2)	Montana, USA	8.02	120–150 ¶	K^+ ¶	17.5 **	$(Mg_{.09}Ca_{.06}K_{1.37})[Al_{2.69}Fe(III)_{.76}Fe(II)_{.06}Mn_{tr}\ Mg_{.43}Ti_{.06}][Si_{6.77}Al_{1.23}]O_{20}(OH)_4$
Vermiculite	Russia	20.2 †	1620 ††	~85% Mg^{2+} 15% Ca^{2+} ††	36 **	$Me^+_{0.70}\ (Si_{3.04}\ Al^{3+}_{0.96})(Mg^{2+}_{2.65}Fe^{3+}_{0.31}Al^{3+}_{0.01})[O_{10}(OH)_2]$ ‡‡

Note: If not noted otherwise, the data are from the Clay Mineral Society (2021).

* Mass loss on ignition at 550 °C

† Steudel et al. (2009)

‡ Mermut et al. (2001)

§ Komadel (2003)

¶ Hower and Mowatt (1966)

** Dogan et al. (2007)

†† Bors et al. (1997)

‡‡ Grain size fraction < 2 µm (Steudel, 2008)

§§ Grim and Kulbicki (1961)

Abberivation: tr, traces.

Table 2.2: Soil type, selected topographical properties of the study sites and selected properties of the topsoil samples used for the clay separation method.

Sample	Soil type*	Substrate	Slope	Land use	Sampling depth [cm]	Latitude Longitude (WGS84)	Elevation [m above sea level]	Annual mean $\delta^2H_{modeled\ precipitation}$ ± SD [‰] †	pH in H_2O
KA-1	Gleyic Luvisol	Alluvial sediments	None	Agricutural	7-13	48.9311° 8.3567°	115	-58 ± 1	5.9
KA-2	Haplic Luvisol	Dilluvial sand dunes	None	Deciduous forest	0-12	48.9623° 8.357°	120	-58 ± 1	6.1
Oso	Dystric Cambisol ‡	Loess on limestone ‡	Upper slope ‡	Coniferous forest	0-10	49.26° 19.71°	1400	-76 ± 1	3.3

* IUSS Working Group WRB (2015)

† Data from OIPC version 3.1 (Bowen, 2021; Bowen & Revenaugh, 2003)

‡ Data from Lobe et al. (1998)

2.2.2 Clay separation

We sieved the three air-dried A-horizon samples to <2 mm. The clay standards IMt-2 and SCa-3 were gently ground to this size with a hand mortar. Depending on the estimated clay content, 5–20 g of air-dry sample were weighed in a 250-mL wide mouth centrifuge bottle (PPCC, Nalgene, Thermo Fisher Scientific, Waltham, MA, USA). To collect enough material for all analyses, we used 3–4 bottles per sample.

The following treatment steps and their sequence were chosen according to the recommendations of Gilg, Girard, and Sheppard (2004) and VanDeVelde and Bowen (2013). We treated the clay mineral standards and the topsoil samples during the clay separation process in the same manner, using the residual sediment of each step for the subsequent step, respectively (Figure 2.1).

To extract iron oxides, we used the DCB method of Mehra and Jackson (1958). We added 100 mL of 0.3 M Na-citrate and 15 mL of 1 M $NaHCO_3$ (both Carl Roth, Karlsruhe, Germany) solutions to the sample and the bottle was shaken for 1 h. Then, we added ~7 g Na-dithionite (Supelco, Merck, Darmstadt, Germany) to each beaker, while stirring at 60 °C in a water bath under a fume hood, until the soil sediment lost the yellowish/ brownish colour. After centrifugation (Heraeus Multifuge X3R with rotor TX-1000, Thermo Fisher Scientific) at a relative centrifugal force of 709 *g* for 5 – 60 min, we decanted the transparent supernatant into a separate beaker and added 100 mL of 0.3 M Na-citrate solution. This step was repeated once and the extracts were combined and made up to 1 L for Fe analysis with an atomic absorption spectrometer (Perkin-Elmer AAS 3100, Waltham, USA). If not noted otherwise, all chemicals used in this study were *pro analysi* quality, and the water was deionised.

Afterwards, we washed the samples three times by shaking the solution with 1 M NaCl solution (Carl Roth) for 1 h on an overhead shaker, centrifuged them for 10–30 min at 4122 *g* and decanted them. A fourth wash was done with 0.5 M NaCl solution.

To remove carbonates, soluble sulphates and salts without dissolving clay minerals, we made up the remaining sediment to 100 mL with deionised water and added 25 mL Na-acetate acetic acid buffer (164 g Na-acetate [water free] + 120 g 100% acetic acid L^{-1} [both Carl Roth]) adjusted to pH 4.8 (Lagaly et al., 2013). If, after stirring sporadically for 2 h in a water bath with 50 °C, the pH was higher than 4.8, more buffer solution was added in 10-mL steps. After all samples had reached the pH value of 4.8, they were left to cool down to room temperature.

To remove organic matter, we added 30 mL of H_2O_2 (30%, Carl Roth). After stirring, we left the bottles overnight at room temperature. Following Hyeong and Capuano (2000), we used a water bath at 50 °C with occasional stirring of the samples. We added 20 mL of H_2O_2 after 2.5–3 h and another 20 mL per beaker after further 2.5–3 h. We used the maximum duration and amount of H_2O_2 required by our soil samples for the clay minerals. When samples started to spill over, we sprayed a small amount of octane-2-ol (pro synthesis, Sigma-Aldrich, St. Louis, MO, USA) into the foam. After washing once with 2 M NaCl solution, the whole H_2O_2 treatment was repeated.

In the following four-fold washing cycle with NaCl solution, we removed the supernatant with a peristaltic pump (ISMATEC MCP Process, Cole-Parmer, Vernon Hills, IL, USA with Tygon® LMT-55 hoses, ID: 8 mm,Tygon®, Saint-Gobain, La Défense, France) to avoid resuspension. We continued the washing of the samples with deionised water until all beakers had an electrical conductivity <400 µS cm^{-1} in the decantate (DIN ISO 11277, 2002). We filled all beakers with deionised water with a pH of ~7.5 (adjusted with NaOH) and shook them overhead for 18 h. Then, we separated the remaining sediments of all clay mineral and soil samples into grain-size fractions starting with wet sieving (63 µm) the sand fraction. The grain-size distribution was determined by pipet analysis according to DIN ISO 11277 (2002), except that we did not use a dispersing agent following the suggestions of Dietrich et al. (1998) and Müller (1964). For kaolinite, we had to add a few millilitres of 0.01 M NaOH (Titripur, Merck) into the suspension and shortly shake it manually to reach full dispersion. Manual shaking for 2 min and letting the sample settle 20 cm in 2-L glass cylinders separated the clay fractions (< 2 µm). We calculated the sedimentation time following Stokes' law considering the current temperature (Gee & Or, 2002). Then, we transferred the supernatant into 10-L buckets with the peristaltic pump and filled the glass cylinder with more deionised water (pH ~ 7.5). We repeated the separation via sedimentation three times to separate >50 % of the clay (Müller, 1964), using always water with a pH of ~7.5. This comparatively fast separation leaves residues of the clay in the silt separates, which we named therefore '≤silt'.

We added 15–25 g $MgCl_2$ (solid, ≥98.5%, Carl Roth) to the bucket to start sedimentation. The next day, we pumped out the clear supernatant and transferred the residual into a 1-L centrifugation beaker (PP, 75007300, Thermo Fisher Scientific). We washed the samples first with 1 M NaCl solution and then once with deionised water.

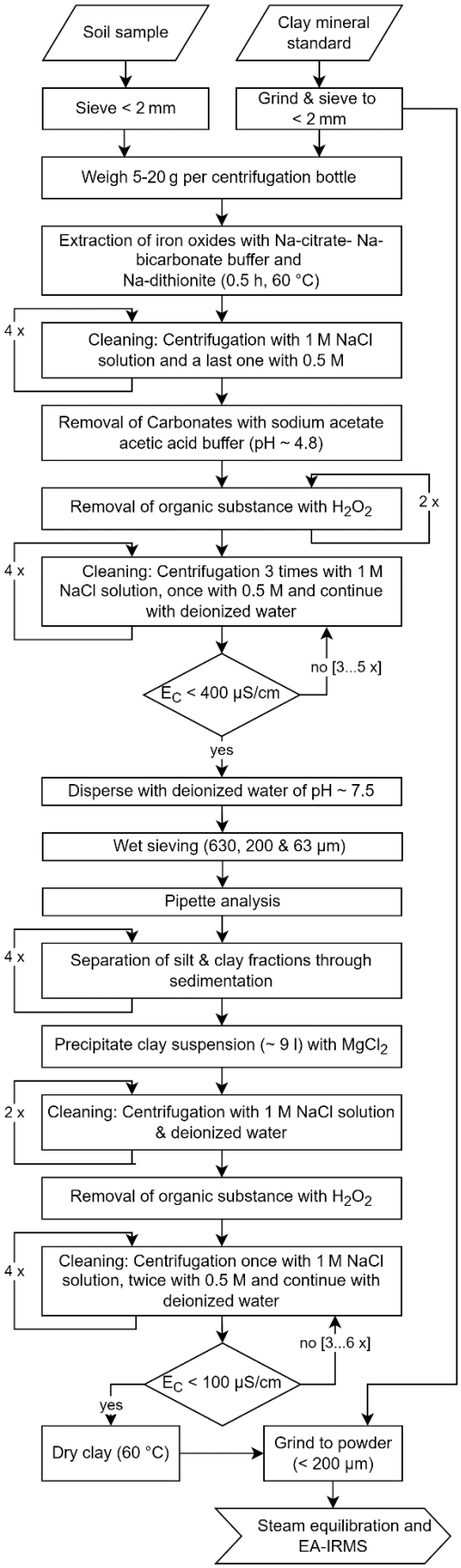

Figure 2.1: Workflow diagram of the clay separation method. EA-IRMS, Elemental Analyser Isotope Ratio Mass Spectrometry.

We treated the clay suspension of the clay minerals and the soils once again with H_2O_2 to further reduce their SOM concentrations. We made the 1-L centrifuge beaker up to 200 mL with deionised water and added 70 mL of 30% H_2O_2 and twice further 45 mL.

The final washing started with 1 M NaCl solution, followed by twice 0.5 M and deionised water until the conductivity of the supernatant was <100 µS cm^{-1}. Some samples needed centrifugation times of up to 4 h at 4122 *g*. The clay suspension was transferred into 250-mL PE wide-mouth beakers (Kautex Textron, Bonn, Germany) and dried at 60 °C. We manually pulverised the '≤silt' and clay fractions to <200 µm in an agate mortar.

The entire clay separation procedure took 10–12 weeks and up to 12 samples could be simultaneously processed (Figure 2.1). The procedure was conducted three times for all samples in separate batches to yield three independent replicates of all clay fractions. After the treatment, the interlayers of all swellable clay minerals should be mostly Na saturated.

2.2.3 Chemical sample properties

The carbon (C) concentrations were measured with an Elemental Analyser (EA) (Flash 2000 HTC, Thermo Fisher Scientific and EuroVector 3000, EuroVector, Pavia, Italy).

The pH was determined with a glass electrode (SenTix® 81 on pH 3310, WTW, Weilheim, Germany) in a deionised water suspension at a soil:water ratio of 1:2.5 (v/v).

The potential cation-exchange capacity (CEC_{pot}) was determined with the Cu(II)-triethylentetramine method (Ammann et al., 2005; Meier & Kahr, 1999). To avoid any pH dependency of the result (Stanjek & Künkel, 2016), we mixed 9.5 mL of the sample with 0.5 mL phosphate buffer (pH = 7.0; 1.814 g KH_2PO_4 [Carl Roth], 3.564 g Na_2HPO_4*$2H_2O$ [Emsure, Merck] in 0.5 L ultrapure water) and shook the suspension for 24 h (Steudel, Weidler, et al., 2009). The removal of the Cu complex by adsorption to the cation-exchange sites was photometrically determined at 577 nm. The potential CEC was referred to oven-dry soil (24 h at 105 °C).

2.2.4 Steam equilibration

We modified the equilibration device of Ruppenthal et al. (2013) (Figure 2.2). We replaced the liquid nitrogen trap with a diaphragm pump (VP 220, VWR, Radnor, PA,

USA) to remove water vapour, which could corrode the rotary vane pump (RZ 2.5, Vacuubrand, Wertheim, Germany), and we added a glove bag (Captair Pyramid, Erlab, Val de Reuil, France), which was filled with Ar to allow for a fast gas-tight sealing of the tin capsules without contact to ambient air.

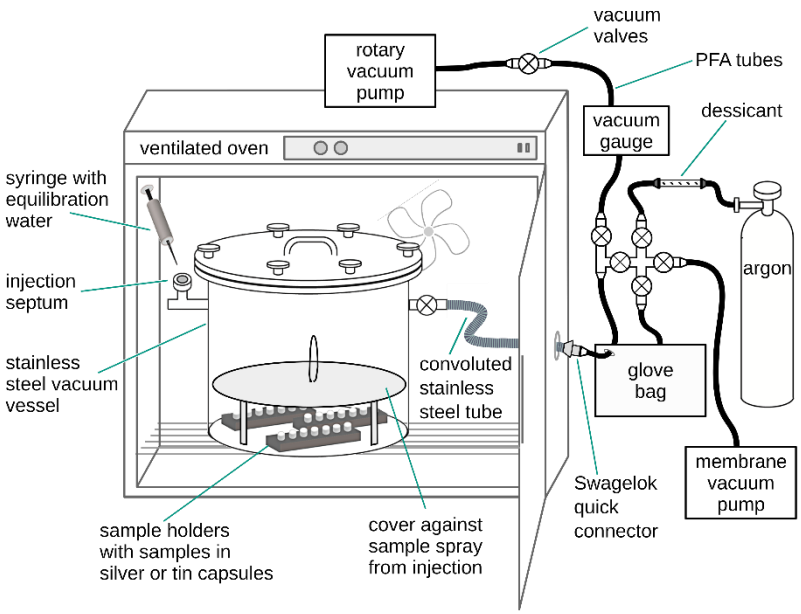

Figure 2.2: Sketch of the modified steam equilibration apparatus of Ruppenthal et al. (2013).

The optimum equilibration time was determined experimentally for two soil samples (the sample KA-2 was not used, Table 2.2) and the clay reference materials following a suggestion of Wassenaar and Hobson (2000). After evacuating the stainless steel vessel (~ 10 L; Rovak, Grumbach, Germany; with steel tubing, fittings and valves from Swagelok, Solon, OH, USA) for 2 h inside a fan-assisted heating oven at 120 °C, we injected 4 mL of equilibration water with a δ^2H value of 335‰ using a syringe (needle: Sterican® G26, B.Braun, Melsungen, Germany) through a high temperature septum (Trajan 041845, Victoria, Australia or Restek 27088, Bellefonte, PA, USA). After 0.25, 1, 4, 16 and 64 h, the vessel was reconnected to the vacuum line and evacuated for 1 h in the oven at 120 °C using the diaphragm pump during the first 15 min. Then, the samples were evacuated for another 2 h at room temperature to cool down, reaching a vacuum ≤1 Pa. Afterwards, we placed the vessel in the glove bag that we evacuated and flushed with Ar (purity grade 4.8) twice. To depressurize the vessel to ambient air pressure, we flooded the vessel with Ar at ~1.3 bar, dried with Sicapent (with indicator, Supelco,

Merck). While the Ar continuously flowed into the vessel, we opened the vessel and directly closed the capsules with a filed and extended concretor's nippler (plier No. 99 10 250, Knipex, Wuppertal, Germany) inside the vessel. This was done in a way that the tin of the capsules was not cut off but compressed to a gas-tight seal (Qi et al., 2010), applying the same force to all capsules. This procedure was necessary to avoid even the slightest contact of the sample with ambient air moisture, which is a prerequisite for the correct determination of the H concentrations and δ^2H values.

For further equilibrations, we chose an equilibration time of 16 h (Figure 2.3). We placed a maximum of 80 samples with an analyte mass of 1–2 mg, each, in the equilibration vessel, corresponding to a ratio of equilibration water-H to exchangeable sample-H >2000:1. We included triplicates of SCa-3 at the beginning and end of each equilibration batch to test for a potential shift in δ^2H values because of diffusing moisture during the sealing process of the samples at the end of the equilibration. For quality control, we included KGa-2 and blanks in triplicates.

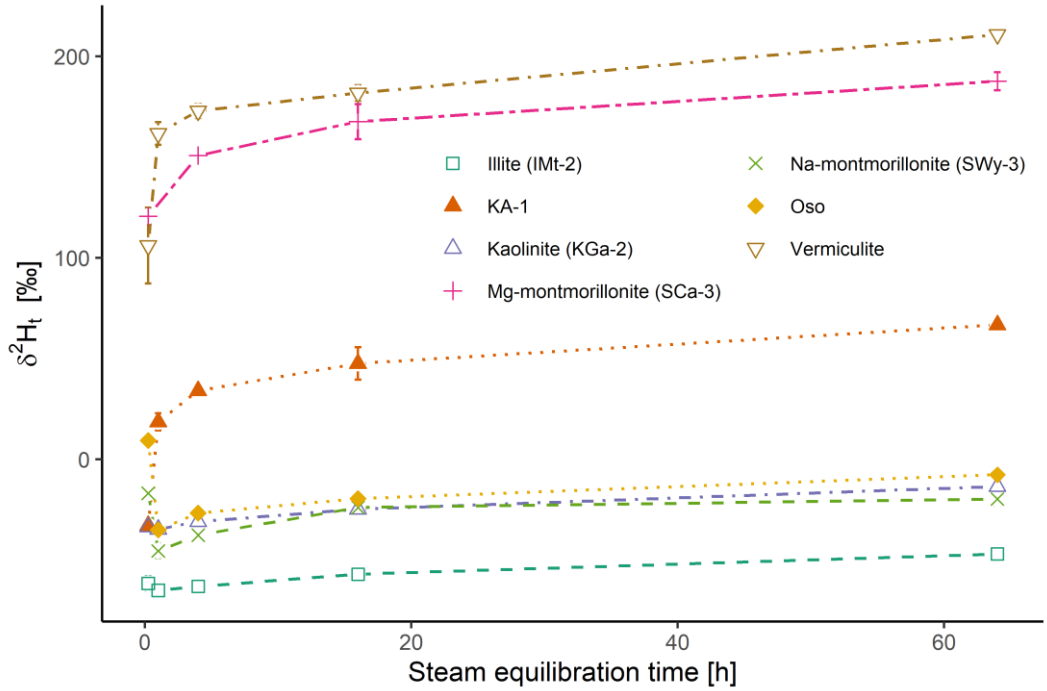

Figure 2.3: Relationship between steam equilibration time and δ^2H_t values of clay minerals and two clay separates (filled symbols) equilibrated with water with a δ^2H_W value of 335‰. Error bars show SD and might be smaller than the symbol size.

We used two to four waters with known δ^2H values (AWI-TD1: -266.4 ± 0.8‰, SD for n = 4 repeated measurements; laboratory water: -57.5 ± 0.8‰, n = 3; medium

deuterium-enriched water: 136.8 ± 0.6‰, n = 3; highly deuterium-enriched water: 334.6 ± 1.8‰, n = 4) to replace all exchangeable H in the sample with the H of the equilibration water and to calculate the contribution of exchangeable H and the δ^2H_n value. We produced the two deuterium-enriched waters by mixing ^2H_2O (HN81.4, Carl Roth) and ultrapure water (Faghihi et al., 2015). The treatment batches one and two were equilibrated with two isotopically different waters and the third batch with four waters.

2.2.5 Hydrogen isotope ratio measurement

The concentrations of H and δ^2H values were determined with an EA-Isotope Ratio Mass Spectrometer (IRMS) (Flash 2000 HTC-Delta V Advantage, Thermo Fisher Scientific). The samples were pyrolyzed in the chromium-filled Al2O3 reactor (Alsint 99.7, IVA, Meerbusch, Germany) at 1250 °C. We used the setup 'A1' described in Gehre et al. (2017), but adapted it for a smaller inner diameter (7 mm) of the inner tube (DEGUSSIT AL23, Friatec, Mannheim, Germany) with a 40 mm octagonal graphite crucible (G52109.001E, OEA Labs, Exeter, UK). In combination with 2 × 5 mm smooth wall tin capsules (IVA184990326, IVA), long sequences of up to 130–150 capsules were possible. We renewed the Cr granulate (1-3 mm, 99+%, ChemPur, Karlsruhe, Germany) after each sequence. The He carrier flow was 80 mL min-1 and the GC oven temperature was 90 °C. The integrated peak area of m/z 2 and 3, calibrated against benzoic acid (SA990747, IVA-Analysentechnik), was used to determine the H concentration. Tin capsules did not show a measurable H_2 blank. The correction factor for H3+ ions produced in the ion source was ascertained before and after each carousel run using the automated procedure of the IRMS software. For normalisation of the measured δ^2H values of each carousel run, we used three international laboratory standards (Vienna Standard Mean Ocean Water [VSMOW], SLAP and IAEA-604). Additionally, we used GISP to test for correct normalisation and to rule out an influence of the halogen release from the Cr-filled reactor on the H isotope measurements (Gehre et al., 2017). We purchased all international laboratory standards from USGS (Reston Stable Isotope Lab, Reston, VA, USA) packed in silver capsules (25 µL). We used polyethylene powder (PE; low density, ≤ 400 µm, 42607 Alfa Aesar, Ward Hill, MA, USA) as an internal laboratory standard for sample bracketing and IAEA-CH7 (IAEA, Vienna, Austria) for quality control at the beginning and end of each sequence. We did not notice drift or residual non-linearity of

the EA-IRMS system. We corrected small memory effects with the help of a pool-wise memory correction algorithm using one or two pools (Guidotti et al., 2013). Over the duration of the experimental period, the PE-powder was measured at a mean δ^2H value of -69.9 ± 1.4‰ (n = 490), GISP at -188.8 ± 1.9‰ (n = 72) and IAEA-CH7 at -100.3 ± 1.5‰ (n = 88). The values were indistinguishable from the certified or recommended values.

2.2.6 Data evaluation

We corrected isotope data and performed statistical analyses with R, version 4.1 (R Core Team, 2021; Wickham et al., 2019). We normalised all stable H isotope ratios to the VSMOW-SLAP scale (Paul et al., 2007) and expressed them in ‰ relative to VSMOW. When the δ^2H_w value was >0‰, we extended the scale with IAEA-604 to 799.9‰. All errors are given as one SD.

We assumed that there is no equilibrium fractionation between the exchangeable H and water-H of the vapour, that is, we assumed a fractionation factor $\alpha_{ex\text{-}w}$ of 1. The fractionation factor $\alpha_{ex\text{-}w}$ is a temperature-dependent material constant, which is difficult to determine. Therefore, it is common practice to use preliminary values for organic materials (Qi & Coplen, 2011; Ruppenthal et al., 2010, 2013, 2015; Sauer et al., 2009; Soto et al., 2017; Wassenaar & Hobson, 2000, 2003). While for some clay minerals, several fractionation factors are available for the equilibrium fractionation between clay mineral H and ambient water-H at the time of mineral formation (Gilg & Sheppard, 1996; Liu & Epstein, 1984; Méheut et al., 2010; O'Neil & Kharaka, 1976; Savin & Epstein, 1970b), we do not know of any reported fractionation factor between exchangeable H in clay minerals and steam-H at 120 °C.

We used the regression equation of the known δ^2H_w values on the measured δ^2H_t values to determine δ^2H_n values and the contribution of the exchangeable to the total H concentration in the clay minerals and soil clay fractions (χ_e; Feng et al., 1993; Filot et al., 2006; Ruppenthal et al., 2010, 2013, 2015; Sauer et al., 2009; Equation (2.1)).

$$\delta^2H_t = \chi_e\,\alpha_{ex-w}\,\delta^2H_w + (1-\chi_e)\delta^2H_n + 1000\,\chi_e(\alpha_{ex-w} - 1) \qquad \textit{(Eq. 2.1)}$$

The slope is the product of χ_e and $\alpha_{ex\text{-}w}$ and the intercept is $(1-\chi_e)\delta^2H_n + 1000\,\chi_e(\alpha_{ex-w} - 1)$. Assuming $\alpha_{ex\text{-}w}$ = 1 and using δ^2H_t from the regression line for δ^2H_w = 0, Equation (2.1) is rearranged to calculate δ^2H_n (Equation (2.2)).

$$\delta^2H_n = \frac{intercept}{1-slope} \qquad (Eq.\ 2.2)$$

Using Gaussian error propagation for Equation (2.2), we estimated the SD of the δ^2H_n values with Equation (2.3), neglecting covariance of slope and intercept.

$$SD = \sqrt{\left(\frac{1}{1-slope} \cdot SD_{intercept}\right)^2 + \left(\frac{intercept}{(slope-1)^2} \cdot SD_{slope}\right)^2} \qquad (Eq.\ 2.3)$$

We removed samples that after the equilibration came into contact with atmospheric humidity. We detected such samples by (a) visual inspection for holes and (b) the absence of an Ar peak after the H_2 peak in the EA chromatogram. Steam equilibrations of the same sample with isotopically different waters need to result in the same contribution of exchangeable H to the total H concentration (same χ_e). Moreover, (c) we removed as outliers individual samples for which H concentrations and the residuals of the equilibration line fell 0.5 times outside the respective interquartile range of all other equilibrations of the same sample.

Because it was not possible to entirely remove all SOM from the clay fractions, we corrected the measured δ^2H values by mathematically removing the influence of the SOM on the δ^2H_n values of the clay minerals and soil clay fractions. Based on the known locations of the three study soils, we took the mean annual δ^2H value of the local precipitation (δ^2H_p) from Bowen and Revenaugh (2003) and Bowen (2021) (Table 2.2). Then, we used the regression function of Ruppenthal et al. (2015) to determine the δ^2H_n value of SOM and calculated the δ^2H_n value of the inorganic clay fraction ($\delta^2H_{n,\ inorg.\ clay}$) with Equation (2.4).

$$\delta^2H_{n,inorg.clay} = \frac{\delta^2H_{n,clay} - f_{n,SOM}\ \delta^2H_{n,SOM}}{1-f_{n,SOM}}, \text{ with } \delta^2H_{n,SOM} = 1.25\ \delta^2H_p - 34 \qquad (Eq.\ 2.4)$$

where $\delta^2H_{n,\ clay}$ is the measured δ^2H_n value of the clay fraction. In this approach, we assume that the clay separation procedure did not change the δ^2H_n value of the SOM.

2.3 Results

2.3.1 Adaptation of the steam equilibration method

In the first step, we determined the optimum equilibration time (Figure 2.3). In our experiment, the δ^2H_t values of the equilibrated samples did not fully reach a plateau after 64 h, but changed little beyond 16 h. The linear regression of the δ^2H_t value of our samples on the δ^2H values of the equilibration water consistently resulted in coefficients of determination >0.99 (Figure 2.4). Only USGS58 muscovite had an R^2 value of 0.82, which we consider a statistical artefact resulting from the small slope of only 0.009

(Figure 2.5). The accuracy of our δ^2H measurement was tested with the USGS57 biotite and USGS58 muscovite standards (Table 2.3). Our δ^2H values were statistically indistinguishable from the results of Qi et al. (2017) illustrating the high accuracy of our δ^2H_t measurements. Our δ^2H_n measurements show that the reference material USGS57 biotite after equilibration at 120 °C for 16 h has an exchangeable H pool size of 4.4% of the total H concentration.

Table 2.3: Stable H isotope ratios of total (δ^2H) and non-exchangeable H (δ^2H_n), contribution of non-exchangeable H to total H concentrations and total H concentrations of the USGS mineral reference materials.

Mineral	Treatment or origin	δ^2H ± SD [‰]	δ^2H_n ± SD [‰]	Exchangeable H ± SD [%]	n	Total H [mg g^{-1}]	n
Biotite	Data from Qi et al. (2017)	-91.5 ± 2.4			24	4.16 ± 0.02	4
	Original sample, air dried	-93.8 ± 1.7			3	4.32 ± 0.09	2
	After steam equilibration		-95.3 ± 0.9	4.4 ± 0.2	3	4.13 ± 0.02	3
Muscovite	Data from Qi et al. 2017	-28.4 ± 1.6			24	4.48 ± 0.02	4
	Original sample, air dried	-31.3 ± 0.9			3	4.68 ± 0.02	2
	After steam equilibration		-30.7 ± 1.4	1.1 ± 0.6	3	4.69 ± 0.02	3

Note: Errors are SD. Replicate measurements (n) refer to the preceding column.

The precision of the δ^2H_n measurements of the three soil clay fractions ranged from ±0.6‰ for Oso to ±6.9‰ for KA-1 (±1 SD); the precision of untreated bulk samples of clay minerals ranged from ±0.9‰ for kaolinite to ±7.5‰ for Mg-montmorillionite (all n = 3; Table 2.4). The kaolinite had the smallest exchangeable H fraction of all studied clay minerals and the Oso clay fraction of all studied soil samples. In contrast, the swellable vermiculites and montmorillonite contain less structural H and much more exchangeable H than kaolinite.

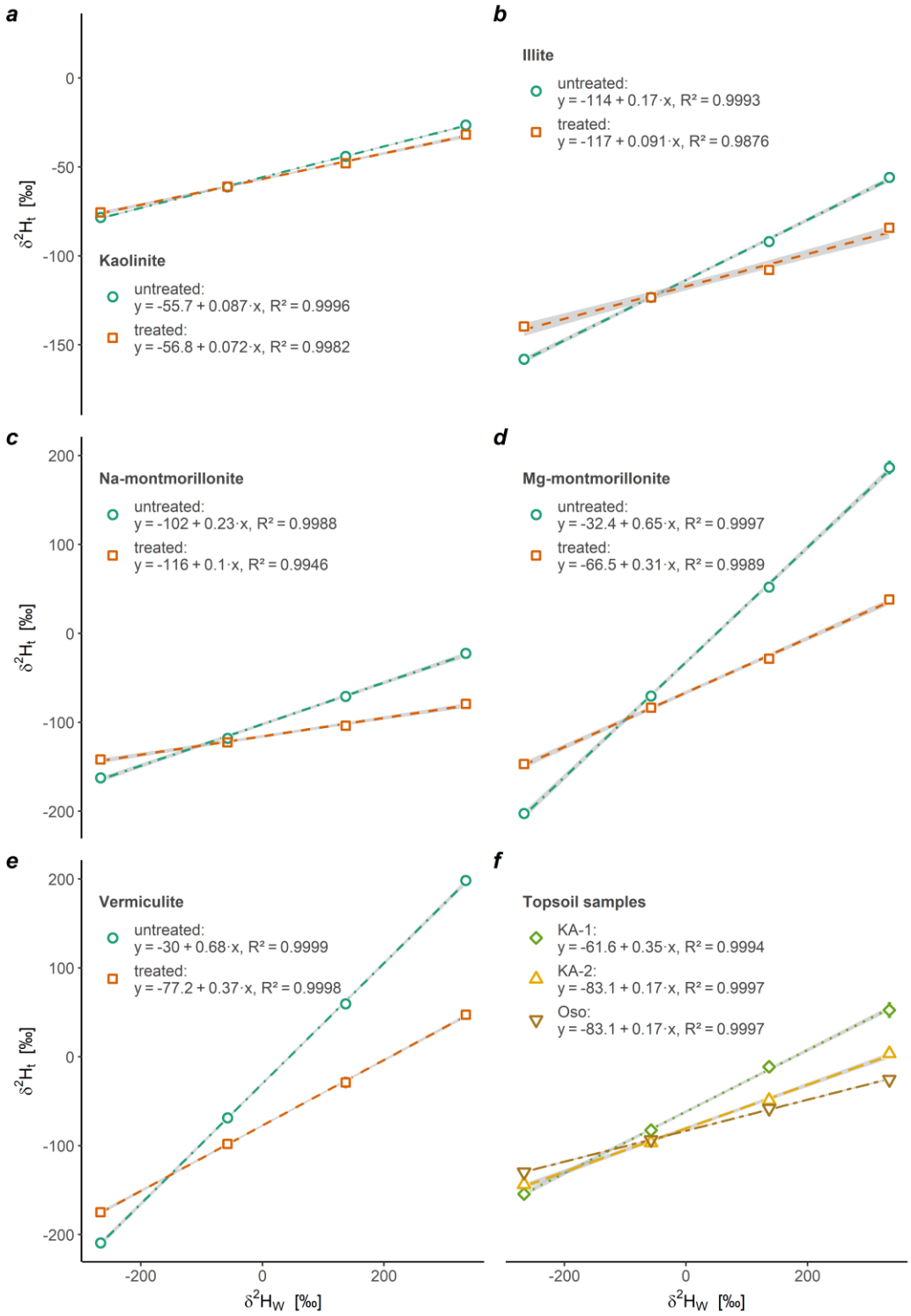

Figure 2.4: Regression lines of the δ^2H_t values of equilibrated samples on the δ^2H_W values of the equilibration waters for untreated, bulk samples (dot-dashed line) and treated clay separates (dashed line) of clay minerals (a–e) and three different soil clay separates (f). Shaded areas illustrate 68% CI.

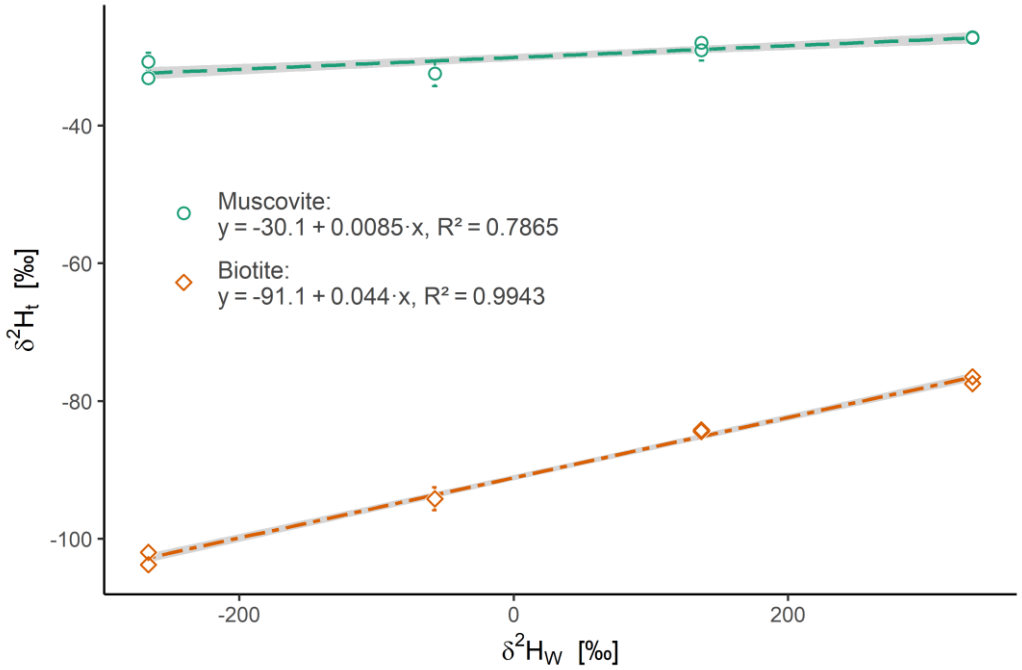

Figure 2.5: Regression lines of the δ^2H_t values of equilibrated samples on the δ^2H_W values of the equilibration waters for the standards USGS57 biotite and USGS58 muscovite. Each point originates from an independent equilibration batch, measured in a separate isotope ratio mass spectrometry sequence. Error bars show SD (n = 2–3) of samples measured in the same equilibration batch and might be smaller than symbol size. Shaded areas illustrate 68% CIs.

2.3.2 Effect of the clay separation on the δ^2H_n values of clay minerals

The δ^2H_n values of the clay mineral samples, which we carried through the clay separation method, fell close to the 1:1 line, when plotted against the δ^2H_n values of the untreated samples, except for the vermiculite (Figure 2.6). With our treatment, we only collected 1% of the bulk sample in the clay fraction of the vermiculite (Table 2.4). As a consequence, the δ^2H_n value of the clay fraction of vermiculite was not representative of the bulk vermiculite. Therefore, we additionally measured the δ^2H_n values of the '≤silt'

Table 2.4: Mean stable isotope ratios of non-exchangeable H (δ^2H_n values) with propagated SD, total H concentrations, contribution of non-exchangeable H to total H concentrations and cumulative yield of the grain-size fractionation procedure.

Name	Batch	Bulk			Clay fraction					
		$\delta^2H_{n,\,bulk}$ ± SD	Total H conc.	Exchangeable H pool	Grain-size fraction	Yield		$\delta^2H_{n,\,clay}$ ± SD	Total H conc.	Exchange-able H pool
		[‰]	[mg g^{-1}]	[%]		[g]	[%]	[‰]	[mg g^{-1}]	[%]
Illite	1	-138.8 ± 2.4	5.5	17.0	Clay	2.4	16	-136.1 ± 1.4	6.3	10.1
	2	-140.3 ± 2.8	5.6	15.9		1.5	11	-128.8 ± 2.6	6.3	6.9
	3	-136.8 ± 3.3	5.3	17.0		2.4	13	-129.3 ± 3.6	6.2	9.2
Kaolinite	1	-62.4 ± 0.5	16.1	8.6	Clay	17.2	79	-63.5 ± 1.5	16.3	7.7
	2	-61.5 ± 1.3	16.4	7.9		11.2	84	-61.6 ± 0.8	16.4	6.1
	3	-61.0 ± 0.8	16.8	8.7		14.5	83	-61.2 ± 1.4	16.5	7.3
Mg-mont-morillonite	1	-102.5 ± 3.3	7.7	65.4	Clay	9.2	92	-100.8 ± 6.2	7.2	34.1
	2	-107.4 ±	8.2	61.9		7.1	94	-103.3 ± 2.4	7.6	32.1
	3	-92.6 ± 14.4	8.0	64.5		8.1	93	-96.2 ± 6.3	7.3	30.6
Na-mont-morillonite	1	-133.4 ± 1.4	6.1	23.4	Clay	7.2	78	-132.9 ± 3.6	6.6	9.3
	2	-140.2 ± 2.8	7.0	21.7		5.7	81	-132.3 ± 1.4	6.8	10.0
	3	-133.4 ± 6.2	6.8	22.8		6.4	79	-128.9 ± 3.2	6.5	10.4
Vermiculite	1				Sand	19.3	94	-105.0 ± 9.2	7.8	50.4
	2					23.5	95	-98.0 ± 5.1	7.8	44.4
	3					23.4	94	-99.5 ± 8.1	6.8	48.4
	1				≤Silt	1.1	5	-123.5 ± 14.6	8.9	45.3
	2					1.0	4	-120.9 ± 6.4	8.8	44.4
	3					1.3	5	-119.8 ± 11.9	8.9	43.9
	1	-101.8 ± 9.4	12.2	66.7	Clay	0.2	1	-125.3 ± 9.9	8.7	44.2
	2	-96.6 ± 12.4	11.9	67.1		0.2	1	-127.7 ± 6.6	8.7	39.0
	3	-92.8 ± 9.9	12.4	67.7		0.3	1	-122.3 ± 7.2	8.6	36.7
KA-1	1				Clay	13.1	51	-107.6 ± 4.2	11.5	36.0
	2					7.4	52	-101.3 ± 1.2	11.1	35.0
	3					10.5	54	-94.1 ± 6.9	11.3	34.7
KA-2	1				Clay	4.0	6	-111.9 ± 2.7	10.6	23.0
	2					0.9	5	-107.3 ± 4.4	9.7	23.0
	3					1.3	6	-106.7 ± 4.1	8.8	24.6
Oso	1				Clay	5.2	13	-99.4 ± 1.7	10.5	18.1
	2					4.6	12	-98.3 ± 1.3	10.7	18.7
	3					4.7	12	-99.2 ± 2.9	10.0	17.2

Note: The subscript 'bulk' refers to the bulk soil and 'clay' to clay fraction, '≤silt' indicates that our silt fraction still included some clay, because of imperfect separation.

and sand fractions of the vermiculite and calculated a mass-weighted mean of the δ^2H_n values of the grain-size fractions. The resulting calculated δ^2H_n value of the bulk vermiculite was similar to that of the untreated sample, illustrating that the clay separation method did not influence the δ^2H_n value of the clay fraction (Figure 2.6). The δ^2H_n values of the soil clay fractions and bulk clay minerals of kaolinite, the two montmorillonites and the directly measured and from the grain-size fractions calculated bulk values of vermiculite were not significantly different between the untreated sample and the clay fraction (t-test, $p \geq 0.09$).

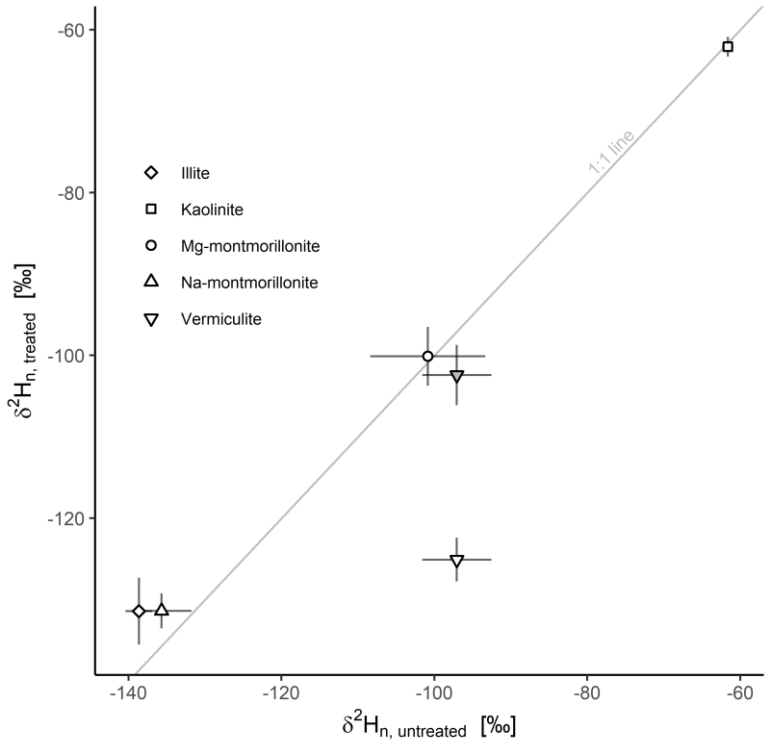

Figure 2.6: Relationship between the δ^2H_n values of untreated bulk clay minerals and those of the clay fraction of kaolinite, illite, Mg- and Na-montmorillonite and vermiculite collected with a clay separation method ("treated") is shown with white filled symbols. For vermiculite, the bulk δ^2H_n value calculated from the separate measurements of the clay, '≤silt' (includes some clay) and sand fractions is additionally shown with gray filled symbol. Error bars show the standard deviation (n = 3, each per treatment batch). For the calculated bulk value of vermiculite, the standard deviation was calculated by Gaussian error propagation from the individual error of the three particle-size fractions.

Because it was not possible to entirely remove SOM from the soil clay fractions, we had to consider the influence of non-exchangeable H in the remaining SOM. The maximum residual organic C concentration in the clay fractions was 35.7 g kg^{-1} (Table

2.5). The organic C concentrations in three of the eight clay fractions including two of the three soil clay fractions were lower than in the bulk samples. This illustrates that the organic matter concentration had been reduced considerably in three samples but less so in the other five ones. To assess the influence of C-bonded H in organic matter on our δ^2H_n values of the three soil clay fractions, we assumed a conversion factor of 2 from organic C to SOM, a H concentration of 50 g kg^{-1} organic matter (Rice & MacCarthy, 1991; Ruppenthal et al., 2013) and a share of non-exchangeable H to total H of 80% (Ruppenthal et al., 2013; Schimmelmann, 1991; Wassenaar & Hobson, 2000). Based on these considerations, the non-exchangeable H from organic matter contributed 15%–34% to the total non-exchangeable H in our three soil clay fractions. This estimate is based on the assumption that the clay separation procedure did not change the δ^2H_n values of the organic matter. Moreover, we assumed that the linear relationship between the δ^2H_n values of SOM and the modelled δ^2H values of the precipitation found for Argentina by Ruppenthal et al. (2015) is also representative of our samples. Our correction of the δ^2H_n values of the soil clay fractions by the contribution of the nonremoved SOM only affected the δ^2H_n value of one of our three soil samples, Oso, more than marginally. In the Oso sample, the corrected δ^2H_n value was shifted by 15‰ (Table 2.6).

Table 2.5: Means and SD (n = 2–3) of organic C concentrations in bulk soils (subscript 'bulk') and the clay fraction (subscript 'clay'), potential cation-exchange capacity (CEC_{pot}) in bulk soils and clay fractions, dithionite-citrate-bicarbonate-soluble Fe concentrations (Fe_d) and contributions of grain-size fractions to the total sample mass.

Sample	$C_{org, bulk}$ [mg g^{-1}]	$CEC_{pot, bulk}$ [$mmol_c$ kg^{-1}]	Fe_d [mg g^{-1}]	Sand [Mass-%]	Silt [Mass-%]	Clay [Mass-%]	$C_{org,clay}$ [mg g^{-1}]	$CEC_{pot, clay}$ [$mmol_c$ kg^{-1}]
Mg-mont-morillonite	0.4 ± 0.02	1113 ± 37	0.6 ± 0.0	1 ± 0.4	11 ± 4	88 ± 4	0.5 ± 0.1	n.a.
Illite	0.6 ± 0.01	89 ± 9	8.9 ± 0.1	49 ± 5.7	32 ± 3	20 ± 9	0.8 ± 0.1	n.a.
Kaolinite	0.2 ± 0.01	29 ± 4	1.2 ± 0.1	1 ± 0.4	16 ± 3	84 ± 2	0.5 ± 0.0	n.a.
Na-mont-morillonite	1.2 ± 0.2	743 ± 12	3.5 ± 0.2	2 ± 0.2	13 ± 4	85 ± 4	0.5 ± 0.1	n.a.
Vermiculite	0.1 ± 0.05	n.a.	0.6 ± 0.1	91 ± 0.4	6 ± 1	3 ± 1	3.6 ± 1.0	n.a.
KA-1	57.7 ± 0.6	247 ± 22	7.5 ± 0.7	10 ± 1.1	25 ± 10	65 ± 10	13.5 ± 1.7	296 ± 12
KA-2	22.5 ± 0.2	57 ± 6	4.1 ± 0.2	62 ± 2.9	22 ± 7	16 ± 7	30.2 ± 3.7	144 ± 3
Oso	61.9 ± 2.2	89 ± 3	9.4 ± 0.1	34 ± 1.0	52 ± 1	15 ± 0	35.7 ± 2.4	121 ± 11

Abbreviation: n.a., not available.

Table 2.6: Mean δ^2H_n values of the clay fractions (subscript 'clay'), the soil organic matter (subscript 'SOM') and δ^2H_n values in the clay fractions corrected by the C-bonded H contribution of residual soil organic matter ($\delta^2H_{n,\ inorg.clay}$).

Sample	$\delta^2H_{n,\ clay}$ ± SD [‰]	$f_{H,SOM}$ [-]	$\delta^2H_{n,\ SOM}$ [‰]	$\delta^2H_{n,\ inorg.clay}$ [‰]
KA-1	-101.0 ± 6.8	0.149	-106.5	-100.0
KA-2	-108.6 ± 2.8	0.326	-106.5	-109.7
Oso	-99.0 ± 0.6	0.334	-129.0	-83.9

Note: $f_{H,SOM}$ is the contribution of H in soil organic matter to the total non-exchangeable H concentration.

2.4 Discussion

2.4.1 Adaptation of the steam equilibration method

Our observation that the δ^2H_t values of the equilibrated samples did not fully reach a plateau after 64 h (Figure 2.3) is in contrast to the findings of Wassenaar and Hobson (2000) and Ruppenthal et al. (2010) for organic materials and bulk soil for which a plateau was already reached between 1 and 2 h. However, a similarly slow increase of the δ^2H_t values with time during vacuum drying at constant temperature was observed for some clay minerals (Faucher & Thomas, 1955; O'Neil & Kharaka, 1976). Likewise, Schimmelmann et al. (2006) reported an asymptotic convergence to a plateau for kerogen-H. Thus, full equilibrium of the clay minerals with the steam occurs only at equilibration times, which are not feasible for routine measurement. Therefore, we decided to run our equilibration for 16 h, because after 16 h the change in the δ^2H_t value was only minor. Thereby, we accept that our δ^2H_n values include some strongly bound interlayer water of phyllosilicates. We consider the associated error as acceptable, because the alternative vacuum-drying methods using constant drying temperatures of 100-250 °C (Bauer & Vennemann, 2014; Gilg et al., 2004; VanDeVelde & Bowen, 2013) also leave an unknown concentration of non-structural H in the sample. The latter is particularly true if the sample consists of a mixture of minerals, which commonly occurs in soil clay fractions. This is related to the fact that the drying temperature required to remove all non-structural H depends on the type of mineral, which has been shown with the help of thermogravimetric analyses (Beyer & von Reichenbach, 2002; Brigatti et al., 2013; Guggenheim & Van Groos, 2001; Joussein et al., 2005; Steudel, 2008). Moreover,

dehydration and dehydroxylation ranges may even overlap for some clay minerals, such as palygorskite (Heller-Kallai, 2013).

Our finding that the biotite standard contained some exchangeable H (Table 2.3) might result in a small variation of the δ^2H values measured in different laboratories at different temperatures if the contribution of exchangeable H is not eliminated as in our approach. However, the size of the exchangeable H pool might even be smaller at room temperature.

We attribute the high precision of the δ^2H_n value of kaolinite and the Oso clay fraction to their large structural H fraction and a corresponding small exchangeable H fraction (Table 2.4). In turn, the bigger error of the δ^2H_n measurements of the swellable vermiculites and partly also the Mg-montmorillonite is attributable to the large exchangeable H fraction (Table 2.4).

We observed large differences between the δ^2H_n values of clay minerals in our study and δ^2H_t measurements of the same material in other studies (Δ^2H_{n-t}). For untreated Mg-montmorillonite (SCa-3), the Δ^2H_{n-t} value was -18‰ and for illite (IMt-1 vs. IMt-2 from the same origin) -36‰ compared with the results of VanDeVelde and Bowen (2013), which we estimated from a figure. For the treated clay fraction of Na-montmorillonite (SWy-1 vs. SWy-3 from the same origin), the Δ^2H_{n-t} value was 14‰ in both cases, relative to the δ^2H_t value for the fraction <2 µm before leaching of Menegatti et al. (1999) and the δ^2H_t of the clay fraction of Fagan (2001), which was similarly treated as ours. We attribute these differences to the fact that the exchangeable H fraction, which ranged from 17% to 64% of the total H concentrations in the three clay minerals (Table 2.4), was less completely removed than in our study, before the δ^2H_t values were determined by Menegatti et al. (1999), Fagan (2001) and VanDeVelde and Bowen (2013). However, our δ^2H_n value for treated Na-montmorillonite (SWy-3) was in close agreement with the measurement of Kanik et al. (2022) of Na-saturated SWy-1 from the same origin, which was similarly treated as ours, showing a Δ^2H_{n-t} value of only 0.5‰. Likewise, the result of Bauer and Vennemann (2014) using 200 °C vacuum drying for untreated SWy-1 was close to ours with a Δ^2H_{n-t} value of -1‰.

2.4.2 Effect of the clay separation on the δ^2H_n values of clay minerals

The recovery of only 1% of the bulk sample in the clay fraction of the vermiculite (Table 2.4) was much lower than the 10% reported in the literature (Steudel et al.,

2009). The major reason for our low yield of the clay fraction was the fact that part of the clay fraction was included in the silt fraction, which we accepted to speed up the clay separation process. We cannot rule out that the H_2O_2 treatment to remove SOM resulted in some swelling of vermiculite moving part of the clay fraction to a larger particle-size class (Obut & Girgin, 2002; Üçgül & Girgin, 2002; Valášková & Martynková, 2012). A similar influence of the particle size on the δ^2H values, like for our vermiculite, was reported for biotite and muscovite (Qi et al., 2014, 2017).

However, macrocrystalline vermiculite originating from a clay deposit differs mineralogically from pedogenic vermiculites in soil clay fractions (Douglas, 1989). The macrocrystalline vermiculite possesses an exclusively trioctahedral structure, includes crystals from sand to clay size, and the OH-dipole of the hydroxyl groups is oriented perpendicular to the sheet plane (Malla, 2002). The usually submicroscopic soil vermiculite can be di- and trioctahedral (Jasmund & Lagaly, 1993). Particularly, dioctahedral vermiculite occurs frequently and is usually smaller than medium silt size (Malla, 2002). Moreover, the OH-dipole of the hydroxyl groups in soil vermiculite is oriented oblique to the dioctahedral sheet plane causing different cation interactions (Malla, 2002). Finally, the potential swelling of vermiculite in our H_2O_2 treatment is less pronounced for microcrystalline soil vermiculite than for macrocrystalline vermiculite from a clay deposit. Therefore, the used macrocrystalline vermiculite is likely not representative for soil vermiculite, so that we consider the observed shift in δ^2H_n values between the bulk vermiculite and its clay fraction as irrelevant for soil clay fractions.

Our finding that there was no effect of the treatment of the samples with H_2O_2 on the δ^2H_n values of the clay minerals contrasted with reports of Hyeong and Capuano (2000) and VanDeVelde and Bowen (2013). We therefore speculate that in the previous work, the apparent effect of the H_2O_2 treatment on the δ^2H values of the treated samples was attributable to re-adsorption of air moisture after drying.

The finding that the organic C concentrations in three of the eight clay fractions were lower than in the bulk samples (Table 2.5), although the clay fraction usually contains a higher organic C concentration than the bulk sample (Eusterhues et al., 2005; Kaiser et al., 2002; von Lützow et al., 2007) underlines the general efficacy of the H_2O_2 treatment. In our approach to mathematically remove the influence of the remaining SOM in the clay fractions after the H_2O_2-treatment (Equation (2.4), Table 2.6), we assumed that the clay separation procedure did not change the δ^2H_n values of the

organic matter. However, Leifeld and Kögel-Knabner (2001) observed that the H_2O_2 treatment attacks non-polycyclic aromatic (e.g., lignin) and O-substituted aliphatic compounds (e.g., sugars) more than alkyl-C, while Mikutta et al. (2005) reported that an H_2O_2 treatment enriches aliphatic and pyrogenic compounds, which includes polycyclic aromatic compounds. Von Lützow et al. (2007) found that SOM was not degraded by H_2O_2 if it was protected by hydrophobic SOM moieties such as alkyl-C and black carbon. We are not aware of any study quantifying how this preferential removal of selected organic compounds influences the δ^2H_n values of residual SOM.

2.5 Conclusions

The steam equilibration method previously used for bulk soils and SOM can be used for precise measurements of δ^2H_n values in clay fractions of soils and clay minerals, provided the contact of the clays with ambient air humidity after equilibration can be entirely avoided. To achieve this, the samples must be handled in a water vapour-free Ar atmosphere. This technique should be universally applicable to other hygroscopic materials. Thus, our first hypothesis is supported.

We did not detect a significant effect of the classical clay fractionation treatment including removal of Fe oxides and carbonates, reduction of SOM and dispersion of the remaining material on the δ^2H_n values of clay minerals. However, the incomplete destruction of SOM required a correction of the data, which relied on the unproven assumption that the H_2O_2 treatment did not change the δ^2H_n values of the SOM. Therefore, we consider our second hypothesis as only supported with this constraint. Future work should focus on a more complete destruction of SOM that does not change the δ^2H_n values of the soil clay fractions.

Author contributions

Stefan Merseburger: Data curation (lead); formal analysis (lead); investigation (lead); methodology (lead); validation (lead); writing – original draft (lead). **Arnim Kessler**: Investigation (supporting); writing – review and editing (supporting). **Yvonne Oelmann**: Conceptualization (equal); funding acquisition (equal); investigation (supporting); supervision (supporting); writing – review and editing (supporting).

Wolfgang Wilcke: Conceptualization (equal); funding acquisition (equal); investigation (supporting); methodology (supporting); project administration (lead); resources (lead); supervision (lead); writing – review and editing (lead).

Acknowledgments

We thank Nadine Gill and Martin Kull for assistance in the laboratory work, Tobias Wirsing for providing soil samples, Nadja Werling and Katja Emmerich for advice and supplementary measurements, Harro Meijer for a working example of the memory correction algorithm, Maria Hoerhold for contributing the deuterium-depleted water ('AWI-TD1') and Stefan Dultz for contributing the vermiculite. This work was funded by the Deutsche Forschungsgemeinschaft (DFG, Wi1601/25-1). Open Access funding enabled and organized by Projekt DEAL.

Conflict of interest statement

The authors declare that they have no conflict of interest.

2.6 References

Ammann, L., Bergaya, F., & Lagaly, G. (2005). Determination of the cation exchange capacity of clays with copper complexes revisited. *Clay Minerals*, *40*(4), 441–453. https://doi.org/10.1180/0009855054040182

Bauer, K. K., & Vennemann, T. W. (2014). Analytical methods for the measurement of hydrogen isotope composition and water content in clay minerals by TC/EA. *Chemical Geology*, *363*, 229–240. https://doi.org/10.1016/j.chemgeo.2013.10.039

Beyer, J., & von Reichenbach, H. (2002). An extended revision of the interlayer structures of one- and two-layer hydrates of Na-vermiculite. *Clay Minerals*, *37*(1), 157–168. https://doi.org/10.1180/0009855023710025

Borden, D., & Giese, R. F. (2001). Baseline studies of the clay minerals society source clays: Cation exchange capacity measurements by the ammonia-electrode method. *Clays and Clay Minerals*, *49*(5), 444–445.

Bors, J., Gorny, A., & Dultz, S. (1997). Iodide, caesium and strontium adsorption by organophilic vermiculite. *Clay Minerals*, *32*(1), 21–28. https://doi.org/10.1180/claymin.1997.032.1.04

Bowen, G. J. (2021). *WaterIsotopes.org*. The Online Isotopes in Precipitation Calculator, Version 3.1. http://wateriso.utah.edu/waterisotopes/pages/data_access/oipc.html

Bowen, G. J., Chesson, L., Nielson, K., Cerling, T. E., & Ehleringer, J. R. (2005). Treatment methods for the determination of δ^2H and $\delta^{18}O$ of hair keratin by continuous-flow isotope-ratio

mass spectrometry. *Rapid Communications in Mass Spectrometry*, *19*(17), 2371–2378. https://doi.org/10.1002/rcm.2069

Bowen, G. J., & Revenaugh, J. (2003). Interpolating the isotopic composition of modern meteoric precipitation: Isotopic composition of modern precipitation. *Water Resources Research*, *39*(10), 1299–1312. https://doi.org/10.1029/2003WR002086

Brigatti, M. F., Galan, E., & Theng, B. K. G. (2013). Structure and mineralogy of clay minerals. In *Developments in clay science* (2nd edition, Vol. 5, pp. 21–81). Elsevier. https://doi.org/10.1016/B978-0-08-098258-8.00014-6

Cerling, T. E. (1984). The stable isotopic composition of modern soil carbonate and its relationship to climate. *Earth and Planetary Science Letters*, *71*(2), 229–240.

Chipera, S. J., & Bish, D. L. (2001). Baseline Studies of the Clay Minerals Society Source Clays: Powder X-Ray Diffraction Analyses. *Clays and Clay Minerals*, *49*(5), 398–409.

Dietrich, H.-G., Dahms, E., Fritz, L., Heimerl, H., & Kühler, E. E. (1998). Korngrößenverteilung. In *Tonmineralogie und Bodenphysik*. Springer Berlin Heidelberg. https://doi.org/10.1007/978-3-642-58852-5

DIN ISO 11277. (2002). *Bodenbeschaffenheit—Bestimmung der Partikelgrößenverteilung in Mineralböden. Verfahren mittels Siebung und Sedimentation*. Beuth Verlag. https://doi.org/10.31030/9283499

Dogan, A. U., Dogan, M., Onal, M., Sarikaya, Y., Aburub, A., & Wurster, D. E. (2006). Baseline studies of the Clay Minerals Society source clays: Specific surface area by the Brunauer Emmett Teller (BET) method. *Clays and Clay Minerals*, *54*(1), 62–66. https://doi.org/10.1346/CCMN.2006.0540108

Dogan, M., Dogan, A. U., Yesilyurt, F. I., Alaygut, D., Buckner, I., & Wurster, D. E. (2007). Baseline studies of the Clay Minerals Society special clays: Specific surface area by the Brunauer Emmett Teller (BET) method. *Clays and Clay Minerals*, *55*(5), 534–541. https://doi.org/10.1346/CCMN.2007.0550508

Douglas, L. A. (1989). Vermiculites. In J. B. Dixon & S. B. Weed (Eds.), *SSSA Book Series* (pp. 635–674). Soil Science Society of America. https://doi.org/10.2136/sssabookser1.2ed.c13

Dultz, S., Riebe, B., & Bunnenberg, C. (2005). Temperature effects on iodine adsorption on organo-clay minerals: II. Structural effects. *Applied Clay Science*, *28*(1), 17–30. https://doi.org/10.1016/j.clay.2004.01.005

Epstein, S., Yapp, C. J., & Hall, J. H. (1976). The determination of the D/H ratio of non-exchangeable hydrogen in cellulose extracted from aquatic and land plants. *Earth and Planetary Science Letters*, *30*(2), 241–251. https://doi.org/10.1016/0012-821X(76)90251-X

Eusterhues, K., Rumpel, C., & Kögel-Knabner, I. (2005). Stabilization of soil organic matter isolated via oxidative degradation. *Organic Geochemistry*, *36*(11), 1567–1575.

Fagan, R. (2001). *Oxygen-and hydrogen-isotope study of hydroxyl-group behavior in standard smectite and kaolinite* [PhD Thesis]. Faculty of Graduate Studies, University of Western Ontario.

Faghihi, V., Meijer, H. a. J., & Gröning, M. (2015). A thoroughly validated spreadsheet for calculating isotopic abundances (^{2}H, ^{17}O, ^{18}O) for mixtures of waters with different isotopic compositions. *Rapid Communications in Mass Spectrometry: RCM*, *29*(15), 1351–1356. https://doi.org/10.1002/rcm.7232

Faucher, J. A., & Thomas, H. C. (1955). Exchange between Heavy Water and Clay Minerals. *The Journal of Physical Chemistry*, *59*(2), 189–191. https://doi.org/10.1021/j150524a026

Feng, X., Krishnamurthy, R. V., & Epstein, S. (1993). Determination of D/H ratios of nonexchangeable hydrogen in cellulose: A method based on the cellulose-water exchange reaction.

Geochimica et Cosmochimica Acta, *57*(17), 4249–4256. https://doi.org/10.1016/0016-7037(93)90320-V

Filot, M. S., Leuenberger, M., Pazdur, A., & Boettger, T. (2006). Rapid online equilibration method to determine the D/H ratios of non-exchangeable hydrogen in cellulose. *Rapid Communications in Mass Spectrometry*, *20*(22), 3337–3344. https://doi.org/10.1002/rcm.2743

Gee, G. W., & Or, D. (2002). Particle-Size Analysis. In *Methods of Soil Analysis: Part 4 Physical Methods* (Vol. 4, pp. 255–293). Soil Science Society of America. https://doi.org/10.2136/sssabookser5.4.c12

Gehre, M., Renpenning, J., Geilmann, H., Qi, H., Coplen, T. B., Kümmel, S., Ivdra, N., Brand, W. A., & Schimmelmann, A. (2017). Optimization of on-line hydrogen stable isotope ratio measurements of halogen- and sulfur-bearing organic compounds using elemental analyzer–chromium/high-temperature conversion isotope ratio mass spectrometry (EA-Cr/HTC-IRMS). *Rapid Communications in Mass Spectrometry*, *31*(6), 475–484. https://doi.org/10.1002/rcm.7810

Gilg, H. A., Girard, J.-P., & Sheppard, S. M. (2004). Conventional and less conventional techniques for hydrogen and oxygen isotope analysis of clays, associated minerals and pore waters in sediments and soils. *Handbook of Stable Isotope Analytical Techniques*, *1*, 38–61.

Gilg, H. A., & Sheppard, S. M. F. (1996). Hydrogen isotope fractionation between kaolinite and water revisited. *Geochimica et Cosmochimica Acta*, *60*(3), 529–533. https://doi.org/10.1016/0016-7037(95)00417-3

Grim, R. E., & Kulbicki, G. (1961). Montmorillonite: High temperature reactions and classification. *American Mineralogist: Journal of Earth and Planetary Materials*, *46*(11–12), 1329–1369.

Guggenheim, S., & Van Groos, A. K. (2001). Baseline studies of the clay minerals society source clays: Thermal analysis. *Clays and Clay Minerals*, *49*(5), 433–443.

Guidotti, S., Jansen, H. G., Aerts-Bijma, A. T., Verstappen-Dumoulin, B. M. a. A., van Dijk, G., & Meijer, H. a. J. (2013). Doubly Labelled Water analysis: Preparation, memory correction, calibration and quality assurance for delta δ^2H and $\delta^{18}O$ measurements over four orders of magnitudes. *Rapid Communications in Mass Spectrometry*, *27*(9), 1055–1066. https://doi.org/10.1002/rcm.6540

Heller-Kallai, L. (2013). Thermally modified clay minerals. In *Developments in clay science* (2nd edition, Vol. 5, pp. 411–433). Elsevier. https://doi.org/10.1016/B978-0-08-098258-8.00014-6

Hobson, K. A., Soto, D. X., Paulson, D. R., Wassenaar, L. I., & Matthews, J. H. (2012). A dragonfly (δ^2H) isoscape for North America: A new tool for determining natal origins of migratory aquatic emergent insects. *Methods in Ecology and Evolution*, *3*(4), 766–772. https://doi.org/10.1111/j.2041-210X.2012.00202.x

Hower, J., & Mowatt, T. C. (1966). The mineralogy of illites and mixed-layer illite/montmorillonites. *American Mineralogist*, *51*(5–6), 825–854. https://doi.org/10.1346/CCMN.1999.0470617

Hsieh, J. C., & Yapp, C. J. (1999). Hydrogen-isotope exchange in halloysite: Insight from room-temperature experiments. *Clays and Clay Minerals*, *47*(6), 811–816.

Hyeong, K., & Capuano, R. M. (2000). The effect of organic matter and the H_2O_2 organic-matter-removal method on the δD of smectite-rich samples. *Geochimica et Cosmochimica Acta*, *64*(22), 3829–3837.

IUSS Working Group WRB. (2015). *World Reference Base for Soil Resources 2014, update 2015, International soil classification system for naming soils and creating legends for soil maps.*

World Soil Resources Reports No. 106. Food and Agriculture Organization of the United Nations (FAO).

Jasmund, K., & Lagaly, G. (Eds.). (1993). *Tonminerale und Tone*. Steinkopff. https://doi.org/10.1007/978-3-642-72488-6

Joussein, E., Petit, S., Churchman, J., Theng, B., Righi, D., & Delvaux, B. (2005). Halloysite clay minerals—A review. *Clay Minerals*, *40*(4), 383–426. https://doi.org/10.1180/0009855054040180

Kaiser, K., Eusterhues, K., Rumpel, C., Guggenberger, G., & Kögel-Knabner, I. (2002). Stabilization of organic matter by soil minerals—Investigations of density and particle-size fractions from two acid forest soils. *Journal of Plant Nutrition and Soil Science*, *165*(4), 451–459. https://doi.org/10.1002/1522-2624(200208)165:4<451::AID-JPLN451>3.0.CO;2-B

Kanik, N. J., Longstaffe, F. J., Kuligiewicz, A., & Derkowski, A. (2022). Systematics of smectite hydrogen-isotope composition: Structural hydrogen versus adsorbed water. *Applied Clay Science*, *216*, 106338. https://doi.org/10.1016/j.clay.2021.106338

Kelly, J. F., Bridge, E. S., Fudickar, A. M., & Wassenaar, L. I. (2009). A test of comparative equilibration for determining non-exchangeable stable hydrogen isotope values in complex organic materials. *Rapid Communications in Mass Spectrometry*, *23*(15), 2316–2320. https://doi.org/10.1002/rcm.4150

Kogel, J. E., & Lewis, S. A. (2001). Baseline studies of the clay minerals society source clays: Chemical analysis by inductively coupled plasma-mass spectroscopy (ICP-MS). *Clays and Clay Minerals*, *49*(5), 387–392.

Komadel, P. (2003). Chemically modified smectites. *Clay Minerals*, *38*(1), 127–138. https://doi.org/10.1180/0009855033810083

Lagaly, G., Schulz, O., & Zimehl, R. (2013). *Dispersionen und Emulsionen: Eine Einführung in die Kolloidik feinverteilter Stoffe einschließlich der Tonminerale*. Springer-Verlag. https://doi.org/10.1007/978-3-642-59248-5

Lawrence, J. R., & Taylor, H. P. (1972). Hydrogen and oxygen isotope systematics in weathering profiles. *Geochimica et Cosmochimica Acta*, *36*(12), 1377–1393. https://doi.org/10.1016/0016-7037(72)90068-3

Leifeld, J., & Kögel-Knabner, I. (2001). Organic carbon and nitrogen in fine soil fractions after treatment with hydrogen peroxide. *Soil Biology and Biochemistry*, *33*(15), 2155–2158. https://doi.org/10.1016/S0038-0717(01)00127-4

Liu, K.-K., & Epstein, S. (1984). The hydrogen isotope fractionation between kaolinite and water. *Chemical Geology*, *46*(4), 335–350. https://doi.org/10.1016/0009-2541(84)90176-1

Lobe, I., Wilcke, W., Kobža, J., & Zech, W. (1998). Heavy metal contamination of soils in Northern Slovakia. *Zeitschrift Für Pflanzenernährung Und Bodenkunde*, *161*(5), 541–546. https://doi.org/10.1002/jpln.1998.3581610507

Malla, P. B. (2002). Vermiculites. In *Soil Mineralogy with Environmental Applications* (pp. 501–529). John Wiley & Sons, Ltd. https://doi.org/10.2136/sssabookser7.c16

Méheut, M., Lazzeri, M., Balan, E., & Mauri, F. (2010). First-principles calculation of H/D isotopic fractionation between hydrous minerals and water. *Geochimica et Cosmochimica Acta*, *74*(14), 3874–3882. https://doi.org/10.1016/j.gca.2010.04.020

Mehra, O. P., & Jackson, M. L. (1958). Iron Oxide Removal from Soils and Clays by a Dithionite-Citrate System Buffered with Sodium Bicarbonate. *Clays and Clay Minerals*, *7*(1), 317–327. https://doi.org/10.1346/CCMN.1958.0070122

Meier, L. P., & Kahr, G. (1999). Determination of the Cation Exchange Capacity (CEC) of Clay Minerals Using the Complexes of Copper(II) Ion with Triethylenetetramine and Tetraethylenepentamine. *Clays and Clay Minerals*, *47*(3), 386–388. https://doi.org/10.1346/CCMN.1999.0470315

Menegatti, A. P., Frueh-Green, G. L., & Stille, P. (1999). Removal of organic matter by disodium peroxodisulphate: Effects on mineral structure, chemical composition and physicochemical properties of some clay minerals. *Clay Minerals*, *34*(2), 247–257.

Mermut, A. R., Angel, & Cano, F. (2001). Baseline studies of the clay minerals society source clays: Chemical analyses of major elements. *Clays and Clay Minerals*, 381–386.

Mikutta, R., Kleber, M., Kaiser, K., & Jahn, R. (2005). Review: Organic Matter Removal from Soils using Hydrogen Peroxide, Sodium Hypochlorite, and Disodium Peroxodisulfate. *Soil Science Society of America Journal*, *69*(1), 120–135. https://doi.org/10.2136/sssaj2005.0120

Müller, G. (1964). *Methoden der Sediment-Untersuchung: Mit 2 Farbtafeln, 29 Tabellen im Text, 1 Tabelle im Anhang sowie 3 Beilagen*. Schweizerbart.

Obut, A., & Girgin, İ. (2002). Hydrogen peroxide exfoliation of vermiculite and phlogopite. *Minerals Engineering*, *15*(9), 683–687. https://doi.org/10.1016/S0892-6875(02)00161-9

O'Neil, J. R., & Kharaka, Y. K. (1976). Hydrogen and oxygen isotope exchange reactions between clay minerals and water. *Geochimica et Cosmochimica Acta*, *40*(2), 241–246. https://doi.org/10.1016/0016-7037(76)90181-2

Paul, D., Skrzypek, G., & Fórizs, I. (2007). Normalization of measured stable isotopic compositions to isotope reference scales – a review. *Rapid Communications in Mass Spectrometry*, *21*(18), 3006–3014. https://doi.org/10.1002/rcm.3185

Qi, H., & Coplen, T. B. (2011). Investigation of preparation techniques for δ^2H analysis of keratin materials and a proposed analytical protocol. *Rapid Communications in Mass Spectrometry*, *25*(15), 2209–2222. https://doi.org/10.1002/rcm.5095

Qi, H., Coplen, T. B., Gehre, M., Vennemann, T. W., Brand, W. A., Geilmann, H., Olack, G., Bindeman, I. N., Palandri, J., Huang, L., & Longstaffe, F. J. (2017). New biotite and muscovite isotopic reference materials, USGS57 and USGS58, for δ^2H measurements–A replacement for NBS 30. *Chemical Geology*, *467*, 89–99. https://doi.org/10.1016/j.chemgeo.2017.07.027

Qi, H., Coplen, T. B., Olack, G. A., & Vennemann, T. W. (2014). Caution on the use of NBS 30 biotite for hydrogen-isotope measurements with on-line high-temperature conversion systems. *Rapid Communications in Mass Spectrometry*, *28*(18), 1987–1994. https://doi.org/10.1002/rcm.6983

Qi, H., Gröning, M., Coplen, T. B., Buck, B., Mroczkowski, S. J., Brand, W. A., Geilmann, H., & Gehre, M. (2010). Novel silver-tubing method for quantitative introduction of water into high-temperature conversion systems for stable hydrogen and oxygen isotopic measurements. *Rapid Communications in Mass Spectrometry*, *24*(13), 1821–1827. https://doi.org/10.1002/rcm.4559

R Core Team. (2021). *R: A language and environment for statistical computing* [Manual]. https://www.R-project.org/

Rice, J. A., & MacCarthy, P. (1991). Statistical evaluation of the elemental composition of humic substances. *Organic Geochemistry*, *17*(5), 635–648. https://doi.org/10.1016/0146-6380(91)90006-6

Ruppenthal, M., Oelmann, Y., del Valle, H. F., & Wilcke, W. (2015). Stable isotope ratios of nonexchangeable hydrogen in organic matter of soils and plants along a 2100-km climosequence in Argentina: New insights into soil organic matter sources and transformations? *Geochimica et Cosmochimica Acta*, *152*, 54–71. https://doi.org/10.1016/j.gca.2014.12.024

Ruppenthal, M., Oelmann, Y., & Wilcke, W. (2010). Isotope ratios of nonexchangeable hydrogen in soils from different climate zones. *Geoderma*, *155*(3–4), 231–241. https://doi.org/10.1016/j.geoderma.2009.12.005

Ruppenthal, M., Oelmann, Y., & Wilcke, W. (2013). Optimized Demineralization Technique for the Measurement of Stable Isotope Ratios of Nonexchangeable H in Soil Organic Matter. *Environmental Science & Technology*, *47*(2), 949–957. https://doi.org/10.1021/es303448g

Sauer, P. E., Schimmelmann, A., Sessions, A. L., & Topalov, K. (2009). Simplified batch equilibration for D/H determination of non-exchangeable hydrogen in solid organic material. *Rapid Communications in Mass Spectrometry*, *23*(7), 949–956. https://doi.org/10.1002/rcm.3954

Savin, S. M., & Epstein, S. (1970a). The oxygen and hydrogen isotope geochemistry of clay minerals. *Geochimica et Cosmochimica Acta*, *34*(1), 25–42. https://doi.org/10.1016/0016-7037(70)90149-3

Savin, S. M., & Epstein, S. (1970b). The oyxgen and hydrogen isotope geochemistry of ocean sediments and shales. *Geochimica et Cosmochimica Acta*, *34*(1), 43–63. https://doi.org/10.1016/0016-7037(70)90150-X

Schimmelmann, A. (1991). Determination of the concentration and stable isotopic composition of nonexchangeable hydrogen in organic matter. *Analytical Chemistry*, *63*(21), 2456–2459. https://doi.org/10.1021/ac00021a013

Schimmelmann, A., Qi, H., Dunn, P. J. H., Camin, F., Bontempo, L., Potočnik, D., Ogrinc, N., Kelly, S., Carter, J. F., Abrahim, A., Reid, L. T., & Coplen, T. B. (2020). Food Matrix Reference Materials for Hydrogen, Carbon, Nitrogen, Oxygen, and Sulfur Stable Isotope-Ratio Measurements: Collagens, Flours, Honeys, and Vegetable Oils. *Journal of Agricultural and Food Chemistry*, *68*(39), 10852–10864. https://doi.org/10.1021/acs.jafc.0c02610

Schimmelmann, A., Sessions, A. L., & Mastalerz, M. (2006). Hydrogen isotopic (D/H) composition of organic matter during diagenesis and thermal maturation. *Annu. Rev. Earth Planet. Sci.*, *34*, 501–533.

Soto, D. X., Koehler, G., Wassenaar, L. I., & Hobson, K. A. (2017). Re-evaluation of the hydrogen stable isotopic composition of keratin calibration standards for wildlife and forensic science applications. *Rapid Communications in Mass Spectrometry*, *31*(14), 1193–1203. https://doi.org/10.1002/rcm.7893

Sprenger, M., Leistert, H., Gimbel, K., & Weiler, M. (2016). Illuminating hydrological processes at the soil-vegetation-atmosphere interface with water stable isotopes. *Reviews of Geophysics*, *54*(3), 674–704. https://doi.org/10.1002/2015RG000515

Stanjek, H., & Künkel, D. (2016). CEC determination with Cu-triethylenetetramine: Recommendations for improving reproducibility and accuracy. *Clay Minerals*, *51*(1), 1–17. https://doi.org/10.1180/claymin.2016.051.1.01

Steudel, A. (2008). *Selection strategy and modification of layer silicates for technical applications* [Univ.-Verlag Karlsruhe]. https://doi.org/10.5445/IR/1000010008

Steudel, A., Batenburg, L. F., Fischer, H. R., Weidler, P. G., & Emmerich, K. (2009). Alteration of swelling clay minerals by acid activation. *Applied Clay Science*, *44*(1–2), 105–115. https://doi.org/10.1016/j.clay.2009.02.002

Steudel, A., Weidler, P. G., Schuhmann, R., & Emmerich, K. (2009). Cation exchange reactions of vermiculite with Cu-triethylenetetramine as affected by mechanical and chemical pretreatment. *Clays and Clay Minerals*, *57*(4), 486–493. Scopus. https://doi.org/10.1346/CCMN.2009.0570409

Üçgül, E., & Girgin, İ. (2002). Chemical Exfoliation Characteristics of Karakoç Phlogopite in Hydrogen Peroxide Solution. *TURKISH JOURNAL OF CHEMISTRY*, *26*(3), 431–440.

Valášková, M., & Martynková, G. S. (2012). Vermiculite: Structural Properties and Examples of the Use. *Clay Minerals in Nature - Their Characterization, Modification and Application*. https://doi.org/10.5772/51237

VanDeVelde, J. H., & Bowen, G. J. (2013). Effects of chemical pretreatments on the hydrogen isotope composition of 2:1 clay minerals: Clay mineral isotope treatment effects. *Rapid Communications in Mass Spectrometry*, *27*(10), 1143–1148. https://doi.org/10.1002/rcm.6554

von Lützow, M., Kögel-Knabner, I., Ekschmitt, K., Flessa, H., Guggenberger, G., Matzner, E., & Marschner, B. (2007). SOM fractionation methods: Relevance to functional pools and to stabilization mechanisms. *Soil Biology and Biochemistry*, *39*(9), 2183–2207. https://doi.org/10.1016/j.soilbio.2007.03.007

Wassenaar, L. I., & Hobson, K. A. (2000). Improved Method for Determining the Stable-Hydrogen Isotopic Composition (δD) of Complex Organic Materials of Environmental Interest. *Environmental Science & Technology*, *34*(11), 2354–2360. https://doi.org/10.1021/es990804i

Wassenaar, L. I., & Hobson, K. A. (2003). Comparative equilibration and online technique for determination of non-exchangeable hydrogen of keratins for use in animal migration studies. *Isotopes in Environmental and Health Studies*, *39*(3), 211–217. https://doi.org/10.1080/1025601031000096781

Wickham, H., Averick, M., Bryan, J., Chang, W., McGowan, L. D., François, R., Grolemund, G., Hayes, A., Henry, L., Hester, J., Kuhn, M., Pedersen, T. L., Miller, E., Bache, S. M., Müller, K., Ooms, J., Robinson, D., Seidel, D. P., Spinu, V., … Yutani, H. (2019). Welcome to the tidyverse. *Journal of Open Source Software*, *4*(43), 1686. https://doi.org/10.21105/joss.01686

3 Global distribution of nonexchangeable stable hydrogen isotope ratios of topsoil clay fractions

Stefan Merseburger [a], Arnim Kessler [b], Sadadi Ojoatre [c], Christoph Berthold [d], Yvonne Oelmann [b], Wolfgang Wilcke [a]

[a] Institute of Geography and Geoecology, Karlsruhe Institute of Technology (KIT), Reinhard-Baumeister-Platz 1, 76131 Karlsruhe, Germany

[b] Geoecology, University of Tübingen, Rümelinstrasse 19-23, 72070 Tübingen, Germany

[c] Lancaster Environment Centre, Lancaster University, LA1 4YQ United Kingdom

[d] Competence Center Archaeometry – Baden-Wuerttemberg (CCA-BW), University of Tübingen, Wilhelmstrasse 56, 72074 Tübingen, Germany

Chapter 3 is published in Geochimica et Cosmochimica Acta 347, 2023; 72–87, https://doi.org/10.1016/j.gca.2023.02.007.

Abstract

Stable isotope ratios of hydrogen (δ^2H values) in local meteoric water correlate with those of nonexchangeable H (δ^2H_n) in bulk soil and organic matter, allowing for probabilistic spatial assignments to soil samples. We hypothesized that there is a similar correlation between the δ^2H values of local meteoric water and the δ^2H_n value of soil clay fractions. The H pool of topsoil clay fractions is usually dominated by pedogenic clay minerals, which contains structural hydroxyl-H, preserving the δ^2H values of ambient water at the time mineral formation. We applied a steam equilibration method with water vapors of known δ^2H values to determine δ^2H_n values in soil clay fractions by eliminating the influence of easily exchangeable H. We collected topsoil samples from 24 locations on five continents with a wide variation in δ^2H values of meteoric water. To calculate δ^2H_n values via steam equilibration the equilibrium fractionation factor between exchangeable H in the clay fractions and equilibration waters ($\alpha_{ex\text{-}w}$) is needed, which is, however, unknown. We therefore assessed the effect of $\alpha_{ex\text{-}w}$ values from 1 (no fractionation) to $\alpha_{ex\text{-}w} = 1.08$, which has been used in steam equilibration approaches of organic matter and bulk soil, on the δ^2H_n values of soil clay fractions. The δ^2H_n values of the clay fractions ranged from -167 ± SD 1‰ for a northern Siberian sample to -44 ± 4‰ in western Kenya for $\alpha_{ex\text{-}w} = 1$ and from -191 ± 3 to -81 ± 4‰ for $\alpha_{ex\text{-}w} = 1.08$. The δ^2H values of local meteoric water correlated significantly with the δ^2H_n values of the clay fractions ($r = 0.85$ for $\alpha_{ex\text{-}w} = 1$ and 0.65 for $\alpha_{ex\text{-}w} = 1.08$, $p < 0.001$). A multiple regression model including hillslope as a possible measure of the accumulation of clay minerals with a slightly different δ^2H_n value from nearby locations by eolian or aqueous transport in addition to the mean seasonal δ^2H values of local meteoric water explained up to 89% of the observed variation in δ^2H values of the clay fractions. Our results demonstrate that the δ^2H_n values of soil clay fractions are driven by the δ^2H values of local precipitation on a global scale, irrespective of the used $\alpha_{ex\text{-}w}$ value and influenced by the mineral type. Overcoming previous methodological limitations opens up opportunities for probabilistic spatial assignments of unknown organic matter-poor topsoil samples, applications to paleosoil problems or to experimentally track clay mineral neoformation in soils by tracer experiments.

3.1 Introduction

The global water cycle distributes hydrogen isotopes unevenly. Since the 1960s, the Global Network of Isotopes in Precipitation (GNIP) surveys this distribution by sampling meteoric water (i.e., rain, dew, hail, and snow; IAEA, 2014). Based on the GNIP data, several studies have reported the modeled long-term distribution of hydrogen isotopes on Earth. Because organisms rely on meteoric water to build up tissue, the H isotope composition of organic matter reflects that of local meteoric water. Usually, there is a process-specific offset of the δ^2H value between the meteoric water and the nonexchangeable H pool of individual chemical compounds or bulk soil organic matter (Wassenaar and Hobson, 1998; Bowen et al., 2005b; Ruppenthal et al., 2015; Werner et al., 2016). In soil organic matter, only C-bonded H conserves the H isotope ratio of its time of formation as nonexchangeable δ^2H (δ^2H_n) value, while H bonded to functional groups involving N, S and O is exchangeable. This exchangeable H pool changes its isotopic composition in contact with ambient water or vapor quickly and thus must be eliminated to determine the δ^2H_n values of materials that contain both, exchangeable and nonexchangeable H such as bulk soil organic matter (Schimmelmann et al., 1999; Wassenaar and Hobson, 2000). The δ^2H_n values of organic substances including collagen, keratin, cellulose or microbial tissue extracted from unburied terrestrial surface environments such as topsoils have previously been used to trace these substances to their likely origins in the H isoscape (West et al., 2010).

Already in the 1970s, a relationship between the δ^2H values of meteoric water and those of clay minerals in soil was observed and attributed to the in-situ formation of clay minerals in equilibrium with the H of ambient water (Savin and Epstein, 1970; Lawrence and Taylor, 1972). The latter correlation was close for kaolinite but less close and disputed for montmorillonite formed by pedogenetic processes in soil, which was attributed to variations in the chemical composition of montmorillonite (Lawrence, 1970; Lawrence and Taylor, 1971; Sheppard and Gilg, 1996). Up to now, methodological limitations prevented a further analysis of the relationship of the δ^2H_n values of montmorillonite and other highly hygroscopic clay minerals with the δ^2H values of meteoric water (Sheppard and Gilg, 1996; Gilg et al., 2004). Because similar to soil organic matter, the H in clay minerals can be exchangeable (adsorbed water on inner and outer surfaces and superficial OH groups) or nonexchangeable (structural water in

the interior of the mineral lattices). The early approaches reduced the influence of exchangeable H by vacuum drying at temperatures of 100–250 °C, which (partly) removes adsorbed water. It can be expected that different temperatures remove different fractions of the adsorbed water, which might moreover also vary among different minerals, so that any H isotope ratio measured with these methods is specific for the used drying temperature (Marumo et al., 1995; Gilg et al., 2004). In addition to the uncertainty created by different drying procedures, there is a risk of rehydration and uncontrolled H isotope exchange by contact with ambient air during the transfer of vacuum-dried samples to the stable isotope measurement, which might have introduced errors into some reported results (Gilg et al., 2004; VanDeVelde and Bowen, 2013; Bauer and Vennemann, 2014; Kanik et al., 2022). These methodological limitations prevented the reliable measurement of the δ^2H value of the nonexchangeable H pool in clay minerals and soil clay fractions and thus also the establishment of an isotopic relationship between meteoric water and the structural H. Such a relationship would allow for a probabilistic spatial assignment of soil samples in the isoscape of meteoric water, opening up new opportunities in environmental forensics. Other research opportunities might lie in the comparison of soil samples formed during different climatic conditions such as interstadial and interglacial soils, in which the climate-determined stable H isotope ratio of meteoric water is conserved in the nonexchangeable H pool of clay minerals. In tracer experiments using ^2H-labeled water in the laboratory or by the exchange of soil monoliths between regions with distinctly different δ^2H values of meteoric water, the clay mineral (neo-)formation might be followed.

In a recent study, Merseburger et al. (2022) adapted and tested the steam equilibration method of Ruppenthal et al. (2013) for clay minerals and soil clay fractions. In this method, the samples were equilibrated with vapors of waters with known H isotope composition. As a result, all vapor-accessible and exchangeable H assumed the isotope signature of the equilibration water. The latter enabled in the next step to calculate the contribution of exchangeable H to the total H pool and the δ^2H_n values of the sample by regression of the measured δ^2H values in the equilibrated samples on the known δ^2H values of the equilibration waters (Eqs. 3.1 and 3.2). Merseburger et al. (2022) avoided rehydration and thus an unwanted post-equilibration H isotope exchange with atmospheric water by airtight closing of the samples in tin

capsules under an Ar atmosphere. Using this technique, Merseburger et al. (2022) did not detect a significant effect of the classical clay fractionation treatment including removal of Fe oxides and carbonates, reduction of soil organic matter and dispersion of the remaining material on the δ^2H_n values of kaolinite, illite, vermiculite and Na-saturated and Mg-rich montmorillonite.

Ruppenthal et al. (2010) found a correlation between the local mean annual δ^2H values of meteoric water and the δ^2H_n values of a global set of bulk soil samples, which was less close than that with the δ^2H_n values of demineralized soil organic matter (Ruppenthal, 2014; Ruppenthal et al., 2015). Ruppenthal et al. (2013) used HF in combination with a recovery procedure for solubilized organic matter and could show that this procedure did not change the stable H isotope ratio of nonexchangeable C-bonded H. This finding suggested that the δ^2H_n values of mineral components of the soil had generally a poorer relationship with the δ^2H values of meteoric water than organic matter or that different minerals showed different relationships resulting in scatter introduced by different mineral compositions. In addition, different ratios of the concentrations of C-bonded, nonexchangeable organic H to those of mineral-bound nonexchangeable H could also have contributed to the poorer relationship. In soils, which are frozen for a longer time, chemical weathering and thus clay mineral formation might be largely restricted to the seasonally nonfrozen period, because mineral formation depends on temperature and the availability of liquid water (Folkoff and Meentemeyer, 1985; Richards and Kump, 2003; Maher, 2010, 2011). Below the freezing point, chemical weathering occurs at a slow rate (Chuvilin et al., 1998; Borden et al., 2010; Lessovaia et al., 2021). Thus, when assessing the relationship between δ^2H values of precipitation and δ^2H_n values of soil clay fractions including periglacial soils, the seasonal mean δ^2H values of meteoric water could be more important than the annual ones.

To eliminate the influence of soil organic matter (SOM) on the δ^2H_n values of pedogenic clay minerals, SOM must be removed, which is commonly done by treatment with H_2O_2 (Hyeong and Capuano, 2000; Gilg et al., 2004; Bauer and Vennemann, 2014). Unfortunately, the SOM removal can be inefficient and selective, especially for samples with a high clay content (Kaiser et al., 2002; Eusterhues et al., 2003; von Lützow et al., 2007). The H_2O_2 treatment removes alkyl-C and aliphatic compounds more completely than aromatic (e.g., lignin) or O-substituted aliphatic ones (e.g., sugars; Leifeld and

Kögel-Knabner, 2001; Mikutta et al., 2005). Therefore, a small contribution of residual C-bonded H to the nonexchangeable H pool of the clay fractions may be unavoidable. However, in previous δ^2H studies of clay fractions, the contribution of C-bonded H to total nonexchangeable H was evaluated and found to be small (Fagan, 2001; Merseburger et al., 2022).

During steam equilibration, exchangeable H is replaced by H of the water vapor, a process that possibly involves equilibrium fractionation of the H isotope ratio with a fractionation factor $\alpha_{ex\text{-}w}$. Equilibrium can be assumed, because Merseburger et al. (2022) tested the time-dependency of the δ^2H value of the steam-treated sample and found that there were almost no changes after a treatment duration of 16 h, which was then suggested as the standard approach. Schimmelmann (1991) found an $\alpha_{ex\text{-}w}$ value of 1.08 for exchangeable H in cellulose, which has thereafter been widely used to determine δ^2H_n values of soil organic matter by steam equilibration assuming that the $\alpha_{ex\text{-}w}$ value found for cellulose is representative for organic matter (Wassenaar and Hobson, 2000, 2003; Sauer et al., 2009; Ruppenthal et al., 2010, 2013, 2015; Soto et al., 2017). Other studies that applied steam equilibration to organic materials and clay minerals neglected equilibrium fractionation thus assuming an $\alpha_{ex\text{-}w}$ value of 1 (Bowen et al., 2005a; Chesson et al., 2009; Qi and Coplen, 2011; Merseburger et al., 2022).

The $\alpha_{ex\text{-}w}$ value needs to be distinguished from the H isotope fractionation factor between ambient water and nonexchangeable H in the clay mineral ($\alpha_{min\text{-}water}$). A variation of the $\alpha_{min\text{-}water}$ values among different clay minerals will blur the potential relationship between the δ^2H values of meteoric water with the δ^2H_n values of clay fractions in unburied topsoils if the clay fractions contain a mixture of different minerals. The $\alpha_{min\text{-}water}$ value for kaolinite is consistently reported as 0.97 in several studies (Savin and Epstein, 1970; Lawrence and Taylor, 1972; Marumo et al., 1980; Gilg and Sheppard, 1996; Méheut et al., 2010). Savin and Epstein (1970) suggested an $\alpha_{min\text{-}water}$ value of 0.93 for montmorillonite, while in other studies 0.97 was reported for montmorillonite and illite (Lawrence, 1970; Lawrence and Taylor, 1972; Taieb, 1990; Sheppard and Gilg, 1996). For glauconite, chlorite, mica and montmorillonite the $\alpha_{min\text{-}water}$ values varied with the octahedral iron concentration (Marumo et al., 1980; Sheppard and Gilg, 1996; Hyeong and Capuano, 2004). The above reported $\alpha_{min\text{-}water}$ values were not determined experimentally but inferred from δ^2H values of clay minerals formed in soils under near-surface conditions. The published $\alpha_{min\text{-}water}$ values

illustrate a small variation among different clay minerals so that we do not expect a strong influence on the hypothesized relationship between the δ^2H values of meteoric water and nonexchangeable H in topsoil clay minerals because of the variable clay mineral composition.

The relationship between the δ^2H values of local meteoric water and the δ^2H_n values of clay minerals could be influenced by study site properties such as hillslope or physical and chemical soil properties. It is e.g., known that translocation processes such as soil erosion might result in the accumulation of allochthonous (i.e., not in-situ formed) clay minerals in colluvial soils (Heimsath et al., 2001; Ferrier and Kirchner, 2008; Schaub et al., 2009; Maher, 2010; Jin et al., 2010), which would then not bear the local δ^2H_n values.

Our overall goal was to evaluate the relationship between the δ^2H values of local meteoric water with the δ^2H_n values of a global set of soil clay fractions collected from unburied topsoils, for which we assumed that the contribution of nonrecrystallized rock-derived clay minerals was negligible. We furthermore only included mineral topsoils (0–10 cm) that were not or in two cases (Gleysols) little influenced by groundwater. We firstly hypothesized that modeled δ^2H values of local meteoric water taken from a GNIP-based model (δ^2H_p) correlated with the δ^2H_n values of soil clay fractions. We secondly hypothesized that the relationship of δ^2H values of local meteoric water and the δ^2H_n values of soil clay fractions is influenced by (a) imperfect removal of soil organic matter, (b) the chosen $\alpha_{ex\text{-}w}$ value needed for evaluating the results of the steam equilibration method, (c) different clay mineral types as assessed via their cation-exchange capacities and XRD analyses and (d) study site properties.

3.2 Material and methods

3.2.1 Samples

We used 30 unburied mineral topsoil samples from nine countries on five continents that cover a wide range of topographical elevations and latitudes and thus δ^2H values of modeled local precipitation (Bowen and Revenaugh, 2003; Bowen, 2017; IAEA/WMO, 2022; see Table 3.1 and Figure 3.1). All samples were taken from the upper mineral horizon, mostly from the first 10 cm, and stored dark and dry for 1–28 years. The soils covered a wide range of parent materials and soil types (Table 3.1). Twenty-

eight of the sampled soils were entirely unaffected by groundwater but two were from groundwater-influenced Gleysols. We collected the latter two samples from the uppermost part of the soil with no or little signs of water influence. We selected 10 samples for mineralogical studies by X-ray powder diffractometry (XRD), which represented both the range of δ^2H values of local meteoric water and the potential cation-exchange capacity (CEC_{pot}). In addition, we made use of XRD mineralogical analyses of topsoil samples from previous studies for samples PA-A9, EC-CAJ, EC-SF1, and EC-BOM (Schrumpf et al., 2001; Messmer et al., 2014).

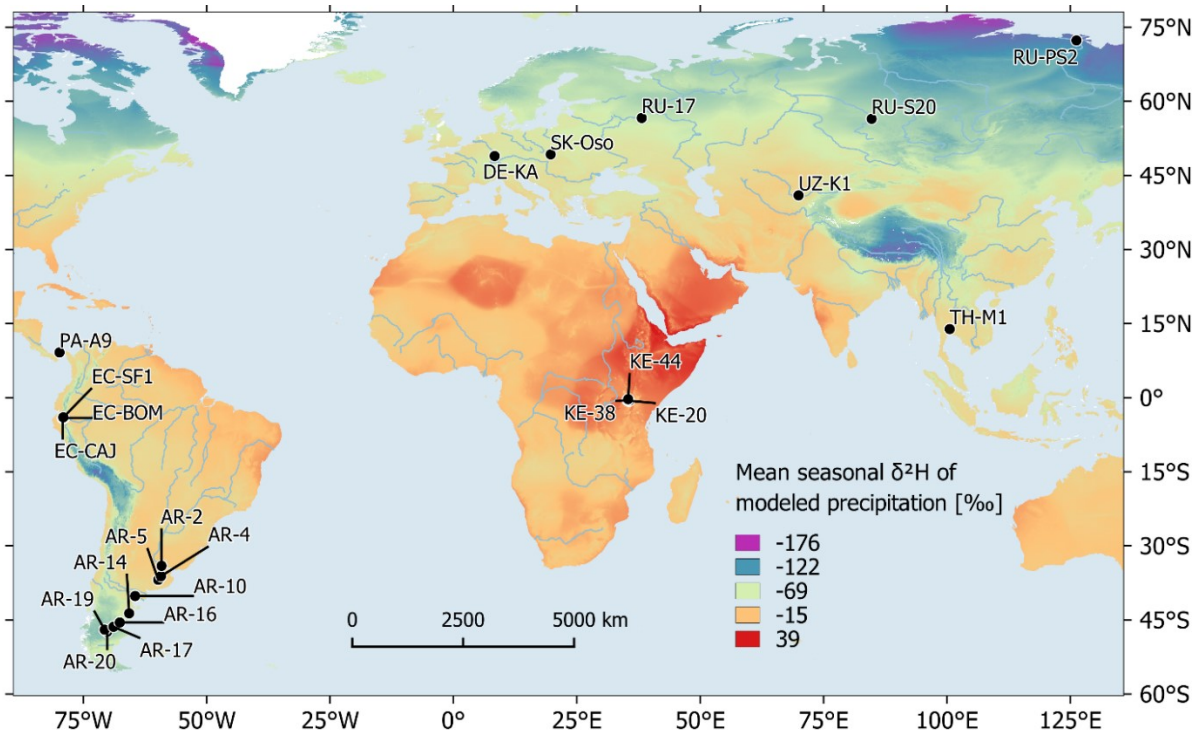

Figure 3.1: Sampling locations and the mean seasonal δ^2H values of meteoric water for months with a mean temperature > 0 °C (Bowen et al., 2005b; IAEA/WMO, 2022).

Table 3.1: Sampling location, topographic position, climatic conditions, δ^2H values and soil properties. The mean δ^2H values of local meteoric water are shown for annual ($\delta^2H_{p,\,annual}$) and seasonal precipitation ($\delta^2H_{p,\,seasonal}$) obtained from the models OIPC3 and RCWIP2.

Sample	Country	Coordinates	Elevation a.s.l	Hillslope	MAT[e]	MAP[e]	PET[f]	Aridity Index[f]	Months > 0 °C	$\delta^2H_{p,annual}$ ± 95% CI (OIPC3)[c]	$\delta^2H_{p,seasonal}$ ±95% CI (OIPC3)[d]	$\delta^2H_{p,annual}$ (RCWIP2)[h]
		[°] [b]	[m]	[°]	[°C]	[mm]					[‰]	
AR-2A	Argentina	-34.061, -59.158	22	2	17.5	1026	1567	0.65	12	-23 ± 1	-26 ± 1	-33
AR-2B		-34.060, -59.159	22	1	17.5	1030	1565	0.66	12	-23 ± 1	-26 ± 1	-33
AR-2C		-34.061, -59.159	22	1	17.5	1030	1565	0.66	12	-23 ± 1	-26 ± 1	-33
AR-4A		-36.147, -59.268	42	0	15.4	992	1426	0.70	12	-28 ± 1	-30 ± 2	-34
AR-5C		-36.878, -59.837	153	0	14.3	930	1413	0.66	12	-33 ± 1	-33 ± 3	-36
AR-10A		-40.169, -64.518	102	0	14.8	266	1908	0.14	12	-48 ± 1	-50 ± 1	-33
AR-10B		-40.169, -64.517	102	0	14.8	266	1908	0.14	12	-48 ± 1	-50 ± 1	-33
AR-10C		-40.168, -64.518	103	1	14.8	266	1908	0.14	12	-48 ± 1	-50 ± 1	-33
AR-14A		-43.677, -65.722	248	0	12.3	186	1792	0.10	12	-61 ± 4	-64 ± 2	-44
AR-16A		-45.526, -67.624	625	2	9.7	194	1742	0.11	12	-84 ± 4	-87 ± 3	-54
AR-17A		-46.388, -68.895	632	7	10.1	170	1791	0.09	12	-93 ± 3	-96 ± 4	-54
AR-19A		-46.987, -70.691	736	7	8.5	155	1571	0.10	12	-97 ± 5	-97 ± 4	-67
AR-19B		-46.989, -70.691	729	7	8.5	155	1571	0.10	12	-97 ± 5	-97 ± 4	-67
AR-19C		-46.987, -70.691	731	7	8.5	155	1571	0.10	12	-97 ± 5	-97 ± 4	-67
AR-20C		-47.409, -70.200	967	2	7.5	180	1619	0.11	12	-102 ± 6	-100 ± 4	-70
DE-KA1	Germany	48.931, 8.357	115	2	10.4	868	917	0.95	12	-58 ± 2	-54 ± 3	-62
DE-KA2		48.962, 8.357	120	1 [a]	10.5	838	922	0.91	12	-58 ± 2	-54 ± 3	-62
EC-BOM	Ecuador	-4.115, -78.968	1065	30 [a]	21.8	1267	1365	0.93	12	-39 ± 2	-40 ± 6	-48
EC-CAJ		-4.108, -79.178	2867	20 [a]	13.1	1119	1142	0.98	12	-66 ± 9	-64 ± 9	-72
EC-SF1		-3.975, -79.075	2057	30 [a]	16.3	911	1132	0.80	12	-54 ± 5	-52 ± 8	-60
KE-20	Kenya	-0.633, 35.593	2386	10	14.7	1323	1427	0.93	12	-5 ± 3	-9 ± 6	-41
KE-38		-0.493, 35.306	2025	4	17.3	1675	1632	1.03	12	0 ± 2	-7 ± 4	-36
KE-44		-0.311, 35.419	2231	19	15.8	1579	1514	1.04	12	-4 ± 2	-9 ± 5	-40
PA-A9	Panama	9.160, -79.838	112	10	26.3	2584	1684	1.53	12	-37 ± 1	-35 ± 2	-19
RU-17	Russia	56.632, 38.173	187	5	4.4	642	751	0.85	7	-88 ± 1	-62 ± 5	-95
RU-PS2		72.339, 126.291	41	0	-13.2	291	364	0.80	4	-167 ± 12	-125 ± 15	-152
RU-S20		56.455, 84.772 [h]	122	1	0.7	514	812	0.63	7	-112 ± 4	-83 ± 5	-105
SK-Oso	Slovakia	49.260, 19.716 [h]	1400	10 [a]	2.8	1284	628	2.04	7	-76 ± 3	-53 ± 2	-85
TH-M1	Thailand	13.890, 100.592	2	1	28.5	1156	1812	0.64	12	-43 ± 1	-39 ± 3	-33
UZ-K1	Uzbekistan	40.959, 69.962 [h]	815	3	12.9	443	1621	0.27	11	-48 ± 2	-44 ± 11	-58

Continued on the next page.

Table 3.1: Continued.

Sample	WRB Soil classification	Depth	C_{org}	N	C_{org}/N	pH	Reference
		[cm]	[g kg^{-1}]				
AR-2A	Phaeozem	0-10	16.3	1.7	9.8	5.3	
AR-2B	Phaeozem	0-10	19.1	1.9	10.1	4.8	
AR-2C	Phaeozem	0-10	18.6	1.9	9.8	5.1	
AR-4A	Phaeozem	0-10	18.9	1.8	10.2	5.2	
AR-5C	Chernozem	0-10	36.7	3.6	10.2	6.2	
AR-10A	Solonetz	0-10	9.1	1.0	8.9	6.9	
AR-10B	Solonetz	0-10	10.4	1.1	9.3	7.0	
AR-10C	Solonetz	0-10	8.5	0.9	9.3	7.0	Ruppenthal et al. (2015)
AR-14A	Calcisol	0-10	4.2	0.8	5.2	6.6	
AR-16A	Solonetz	0-10	12.8	1.4	9.2	6.8	
AR-17A	Luvisol	0-10	19.1	1.4	13.9	6.6	
AR-19A	Vertisol (eroded)	0-10	17.0	1.3	13.2	6.9	
AR-19B	Vertisol (eroded)	0-10	13.1	0.9	13.9	7.1	
AR-19C	Vertisol (eroded)	0-10	14.0	1.0	13.7	7.4	
AR-20C	Planosol (Pseudogley)	0-10	22.6	1.9	12.1	6.1	
DE-KA1	Vertic Eutric Gleysol	7-13	55.0	4.9	11.3	5.9	Merseburger et al. (2022)
DE-KA2	Luvisol	0-12	20.3	1.3	15.3	6.1	
EC-BOM	Dystric Colluvic Cambisol	0-25	24.3	1.9	12.6	4.6	Fabian et al. (2019, 2020)
EC-CAJ	Skeletic Dystric Cambisol	0-11	64.4	4.5	14.3	3.8	Fabian et al. (2020)
EC-SF1	Stagnic Dystric Cambisol	0-15	22.2	1.3	17.4	4.3	Fabian et al. (2019), Wilcke et al. (2002)
KE-20	Humic Cambisol [g]	0-10	48.8	3.9	12.5	5.1	
KE-38	Eutric Cambisol [g]	0-10	37.3	3.9	9.6	5.2	Ojoatre (2022)
KE-44	Eutric Cambisol [g]	0-10	48.4	4.4	11.0	5.7	
PA-A9	Luvisol	0-10	28.2	2.9	0.1	6.5	Messmer (2014), Messmer et al. (2014)
RU-17	Albic Luvisol	0-30	21.6	1.7	12.5	6.7	Siewert (2001, 2004)
RU-PS2	Cryosol	0-8	77.8	5.2	15.0	4.9	Knoblauch et al. (2021)
RU-S20	Lamellic Luvisol	0-10	20.3	0.8	25.8	5.3	Siewert et al. (2004; 2009)
SK-Oso	Dystric Cambisol	0-10	60.0	4.4	13.6	3.6	Lobe et al. (1997; 1998), Merseburger et al. (2022)
TH-M1	Eutric Gleysol	0-5	23.1	2.2	10.5	7.2	Müller et al. (1998; 2000), Wilcke et al. (1998)
UZ-K1	Haplic Calcisol	0-10	14.0	not available		7.8	Bandowe et al. (2010), Shukurov et al. (2009)

n.a. is not applicable.

[a] Slopes were measured in the field. The other slopes are derived from ALOS Global Digital Surface Model „ALOS WORLD 3D – 30m“ (version 3.2, Japan Aerospace Exploration Agency, 2021).

[b] Coordinates are in decimal degree WGS84, noted as north-positive latitude and east-positive longitude.

[c] OIPC3 is the Online Isotopes in Precipitation Calculator (version 3.1) from Bowen (2017) and Bowen and Revenaugh (2003), “CI” is the confidence interval.

[d] Mean δ^2H values of the mean annual meteoric water in months with a mean temperature > 0 °C (weighted by volume), “CI” is the confidence interval.

[e] MAT is mean annual temperature. MAP is mean annual precipitation. Data from the Worldclim dataset of the years 1970–2000 (Fick and Hijmans, 2017).

[f] PET is the annual average potential evapotranspiration for a reference crop. From Trabucco and Zomer (2019).

[g] From the Soil and Terrain database for Kenya (ISRIC World Soil Information, 2007).

[h] RCWIP2 is the Regionalized Cluster-Based Water Isotope Prediction model (version 2) from Terzer-Wassmuth et al. (2021).

3.2.2 Clay separation, steam equilibration and hydrogen isotope ratio measurement

We used the clay separation, steam equilibration and isotope ratio mass spectrometry (IRMS) methods of Merseburger et al. (2022). In short, we first collected the fine earth fraction of the soil samples by sieving the air-dry soil to <2 mm, including gentle crushing of soil aggregates. From the fine earth we removed Fe oxides with the dithionite-citrate-buffer (DCB) method of Mehra and Jackson (1960). To remove carbonates, we used a Na-acetate acetic acid buffer adjusted to pH 4.8. To remove organic matter, we added H_2O_2 in a water bath at 50 °C. After each sample treatment, we removed water-soluble salts by washing with deionized water and measured electrical conductivity (EC). Washing was repeated until the EC of the supernatants had reached <400 µS/cm. We determined the grain sizes by pipet analysis according to DIN ISO 11277 (2002), but instead of a dispersion agent we used water with a pH of ~7.5. In this water, we separated the grain sizes by a repeated sedimentation in 2-L cylinders. The clay fractions (<2 µm) were precipitated with $MgCl_2$. A H_2O_2 treatment of the precipitate reduced the organic matter concentration in the clay fractions further. After final washings until the EC of the supernatant had reached <100 µS/cm, the clay fractions were dried at 60 °C and pulverized. Merseburger et al. (2022) had shown that this treatment did not change the δ^2H value of the nonexchangeable H pool (δ^2H_n), while possible changes of the δ^2H value of the exchangeable H pool did not matter, because we removed the influence of the exchangeable H pool on the δ^2H_n values by steam equilibration with waters of known H-isotopic compositions (see below).

The 30 samples were distributed among four treatment batches. Each treatment batch was processed in approximately 10–12 weeks. As quality check, we included the sample SK-Oso in each treatment batch. Based on the repeated measurements of this sample, we quantified the precision of our methods, which showed a relative standard deviation (RSD, in % of the mean) of 2% for each of the sand, silt and clay contents, 2% for the dithionite-citrate-extractable Fe concentration (Fe_d), 6, 5 and 4% for the C, N and H concentrations, respectively and 5% for the potential cation-exchange capacity (CEC_{pot}). As a measure for the spatial variation of the studied soils we analyzed three samples from northern, central and southern Argentina (AR-2, AR-10, AR-19) in triplicates (-A, -B and -C), collected in the field with approximately 100 m distance from each other (Ruppenthal et al., 2015, Table 3.1). The three replicate sites showed the

same modeled δ^2H values of meteoric water. The three replicates were each treated in separate batches, steam equilibration and IRMS measurement runs to guarantee statistical independence and thus allow for statistical evaluation. For steam equilibration, we weighed 1–2 mg of the clay fractions (<2 µm, collected by sedimentation) into smooth-walled tin capsules. In previous work, both tin and silver capsules were successfully used for H isotope ratio measurements (Qi et al., 2014; Gehre et al., 2015; Oerter et al., 2017; Schimmelmann et al., 2020). We chose Sn instead of Ag capsules, because Sn is softer than Ag and thus can be more easily crimp-sealed so that we could more reliably ensure that the capsules were air-tight. The samples were vacuum-dried for 2 h at 120 °C. Then, we injected water of known isotopic composition into the closed stainless-steel vessel. Following Merseburger et al. (2022) who found that there were only little changes in the δ^2H value of the steam-treated sample after 16 h, we used this duration for steam-equilibration of our samples. This was followed by 1 h of vacuum drying at 120 °C and a 2-h cooling phase at room temperature (<1 Pa). We transferred the vacuum chamber into a glove bag, flushed twice with dried Ar for a moisture-free atmosphere. We sealed each of the up to 80 capsules in the vacuum vessel with a gas-tight pressing in the Ar atmosphere so that some Ar was enclosed with the sample. Later, we discarded all IRMS measurements of capsules, for which the thermal conductivity sensor of the EA-IRMS could not detect an Ar peak after the H_2 peak in the gas chromatogram, because we interpreted the lack of an Ar peak as indication of a leak through which the enclosed Ar had escaped (and ambient air possibly entered the sample). We steam equilibrated our samples with three different waters of known δ^2H values (AWI–TD1: -266‰, medium deuterium-enriched water: 137‰; highly deuterium-enriched water: 335‰). We produced the two deuterium-enriched waters by mixing ^2H_2O and ultrapure water (Faghihi et al., 2015).

After weighing the cooled capsules, we measured them with an Elemental Analyzer-Isotope Ratio Mass Spectrometer by pyrolysis in a chromium-filled Al_2O_3 reactor at 1250 °C. For normalization, VSMOW, SLAP and, when the steam equilibration was performed with deuterium-enriched water, IAEA-604 were included as silver capsule triplicates (25 µL, USGS, Reston, VA, USA) in each IRMS sequence. Over the duration of the experimental period, a PE-powder used as in-house standard was measured with a mean δ^2H value of -61.4 ± standard deviation 1.4‰ (n = 490), GISP with -188.8 ± 1.9‰ (n = 72) and IAEA-CH7 with -100.3 ± 1.5‰ (n = 88). The values were

undistinguishable from the certified or recommended values. The four times separately treated sample SK-Oso showed a standard deviation of the δ^2H_n values of 2.8‰ and for the contributions of the exchangeable H to the total H pool (χ_e) an RSD of 4%.

3.2.3 Chemical sample properties

The C concentrations of the clay fractions were determined with an Elemental Analyzer (Flash 2000 HTC, Thermo Fisher, Waltham, MA, USA and EuroVector 3000, EuroVector, Pavia, Italy). The pH of the topsoil samples was measured with a glass electrode (SenTix® 81 on pH 3310, WTW, Weilheim, Germany) in a deionized water suspension at a soil:water ratio of 1:2.5 (v/v). The potential cation-exchange capacity (CEC_{pot}) of the clay fractions collected by sedimentation was determined with the Cu(II)-triethylentetramine method (Meier and Kahr, 1999; Ammann et al., 2005), using additionally a phosphate puffer (pH = 7.0) and 24 h shaking time. We used the CEC_{pot} of the clay fractions to distinguish two sample groups. Following international soil classification systems (Soil Survey Staff, 2014) we used a CEC_{pot} of 160 $mmol_c\ kg^{-1}$ as threshold to distinguish samples which were dominated by nonswellable clay minerals including kaolinite, illite and chlorite, indicating an advanced state of acidification and weathering, from samples which were dominated by swellable three-layer clay minerals such as smectites and vermiculites indicating a less advanced soil development. This rough grouping was confirmed by our XRD analyses of 10 selected samples and by the results of Schrumpf et al. (2001) and Messmer et al. (2014), who reported clay mineralogical results from nearby sites in Ecuador and the same sample as we studied from Panama, respectively (Table 3.1).

To determine the concentrations of Na, Mg, Al, K, Ca and Fe, we weighed 0.1 g of the clay fractions in 55-mL pressure vessels (TFM, MARS XPress, CEM, Matthews, NC, USA). We added 2 mL HNO_3 (69% suprapur, HN50.3, Carl Roth, Karlsruhe, Germany), 0.5 mL H_2O_2 (30%, suprapur Merck, Darmstadt, Germany) and 1.5 mL HF (48%, suprapur, HN54.1, Carl Roth, Karlsruhe, Germany). The samples were digested in a microwave oven (MARS XPress, CEM, Matthews, NC, USA) for 1 h (max. 200 °C). After >20 min cooling time, we added 10 mL 5% H_3BO_3 (P6943.1, Carl Roth, Karlsruhe, Germany) to complex residual HF in the microwave oven for security reasons. Afterwards, the solutions were transferred into a volumetric flask and made up to 50 mL with ultrapure water. An aliquot of 100 µL was diluted with 1% HNO_3 solution to 10 mL

for the ICP-MS (Agilent 7900, Santa Clara, CA, USA) and ICP-OES (Agilent 5100, Santa Clara, CA, USA) measurements, calibrated with the Multielement Standard IV (Merck 1.11355.0100, Darmstadt, Germany) in a similar matrix (0.3 mL H_3BO_3 (p.a.) and 1 mL 69% HNO_3). The accuracy of concentration measurements was checked by repeated analysis of the reference materials BCR-2 (Basalt, Columbia River, USGS, Denver, CO, USA) in each digestion batch (n = 2). If the recovery of BCR-2 deviated by > 10% from the certified elemental value, we repeated the digestion batch. The RSD of BCR-2 was 4% for Na, 1% for Mg, Al, K and Ca and 3% for Fe.

3.2.4 XRD analysis of the clay fractions

We selected 10 samples for qualitative mineralogical studies by X-ray powder diffractometry (XRD) to equally cover a representative range of δ^2H values of modeled local precipitation and potential cation exchange capacity (CEC_{pot}). The qualitative characterization of the clay minerals by X-ray diffraction was performed at the CCA-BW of the University of Tübingen, Germany using the air-dried clay fractions. The samples were prepared like random-oriented powders with a final smoothing out of the sample surface in standard powder sample holders. Thus, a preferential orientation of the clay particles is still to be expected, which increases the 00l-intensities of the clay minerals compared to the other lattice directions. For the measurements a BRUKER D8-advance powder diffractometer was used, equipped with a Cu-sealed tube running at 40 kV/20 mA, a Göbel mirror optics for parallel beam and Kα-radiation, a 0.2 mm divergence slit and a VANTEC-1 detector in scanning mode with a step size of 0.008°. The samples were rotated during the measurement from 2° to 30° 2θ, average measurement time was 1.5 h. The resulting pattern of the air-dried samples permitted a semiqualitative identification of all containing mineral phases in the clay fraction and allowed for an estimation whether two-layer or three-layer clay minerals were present, using Brindley and Brown (1980).

3.2.5 Data evaluation

We normalized all stable H isotope ratios to the VSMOW-SLAP scale (Paul et al., 2007), which we extended with IAEA-604 to 799.9‰, and expressed them in ‰ relative to Vienna Standard Mean Ocean Water (VSMOW). We used the R statistical

computing environment (Wickham et al., 2019; R Core Team, 2022) to calculate stable H isotope data and for statistical analysis. Significance was set to $p < 0.05$.

We regressed the known H isotope composition of the equilibration waters (δ^2H_w) on the measured δ^2H_t (t = total) values of the clay fractions and used Eq. 3.1 to determine δ^2H_n values and the contribution of the exchangeable to the total H concentration (χ_e) (Feng et al., 1993; Wassenaar and Hobson, 2000; Sessions and Hayes, 2005; Ruppenthal et al., 2010).

$$\delta^2H_t = \chi_e\, \alpha_{ex-w}\, \delta^2H_w + (1-\chi_e)\delta^2H_n + 1000\, \chi_e(\alpha_{ex-w} - 1) \qquad (Eq.\ 3.1)$$

The intercept is a function of χ_e, δ^2H_n and $\alpha_{ex\text{-}w}$. The slope is the product of χ_e and $\alpha_{ex\text{-}w}$. Using the latter and δ^2H_t from the regression line for $\delta^2H_w = 0$, Eq. 3.1 is solved for δ^2H_n (Eq. 3.2).

$$\delta^2H_n = \frac{\alpha_{ex-w}\ \text{intercept} - 1000\ \text{slope}\ (\alpha_{ex-w}-1)}{\alpha_{ex-w} - \text{slope}} \qquad (Eq.\ 3.2)$$

For Eq. 3.2, we assumed either no fractionation ($\alpha_{ex\text{-}w}$=1; Bowen et al., 2005a; Chesson et al., 2009; Qi and Coplen, 2011; Merseburger et al., 2022) or $\alpha_{ex\text{-}w}$ =1.08 (Wassenaar and Hobson, 2000, 2003; Sauer et al., 2009; Ruppenthal et al., 2010, 2013, 2015; Soto et al., 2017), which covered the range of $\alpha_{ex\text{-}w}$ values reported in the literature. The standard deviation (SD) of the δ^2H_n values was estimated by using Gaussian error propagation (Merseburger et al., 2022). We recalculated the δ^2H_n values for bulk soil and SOM reported by Ruppenthal et al. (2014; 2015) for $\alpha_{ex\text{-}w}$ = 1 with the help of the reported χ_e values.

We calculated the mean annual δ^2H values of local meteoric water, called "precipitation" (p) in the cited literature source ($\delta^2H_{p,\,annual}$) for all our study sites with the Online Isotopes in Precipitation Calculator (OIPC3, version 3.1; Bowen, 2017; Bowen & Revenaugh, 2003). Additionally, $\delta^2H_{p,\,annual}$ was extracted from the gridded maps of a Regionalized Cluster-Based Water Isotope Prediction model (RCWIP2) from Terzer-Wassmuth et al. (2021). To calculate mean seasonal δ^2H_p values ($\delta^2H_{p,\,seasonal}$) representing the volume-weighted mean δ^2H_p value of the months with an average temperature >0 °C (Bowen et al., 2005b), we used the δ^2H_p values of the OIPC3 and temperature and precipitation data of the sampling locations from the years 1970–2000 (Fick and Hijmans, 2017). The 95% confidence intervals of the $\delta^2H_{p,\,seasonal}$ values were taken from raster grids (Bowen et al., 2005b).

To test for normal distribution, we used the Shapiro-Wilk Normality test. If necessary, we transformed the variables to their logarithmic, reciprocal or square root

values based on the skewness of the original distribution (Webster, 2001). Linear models were validated by investigating their residuals with the Shapiro-Wilk test for normal distribution and using the Breusch-Pagan test for homoscedasticity. For the multiple regression, we used globally available climatic and topographic variables (Table 3.1). We used principal component analysis (normalized and varimax rotated) to identify statistically independent explanatory variables and only accepted principal components with eigenvalues > 1 (Revelle, 2021). As independent explanatory variables, we used the highest loading variable of each principal component. We implemented stepwise multiple regression analysis with the R packages "StepReg" (Li et al., 2021), using the corrected Akaike information criterion to choose the best model in a bi-directional model selection process with 0.05 as significance threshold for in- or exclusion of variables. Relative weights were determined with the R package "relaimpo" (Grömping, 2007).

In line with reports from the literature, we did not fully get rid of some remaining organic matter in the clay fractions, particularly at high clay concentrations (Kaiser et al., 2002; Mikutta et al., 2005; von Lützow et al., 2007). Therefore, we roughly corrected the measured δ^2H values of the clay fractions ($\delta^2H_{n,clay}$) with Eq. 3.3 and 3.4. For this purpose, we used an updated regression of the δ^2H_n values of soil organic C concentrations on δ^2H values of the mean annual local precipitation of Ruppenthal et al. (2014; 2015), because the number of worldwide stations contributing to the Online Isotopes in Precipitation Calculator had tripled since 2015 (Bowen, 2017).

$$\delta^2H_{n,inorg.clay} = \frac{\delta^2H_{n,clay} - f_{n,SOM}\,\delta^2H_{n,SOM}}{1 - f_{n,SOM}} \qquad (Eq.\ 3.3)$$

$$\delta^2H_{n,SOM} = 0.985\,\delta^2H_p - 54.6‰ \qquad (Eq.\ 3.4)$$

$\delta^2H_{n,\ inorg.\ clay}$ is the δ^2H_n value corrected for the contribution of SOM and thus that of the inorganic part of the clay fractions. $f_{n,\ SOM}$ is the contribution of C-bonded H in SOM to the total nonexchangeable H in our soil clay fractions. The C-bonded H from SOM was estimated by assuming 25 g of H per kg of C_{org} (Rice and MacCarthy, 1991; additionally assuming that SOM contains 50% C) and that 80% of this H was nonexchangeable (Schimmelmann, 1991; Wassenaar and Hobson, 2000; Ruppenthal et al., 2013). We furthermore assumed that the clay separation procedure did not change the δ^2H_n value of the SOM. We are aware of the fact that all these assumptions include an unknown uncertainty. However, our purpose was to qualitatively assess the importance of the

organic matter, which we couldn't get rid of with our treatment for our measures of the δ^2H_n values of soil clay separates.

3.3 Results

3.3.1 Relationship of the δ^2H values of meteoric water with the δ^2H_n values of clay fractions

The δ^2H_n values of the clay fractions, calculated with Eq. 3.2, ranged from -167‰ for north Siberia to -44‰ for west Kenia, calculated with $\alpha_{ex\text{-}w} = 1$ and from -191‰ for south Argentina (-181‰ for north Siberia) to -81‰ for west Kenia for $\alpha_{ex\text{-}w} = 1.08$ (Table 3.2). No matter which $\alpha_{ex\text{-}w}$ was used, there was always a significant correlation between the local mean annual and seasonal δ^2H values of meteoric water obtained from the OIPC3 model (Bowen, 2017) and the δ^2H_n values of the clay fractions (Figure 3.2). Without the low δ^2H_n values of the clay fractions at the sites AR-5C and AR-4A, which could be considered as outliers, the R^2 values of the four regression lines in Figure 3.2 improved from 0.42–0.77 to 0.58–0.88. When we used the RCWIP2 model (Terzer-Wasmuth et al., 2021) to generate the δ^2H values of local mean annual meteoric water, the results changed little except that the p value of the correlation between the δ^2H values of meteoric water and the nonexchangeable H pool in the soil clay fractions was just not significant anymore for $\alpha_{ex\text{-}w} = 1.08$ ($p = 0.102$, Figure 3.S1).

For the Argentinian climosequence (Sites AR-2 to AR-20, Table 3.2) described by Ruppenthal et al. (2015), the δ^2H_n values of the clay fractions were at all study sites consistently lower than those of demineralized SOM (data taken from Ruppenthal et al., 2015 and recalculated for $\alpha_{ex\text{-}w} = 1$; the difference in the δ^2H_n values of the clay fractions and the demineralized organic matter (Δ^2H) ranged from 4 to 54‰ for $\alpha_{ex\text{-}w} = 1$ and from 21 to 86‰ for $\alpha_{ex\text{-}w} = 1.08$; Figure 3.3). As expected, the bulk soil (data taken from Ruppenthal, 2014, and recalculated for $\alpha_{ex\text{-}w} = 1$) fell in between demineralized organic matter following the procedure of Ruppenthal et al. (2013) and clay fractions for both $\alpha_{ex\text{-}w}$ values.

Table 3.2: Selected physical and chemical properties of the studied bulk soil samples and clay fractions.

Sample	Bulk samples				Clay fractions													
	Sand	Silt	Clay	Fe_d	C_{org}	N	Na	Mg	Al	K	Ca	Fe	CEC [a]	$\delta^2H_{n,\alpha=1} \pm SD$ [b]	$\chi_{e,\alpha=1} \pm SD$ [bc]	$\delta^2H_{n,\alpha=1.08} \pm SD$ [b]	$\chi_{e,\alpha=1.08} \pm SD$ [bc]	$H \pm SD$ [d]
	[%]				[g kg^{-1}]								[mmol$_c$ kg^{-1}]	[‰]	[%]	[‰]	[%]	[mg g^{-1}]
AR-2A	7.9	68.3	23.8	5.9	2.9	0.7	9.3	10.0	105	22.2	1.5	40.9	261	-91 ± 10	42.9 ± 2	-138 ± 9	39.7 ± 2	7.2 ± 0.1
AR-2B	5.4	69.5	25.1	5.3	2.8	0.6	10.1	9.4	97.3	22.7	1.5	39.9	283	-88 ± 7	41.1 ± 1.6	-133 ± 7	38.1 ± 1.6	7.4 ± 0.4
AR-2C	6.7	72.0	21.3	6.3	3.8	0.7	9.8	9.3	98.7	22.8	1.4	38.6	257	-93 ± 3	46.2 ± 0.7	-148 ± 3	42.8 ± 1	7.4 ± 0.1
AR-4A	47.4	40.4	12.2	3.1	8.4	0.9	9.2	7.1	81.9	13.6	2.5	32.7	199	-108 ± 8	50.9 ± 1.4	-172 ± 7	47.1 ± 1.5	8 ± 0.2
AR-5C	30.3	52.5	17.3	2.7	8.4	0.6	14.7	8.6	83.2	13.9	5.4	38.9	217	-118 ± 5	40.1 ± 1.1	-160 ± 5	37.1 ± 1.2	6.5 ± 0.1
AR-10A	49.6	25.8	24.7	5.3	1.0	0.2	16.3	20.2	94.5	19.0	3.7	50.2	531	-106 ± 2	39.9 ± 0.5	-148 ± 2	37 ± 0.8	7.2 ± 0.1
AR-10B	49.3	28.1	22.6	4.9	1.0	0.2	15.4	17.2	86.0	17.5	3.6	47.4	554	-105 ± 5	39.8 ± 1.2	-147 ± 5	36.8 ± 1.3	7.5 ± 0.3
AR-10C	49.0	31.2	19.7	6	1.1	0.2	13.4	16.5	89.6	16.6	3.8	47.4	499	-113 ± 2	44.4 ± 0.3	-162 ± 2	41.1 ± 0.8	7.2 ± 0.1
AR-14A	75.7	12.4	11.9	3.8	1.1	0.2	16.3	15.5	89.0	17.2	4.4	47.4	248	-118 ± 8	40.8 ± 1.6	-161 ± 8	37.8 ± 1.7	7.6 ± 0.6
AR-16A	71.4	13.9	14.7	4.5	3.7	0.3	13.9	11.4	96.5	13.3	3.3	51.7	497	-128 ± 6	41.6 ± 1.3	-172 ± 6	38.5 ± 1.4	8.4 ± 0.4
AR-17A	71.1	13.3	15.6	5.7	4.8	0.3	14.8	13.8	93.9	10.0	2.2	55.7	664	-130 ± 9	42.6 ± 1.7	-176 ± 8	39.5 ± 1.7	9.8 ± 5.2
AR-19A	58.3	17.6	24.1	3.5	3.2	0.2	15.7	16.9	93.3	12.3	3.3	49.5	640	-132 ± 2	37 ± 0.4	-168 ± 2	34.3 ± 0.7	7.1 ± 0.1
AR-19B	60.2	20.1	19.7	2.9	3.0	0.2	17.8	15.0	83.7	12.9	4.2	47.3	598	-142 ± 3	38 ± 0.6	-179 ± 3	35.2 ± 0.8	6.7 ± 0.1
AR-19C	46.9	23.5	29.6	4	2.6	0.2	15.7	17.6	90.1	9.4	1.8	50.7	796	-139 ± 6	35.2 ± 1.2	-172 ± 5	32.6 ± 1.2	7.2 ± 0.1
AR-20C	73.5	16.7	9.8	7.5	5.3	0.4	n.a.	n.a.	n.a.	n.a.	n.a.	n.a.	423	-132 ± 5	49.8 ± 0.9	-191 ± 5	46.1 ± 1.2	8.5 ± 0.1
DE-KA1	9.2	33.0	57.7	7.7	12.5	1.6	8.3	12.1	132	21.6	0.7	28.3	296	-94 ± 7	34.7 ± 1.9	-128 ± 7	32.2 ± 1.8	11.3 ± 0.4
DE-KA2	62.4	29.2	8.4	4	27.6	0.8	10.4	14.1	106	21.6	2.9	28.8	145	-107 ± 4	4.1 ± 1.3	-128 ± 4	22.8 ± 1.2	8.8 ± 2.3
EC-BOM	57.5	13.9	28.6	11.7	12.6	1.1	2.8	2.1	221	9.3	n.d.	10.1	127	-61 ± 2	30.1 ± 0.6	-90 ± 2	27.9 ± 0.8	20.4 ± 0.3
EC-CAJ	21.8	51.0	27.2	2.1	58.9	3.0	11.5	7.9	141	26.9	n.d.	16.8	153	-109 ± 2	14.3 ± 0.6	-120 ± 2	13.2 ± 0.6	13.7 ± 0.4
EC-SF1	24.2	54.1	21.7	23.2	7.0	1.1	8.0	6.9	165	35.2	n.d.	16.9	143	-71 ± 2	17 ± 0.6	-85 ± 2	15.7 ± 0.6	10 ± 0.4
KE-20	8.8	26.6	64.6	74.9	6.9	1.0	4.3	2.7	173	5.1	0.1	26.8	204	-44 ± 4	41.3 ± 0.9	-91 ± 4	38.3 ± 1.1	14.8 ± 0.2
KE-38	6.9	19.5	73.6	56.2	4.5	0.8	3.8	2.0	172	3.2	0.0	24.0	189	-44 ± 6	35.1 ± 1.4	-81 ± 5	32.5 ± 1.4	16.3 ± 0.8
KE-44	4.1	25.1	70.8	63.3	4.5	0.9	7.1	4.8	167	8.3	0.1	43.6	344	-56 ± 3	43.2 ± 0.6	-106 ± 3	40 ± 0.9	13.5 ± 0.1
PA-A9	1.9	14.1	84.0	18.6	1.9	0.2	16.0	17.9	118	1.8	0.0	55.9	872	-85 ± 5	28.3 ± 1.3	-111 ± 5	26.2 ± 1.3	8.4 ± 0.4
RU-17	2.6	84.5	12.9	6.4	7.2	1.0	8.0	14.6	111	22.8	0.9	39.3	241	-101 ± 6	32.9 ± 1.5	-133 ± 6	30.5 ± 1.5	8.6 ± 0.6
RU-PS2	19.0	68.3	12.7	12.2	31.5	1.0	11.7	17.3	117	22.1	1.6	43.5	240	-167 ± 1	19.4 ± 0.2	-181 ± 1	17.9 ± 0.4	11.6 ± 0.6
RU-S20	83.5	12.4	4.1	3.1	29.3	0.7	10.6	19.5	119	16.7	3.2	36.3	114	-136 ± 2	31.5 ± 0.5	-164 ± 2	29.2 ± 0.7	11 ± 0.5
SK-Oso	33.5	51.2	15.1	9.5	35.5	2.8	6.6	18.7	111	40.6	0.2	8.5	121	-99 ± 3	17.8 ± 0.8	-113 ± 3	16.1 ± 0.9	10.3 ± 0.4
TH-M1	15.9	47.2	36.9	17.6	2.0	0.5	7.3	13.0	257	20.4	0.4	59.9	297	-84 ± 14	18.9 ± 4.7	-100 ± 13	17.5 ± 4.3	9.8 ± 0.5
UZ-K1	9.5	60.9	29.6	7.3	1.5	0.5	8.8	25.4	106	32.1	1.4	46.2	311	-102 ± 6	23.8 ± 1.7	-123 ± 6	22 ± 1.6	8.3 ± 0.3

n.a. – not available.
n.d. – not detected.
SD – standard deviation.
[a] CEC is the potential cation-exchange capacity.
[b] n = 1, SD is derived by Gaussian error propagation, except for SK-Oso with n=4.
[c] χ_e is the exchangeable fraction of the total H.
[d] n = 5–15 repeated measurements after one treatment, except for SK-Oso (four separate treatments).

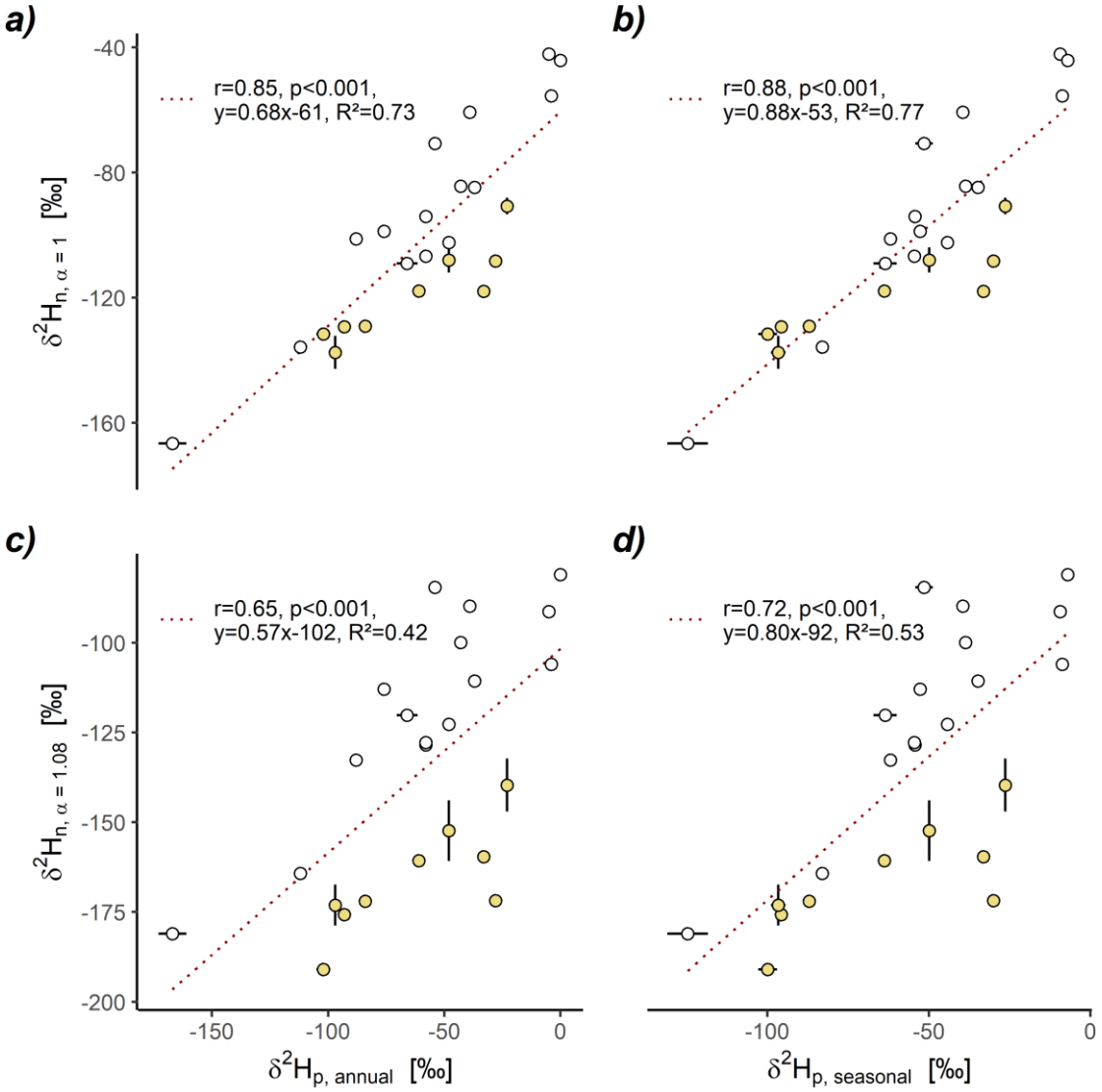

Figure 3.2: Relationship between the δ^2H values of local mean annual (a, c) or seasonal (b, d) meteoric water (δ^2H_p) and the δ^2H_n values of soil clay fractions for an equilibrium fractionation factor between water-H (in the steam) and exchangeable H ($\alpha_{ex\text{-}w}$) of 1 (a, b) and 1.08 (c, d). δ^2H_p is from the Online Isotopes in Precipitation Calculator, version 3.1 (Bowen 2017). The yellow filling marks the samples from Argentina. The error bars of δ^2H_p values indicate the 68% confidence interval and might be smaller than the symbol size. The error bars of δ^2H_n values indicate the standard deviation from field triplicates, available for only three sample locations from Argentina.

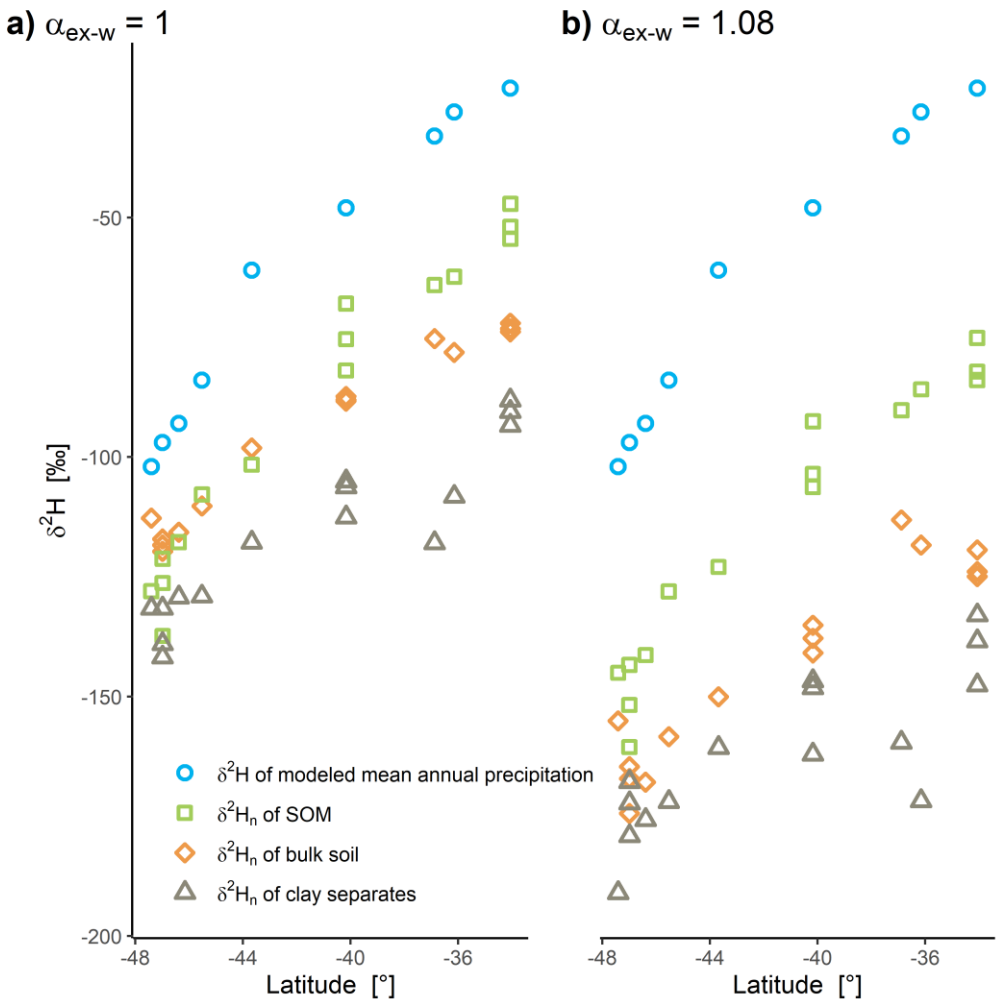

Figure 3.3: Relationship between latitude and the δ^2H values of local mean annual meteoric water and the δ^2H_n values of demineralized soil organic matter (SOM), bulk soil and soil clay fractions for an equilibrium fractionation factor between water-H (in the steam) and exchangeable H (α_{ex-w}) of 1 (a) and 1.08 (b). The data for the bulk soil and the demineralized soil organic matter from a 2100-km climosequence from north to south Argentina were taken from Ruppenthal (2014) and Ruppenthal et al. (2015) who used an α_{ex-w} value of 1.08 (b), which we additionally recalculated for α_{ex-w} = 1 (a). The δ^2H values of meteoric water were taken from the Online Isotopes in Precipitation Calculator, version 3.1, where precipitation includes rain, snow, dew and hail (Bowen, 2017).

3.3.2 Influence of the soil organic matter removal

Two of the 30 samples (DE-KA2 and SK-Oso) had higher C_{org} concentrations in the clay fractions than in the bulk soils, while the inorganic C had been destroyed during the clay separation procedure (Table 3.1 and 3.2). With a minimum concentration of 1.0 mg g^{-1} C_{org}, none of the clay fractions was completely free of SOM (Table 3.2). When

we roughly estimated the influence of the organic matter on the δ^2H_n values of the clay fractions with Eqs. 3.3 and 3.4, the δ^2H_n values of the clay fractions on average only changed by <3.4‰ but by up to 19‰ in the individual samples (Table 3.3).

Table 3.3: Effect of the correction for C-bonded H in soil organic matter on the δ^2H_n values in the clay fractions (expressed as difference between the δ^2H_n values before and after correction, δ^2H_{uncorr}-SOM_{corr}) and on the properties of the regression line of the δ^2H_n values of soil clay fractions on the δ^2H values of meteoric water (expressed as differences, subscript diff, in intercept, slope and coefficient of determination for two different fractionation factors between steam and exchangeable H ($\alpha_{ex\text{-}w}$) and local mean annual and mean seasonal meteoric water (δ^2H_p values taken from Bowen 2017).

$\alpha_{ex\text{-}w}$	δ^2H_p	$\Delta^2H_{uncorr\text{-}SOM\ corr}$				linear regression $\delta^2H_{n,\,clay}$–$\delta^2H_{p\ uncorr\text{-}SOMcorr}$		
		mean	SD	min.	max.	$intercept_{diff}$	$slope_{diff}$	R^2_{diff}
		[‰]						
1.08	annual	1.6	5.9	-14	17	6.2	0.078	0.13
1.08	seasonal	3.4	4.7	-2	17	3.9	0.01	0.07
1	annual	-2.7	5.9	-19	6	3.5	0.105	0.15
1	seasonal	-0.8	2.5	-5	6	0.9	0.031	0.06

3.3.3 Influence of the preliminary $\alpha_{ex\text{-}w}$ values

The differences between the δ^2H_n values calculated with $\alpha_{ex\text{-}w}$ = 1.08 and $\alpha_{ex\text{-}w}$ = 1, respectively, for the same sample ranged from 11‰ to 64‰ with a mean of 35‰. The size of these differences was positively related with the concentrations of exchangeable H (χ_e) which can be derived from Eq. 3.2 indicating that the choice of the $\alpha_{ex\text{-}w}$ value influenced the calculated δ^2H_n values the more the smaller the nonexchangeable H pool was relative to the total H pool. The differences in the δ^2H_n values calculated with different $\alpha_{ex\text{-}w}$ values influenced the regression lines in Figure 3.2 but did not change the general positive relationship between the δ^2H values of meteoric water and the δ^2H_n values of clay fractions.

3.3.4 Influence of the dominant clay mineral type

To distinguish between samples dominated by nonswellable clay minerals and swellable clay minerals, we used the CEC_{pot} of the clay fraction. Following the common practice in international soil classification systems (Soil Survey Staff, 2014; IUSS Working Group WRB, 2022), we used a CEC_{pot} of 160 $mmol_c$ $(kg\ clay)^{-1}$ to distinguish

strongly and less strongly weathered soil environments. We tested this grouping with the help of XRD analyses (Figure 3.4).

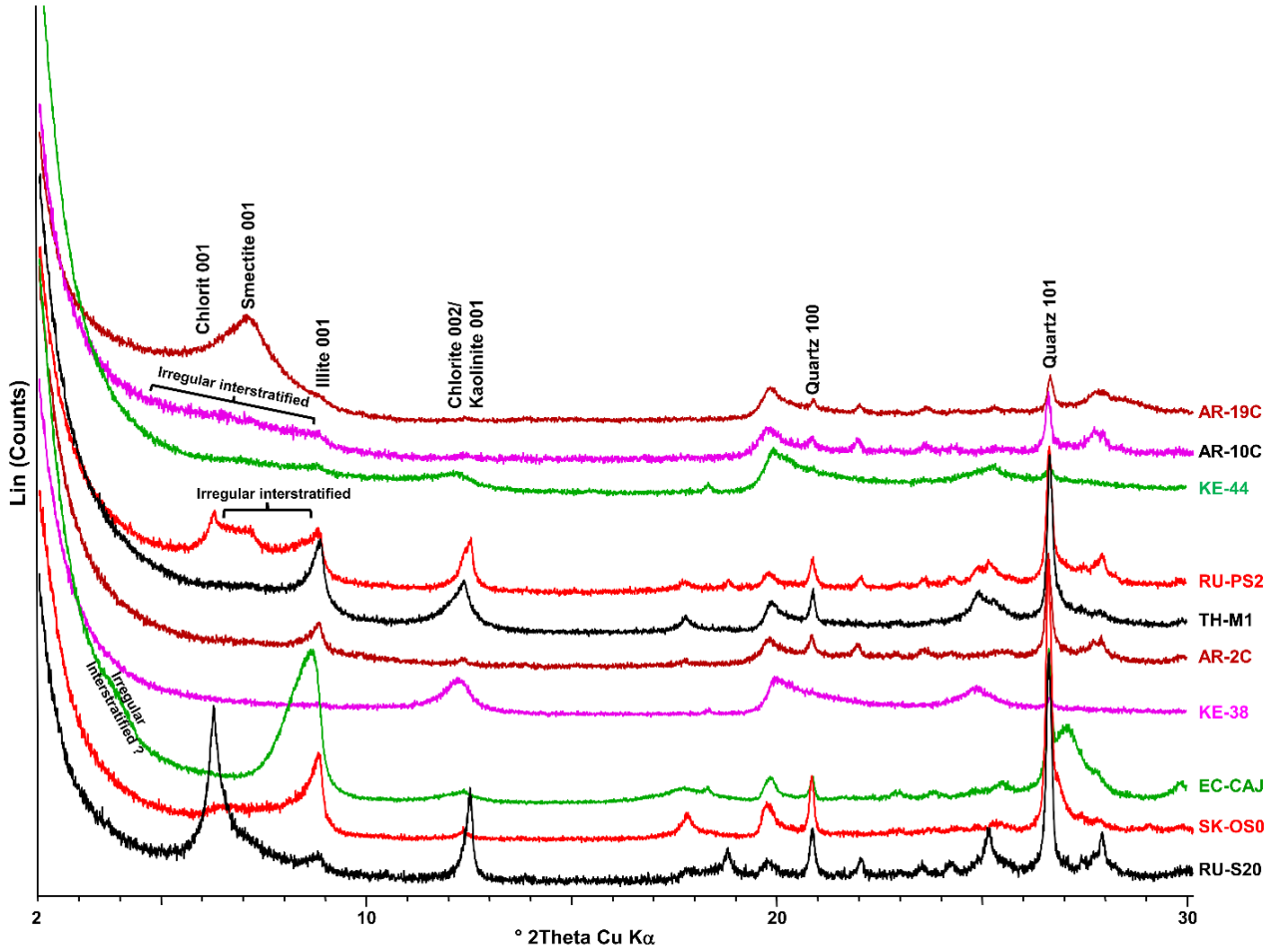

Figure 3.4: X-ray powder diffraction (XRD) spectra of ten topsoil clay fractions (with smoothed out sample surface), sorted according to their potential cation-exchange capacity from high (top) to low (bottom). See Tables 3.1 and 3.2 for an explanation of the sample designations and properties.

The samples with the highest CEC_{pot} (AR-19C) only contained smectites, which was probably also present in irregular interstratified form besides illites in the samples with the next highest CEC_{pot} (AR-10C, KE-44, Figure 3.4). Together with KE-44, these four samples appeared to be dominated by three-layer clay minerals. Samples RU-PS2, TH-M1, AR-2C, and SK-Oso showed peaks in a range associated with the presence of illites, some in interstratified form, and kaolinite. TH-M1, AR-2C, KE-28 did not show patterns of swellable phases, which is typical for hot-humid weathering condition and sufficient

drainage. The broad intensity of KE-38 at ~12.2 °2 θ (~7 Å) is typical for the 001-main intensity of poorly ordered kaolinite. EC-CAJ exhibited patterns of mixed-layer illites or K/Na-scmectites. In the sample RUS20 with the lowest CEC of 114 $mmol_c\ kg^{-1}$ and RU-PS2 it was not clear whether only chlorite, or also small amounts of kaolinite were present due to the overlap of the Chlorite 002 and Kaolinite 001 intensities at ~12,2 °2 θ (~7 Å). Typical for recent topsoils and consistent with the C_{org} results for the clay fractions (Table 3.2), the XRD scans revealed large amounts of amorphous content, especially KE-44, due to the weak intensities of the clay minerals in relation to the background intensity. The clay fraction of sample PA-A9, collected from a depression in Panama, contained only smectite (Messmer et al., 2014). Schrumpf et al. (2001) examined soil samples near our sampling sites EC-CAJ (3050 m a.s.l.), EC-SF1 (1950 m a.s.l.), and EC-BOM (1010 m a.s.l.). The results of Schrumpf et al. (2001) illustrated that illite and kaolinite were found at all three elevations. The concentrations of illites increased with elevation while that of kaolinite decreased. Fully swellable three-layer clay minerals such as vermiculites were absent (EC-CAJ) or occurred in traces (EC-BOM, EC-SF1). Thus, our own XRD analyses and the cited literature confirm that the CEC_{pot} of the clay fraction reflected the mineralogy well.

The regression of the δ^2H_n values of the sample group dominated by nonswellable clay minerals with a low CEC_{pot} <160 $mmol_c\ kg^{-1}$ (n = 6) on the δ^2H values of meteoric water showed a steeper slope than that dominated by swellable clay minerals with a high CEC_{pot} ≥160 $mmol_c\ kg^{-1}$ (n=18) for both $\alpha_{ex\text{-}w}$ values and both measures of local meteoric water (Figure 3.5). The difference in slope was less pronounced for $\alpha_{ex\text{-}w} = 1$ than for $\alpha_{ex\text{-}w} = 1.08$ and for local mean seasonal meteoric water than for local mean annual meteoric water. The separate regressions showed higher coefficients of determination than the joint regression of all samples (Figures 3.2, 3.5 and 3.S1).

3.3.5 Influence of climatic, topographic and soil properties

To explain the scatter around the regression lines of the δ^2H_n values of clay fractions on the δ^2H values of meteoric water, we set up multiple regression models of the climatic, topographic, and soil properties shown in Table 3.1. To ensure that we only used independent explanatory variables in our multiple regression model, we selected the highest loading variables from independent principal components. The best

regression model according to the Akaike information criterion for $\alpha_{ex\text{-}w} = 1$ is shown in Eq. 3.5 and the best one for $\alpha_{ex\text{-}w} = 1.08$ in Eq. 3.6.

$\delta^2H_{n,\,\alpha=1,\,predicted} = 0.78\ \delta^2H_{p,\,seasonal}$ *[0.68]* $+ 9.65\ \ln(\text{hillslope} + 1)$ *[0.20]* $- 74,$ (*Eq. 3.5*)

with $r = 0.94$, $p < 0.001$ and $R^2 = 0.89$.

$\delta^2H_{n,\,\alpha=1.08,\,predicted} = 0.70\ \delta^2H_{p,\,seasonal}$ *[0.47]* $+ 13.6\ \ln(\text{hillslope} + 1)$ *[0.29]*

$+ 0.28\ \text{latitude}$ *[0.10]* $- 118,$ (*Eq. 3.6*)

with $r = 0.93$, $p < 0.001$, $R^2 = 0.86$. The italic numbers in square brackets of Eqs. 3.5 and 3.6 are the fractions of the total variance explained by the individual explanatory variables. In Eqs. 3.5 and 3.6, the local mean seasonal meteoric water was favored over the local mean annual meteoric water and hillslope was chosen as an explanatory variable in the best model.

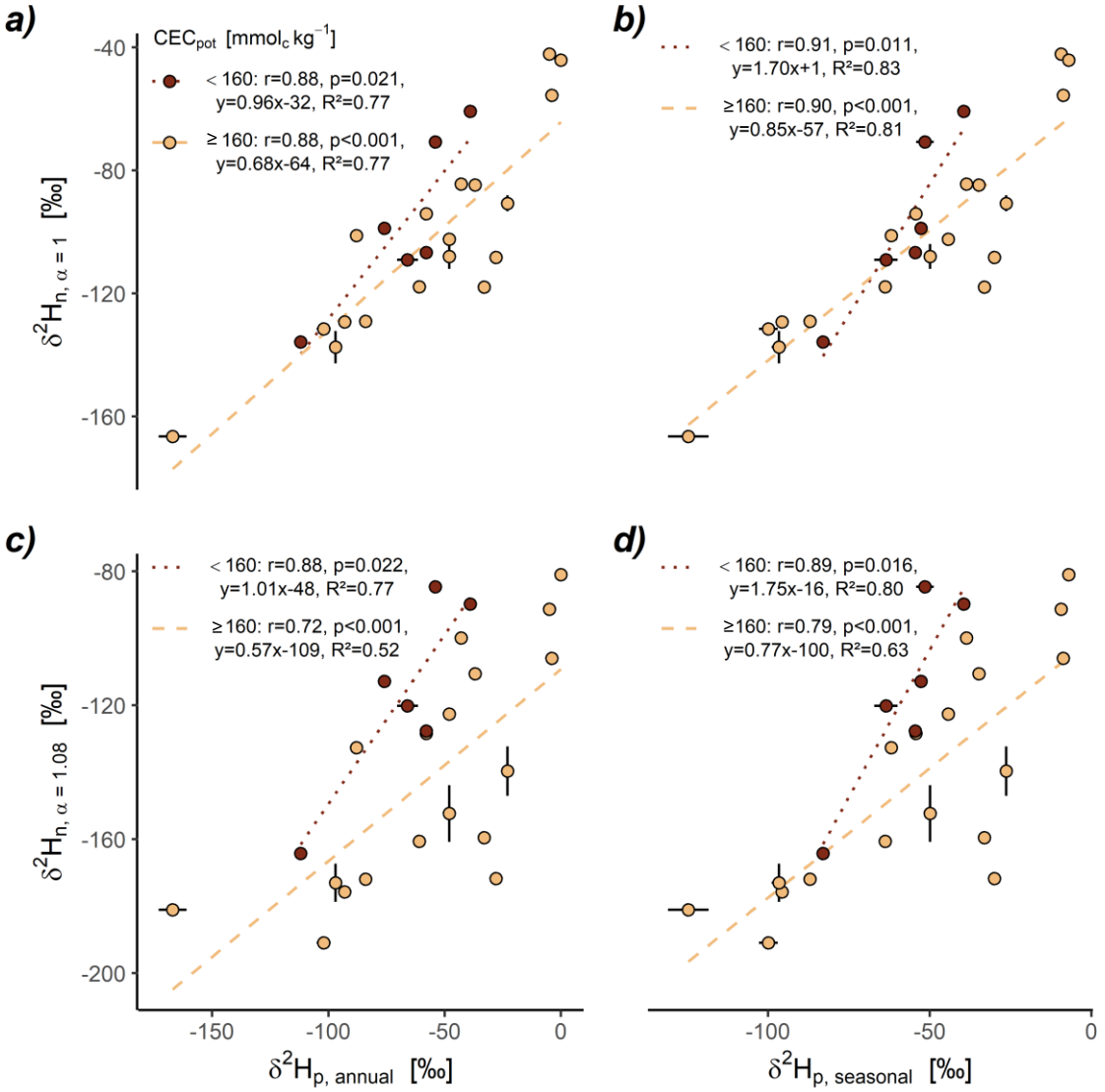

Figure 3.5: Relationship between the δ^2H values of local mean annual (a, c) or seasonal (b, d) precipitation (δ^2H_p) and the δ^2H_n values of soil clay fractions for an equilibrium fractionation factor between water-H (in the steam) and exchangeable H ($\alpha_{ex\text{-}w}$) of 1 (a, b) and 1.08 (c, d). δ^2H_p is from the Online Isotopes in Precipitation Calculator, version 3.1 (Bowen 2017). The yellow filling marks clay separates with a potential cation-exchange capacity (CEC) <160 mmol$_c$ kg^{-1} and the dark brown filling clay separates with a CEC$_{pot}$ ≥160 mmol$_c$ kg^{-1}. The yellow dashed line shows the regression of the δ^2H_n values of the soil clay fractions on the δ^2H values of local meteoric water for the clay separates with a CEC <160 mmol$_c$ kg^{-1} (deemed to be dominated by nonswellable clay minerals) and the dark brown dotted line for soil clay fractions with a CEC ≥160 mmol$_c$ kg^{-1} (deemed to be dominated by swellableclay minerals). The error bars of δ^2H_p indicate the 68% confidence interval and might be smaller than the symbol size. The error bars of δ^2H_n values indicate the standard deviation from field triplicates, available for three sample locations from Argentina.

3.4 Discussion

3.4.1 Relationship of the δ^2H values of precipitation with the δ^2H_n values of clay fractions

Our range of δ^2H_n values of clay fractions for both $\alpha_{ex\text{-}w}$ values is similar to that reported by Lawrence and Taylor (1971) of -30 to -165‰ for clay minerals and hydroxides in soils of the USA (Table 3.2). The finding of a significant correlation of the δ^2H values of meteoric water with the δ^2H_n values of clay fractions is consistent with previous work that also used the OIPC model to analyze relationships of the H isotopic composition of meteoric water with those of various natural materials (Table 3.4). Ruppenthal et al. (2010) found a correlation of the δ^2H values of local mean annual meteoric water with the δ^2H_n values of a global data set of 12 bulk soil samples, Ruppenthal et al. (2015) with demineralized soil organic matter at 20 locations along a climosequence in Argentina, Hobson et al. (2012) with wing chitin of dragonflies, and Sachse et al. (2012) with leaf-wax n-C_{29} alkanes in shrubs, trees, forbs, graminoids and sediments from various studies. These results illustrate that the H isotopic composition of meteoric water has a consistent and widespread influence on the δ^2H_n values in various natural materials. The slightly higher R^2 values of the regressions if only meteoric water of the nonfrozen period was considered might indicate that indeed only H of liquid water can be incorporated into clay minerals.

The fact that the δ^2H_n values of the bulk soils of the Argentinean subset of samples could be explained as a mixture of those of demineralized organic matter and the clay fractions illustrated that the nonexchangeable H pool of different soil constituents such as organic matter and clay minerals showed a different H isotope fractionation between ambient water and the individual constituents at the time of their formation (i.e., different $\alpha_{min|SOM\text{-}water}$ values; Figure 3.3). Nonexchangeable H in soil clay fractions showed a stronger fractionation relative to ambient water-H than the soil organic matter as reflected by the different $\Delta^2H_{meteoric\ water\text{-}soil\ constituent}$ values.

The results support our first hypothesis that there is a global correlation between the δ^2H values of meteoric water and the δ^2H_n values of clay fractions (Figure 3.2). However, slope and y-axis intercept of the regression of the δ^2H_n values of clay fractions on the δ^2H values of local meteoric water vary with the choice of the $\alpha_{ex\text{-}w}$ values and among the two precipitation models (Bowen and Revenaugh, 2003; Terzer-Wassmuth et

al., 2021; see Supplementary Material). To define a universally valid regression line therefore requires to better constrain the $\alpha_{ex\text{-}w}$ values, which likely differ among different minerals. Moreover, the data shows a larger scatter around the regression lines than reported by Ruppenthal et al. (2014) for demineralized soil organic matter as can also be seen in Figure 3.3. This larger scatter is related with the different mineralogical composition of the studied soil clay fractions (Figure 3.4 and 3.5).

Table 3.4: Properties of regression lines of the nonexchangeable hydrogen isotope ratios (δ^2H_n values) in different environmental media on the δ^2H values of the meteoric water (δ^2H_p).

Type	$\delta^2H_{(n)}$	$\alpha_{ex\text{-}w}$	δ^2H_p	OIPC[a] version	slope	intercept [‰]	R^2	Source and Remark
steam equilibration	clay fractions	1	annual	3.1	0.74	-54	0.83	this study, excl. two outliers (n=22)
		1.08	annual	3.1	0.66	-92	0.58	
		1	seasonal	3.1	0.96	-46	0.88	
		1.08	seasonal	3.1	0.92	-80	0.71	
	bulk soil	1.08	annual	2.2	0.9	-34	0.79	Ruppenthal et al. (2010)
	dragonfly wing chitin	1.08	seasonal	2.2	0.91	-43	0.75	Hobson et al. (2012)
	SOM	1.08	annual[b]	2.2	1.25	-38	0.94	Ruppenthal et al. (2015)
	SOM	1	annual[b]	3.1	0.88	-32	0.91	δ^2H_n from Ruppenthal et al. (2015) recalculated with different $\alpha_{ex\text{-}w}$, δ^2H_p updated
	SOM	1.08	annual[b]	3.1	0.99	-54	0.87	δ^2H_n from Ruppenthal et al. (2015), δ^2H_p updated
	bulk soil	1.08	annual[b]	2.2	0.97	-85	0.74	Ruppenthal (2014)
	bulk soil	1	annual[b]	3.1	0.65	-56	0.92	δ^2H_n from Ruppenthal (2014) recalculated with different $\alpha_{ex\text{-}w}$, δ^2H_p updated
	bulk soil	1.08	annual[b]	3.1	0.68	-101	0.79	δ^2H_n from Ruppenthal (2014), δ^2H_p updated
CISA, n-C29 alkane	shrubs	not applicable	annual	2.2	0.87	-112	0.21	Sachse et al. (2012)
	trees				0.52	-134	0.46	
	forbs				1.16	-120	0.83	
	C_3 graminoids				1.21	-129	0.49	
	C_4 graminoids				0.78	-142	0.48	
	lake-surface sediments				0.55	-148	0.80	

[a] OIPC is Online Isotopes in Precipitation Calculator from Bowen (20217) and Bowen and Revenaugh (2003). For the annual average δ^2H_p model from version 2.2 to 3.1 the number of included monitoring station tripled.

b No systematic difference between both models, because all months have an average temperature > 0 °C.

3.4.2 Influence of the soil organic matter removal

We attribute the remaining C_{org} concentrations of the clay fractions (Table 3.2) to the well-known incomplete and selective SOM removal by H_2O_2 (Leifeld and Kögel-Knabner, 2001; Mikutta et al., 2005; Merseburger et al., 2022). However, our correction of the δ^2H_n values of the clay fractions considering the δ^2H_n values of SOM with Eq. 3.3 resulted in only small changes of the δ^2H_n values of the clay fractions that were on average in the range of the analytical uncertainty (Table 3.3). This finding is in line with Fagan (2001) who found the C-bonded H concentrations in clay mineral standards too low to contribute to the δ^2H measurements. Thus, the influence of the remaining C_{org} concentrations in the soil clay fractions on their δ^2H_n values can be neglected.

3.4.3 Influence of the preliminary $\alpha_{ex\text{-}w}$ values

The choice of the $\alpha_{ex\text{-}w}$ value had a considerable impact on the δ^2H_n values of the clay fractions (Table 3.2, Figures 3.2-3.4). Because the difference in the δ^2H_n values of the clay fractions between the two $\alpha_{ex\text{-}w}$ values of 1 and 1.08 was related with the exchangeable H concentrations (χ_e) as can be derived from Eq. 3.2, the choice of the $\alpha_{ex\text{-}w}$ value had a stronger impact on the δ^2H_n values of samples with a CEC_{pot} ≥160 $mmol_c\ kg^{-1}$, which are dominated by swellable clay minerals and therefore show more adsorption water contributing to the exchangeable H pool than the nonswellable minerals with a CEC_{pot} <160 $mmol_c\ kg^{-1}$ (O'Neil and Kharaka, 1976; Merseburger et al., 2022). Our results illustrate that the $\alpha_{ex\text{-}w}$ values, particularly of the swellable clay minerals, need to be better constrained to reduce the scatter around the regression lines of the δ^2H_n values of clay fractions on the δ^2H values of local precipitation.

3.4.4 Influence of the dominant clay mineral type

Our finding that the slopes of the regression lines of the δ^2H_n values of the clay fractions on the δ^2H values of local meteoric water differed between samples dominated by nonswellable and swellable clay minerals (Figure 3.5) is in line with the results of Savin and Epstein (1970) that kaolinite had a higher $\alpha_{min\text{-}water}$ value of 0.97 than montmorillonite with an $\alpha_{min\text{-}water}$ value of 0.94. As a consequence, separate regression lines of δ^2H_n values of the clay fractions on the δ^2H values of meteoric water are needed for soils differing in clay mineral composition if this regression is to be used to reconstruct the local δ^2H values of meteoric water or probabilistically assign a soil

sample to its spatial origin. Because of the partly systematic variation in clay mineral composition among different climatic zones with e.g., more frequent occurrence of of nonswellable clay minerals in the hot-humid inner tropical zone vs. a more frequent dominance of swellable clay minerals in the temperate zone (FAO, 2009; Ito and Wagai, 2017), the regression lines of δ^2H_n values of the clay fractions on δ^2H values of meteoric water likely vary among different climate zones. As a consequence, there is no unique regression line for soil clay fractions which is globally valid. This might be different to soil organic matter (Ruppenthal et al., 2014). Moreover, mixtures of different clay mineral types in soil clay fractions will increase the scatter around the regression lines. The same is true for cases in which clay minerals formed under distinctly different conditions than in the studied topsoil environments that could be inherited from the parent material contribute to the soil clay fraction.

3.4.5 Influence of climatic, topographic and soil properties

The fact that our model selection procedure preferred the δ^2H values of seasonal over annual meteoric water (Eqs. 3.5 and 3.6) further supports the conclusion that at sites with a longer period during which soils are frozen, the δ^2H_n values of the clay minerals only reflect the H isotopic composition of the liquid water during the growing season, because chemical weathering is strongly reduced in frozen soil (Chuvilin et al., 1998; Borden et al., 2010; Lessovaia et al., 2021). The influence of the hillslope on the δ^2H_n values of clay fractions possibly reflects the degree to which the local clay minerals have been formed in situ. Flat areas tend to accumulate colluvial material from upslope or eolian deposition and thus may contain clay minerals formed at adjacent locations with different δ^2H values of meteoric water, while steep areas tend to be eroded and thus only contain clay minerals formed in situ. Similar to this assumption, Schaub et al. (2009) observed that the $\delta^{18}O$ values of bulk soils reflected the extent of erosion. Interestingly, in the multiple regression models including hillslope as explanatory variables, the Argentinian samples AR-5C and AR-4A, which originate from Phaeozems in a flat steppe likely influenced by eolian input of clay minerals from surrounding soils, were no longer outliers. The small additional contribution of latitude to the explanation of the total variation in the δ^2H_n values of clay fractions in Eq. 3.6 might further confirm that the climate had an influence on clay mineral composition and thus influences the δ^2H_n values of soil clay fractions.

3.5 Conclusions

Our results confirmed the first hypothesis, that there is a significant correlation between the δ^2H values of local meteoric water and the δ^2H_n values of soil clay fractions at a global scale. However, this relationship is less close than previously observed for soil organic matter. The remaining organic matter in the soil clay fractions which could not be completely destroyed did not substantially influence the δ^2H_n values of the soil clay fractions, while the $\alpha_{ex\text{-}w}$ values, the equilibrium fractionation factor between ambient water-H and exchangeable H in the clay fraction, needed to calculate the δ^2H_n values from steam equilibration, the mineral types and some properties of the study sites had a strong influence confirming our second hypothesis except for the assumed influence of the remaining organic matter in the clay fractions.

The choice of the $\alpha_{ex\text{-}w}$ values of the clay fractions in the range of 1–1.08 as reported in the literature influenced the regression of the δ^2H_n values of soil clay fractions on the δ^2H values of local meteoric water but did not change the overall positive relationship. Thus, for a more precise determination of the δ^2H_n values of soil clay fractions with the steam equilibration approach, the $\alpha_{ex\text{-}w}$ values need to be better constrained.

The slope and y intercept of the regression of the δ^2H_n values of soil clay fractions on the δ^2H values of local meteoric water varied with the CEC_{pot} of the soil clay fractions. The subset of samples dominated by nonswellable clay minerals as indicated by a CEC_{pot} < 160 $mmol_c\ kg^{-1}$ clay and the presence of kaolinite, illite or chlorite showed a steeper slope than that dominated by swellable clay minerals with a CEC ≥ 160 $mmol_c\ kg^{-1}$ and the presence of smectites and vermiculites confirming that the $\alpha_{mineral\text{-}water}$ value, the equilibrium fractionation factor between ambient water-H and nonexchangeable H in the clay fraction, which is conserved from the time of mineral formation, is mineral-specific.

The inclusion of seasonal local meteoric water, hillslope and latitude in a multiple regression model explained up to 89% of the variation in the δ^2H_n values of soil clay fractions. This suggested that only the ambient water-H during nonfrozen periods contributes to the nonexchangeable H of soil clay fractions. We interpreted the choice of hillslope as explanatory variable as indication of an influence of the degree to which clay minerals are formed in situ which is more likely at steeper, more strongly eroded than at

less steep or flat sites where colluvial or eolian material accumulates. Finally, the choice of latitude as explanatory variable might reflect the climatic influence on the formation of clay minerals.

Declaration of competing interest

The authors declare that they have no known competing financial interests or personal relationships that could have appeared to influence the work reported in this paper.

Acknowledgments

We thank Nadine Gill for help in the laboratory, Andre Velescu for support with the ICP-MS and ICP-OES measurements, Harald Neidhardt for coordinative help concerning XRD analysis, Annette Flicker for running the XRD-analysis at the CCA-BW in Tübingen, Harro Meijer for a working example of the memory correction algorithm and Maria Hoerhold for contributing the deuterium-depleted water (AWI-TD1). We thank all providers of soil samples: Lars Kutzbach and Christian Knoblauch (RU-PS2), Christian Siewert (RU-17, RU-S20), Suzanne Robin Jacobs (KE-20, KE-38, KE-44), Tobias Wirsing (DE-KA1, DE-KA2), Benjamin A.M. Bandowe (UZ-K1), Andre Velescu and Tobias Fabian (EC-BOM, EC-CAJ, EC-SF1). This work was funded by the Deutsche Forschungsgemeinschaft (DFG, Wi1601/25-1).

3.6 References

Ammann, L., Bergaya, F., Lagaly, G., 2005. Determination of the cation exchange capacity of clays with copper complexes revisited. Clay Miner. 40, 441–453.

Bauer, K.K., Vennemann, T.W., 2014. Analytical methods for the measurement of hydrogen isotope composition and water content in clay minerals by TC/EA. Chem. Geol. 363, 229–240.

Borden, P.W., Ping, C.-L., McCarthy, P.J., Naidu, S., 2010. Clay mineralogy in arctic tundra Gelisols, northern Alaska. Soil Sci. Soc. Am. J. 74, 580–592.

Bowen, G.J., Revenaugh, J., 2003. Interpolating the isotopic composition of modern meteoric precipitation: isotopic composition of modern precipitation. Water Resour. Res. 39, 1299–1312.

Bowen, G.J., Chesson, L., Nielson, K., Cerling, T.E., Ehleringer, J.R., 2005a. Treatment methods for the determination of δ^2H and $\delta^{18}O$ of hair keratin by continuous- flow isotope-ratio mass spectrometry. Rapid Commun. Mass Spectrom. 19, 2371–2378.

Bowen, G.J., Wassenaar, L.I., Hobson, K.A., 2005b. Global application of stable hydrogen and oxygen isotopes to wildlife forensics. Oecologia 143, 337–348.

Bowen, G.J., 2017. WaterIsotopes.org. Online Isotopes in Precipitation Calculator, Version 3.1.

Brindley, G.W., Brown, G., 1980. X-ray diffraction procedures for clay mineral identification. In: Brindley, G.W., Brown, G. (Eds.), Crystal Structures of Clay Minerals and Their X-Ray Identification. Mineralogical Society, pp. 305–356.

Chesson, L.A., Podlesak, D.W., Cerling, T.E., Ehleringer, J.R., 2009. Evaluating uncertainty in the calculation of non-exchangeable hydrogen fractions within organic materials. Rapid Commun. Mass Spectrom. 23, 1275–1280.

Chuvilin, E.M., Ershov, E.D., Smirnova, O.G., 1998. Ionic migration in frozen soils and ice. In: Proceedings of the 7th International Permafrost Conference, Yellowknife, NWT, 23–27 June 1998 Centre d'études nordiques, Université Laval Laval, Que. pp. 167–171.

DIN ISO 11277 (2002) Bodenbeschaffenheit - Bestimmung der Partikelgrößenverteilung in Mineralböden. Verfahren mittels Siebung und Sedimentation., Beuth Verlag, Berlin.

Eusterhues, K., Rumpel, C., Kleber, M., Kögel-Knabner, I., 2003. Stabilisation of soil organic matter by interactions with minerals as revealed by mineral dissolution and oxidative degradation. Org. Geochem. 34, 1591–1600.

Fabian, T., Velescu, A., Wilcke, W., 2019. Soil development on heterogeneous parent material under tropical montane forest in South Ecuador. Tabebuia Bull. 6, 7.

Fabian, T., Velescu, A., Harteif, K., Wilcke, W., 2020. Soil properties of the cloud forest in Cajanuma and of the pastures along an elevation gradient from 1000 to 3000 m a.s.l. Tabebuia Bull. 7, 9.

Fagan, R., 2001. Oxygen-and hydrogen-isotope study of hydroxyl-group behavior in standard smectite and kaolinite. Faculty of Graduate Studies, University of Western Ontario. PhD Thesis.

Faghihi, V., Meijer, H.A.J., Gröning, M., 2015. A thoroughly validated spreadsheet for calculating isotopic abundances (δ^2H, $\delta^{17}O$, $\delta^{18}O$) for mixtures of waters with different isotopic compositions. Rapid Commun. Mass Spectrom. 29, 1351– 1356.

FAO, 2009. Harmonized World Soil Database: Topsoil CEC (clay), Version 1.1.

Feng, X., Krishnamurthy, R.V., Epstein, S., 1993. Determination of D/H ratios of nonexchangeable hydrogen in cellulose: A method based on the cellulose-water exchange reaction. Geochim. Cosmochim. Acta 57, 4249–4256.

Ferrier, K.L., Kirchner, J.W., 2008. Effects of physical erosion on chemical denudation rates: A numerical modeling study of soil-mantled hillslopes. Earth Planet. Sci. Lett. 272, 591–599.

Fick, S.E., Hijmans, R.J., 2017. WorldClim 2: new 1-km spatial resolution climate surfaces for global land areas. Int. J. Climatol. 37, 4302–4315.

Folkoff, M.E., Meentemeyer, V., 1985. Climatic control of the assemblages of secondary clay minerals in the A-horizon of United States soils. Earth Surf. Process. Landf. 10, 621–633.

Gehre, M., Renpenning, J., Gilevska, T., Qi, H., Coplen, T.B., Meijer, H.A., Brand, W.A., Schimmelmann, A., 2015. On-line hydrogen-isotope measurements of organic samples using elemental chromium: an extension for high temperature elemental-analyzer techniques. Anal. Chem. 87, 5198–5205.

Gilg, H.A., Sheppard, S.M.F., 1996. Hydrogen isotope fractionation between kaolinite and water revisited. Geochim. Cosmochim. Acta 60, 529–533.

Gilg, H.A., Girard, J.-P., Sheppard, S.M.F., 2004. Conventional and Less Conventional Techniques for Hydrogen and Oxygen Isotope Analysis of Clays, Associated Minerals and Pore Waters

in Sediments and Soils. In: Handbook of Stable Isotope Analytical Techniques. Volume 1. Elsevier, pp. 38–61.

Grömping, U., 2007. Relative importance for linear regression in R: the package relaimpo. J. Stat. Softw. 17, 1–27.

Heimsath, A.M., Dietrich, W.E., Nishiizumi, K., Finkel, R.C., 2001. Stochastic processes of soil production and transport: erosion rates, topographic variation and cosmogenic nuclides in the Oregon Coast Range. Earth Surf. Process. Landf. 26, 531–552.

Hobson, K.A., Soto, D.X., Paulson, D.R., Wassenaar, L.I., Matthews, J.H., 2012. A dragonfly (δ^2H) isoscape for North America: a new tool for determining natal origins of migratory aquatic emergent insects. Methods Ecol. Evol. 3, 766– 772.

Hyeong, K., Capuano, R.M., 2000. The effect of organic matter and the H_2O_2 organic- matter-removal method on the δD of smectite-rich samples. Geochim. Cosmochim. Acta 64, 3829–3837.

Hyeong, K., Capuano, R.M., 2004. Hydrogen isotope fractionation factor for mixed-layer illite/smectite at 60° to 150°C: new data from the northeast Texas Gulf Coast 1. Geochim. Cosmochim. Acta 68, 1529–1543. IAEA, 2014.

IAEA/GNIP, 2014. Precipitation Sampling Guide (V2.02).

IAEA/WMO, 2022. Global Network of Isotopes in Precipitation. The GNIP Database.

ISRIC World Soil Information, 2007. Soil and Terrain database for Kenya, version 2.0, at scale 1:1 million (KENSOTER).

Ito, A., Wagai, R., 2017. Global distribution of clay-size minerals on land surface for biogeochemical and climatological studies. Sci. Data 4, sdata2017103.

IUSS Working Group WRB, 2022. World Reference Base for Soil Resources. International soil classification system for naming soils and creating legends for soil maps. International Union of Soil Sciences (IUSS), Vienna, Austria.

Japan Aerospace Exploration Agency, 2021. ALOS Global Digital Surface Model "ALOS World 3D - 30m" (AW3D30).

Jin, L., Ravella, R., Ketchum, B., Bierman, P.R., Heaney, P., White, T., Brantley, S.L., 2010. Mineral weathering and elemental transport during hillslope evolution at the Susquehanna/Shale Hills Critical Zone Observatory. Geochim. Cosmochim. Acta 74, 3669–3691.

Kaiser, K., Eusterhues, K., Rumpel, C., Guggenberger, G., Kögel-Knabner, I., 2002. Stabilization of organic matter by soil minerals—investigations of density and particle-size fractions from two acid forest soils. J. Plant Nutr. Soil Sci. 165, 451– 459.

Kanik, N.J., Longstaffe, F.J., Kuligiewicz, A., Derkowski, A., 2022. Systematics of smectite hydrogen-isotope composition: Structural hydrogen versus adsorbed water. Appl. Clay Sci. 216 106338.

Knoblauch, C., Beer, C., Schuett, A., Sauerland, L., Liebner, S., Steinhof, A., Rethemeyer, J., Grigoriev, M.N., Faguet, A., Pfeiffer, E.-M., 2021. Carbon dioxide and methane release following abrupt thaw of pleistocene permafrost deposits in Arctic Siberia. J. Geophys. Res Biogeosci. 126 e2021JG006543.

Lawrence, J.R., Taylor, H.P., 1971. Deuterium and oxygen-18 correlation: Clay minerals and hydroxides in Quaternary soils compared to meteoric waters. Geochim. Cosmochim. Acta 35, 993–1003.

Lawrence, J.R., Taylor, H.P., 1972. Hydrogen and oxygen isotope systematics in weathering profiles. Geochim. Cosmochim. Acta 36, 1377–1393.

Lawrence, J.R., 1970. O^{18}/O^{16} and D/H ratios of soils, weathering zones and clay deposits. California Institute of Technology. PhD Thesis,.

Leifeld, J., Kögel-Knabner, I., 2001. Organic carbon and nitrogen in fine soil fractions after treatment with hydrogen peroxide. Soil Biol. Biochem. 33, 2155–2158.

Lessovaia, S.N., Desyatkin, R.V., Okoneshnikova, M.V., Ivanova, A.Z., 2021. Clay mineralogy of Cryosols formed in an ultra-continental climate of Siberia. IOP Conf. Ser. Earth Environ. Sci. 862, 012070.

Li, J., Lu, X., Cheng, K., Liu, W., 2021. StepReg: Stepwise regression analysis.

Lobe, I., Wilcke, W., Kobža, J., Zech, W., 1998. Heavy metal contamination of soils in Northern Slovakia. Z. Pflanzenernähr. Bodenkd. 161, 541–546.

Lobe, I., 1997. Untersuchungen zur Schwermetallbelastung von Böden der Nord- Slowakei. University Bayreuth. Diploma thesis.

Maher, K., 2010. The dependence of chemical weathering rates on fluid residence time. Earth Planet. Sci. Lett. 294, 101–110.

Maher, K., 2011. The role of fluid residence time and topographic scales in determining chemical fluxes from landscapes. Earth Planet. Sci. Lett. 312, 48–58.

Marumo, K., Nagasawa, K., Kuroda, Y., 1980. Mineralogy and hydrogen isotope geochemistry of clay minerals in the Ohnuma geothermal area, Northeastern Japan. Earth Planet. Sci. Lett. 47, 255–262.

Marumo, K., Longstaffe, F.J., Matsubaya, O., 1995. Stable isotope geochemistry of clay minerals from fossil and active hydrothermal systems, southwestern Hokkaido, Japan. Geochim. Cosmochim. Acta 59, 2545–2559.

Méheut, M., Lazzeri, M., Balan, E., Mauri, F., 2010. First-principles calculation of H/D isotopic fractionation between hydrous minerals and water. Geochim. Cosmochim. Acta 74, 3874–3882.

Mehra, O.P., Jackson, M.L., 1960. Iron oxide removal from soils and clays by a dithionite-citrate system buffered with sodium bicarbonate. In: Proceedings 7th National Conference on Clays and Clay Minerals, 317–327.

Meier, L.P., Kahr, G., 1999. Determination of the Cation Exchange Capacity (CEC) of Clay Minerals Using the Complexes of Copper(II) Ion with Triethylenetetramine and Tetraethylenepentamine. Clays Clay Miner. 47, 386–388.

Merseburger, S., Kessler, A., Oelmann, Y., Wilcke, W., 2022. Nonexchangeable stable hydrogen isotope ratios in clay minerals and soil clay fractions: A method test. Eur. J. Soil Sci. 73 e13285.

Messmer, S.T., Elsenbeer, H., Wilcke, W., 2014. High exchangeable calcium concentrations in soils on Barro Colorado Island, Panama. Geoderma 217–218, 212–224.

Messmer, S.T., 2014. Biotic and abiotic drivers of the base metal cycling in a tropical lowland rain forest in Panama. Univerity of Bern. PhD Thesis.

Mikutta, R., Kleber, M., Kaiser, K., Jahn, R., 2005. Review: Organic matter removal from soils using hydrogen peroxide, sodium hypochlorite, and disodium peroxodisulfate. Soil Sci. Soc. Am. J. 69, 120–135.

Müller, S., Wilcke, W., Kanchanakool, N., Zech, W., 2000. Polycyclic aromatic hydrocarbons (PAHs) and polychlorinated biphenyls (PCBs) in particle-size separates of urban soils in Bangkok, Thailand. Soil Sci. 165, 412.

Müller, S., 1998. Polyzyklische aromatische Kohlenwasserstoffe (PAK) und polychlorierte Biphenyle (PCB) in Korngrößen- und Dichtefraktionen urbaner Böden Bangkoks. University Bayreuth. Diploma thesis.

Oerter, E., Singleton, M., Davisson, L., 2017. Hydrogen and oxygen stable isotope signatures of goethite hydration waters by thermogravimetry-enabled laser spectroscopy. Chem. Geol. 475, 14–23.

Ojoatre, S., 2022. Deforestation and Recovery of the Tropical Montane forests of East Africa. Lancaster University. PhD Thesis,.

O'Neil, J.R., Kharaka, Y.K., 1976. Hydrogen and oxygen isotope exchange reactions between clay minerals and water. Geochim. Cosmochim. Acta 40, 241–246.

Paul, D., Skrzypek, G., Fórizs, I., 2007. Normalization of measured stable isotopic compositions to isotope reference scales – a review. Rapid Commun. Mass Spectrom. 21, 3006–3014.

Qi, H., Coplen, T.B., 2011. Investigation of preparation techniques for δ^2H analysis of keratin materials and a proposed analytical protocol. Rapid Commun. Mass Spectrom. 25, 2209–2222.

Qi, H., Coplen, T.B., Olack, G.A., Vennemann, T.W., 2014. Caution on the use of NBS 30 biotite for hydrogen-isotope measurements with on-line high-temperature conversion systems. Rapid Commun. Mass Spectrom. 28, 1987–1994.

R Core Team, 2022. R: A language and environment for statistical computing. Vienna, Austria.

Revelle, W., 2021. psych: Procedures for psychological, psychometric, and personality research. Evanston, Illinois.

Rice, J.A., MacCarthy, P., 1991. Statistical evaluation of the elemental composition of humic substances. Org. Geochem. 17, 635–648.

Richards, P.L., Kump, L.R., 2003. Soil pore-water distributions and the temperature feedback of weathering in soils. Geochim. Cosmochim. Acta 67, 3803–3815.

Ruppenthal, M., Oelmann, Y., Wilcke, W., 2010. Isotope ratios of nonexchangeable hydrogen in soils from different climate zones. Geoderma 155, 231–241.

Ruppenthal, M., Oelmann, Y., Wilcke, W., 2013. Optimized demineralization technique for the measurement of stable isotope ratios of nonexchangeable H in soil organic matter. Environ. Sci. Technol. 47, 949–957.

Ruppenthal, M., Oelmann, Y., del Valle, H.F., Wilcke, W., 2015. Stable isotope ratios of nonexchangeable hydrogen in organic matter of soils and plants along a 2100-km climosequence in Argentina: New insights into soil organic matter sources and transformations? Geochim. Cosmochim. Acta 152, 54–71.

Ruppenthal, M., 2014. Stable isotope ratios of nonexchangeable hydrogen in bulk organic matter as novel biogeochemical tracer. University of Tübingen. PhD Thesis.

Sachse, D., Billault, I., Bowen, G.J., Chikaraishi, Y., Dawson, T.E., Feakins, S.J., Freeman, K.H., Magill, C.R., McInerney, F.A., van der Meer, M.T.J., Polissar, P., Robins, R.J., Sachs, J.P., Schmidt, H.-L., Sessions, A.L., White, J.W.C., West, J.B., Kahmen, A., 2012. Molecular Paleohydrology: Interpreting the hydrogen- isotopic composition of lipid biomarkers from photosynthesizing organisms. Annu. Rev. Earth Planet. Sci. 40, 221–249.

Sauer, P.E., Schimmelmann, A., Sessions, A.L., Topalov, K., 2009. Simplified batch equilibration for D/H determination of non-exchangeable hydrogen in solid organic material. Rapid Commun. Mass Spectrom. 23, 949–956.

Savin, S.M., Epstein, S., 1970. The oxygen and hydrogen isotope geochemistry of clay minerals. Geochim. Cosmochim. Acta 34, 25–42.

Schaub, M., Seth, B., Alewell, C., 2009. Determination of $\delta^{18}O$ in soils: measuring conditions and a potential application. Rapid Commun. Mass Spectrom. 23, 313–318.

Schimmelmann, A., Lewan, M.D., Wintsch, R.P., 1999. D/H isotope ratios of kerogen, bitumen, oil, and water in hydrous pyrolysis of source rocks containing kerogen types I, II, IIS, and III. Geochim. Cosmochim. Acta 63, 3751–3766.

Schimmelmann, A., Qi, H., Dunn, P.J.H., Camin, F., Bontempo, L., Potoc̆nik, D., Ogrinc, N., Kelly, S., Carter, J.F., Abrahim, A., Reid, L.T., Coplen, T.B., 2020. Food matrix reference materials for hydrogen, carbon, nitrogen, oxygen, and sulfur stable isotope-ratio measurements: Collagens, flours, honeys, and vegetable oils. J. Agric. Food Chem. 68, 10852–10864.

Schimmelmann, A., 1991. Determination of the concentration and stable isotopic composition of nonexchangeable hydrogen in organic matter. Anal. Chem. 63, 2456–2459.

Schrumpf, M., Guggenberger, G., Valarezo, C., Zech, W., 2001. Tropical montane rain forest soils: Development and nutrient Status along an altitudinal gradient in the South Ecuadorian Andes. Erde 132, 43–59.

Sessions, A.L., Hayes, J.M., 2005. Calculation of hydrogen isotopic fractionations in biogeochemical systems. Geochim. Cosmochim. Acta 69, 593–597.

Sheppard, S.M.F., Gilg, H.A., 1996. Stable isotope geochemistry of clay minerals. Clay Miner. 31, 1–24.

Shukurov, N., Pen-Mouratov, S., Steinberger, Y., Kersten, M., 2009. Soil biogeochemical properties of Angren industrial area, Uzbekistan. J. Soils Sediments 9, 206–215.

Siewert, C., Paillan, H., Barsukov, P., 2009. Nachweisbarkeit von Bodenveränderungen. In Jahrestagung der DBG 2009: Böden - eine endliche Ressource. Bonn.

Siewert, C., 2001. Investigation of the thermal and biological stability of soil organic matter. Shaker, Aachen.

Siewert, C., 2004. Rapid screening of soil properties using Thermogravimetry. Soil Sci. Soc. Am. J. 68, 1656.

Soil Survey Staff, 2014. Keys to Soil Taxonomy. United States Department of Agriculture, Natural Resources Conservation Service, Washington, DC.

Soto, D.X., Koehler, G., Wassenaar, L.I., Hobson, K.A., 2017. Re-evaluation of the hydrogen stable isotopic composition of keratin calibration standards for wildlife and forensic science applications. Rapid Commun. Mass Spectrom. 31, 1193–1203.

Taieb, R., 1990. Les isotopes de l'hydrogène, du carbone et de l'oxygène dans les sédiments argileux et les eaux de formation. PhD Thesis, Vandoeuvre-les- Nancy, INPL.

Terzer-Wassmuth, S., Wassenaar, L.I., Welker, J.M., Araguás-Araguás, L.J., 2021. Improved high-resolution global and regionalized isoscapes of $\delta^{18}O$, $\delta^{2}H$ and D- excess in precipitation. Hydrol. Process. 35, e14254.

Trabucco, A., Zomer, R., 2019. Global Aridity Index and Potential Evapotranspiration (ET0). Climate Database 2.

VanDeVelde, J.H., Bowen, G.J., 2013. Effects of chemical pretreatments on the hydrogen isotope composition of 2:1 clay minerals: Clay mineral isotope treatment effects. Rapid Commun. Mass Spectrom. 27, 1143–1148.

von Lützow, M., Kögel-Knabner, I., Ekschmitt, K., Flessa, H., Guggenberger, G., Matzner, E., Marschner, B., 2007. SOM fractionation methods: Relevance to functional pools and to stabilization mechanisms. Soil Biol. Biochem. 39, 2183– 2207.

Wassenaar, L.I., Hobson, K.A., 1998. Natal origins of migratory monarch butterflies at wintering colonies in Mexico: new isotopic evidence. Proc. Natl. Acad. Sci. 95, 15436–15439.

Wassenaar, L.I., Hobson, K.A., 2000. Improved method for determining the stable- hydrogen isotopic composition (δD) of complex organic materials of environmental interest. Environ. Sci. Technol. 34, 2354–2360.

Wassenaar, L.I., Hobson, K.A., 2003. Comparative equilibration and online technique for determination of non-exchangeable hydrogen of keratins for use in animal migration studies. Isotopes Environ. Health Stud. 39, 211–217.

Webster, R., 2001. Statistics to support soil research and their presentation: Statistics to support soil research. Eur. J. Soil Sci. 52, 331–340.

Werner, S.J., Hobson, K.A., Wilgenburg, S.L.V., Fischer, J.W., 2016. Multi-isotopic (δ^2H, δ^{13}C, δ^{15}N) tracing of molt origin for red-winged blackbirds associated with agro-ecosystems. PLOS ONE 11, e0165996.

West, J.B., Bowen, G.J., Dawson, T.E., Tu, K.P. (Eds.), 2010. Isoscapes. Springer Netherlands, Dordrecht.

Wickham, H., Averick, M., Bryan, J., Chang, W., McGowan, L.D., François, R., Grolemund, G., Hayes, A., Henry, L., Hester, J., Kuhn, M., Pedersen, T.L., Miller, E., Bache, S.M., Müller, K., Ooms, J., Robinson, D., Seidel, D.P., Spinu, V., Takahashi, K., Vaughan, D., Wilke, C., Woo, K., Yutani, H., 2019. Welcome to the tidyverse. J. Open Source Softw. 4, 1686.

Wilcke, W., Müller, S., Kanchanakool, N., Zech, W., 1998. Urban soil contamination in Bangkok: heavy metal and aluminium partitioning in topsoils. Geoderma 86, 211–228.

Wilcke, W., Yasin, S., Abramowski, U., Valarezo, C., Zech, W., 2002. Nutrient storage and turnover in organic layers under tropical montane rain forest in Ecuador. Eur. J. Soil Sci. 53, 15–27.

3.7 Supplementary material

(1) Supplementary Figure 3.S1 shows the relationship between the δ^2H values of local mean annual meteoric water (δ^2H_p) and the δ^2H_n values of the soil clay fractions.

(2) Supplementary Research Data include properties of the bulk soil samples (sampling locations, particle-size distributions, dithionite-citrate-buffer-extractable Fe concentrations) and the clay fractions (elemental concentrations, cation-exchange capacities, results of the X-ray diffractometric measurements) and details of the δ^2H analyses. Supplementary material to this article can be found online at https://doi.org/10. 1016/j.gca.2023.02.007.

3.7.1 Supplementary Figure S1

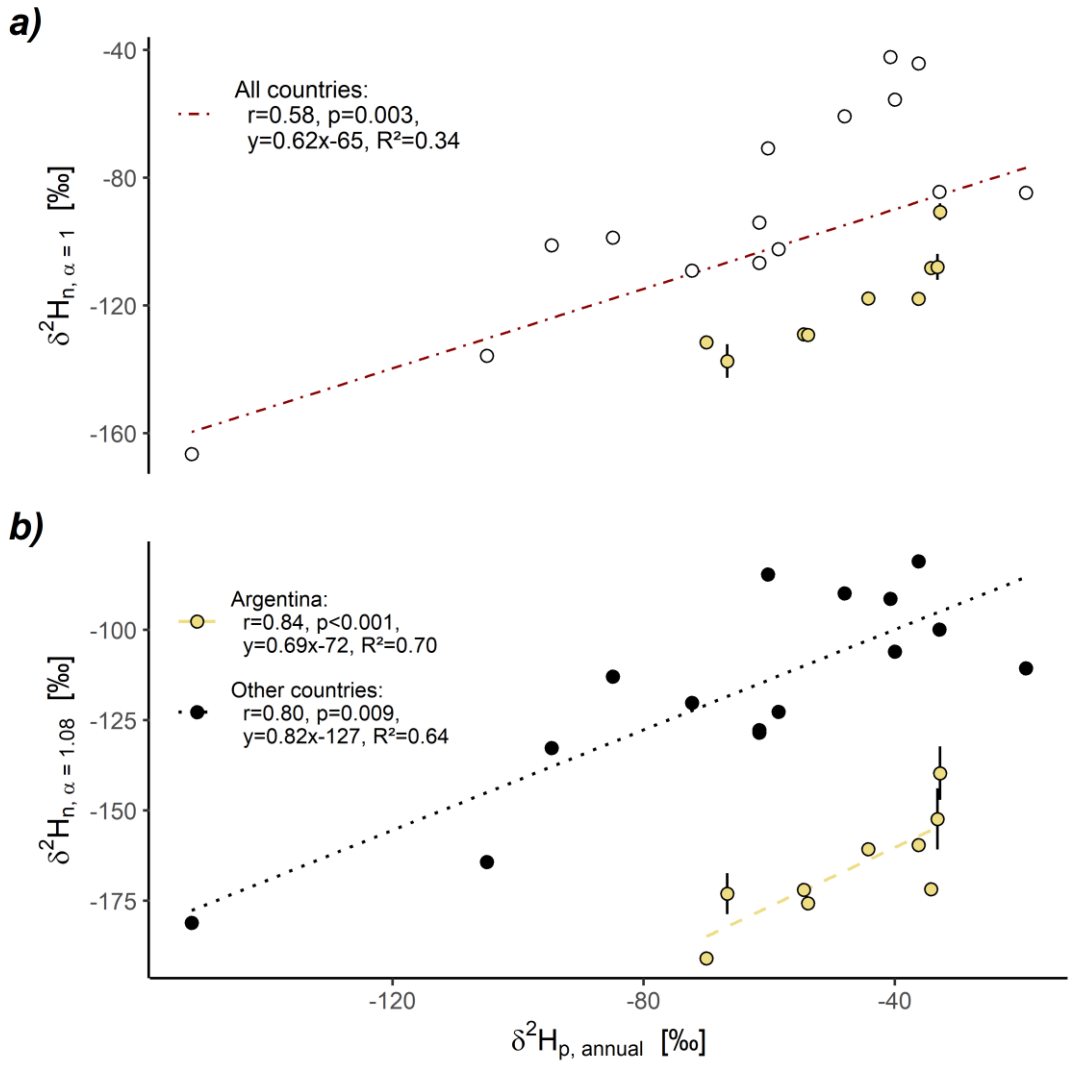

Figure 3.S1: Relationship between the δ^2H values of mean annual local meteoric water (δ^2H_p) and the δ^2H_n values of soil clay fractions for an equilibrium fractionation factor between water-H (in the steam) and exchangeable H ($\alpha_{ex\text{-}w}$) of 1 (a) and 1.08 (b). $\delta^2H_{p,\ annual}$ is from the Regionalized Cluster-Based Water Isotope Prediction model (RCWIP2) of Terzer-Wassmuth et al. (2021). The yellow filling marks the samples from Argentina. The error bars of δ^2H_n values indicate the standard deviation from field triplicates, available for only three sample locations from Argentina.

4 Equilibrium isotope fractionation factors of the H exchange between steam and soil clay fractions

Stefan Merseburger [1], Arnim Kessler [2], Yvonne Oelmann [2], Wolfgang Wilcke [1]

[1] Institute of Geography and Geoecology, Karlsruhe Institute of Technology (KIT), Karlsruhe, Germany
[2] Geoecology, University of Tübingen, Tübingen, Germany

Chapter 4 is online published on 27/02/2023 in Rapid Communications in Mass Spectrometry, https://doi.org/10.1002/rcm.9499, open access.

Abstract

RATIONALE: Steam equilibration overcomes the problem of the traditional measurements of H isotope compositions, which leave an arbitrary amount of adsorbed water in the sample, by controlling for the entire exchangeable H pool, including adsorbed water and hydroxyl-H. However, the use of steam equilibration to determine nonexchangeable stable H isotope compositions in environmental media (expressed as δ^2H_n values) by mathematically eliminating the influence of exchangeable H after sample equilibration with waters of known H-isotopic composition requires the knowledge of the equilibrium isotope fractionation factor between steam-H and exchangeable H of the sample ($\alpha_{ex\text{-}w}$), which is frequently unknown.

METHODS: We developed a new method to determine the $\alpha_{ex\text{-}w}$ values for clay minerals, topsoil clay fractions, and mica by manipulating the contributions of exchangeable H to the total H pool via different degrees of post-equilibration sample drying. We measured the δ^2H values of steam-equilibrated mineral and soil samples using elemental analyzer-pyrolysis-isotope ratio mass spectrometry.

RESULTS: The $\alpha_{ex\text{-}w}$ values of seven clay minerals ranged from 1.071 to 1.140, and those of 19 topsoil clay fractions ranged from 0.885 to 1.216. The $\alpha_{ex\text{-}w}$ value of USGS57 biotite, USGS58 muscovite, and of cellulose was 0.965, 0.871, and 1.175, respectively. The method did not work for kaolinite, because its small exchangeable H pool did not respond to the selected drying conditions. Structurally different mineral groups such as two- and three-layer clay minerals or mica showed systematically different $\alpha_{ex\text{-}w}$ values. The $\alpha_{ex\text{-}w}$ value of the topsoil clay fractions correlated with the soil clay content ($r = 0.63$, $p = 0.004$), the local mean annual temperature ($r = 0.68$, $p = 0.001$), and the δ^2H values of local precipitation ($r = 0.72$, $p < 0.001$), likely to reflect the different clay mineralogy under different weathering regimes.

CONCLUSIONS: Our new $\alpha_{ex\text{-}w}$ determination method yielded realistic results in line with the few previously published values for cellulose. The determined $\alpha_{ex\text{-}w}$ values were similar to the widely assumed values of 1.00–1.08 in the literature, suggesting that the adoption of one of these values in steam equilibration approaches is appropriate.

4.1 Introduction

Stable hydrogen isotope compositions (expressed as δ^2H values relative to the standard mean ocean water) are widely used to investigate the provenance of organic substances like collagen, keratin, cellulose, or microbial tissue.[1] When complex materials like soil and plant samples are studied, the measurement of the δ^2H values can be influenced by unwanted exchange of part of the H pool, termed "exchangeable", with ambient atmospheric water vapor during sample preparation, for example. The latter does not affect the "nonexchangeable" part of the H pool stored as C-bonded H in organic matter or structural H in hydroxyl groups. However, the quickly exchanging H can blur the stable H isotope signal of the nonexchangeable H pool.[2–5] Steam equilibration avoids this problem by controlling the influence of the exchangeable H on the δ^2H values of the nonexchangeable H pool. The latter is reached by equilibrating the H isotope composition of exchangeable H with water vapors of known H-isotopic composition. After steam equilibration, the contribution of exchangeable to total H (χ_e) and the nonexchangeable H isotope ratios (δ^2H_n) can be determined by a regression of the measured δ^2H values (δ^2H_t) in equilibrated samples on the known δ^2H values of equilibration water vapors (δ^2H_w; Eq. 4.1).

$$\delta^2 H_t = \chi_e \, \alpha_{ex-w} \, \delta^2 H_w + (1 - \chi_e) \, \delta^2 H_n + 1000 \, \chi_e \, (\alpha_{ex-w} - 1) \qquad \text{(Eq. 4.1)}$$

From this empirical regression line, χ_e (included in the slope) and the δ^2H_n value (included in the y-axis intercept) can be calculated if the equilibrium fractionation factor between exchangeable H of the sample and equilibration water (α_{ex-w}) is known. α_{ex-w} is defined as the ratio of the stable isotope ratio of the exchangeable H in the samples to the stable H isotope ratio of the steam. To the best of our knowledge, there is no established method to determine α_{ex-w} values for complex mixtures of compounds commonly occurring in soils in the temperature range used for steam equilibration at 110 °C–130 °C. Schimmelmann[6] determined the α_{ex-w} value of cellulose by steam equilibration of fibrous cellulose and its nitrated counterpart using a reduced exchangeable H concentration at 114 °C for 20 h. From the intersection of the two resulting regression lines for the original cellulose and the nitrated cellulose, Schimmelmann[6] calculated an α_{ex-w} value of 1.08. This α_{ex-w} value has been widely used to determine δ^2H_n values of various organic compounds, plants, soil organic matter, and bulk soil by steam equilibration[7–15], although it is known that the α_{ex-w} values of cellulose

can range from 1.063 to 1.243 depending on its crystallinity.[16–19] Other studies that applied a steam equilibration method to organic materials and clay minerals ignored equilibrium fractionation between exchangeable H in the studied material and ambient water vapor-H, thus assuming an $\alpha_{ex\text{-}w}$ value of 1.[17,20–23]

Recently, Merseburger et al.[23] adapted and tested the steam equilibration method of Ruppenthal et al.[9] for clay minerals and soil clay fractions. In the hygroscopic clay minerals, in which not only adsorbed water contributes to the exchangeable H pool but also hydroxyl-H at the mineral edges, which cannot be removed by drying[2], there is a particular risk of exchanging H with ambient atmospheric water vapor after steam equilibration, which needs to be avoided.[2–5] The latter can be reached by closing the samples in airtight tin capsules under an Ar atmosphere, which require less mechanical force for crimping than Ag capsules.[23–25] For samples with a high χ_e value, the calculated δ^2H_n values respond sensitively to variations in the $\alpha_{ex\text{-}w}$ value, because the $\alpha_{ex\text{-}w}$ value influences both the slope and the intercept of the regression line of δ^2H_t values of the studied sample on the δ^2H_w values used for the exchange (Eq. 4.1).[8,13,19,22,26] Thus, the knowledge of a sample-specific $\alpha_{ex\text{-}w}$ value might improve the measurement of δ^2H_n, particularly if the sample consists of an unknown mixture of different minerals.

The fact that the χ_e value influences the slope of the regression line of measured δ^2H_t values on the known δ^2H_w values provides the opportunity to determine the $\alpha_{ex\text{-}w}$ value by manipulating χ_e, provided that the $\alpha_{ex\text{-}w}$ values remain unchanged. Because part of the exchangeable H pool consists of adsorbed water, different sample drying conditions result in different χ_e values. Analogous to the approach of Schimmelmann[6], from the intersection point of the pair of regression lines with different slopes resulting from two different drying conditions, $\alpha_{ex\text{-}w}$ can be calculated, provided the difference in the slopes is sufficiently large to precisely determine the intersection point.[6]

In a previous work, Merseburger et al.[23] tested whether the classic clay separation treatment, including the removal of Fe oxides and carbonates, reduction of soil organic matter (SOM), and dispersion of the remaining material, affects the δ^2H_n values of clay minerals. In the absence of a known $\alpha_{ex\text{-}w}$ value, the equilibrium fractionation between the exchangeable H pool and the steam-H was ignored (i.e., $\alpha_{ex\text{-}w} = 1$). Merseburger et al.[23] found that the differences in δ^2H_n values between clay minerals (kaolinite, illite, montmorillonite, and vermiculite) subjected and not subjected to the clay separation treatment were not significant and concluded that the clay separation treatment did not

affect the δ^2H_n values of clay minerals and soil clay fractions. However, this conclusion can be maintained only if the clay separation treatment did not change $\alpha_{ex\text{-}w}$, which remains to be tested.

Ruppenthal et al.[8] reported a correlation between the modeled δ^2H values of local mean annual precipitation and the δ^2H_n values of a global set of bulk soil samples. A study of an Argentinian climosequence demonstrated a weaker correlation of the δ^2H values of local precipitation with the δ^2H_n values of bulk soil than with the δ^2H_n values of demineralized SOM.[10,27] Merseburger et al.[24] showed that one reason for the weaker correlation of the δ^2H values of local precipitation with the δ^2H_n values of bulk soil than of SOM is the weaker correlation of the δ^2H values of local precipitation with the δ^2H_n values of clay fractions than of SOM assuming the same constant $\alpha_{ex\text{-}w}$ values for all samples. The larger scatter in the relationship between the δ^2H_n values of soil clay fractions and the δ^2H values of local precipitation was attributed to different isotope fractionation between ambient water-H and H of clay minerals ($\alpha_{min\text{-}water}$) during their formation[28] and a minor contribution of rock-derived clay minerals that were not formed under the current climatic conditions. It is, however, additionally possible that this larger scatter compared to the work of Ruppenthal et al.[8,10,27] is also attributable to a potential difference in the $\alpha_{ex\text{-}w}$ values, which might reflect the types of clay minerals. Different types of clay minerals (a) tend to form under different weathering regimes.[29–32] (b) Savin and Epstein[28] found different $\alpha_{min\text{-}water}$ values for kaolinite typically formed under strong chemical weathering conditions (0.97) and montmorillonite more characteristic of moderate weathering (0.94), and it seems possible that similar differences exist for $\alpha_{ex\text{-}w}$. Furthermore, (c) for glauconite, chlorite, mica and montmorillonite the $\alpha_{min\text{-}water}$ values varied with the octahedral Fe concentration,[33–35] and the chemical composition of clay minerals and soil clay fractions could also influence $\alpha_{ex\text{-}w}$. In addition, the Fe oxide concentration in soil is strongly linked to the weathering regime, with Fe oxides being an important component of soil clay fractions,[30,36] and the octahedral Fe concentrations might be related with the Fe oxide concentrations. Moreover, (d) the different crystal structures and imperfect lattices can influence the availability of hydroxyl groups for H exchange.[11,18,35,37–39] For instance, kaolinite has one quarter of the hydroxyl groups in the same layer as the non-bridging oxygen atoms of the tetrahedral sheet, which are less accessible than the rest of hydroxyl groups on the surface of the microcrystals, which show different vibrational

energies and different H exchange rates.[35,39,40] As a consequence, Méheut et al.[41] calculated different equilibrium fractionation factors with water for both hydroxyl types of kaolinite.

Our aims were (a) to determine sample-specific $\alpha_{ex\text{-}w}$ values for individual clay minerals and soil clay fractions by manipulating the contribution of exchangeable to total H (χ_e) via differently intensive drying assuming that this does not change the $\alpha_{ex\text{-}w}$ values and (b) to test whether the conventional method to collect soil clay fractions influences $\alpha_{ex\text{-}w}$. Moreover, (c) we tested the hypothesis that the $\alpha_{ex\text{-}w}$ values of soil clay fractions are influenced by their mineralogical composition as assessed via the potential cation-exchange capacity (CEC_{pot}) and their latitudinal and elevational position assessed via the δ^2H value of the local precipitation at the sampling location.

4.2 Material and methods

4.2.1 Samples

We used kaolinite (KGa-2), dioctahedral illite (IMt-2), Na-saturated montmorillonite (SWy-3) and Mg-rich trioctahedral montmorillonite (SCa-3) provided by the Clay Mineral Society (Chantilly, VA, USA) and a trioctahedral vermiculite (contributed by Stefan Dultz, Hannover, Germany) as clay mineral reference materials. SCa-3 and IMt-2 were delivered as brittle rock chips, with a macroscopically visible heterogeneity in grain sizes and colors. SWy-3 and KGa-2 were delivered as fine-grained powders. The standards are described by the baseline studies of the Clay Minerals Society Source Clays[42–48] and by Hower and Mowatt[49] for IMt-2. Trioctahedral vermiculite was characterized by Dultz et al.[50], Bors et al.[51] and Steudel et al.[52,53]. Furthermore, we included USGS57 biotite and USGS58 muscovite described by Qi et al.[54] and microcrystalline cellulose (A17730 Alfa Aesar, Ward Hill, MA, USA).

We used 22 topsoil samples from nine countries on five continents (Table 4.1 and 4.S1). Nine samples originated from a climosequence in Argentina (signature “AR”), which are described in detail in Ruppenthal et al.[10] The Argentinian samples were collected from the 0–10 cm mineral soil layer of Phaeozems (AR-2A and AR-4A), a Chernozem (AR-5C), a Calcisol (AR-14A), a Solonetz (AR-16A), a Luvisol (AR-17A), a Vertisol (AR-19A) and a Planosol (AR-20C). The clay contents ranged from 10% to 30% and organic C concentrations from 5 to 14 g kg^{-1}. The sample DE-KA1 originated from

the 7-13 cm depth layer of a Gleysol near Karlsruhe, Germany, with a clay content of 58% and an organic C concentration of 55 g kg^{-1}.[23] The signature "EC" refers to samples from tropical forest sites in south Ecuador.[55–58] EC-BOM was collected from the 0-25 cm layer of a Cambisol at an elevation of ~3000 m above sea level and EC-SF from the 0-15 cm layer of a Cambisol at an elevation of ~2000 m above sea level. The clay contents were 29% and 22%, and the organic C concentrations were 24 and 22 g kg^{-1}. The sample KE-44 originated from the 0–10 cm layer of a Cambisol in Kenya, had a clay content of 71% and an organic C concentration of 48 g kg^{-1} and was provided by Sadadi Ojoatre.[59] Sample PA-A9 originated from the 0–10 cm layer of a Luvisol on Barro Colorado Island, Panama and had a clay content of 84% and an organic C concentration of 28 g kg^{-1}.[60,61] The signature "RU" refers to Russia. Sample RU-17 was collected from the 0–30 cm layer of a Luvisol, RU-PS2 from the 0–8 cm layer of a Cryosol, and RU-S20 from the 0–10 cm layer of a Luvisol. The Russian samples had a clay content of 4%–13% and an organic C concentration of 20–78 g kg^{-1}.[62–64] Sample SK-Oso originated from the 0–10 cm layer of a Cambisol in Slovakia and had a clay content of 15% and an organic C concentration of 60 g kg^{-1}.[65,66] Finally, UZ-K1 originated from the 0–10 cm layer of a Calcisol in Uzbekistan with a clay content of 30% and an organic C concentration of 14 g kg^{-1}.[67,68] All samples were dried and stored in the dark for 1–28 years. Further properties of the used soil samples, including X-ray powder diffractometric patterns of six samples, can be found in Merseburger et al.[24] Additional X-ray powder diffractometric patterns have been published for sample PA-A9 [60] and from soils nearby the locations from where our two Ecuadorian samples were collected.[58]

4.2.2 Clay separation

We used the clay separation method of Merseburger et al.[23], which was thoroughly tested and found to not affect the δ^2H_n values of clay minerals typically occurring in soils. In contrast, the clay separation method of course influences the δ^2H values of the exchangeable H pool. This is, however, not relevant for our measurement of δ^2H values, because we anyway equilibrate all exchangeable H with water vapors of known H isotopic composition in our steam equilibration method (Eq. 4.1). Briefly, after sieving to < 2 mm we removed Fe oxides by applying the dithionite-citrate-buffer method of Mehra and Jackson[69] once. To remove carbonates, we used a Na-acetate acetic acid buffer adjusted to pH 4.8. To remove organic matter, we added H_2O_2 in a water bath at 50 °C.

We removed water-soluble salts with several washing cycles using water or salt solutions after each mineral or SOM destruction step. After the electrical conductivity of the sample solution had reached < 400 µS cm^{-1}, we determined the grain sizes by pipette analysis according to DIN ISO 11277,[70] but instead of a dispersion agent we used water with a pH of ~7.5. In this water, we separated the grain sizes by repeated sedimentation in 2-L cylinders. Clay separates were precipitated using $MgCl_2$. A H_2O_2 treatment of the precipitate reduced the organic matter concentration in the clay fractions further. After final washings until the conductivity of the supernatant had reached <100 µS cm^{-1}, we dried the clay fractions at 60 °C and pulverized them manually in a mortar.

All samples were distributed among four treatment batches each taking ~10–12 weeks. As quality check, we included sample SK-Oso in each treatment batch, which resulted in relative standard deviations of 2% for each of the sand, silt and clay fractions. In a previous study,[23] we found that the differences between clay minerals (kaolinite, illite, montmorillonite, vermiculite) that were subjected ("treated") and not subjected to the clay separation procedure ("untreated") were not significant and concluded that the clay separation treatment did not affect the δ^2H_n values of clay minerals and soil clay fractions.

4.2.3 Steam equilibration

We steam equilibrated all samples, which included the soil clay fractions and the pure minerals that were both subjected to the clay separation procedure ("treated") and measured directly ("untreated"). We weighed 1–2 mg of the air-dry and homogeneous sample (2–3.5 mg for USGS biotite and muscovite) in triplicates and transferred into smooth-walled tin capsules of known weight. The samples were vacuum-dried for 2 h at 120 °C. Then, we injected water of known isotopic composition into the closed stainless-steel vessel. We steam equilibrated our samples with three to four different waters of known isotopic composition per batch (AWI-TD1: -266.4 ± SD 0.8‰, n = 4; laboratory water: -57.5 ± 0.8‰, n=3; medium deuterium-enriched water: 136.8 ± 0.6‰, n = 3; and highly deuterium-enriched water: 334.6 ± 1.8‰, n = 4). Within 16 h at the same temperature, the steam-H equilibrated with the exchangeable H fraction of the samples. This was followed by 15 min of vacuum drying using a diaphragm pump (VP 220, VWR, Radnor, PA, USA) and 45 min using a rotary vane pump (RZ 2.5, Vacuubrand, Wertheim, Germany), both at 120 °C and a 2-h cooling phase at room temperature under

continuous evacuation (≤ 1 Pa), which we called “medium” drying intensity. We transferred the vacuum chamber into a glove bag, self-made from 100 µm polyethylene foil bags[71] and flushed twice with dried Ar to reach a water vapor-free atmosphere. In the Ar atmosphere, we sealed each of the approximately 80 capsules in the vacuum vessel with a gastight pressing. After cooling, each capsule was weighed.

In addition to medium drying, we realized a weaker and a stronger drying intensity. For the weaker drying intensity, the temperature was maintained at 120 °C after the 16-h equilibration, and the stainless-steel vessel was evacuated using the diaphragm pump for 1 h. Then, the vessel was cooled for 2 h at room temperature outside the oven while evacuating with the diaphragm pump to a final pressure of 150–300 Pa. For the stronger drying intensity, the temperature was maintained at 120 °C after the 16-h equilibration, and the stainless-steel vessel was evacuated using the diaphragm pump for 15 min and additionally with the rotary vane pump for another 45 min. Then, the temperature was increased to 200 °C for 2 h, cooled for 3 h at room temperature outside the oven and evacuated continuously using the rotary vane pump to a final vacuum < 1 Pa (Figure 4.1). To test additionally whether there was an effect of remoistening of the samples after the different drying procedures on their δ^2H_t values, we included SCa-3 montmorillonite (as provided by the Clay Mineral Society but gently ground to < 200 µm by hand) considered as particularly hygroscopic in each equilibration batch. We sealed the tin capsules with SCa-3 montmorillonite in triplicate before all other samples in the equilibration batch and again at the end, also in triplicate. We found only a small difference of 2.2 ± SD 2.0‰ between the mean of the triplicate samples sealed at the beginning and the mean of the triplicate samples sealed at the end, because of slight remoistening during which we sealed the tin capsules of all samples.

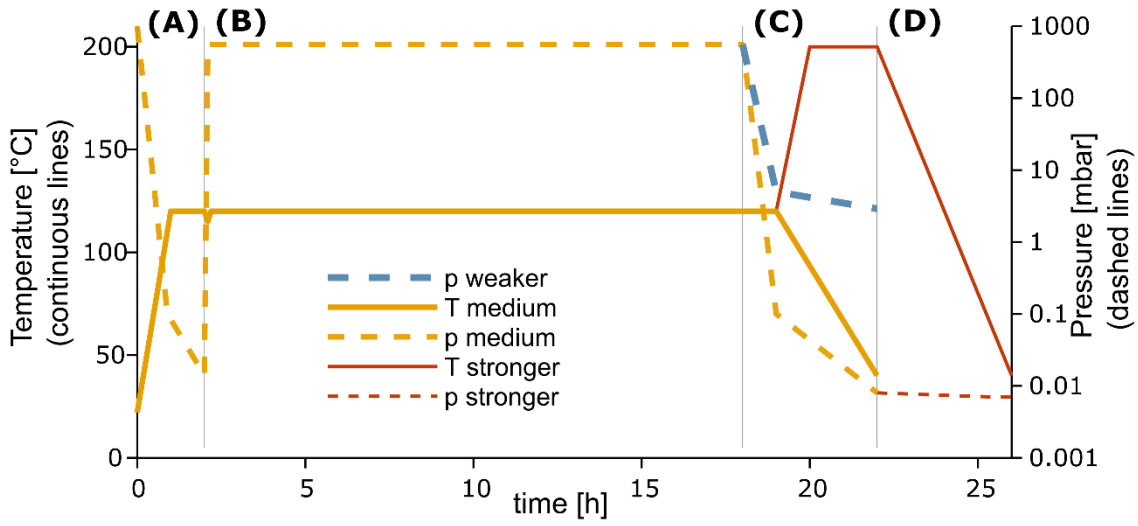

Figure 4.1: Temperature and pressure conditions during equilibration of soil clay fractions and clay minerals with water vapor of known H-isotopic composition. A, the drying phase before equilibration; B, the equilibration phase; C and D, two stages of the drying phase. The continuous yellow line shows the standard procedure (medium drying). If deviating from the standard procedure, temperature (continuous lines) and pressure (dashed lines) are plotted for stronger drying (red, thin lines) and for weaker drying (blue, thick, dashed line), for which only the pressure was less decreased.

Our different drying intensities reflect conditions used in previous studies in which steam equilibration was applied. For example, the final pressure of our weaker drying intensity is close to the 100 Pa used by Ruppenthal et al.[8] and the <500 Pa recommended by Wassenaar et al.[72] The stronger drying intensity at 200 °C is by ±50 °C similar to the vacuum-drying temperatures used for durations of 2–4 h before conventional δ^2H measurements of clays. Studies investigating the optimum temperature for vacuum drying found that 200 °C removes most of the adsorbed water, although some water residues remain depending on the clay mineral type and the degree of crystallinity.[2,5,37,40] Our approach is based on the assumption that the variation in drying procedures did not affect the $\alpha_{ex\text{-}w}$ values. It is reported that the pressure sensitivity of the equilibrium fractionation factor is negligible below 130 °C[41,73] and likely still small up to our maximum temperature of 200 °C. However, there are two possible problems with this assumption. (a) With the variation in the temperature between 120 °C and 200 °C, we might slightly change the $\alpha_{ex\text{-}w}$ value, which is an equilibrium constant that is related with temperature. For pure water, the difference in $\alpha_{liquid\text{-}vapor}$ between our lowest temperature of 120 °C and our highest one of 200 °C was reported to be 0.018 at high pressure.[74] Because we studied adsorbed water, which does not similarly freely

exchange between the liquid and gaseous phases under a lower pressure, we assume that the variation in the $\alpha_{ex\text{-}w}$ value created by the different drying pressures is < 0.018. (b) We removed different amounts of adsorbed water with different drying intensities. If the removed water had a different H isotope composition than the total exchangeable H pool, then the different removed amounts could also have a small influence on our estimate of the $\alpha_{ex\text{-}w}$ value of the remaining exchangeable H. The latter we have not checked, because this would require to determine specific $\alpha_{ex\text{-}w}$ value for different fractions of exchangeable H, which was beyond our time and money resources.

4.2.4 Hydrogen isotope ratio measurement

We used the H isotope ratio measurement, clay separation and steam equilibration methods of Merseburger et al.[23,24] Briefly, after weighing the cooled capsules, we measured the δ^2H values using an elemental analyzer-pyrolysis-isotope ratio mass spectrometer (Flash 2000 HTC–Delta V Advantage, Thermo Fisher, Waltham, MA, USA) in a chromium-filled Al_2O_3 reactor at 1250 °C. We corrected small memory effects with the help of a pool-wise memory correction algorithm using one or two pools.[75] For normalization, we used VSMOW (Vienna Standard Mean Ocean Water), SLAP and IAEA-604 in silver capsule triplicates (25 µl, USGS, Reston, VA, USA) for each measurement sequence.

To control for instrumental drift between October 20, 2020, and May 21, 2021, we measured in each elemental analyzer-pyrolysis-isotope ratio mass spectrometry (EA–IRMS) sequence a polyethylene powder used as in-house standard with a mean δ^2H value of -70.2 ± SD 1.7‰ (n=264), GISP with -189.3 ± 1.1‰ (n=46) and IAEA-CH7 with -100.6 ± 1.7‰ (n=90). The standards were not steam equilibrated. These values were indistinguishable from the certified or recommended values. The sample SK-Oso, for which we collected the clay fraction four times in separate runs to generate independent replicates and which were steam-equilibrated had a δ^2H_n value of -99 ± SD 3‰ and a χ_e of 17.8 ± 0.8% ($\alpha_{ex\text{-}w}$ = 1, medium drying intensity).

4.2.5 Chemical sample properties

The C concentrations were determined using an elemental analyzer (Flash 2000 HTC, Thermo Fisher, Waltham, MA, USA and EuroVector 3000 (EuroVector, Pavia, Italy). The pH value was measured with a glass electrode (SenTix® 81 on pH 3310, WTW,

Weilheim, Germany) in a deionized water suspension at a soil to water ratio of 1:2.5 (v/v). The CEC_{pot} of the clay fractions was determined using the Cu(II)-triethylentetramine method[76,77], in a phosphate buffer (pH = 7.0) and with 24 h shaking time. To differentiate between nonswellable two-layer clay minerals and chlorite and swellable three-layer clay minerals and illite in soil clay separates, which contain a complex mixture of minerals not only consisting of clay minerals, we used a value of 160 $mmol_c\ kg^{-1}$ below which we assumed a dominance of two-layer clay minerals and/or chlorite and above which one of three-layer clay minerals following international soil classification systems.[78] For pure clay minerals, the threshold value of the CEC_{pot} to distinguish between two- and three-layer clay minerals was 400 $mmol_c\ kg^{-1}$.[79] Previous XRD measurements of a subset of our soil clay fractions confirmed that the CEC_{pot} is suitable to approximatly assign the clay fractions of the soil samples to the dominant clay mineral groups.[24,58,60]

4.2.6 Data evaluation

We normalized all stable H isotope ratios to the VSMOW-SLAP scale [80], which we extended with IAEA-604 to 799.9‰, and expressed them in ‰ relative to VSMOW.

We used the R statistical computing environment[81,82] to calculate stable H isotope data and for statistical analysis. To determine reliable δ^2H_n values, we removed samples that came into contact with atmospheric humidity after the equilibration. We detected such samples by (a) visual inspection for holes and (b) the absence of an Ar peak after the H_2 peak in the elemental analyzer chromatogram. Steam equilibrations of the same sample with isotopically different waters need to result in the same contribution of exchangeable H to the total H concentration (same χ_e). Moreover, (c) we removed individual H isotope measurements in which both the H concentration and the residual of the equilibrium line were 0.5 times outside the interquartile range of all other equilibrations of the same sample as outliers. This quality check was performed individually for all capsules subjected to steam equilibration by performing steps (b) and (c) simultaneously in an automated script. We regressed the measured δ^2H_t values on the known isotopic H composition of the equilibration waters (δ^2H_w) and used Eq. 4.1 to determine δ^2H_n values and the contribution of exchangeable to the total H concentration (χ_e).[8–10,13,16,19,26] The intercept (b) of the regression line is a function of χ_e, δ^2H_n and $\alpha_{ex\text{-}w}$. The slope (m) is the product of χ_e and $\alpha_{ex\text{-}w}$. For $\delta^2H_w = 0$, Equation 4.1 can

be solved for δ^2H_n using each individual regression line (i) originating from a specific drying procedure (Eq. 4.2):

$$\delta^2H_{n,i} = \frac{\alpha_{ex-w}\, b_i - 1000\, m_i\, (\alpha_{ex-w} - 1)}{\alpha_{ex-w} - m_i} \quad . \qquad \text{(Eq. 4.2)}$$

By drying the samples after equilibration differently, the slope (m_i) and intercept (b_i) of the equilibration line can be manipulated because χ_e is varied and as a consequence also the δ^2H_t values. Assuming that $\alpha_{ex\text{-}w}$ and δ^2H_n values of the different drying procedures are the same and solving Eq. 4.2 for $\alpha_{ex\text{-}w}$ yields Eq. 4.3:

$$\alpha_{ex-w} = \frac{b_1\, m_2 - b_2\, m_1 + 1000\, (m_2 - m_1)}{b_1 - b_2 + 1000\, (m_2 - m_1)}. \qquad \text{(Eq. 4.3)}$$

For confirmation, we calculated $\alpha_{ex\text{-}w}$ using two other methods with the identical result (Supporting Information Text S1). We estimated the standard error of $\alpha_{ex\text{-}w}$ by applying Gaussian error propagation (Supporting Information Text S2). A larger difference between the slopes and a smaller scatter around the equilibration lines resulted in a smaller propagated error. We accepted only $\alpha_{ex\text{-}w}$ values with a propagated SD < 0.2. Moreover, we used pairs of equilibration lines only if the stronger drying resulted in a steeper slope than the weaker drying. Including the medium-drying equilibration line taken from Merseburger et al.[23,24], when available, yielded a maximum of three possible equilibration line pairs, and thus three opportunities for deriving $\alpha_{ex\text{-}w}$. We then calculated the arithmetic mean and standard error as a measure of the precision of the estimate of the mean of the $\alpha_{ex\text{-}w}$ values from different combinations of equilibration line pairs.

For the sampling locations of the topsoil clay fractions we considered mean annual precipitation and temperature using the Worldclim data set (version 2) for the years 1970–2000 [83] with derived evapotranspiration and aridity index[84]. Annual mean δ^2H values of precipitation (δ^2H_p) were computed using the Online Isotopes in Precipitation Calculator.[85,86]

4.3 Results and Discussion

4.3.1 Determination of sample-specific $\alpha_{ex\text{-}w}$ value

In line with the sufficiently different slopes of the regression lines, there was a significant difference between the contributions of exchangeable H to total H (χ_e) in the minerals and clay fractions after weaker and stronger drying (paired t-tests, mean

difference 11.2%, $p < 0.001$), ranging from 1% to 24% (Table 4.1). Thus, the different drying procedures allowed for the calculation of a sample-specific $\alpha_{ex\text{-}w}$ value.

We were able to determine the $\alpha_{ex\text{-}w}$ value for 7 of 10 clay minerals, 19 of 22 topsoil clay fractions, and all 3 other materials (two different types of mica and cellulose, Table 4.1). The missing data are attributable to the fact that the slopes of the regression lines of the δ^2H_t values of the sample on the δ^2H_w values after the different drying procedures were not sufficiently different to reliably determine the intersection point of the two regression lines in all three considered pairs (weaker-medium, weaker-stronger, and medium-stronger drying). The overall mean $\alpha_{ex\text{-}w}$ value was 1.080 ± standard error (SE) 0.015 (n=29) and thus identical with the $\alpha_{ex\text{-}w}$ value frequently chosen in the literature for bulk soil and organic matter.[8] Thus, an $\alpha_{ex\text{-}w}$ value of 1.080 is a suitable estimate for soil minerals.

For USGS57 biotite, only the slopes of the regression lines of the δ^2H_t values of the sample on the δ^2H_w values between weaker drying and medium-stronger drying were sufficiently different, whereas medium and stronger drying resulted in indistinguishable slopes, leaving two of three possible combinations of regression lines for deriving $\alpha_{ex\text{-}w}$ (Figure 4.2A; Table 4.1). For untreated kaolinite, that is kaolinite not subjected to clay separation, the regression lines of the three different drying procedures were almost identical, preventing the calculation of an $\alpha_{ex\text{-}w}$ value of this nonswellable two-layer clay mineral (Figure 4.2B). Kaolinite showed a contribution of exchangeable to total H of 7 ± SD 1 % and USGS58 muscovite of 1.1 ± 0.6 %, (for medium drying). In contrast to kaolinite, the $\alpha_{ex\text{-}w}$ determination of the muscovite was possible, because the exchangeable H pool responded to the different drying intensities. This indicated that the exchangeable H pool of the muscovite contained more adsorbed water, whereas that of the kaolinite contained more hydroxyl-H. The swellable two-layer clay minerals, SCa-3 montmorillonite (Figure 4.2C) and trioctahedral vermiculite (Supporting Information Table 4.S1) strongly responded to the different drying procedures. However, the regression line of the treated trioctahedral vermiculite showed a low coefficient of determination, because of a large scatter around the regression lines (Supporting Information Table 4.S1), so that the SD of $\alpha_{ex\text{-}w}$ was with 0.224 above our proposed threshold for acceptable precision. Consequently, we could not determine a reliable $\alpha_{ex\text{-}w}$ value for treated trioctahedral vermiculite.

The two regression lines after weaker and stronger drying for commercially available cellulose were sufficiently different to determine the $\alpha_{ex\text{-}w}$ value at 1.175 (Figure 4.2D). This is higher than the $\alpha_{ex\text{-}w}$ value of 1.08 determined at 114 °C reported by Schimmelmann[6] and of 1.082 determined at 105 °C reported by Filot et al.[16] who found a variation of the $\alpha_{ex\text{-}w}$ value for cellulose extracted from different years of tree rings from 1.063 to 1.112. However, our $\alpha_{ex\text{-}w}$ value for cellulose is lower than the reported $\alpha_{ex\text{-}w}$ values of 1.213–1.243 determined at 0 and 92 °C for cellulose extracted from different tree species.[17–19] The differences in the $\alpha_{ex\text{-}w}$ values cannot be explained by the different equilibration temperatures, because there is no obvious relationship between temperature and the $\alpha_{ex\text{-}w}$ value. We therefore speculate that the different reported $\alpha_{ex\text{-}w}$ values of cellulose are related with its crystallinity and thus represent a natural variation. While in the microcrystalline cellulose, which we studied, steam might reach all hydroxyl-H, this is possibly not the case in more crystalline cellulose, where some hydroxyl-H is shielded from the access of steam.[11,18]

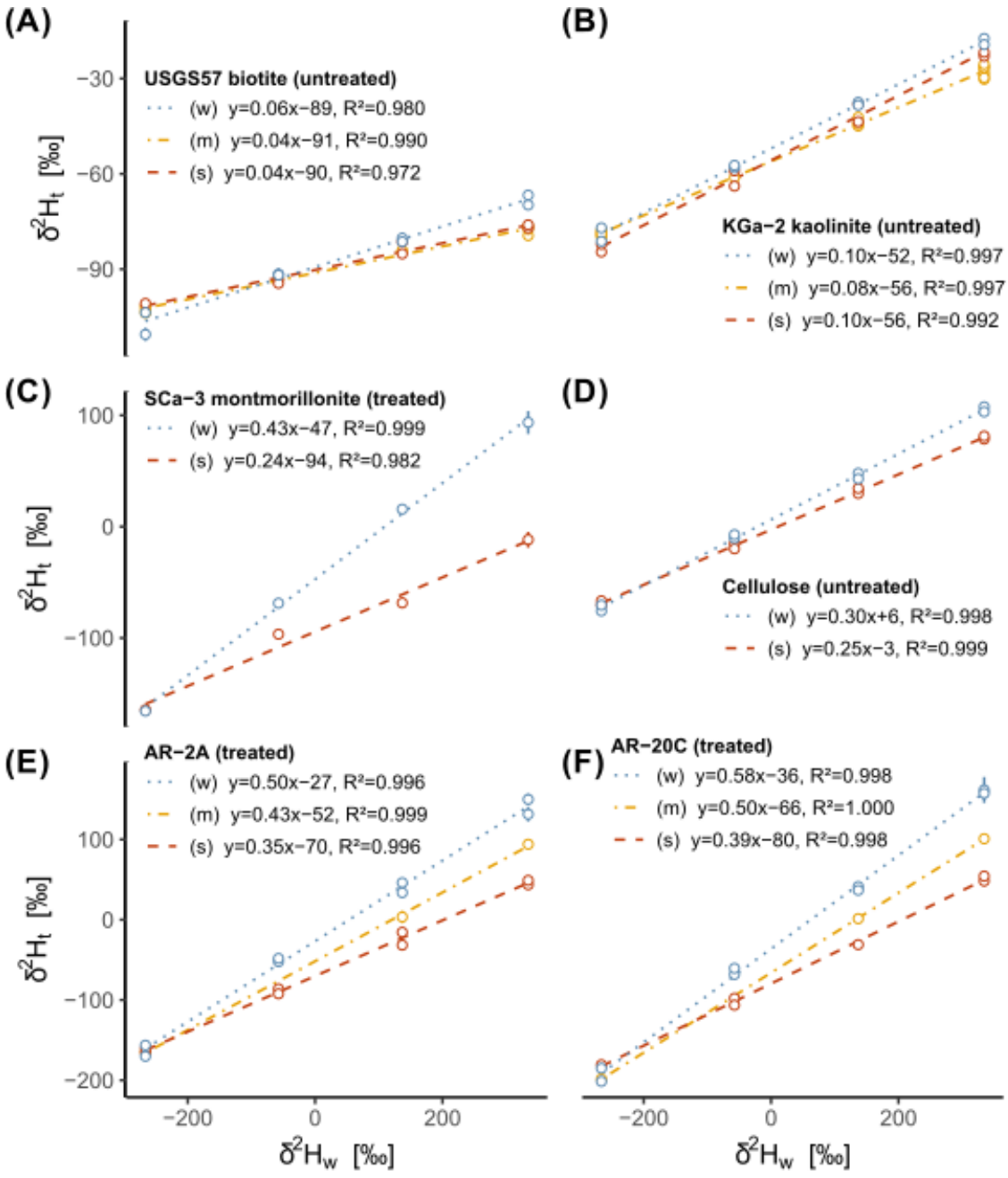

Figure 4.2: Regression lines of the total δ^2H values of the mineral samples and clay fraction (δ^2H_t) on the δ^2H values of different equilibration waters (δ^2H_w) of selected samples after weaker ("w"), medium ("m") and stronger ("s") drying. "AR" denotes soil clay fractions from Argentina (Table 4.1). "Untreated" and "treated" indicate samples not subjected and subjected to clay separation (Section 2.2), respectively. For C, *SCa-3 montmorillonite and* D, *microcrystalline cellulose, no medium drying intensity was realized. Each point originates from an independent equilibration run, measured in a separate* EA-*IRMS sequence. Error bars show standard deviations (n=1–3) and might be smaller than the symbol size.*

Table 4.1: *Results of steam equilibration with weaker ("w"), medium ("m") and stronger ("s") drying intensities (see Figure 1) including the equilibrium fractionation factor between the exchangeable H pool of the sample and the H of the steam ($\alpha_{ex\text{-}w}$), the contribution of exchangeable H to total H (χ_e) after weaker and stronger drying, the δ^2H_n values calculated using sample-specific $\alpha_{ex\text{-}w}$ value and for $\alpha_{ex\text{-}w}$ = 1 and the potential cation-exchange capacity (CEC_{pot}).*

Type	Sample (reference)	Treatment	Equilibration line pairs	$\alpha_{ex\text{-}w}$ ‡	$\chi_{e,weaker}$ *	$\chi_{e,stronger}$ *	δ^2H_n *	$\delta^2H_{n,\alpha=1}$ *	CEC_{pot}
					[%]		[‰]		$mmol_c\ kg^{-1}$
clay mineral	IMt-2 illite §	treated	ws	1.079	13	8	-141	n.d.	n.d.
		untreated	wm, ws	1.134 ± 0.005	21 ± 2	14 ± 1	-158 ± 4	-138 ± 4	89
	SCa-3 montmorillonite §	treated	ws	1.140	38	22	-160	n.d.	n.d.
		untreated	wm, ws, ms	1.084 ± 0.015	75 ± 5	54 ± 4	-202 ± 15	-98 ± 17	1113
	SWy-3 montmorillonite §	treated	ws	1.122	16	10	-150	n.d.	n.d.
		untreated	wm, ws	1.071 ± 0.032	31 ± 3	22 ± 2	-150 ± 7	-133 ± 7	743
	Trioctahedral vermiculite #,§	untreated	ws, ms	1.090 ± 0.039	71 ± 6	54 ± 3	-225 ± 13	-95 ± 13	n.d.
other	USGS57 biotite [54]	untreated	wm, ws	0.965 ± 0.019	7 ± 1	4 ± 1	-94 ± 1	-95 ± 1	n.d.
	Microcrystalline cellulose		ws	1.175	25	21	-51	n.d.	n.d.
	USGS58 muscovite [54]		wm	0.871	3	2	-29	-31 ± 1	n.d.
topsoil clay fraction	AR-2A [10]	treated	ws, ms	1.129 ± 0.030	45 ± 3	31 ± 3	-162 ± 9	-91 ± 10	261
	AR-4A [10]		wm, ws, ms	1.060 ± 0.027	57 ± 4	40 ± 3	-158 ± 8	-108 ± 8	199
	AR-5C [10]		ws, ms	1.099 ± 0.077	41 ± 4	31 ± 3	-168 ± 8	-118 ± 5	217
	AR-10A [10]		wm, ws, ms	1.100 ± 0.006	49 ± 3	28 ± 2	-157 ± 2	-106 ± 2	531
	AR-14A [10]		wm, ws, ms	1.070 ± 0.019	53 ± 4	30 ± 4	-156 ± 8	-118 ± 8	248
	AR-16A [10]		wm, ws, ms	1.087 ± 0.046	51 ± 5	33 ± 5	-176 ± 7	-129 ± 5	497
	AR-17A [10]		wm, ws, ms	1.091 ± 0.042	49 ± 4	32 ± 3	-180 ± 9	-129 ± 8	664
	AR-19A [10]		wm, ws, ms	1.080 ± 0.000	45 ± 2	26 ± 3	-168 ± 2	-132 ± 2	640
	AR-20C [10]		wm, ws, ms	1.080 ± 0.052	54 ± 6	36 ± 4	-191 ± 10	-132 ± 5	423
	DE-KA1 [23]		wm, ws	1.129 ± 0.023	37 ± 2	28 ± 2	-146 ± 6	-94 ± 7	296
	EC-BOM [55,56,58]		wm	1.114	31	30	-101	-61 ± 2	127
	EC-SF1 [55,57,58]		wm	0.979	19	16	-67	-71 ± 2	143
	KE-44 [59]		ws	1.216	41	32	-168	-56 ± 2	344
	PA-A9 [60,61]		wm, ws	1.150 ± 0.035	35 ± 2	22 ± 2	-129 ± 5	-85 ± 5	872
	RU-17 [62,63]		wm, ws	1.094 ± 0.011	39 ± 3	26 ± 2	-138 ± 6	-101 ± 6	241
	RU-PS2 [64]		ws, ms	0.885 ± 0.105	26 ± 5	20 ± 4	-140 ± 8	-167 ± 1	240
	RU-S20 [62,63]		wm, ws, ms	1.007 ± 0.036	40 ± 3	26 ± 2	-139 ± 4	-136 ± 2	114
	SK-Oso [65,66]		wm, ws, ms	1.024 ± 0.024	21 ± 1	16 ± 1	-105 ± 3	-99 ± 3 †	121
	UZ-K1 [67,68]		wm, ws	1.205 ± 0.011	26 ± 1	17 ± 2	-148 ± 6	-102 ± 6	311

Notes: The δ^2H_n values for $\alpha_{ex\text{-}w}$ = 1 and the CEC_{pot} were taken from previous studies.[23,24] "Untreated" and "treated" indicate samples not subjected and subjected to clay separation, including removal of Fe oxides and carbonates, reduction in SOM and dispersion of the remaining material. Abbreviations: n.d. – not determined; SOM – soil organic matter.

‡ Mean ± standard error calculated from $\alpha_{ex\text{-}w}$ determinations with the help of two or three pairs of regression lines of the δ^2H value of the sample on the δ^2H value of the waters used for steam equilibration.

* With standard deviation, derived by Gaussian error propagation (see Supporting Information Text S2)

The result of the treated trioctahedral vermiculite showed an inacceptable standard deviation above 0.2 and was therefore omitted.

† Mean and standard deviation of δ^2H_n from four independent measurements.

§ Reference is given in the text section 2.1.

For both micas (USGS57 biotite and USGS58 muscovite[54]) we found, as the only samples, $\alpha_{ex\text{-}w}$ values < 1 (Table 4.1). We speculated that this might be attributable to the particularly low isoelectric point of pH < 2, which is lower than that of many clay minerals, indicating that hydroxyl groups at the mineral edges do not strongly bind protons, which commonly favors the binding of the light H isotope.[87,88]

For most topsoil clay fractions, our different drying procedures resulted in sufficiently different slopes of the regression lines as illustrated for two soil clay fractions from Argentina in Figure 4.2E and 2F. For 19 soil clay samples, the mean $\alpha_{ex\text{-}w}$ value was 1.084 ± SE 0.017 (Table 4.1), which was significantly greater than 1.00 (t-test, $p < 0.001$) and thus indicated that there was indeed an equilibrium fractionation between steam-H and the exchangeable H pool. The three topsoil clay fractions for which we could not successfully determine $\alpha_{ex\text{-}w}$ values originated from Thailand and Kenya. The Kenyan samples had high concentrations of dithionite-soluble Fe ranging from 56 to 75 mg g^{-1}. This could be problematic, because octahedral Fe was reported to influence the H isotope fractionation between clay minerals and ambient water at the time of mineral precipitation (i.e., the $\alpha_{min\text{-}water}$ value)[33–35] and by inference might also influence the $\alpha_{ex\text{-}w}$ value. However, this high Fe concentration did not prevent us from determining a meaningful $\alpha_{ex\text{-}w}$ value for the clay fraction of sample KE-44 (Table 4.1). Moreover, these tropical soil samples possibly contained some kaolinite, for which our approach did not work (Figure 4.2B). We attribute this to a small exchangeable H pool not responsive to the selected drying conditions in kaolinite and strongly weathered tropical soil samples.

Overall, we found systematic differences in the $\alpha_{ex\text{-}w}$ values of well-defined materials with the micas showing the lowest, the three-layer clay minerals intermediate, and cellulose the highest values (Table 4.1), revealing that these minerals provided different bonding environments for exchangeable H. Because in equilibrium fractionation, the heavy isotopes tend to accumulate in the stronger bonds, a higher $\alpha_{ex\text{-}w}$ value reflects a stronger bonding environment for H.[87] The $\alpha_{ex\text{-}w}$ values of our topsoil clay fractions almost spanned the whole range of $\alpha_{ex\text{-}w}$ values of the well-defined materials reflecting the heterogeneous mineral composition of these samples (Table 4.1).

4.3.2 Influence of the clay separation on the $\alpha_{ex\text{-}w}$ values of clay minerals

The differences in the $\alpha_{ex\text{-}w}$ values of the three clay minerals provided by the Clay Mineral Society (IMt-2 illite: 0.055, SCa-3 montmorillonite: -0.056, and SWy-3 montmorillonite: -0.051) between samples not subjected to clay separation ("untreated") and samples subjected to clay separation ("treated") were consistently smaller than the propagated SD of each treated sample (0.099, 0.089 and 0.172, respectively; Table 4.1; Supporting Information Section 4.6.2). Additionally, a t-test for the three pairs of treated and untreated $\alpha_{ex\text{-}w}$ values did not indicate a significant difference ($p = 0.68$). Thus, the clay separation procedure did not change the properties of the studied clay minerals in a way that significantly influenced their $\alpha_{ex\text{-}w}$ values.

For some of the swellable three-layer clay minerals such as trioctahedral vermiculite and SCa-3 montmorillonite, the error of the $\alpha_{ex\text{-}w}$ value determination using our approach was comparatively high and for the treated trioctahedral vermiculite even above the acceptable SD of 0.2 (Table 4.1 We attribute this to an insufficient control of the final vacuum for weaker drying conditions and still slight remoistening after steam equilibration and drying, because of the particularly high hygroscopicity of these minerals, which should be further reduced in future studies (Supporting Information Text 3). We quantified the influence of remoistening in the time interval between opening the vacuum vessel in a dried Ar atmosphere and gas-tight sealing of the last capsules using SCa-3-montmorillonite, our most hygroscopic sample (Table 4.1), in each steam equilibration run. The difference in the δ^2H_t values of SCa-3 montmorillonite between the first and the last capsules averaged 2.2 ± SD 2.0‰. Because of a consistently much flatter slope of the regression lines of the δ^2H_t values of the sample on the δ^2H_w values, we assume this small influence to be negligible for the less hygroscopic soil clay fractions (Supporting Information Table 4.S1).

For the soil clay fractions, we cannot test the influence of the clay separation as for pure minerals, because the soil clay fractions exist only after this treatment. However, from the lack of an influence of clay separation on the $\alpha_{ex\text{-}w}$ values of several common minerals in soils, we infer that the clay separation did not affect the $\alpha_{ex\text{-}w}$ values of the soil clay fractions.

4.3.3 Influence of the CEC_{pot} and the δ^2H value of local precipitation on the $\alpha_{ex\text{-}w}$ values of soil clay fractions

The $\alpha_{ex\text{-}w}$ values of the group of soil clay fractions with a $CEC_{pot} \leq 160$ $mmol_c$ kg^{-1}, which was presumably dominated by nonswellable clay minerals with a low surface charge, including two-layer minerals and pedogenic chlorite[78] are indicative of a strong weathering environment.[29,32] The group of soil clay fractions with a $CEC_{pot} \leq 160$ $mmol_c$ kg^{-1} was unrelated with the mean annual δ^2H value of local precipitation (δ^2H_p), which we used as a proxy of the climatic influence at the various latitudinal and elevational locations with decreasing δ^2H_p values from the equator to the pole and from sea level to mountain tops (Figure 4.3). We attribute this to the small number of four samples, the small variation in δ^2H_p values and the comparatively large error of the $\alpha_{ex\text{-}w}$ values because of the small χ_e values of these samples.

The $\alpha_{ex\text{-}w}$ values of the group of soil clay fractions with a CEC_{pot} of 160–400 $mmol_c$ kg^{-1} presumably containing a mixture of different clay minerals with a higher surface charge, including nonswellable three-layer minerals such as illites and swellable three-layer minerals such as smectites and vermiculite, correlated significantly with the δ^2H_p values. This might reflect an increasing contribution of three-layer clay minerals with increasing latitude and climatically determined decreasing weathering intensity. This is corroborated by the increasing χ_e values with increasing latitude in this group of soil clay fractions (Table 4.1), because it is known that the χ_e values decrease in the order, swellable three-layer clay minerals > nonswellable three-layer clay minerals (illite) > two-layer clay minerals > mica.[23,24]

The $\alpha_{ex\text{-}w}$ values of the group of soil clay fractions with a $CEC_{pot} > 400$ $mmol_c$ kg^{-1}, presumably dominated by swellable three-layer clay minerals correlated with the δ^2H_p values, but the slope was flatter than that for the group of soil clay fractions with a CEC_{pot} of 160–400 $mmol_c$ kg^{-1} (Figure 4.3). We attribute this finding to the fact that the group of soil clay fractions with a $CEC_{pot} > 400$ $mmol_c$ kg^{-1} contained a less heterogeneous mixture of minerals, possibly dominated by a single three-layer clay mineral.

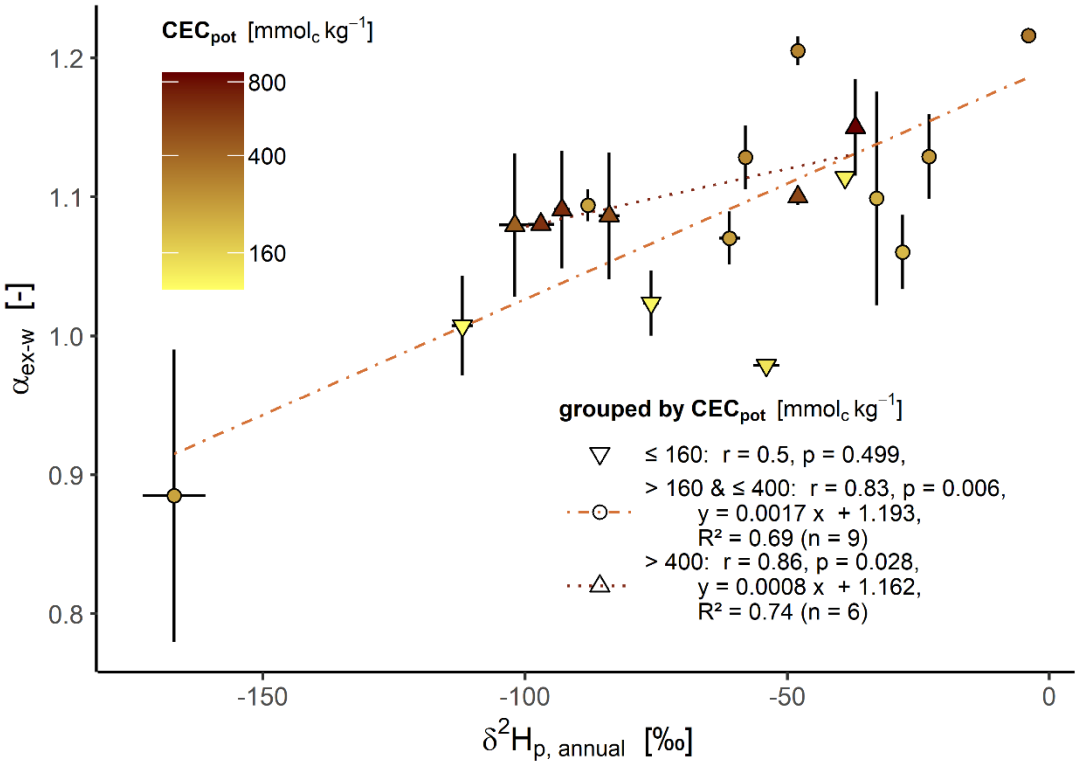

Figure 4.3: Relationship between the δ^2H values of mean annual local precipitation ($\delta^2H_{p,\ annual}$; taken from Bowen[86]) and the specific $\alpha_{ex\text{-}w}$ values of the soil clay fractions. The soil clay fractions are grouped based on the potential cation-exchange capacity (CEC_{pot}) into samples with a $CEC_{pot} \leq 160$ mmol$_c$ kg^{-1} presumably dominated by nonswellabe clay minerals such as kaolinite and pedogenic chlorite and a CEC_{pot} >160 to ≤ 400 mmol$_c$ kg^{-1} presumably containing a mixture of different swellable and nonswellable clay minerals such as illite, smectites and vermiculite, and >400 mmol$_c$ kg^{-1} presumably dominated by swellable three-layer clay minerals such as smectites and vermiculite. To illustrate the variation in CEC_{pot} values within these groups, we furthermore color-coded the CEC_{pot}. The horizontal error bars indicate the 68% confidence interval and might be smaller than the symbol size. The vertical error bars indicate the standard error (n=2–3), if available.

Our findings are in line with the fact that the hot-humid inner tropical zone at low latitude (and δ^2H_p values near 0) tends to be dominated by two-layer clay minerals, whereas the temperate zone at intermediate latitude and δ^2H_p values show a prevalence of three-layer clay minerals.[29,31,32] The climatic influence on the $\alpha_{ex\text{-}w}$ values is corroborated by the finding that the $\alpha_{ex\text{-}w}$ values correlated significantly with the clay content of the bulk soil and the mean annual temperature (Figure 4.4). Intensely weathered tropical soils frequently show higher clay content and a higher mean annual temperature than soils at higher latitude.

Our finding has implications for the interpretation of earlier observations of correlations between δ^2H values of local precipitation and δ^2H values of clay minerals, soil clay fractions and bulk soils, if the δ^2H values were determined by steam equilibration such as in Merseburger et al.[23] and Ruppenthal et al.[8,10,27] The relationship between δ^2H values of local precipitation and δ^2H_n values of clay minerals of the soil clay fraction or bulk soil can, in these cases, be influenced by the varying $\alpha_{ex\text{-}w}$ values of the clay mineral mixture in different soils.

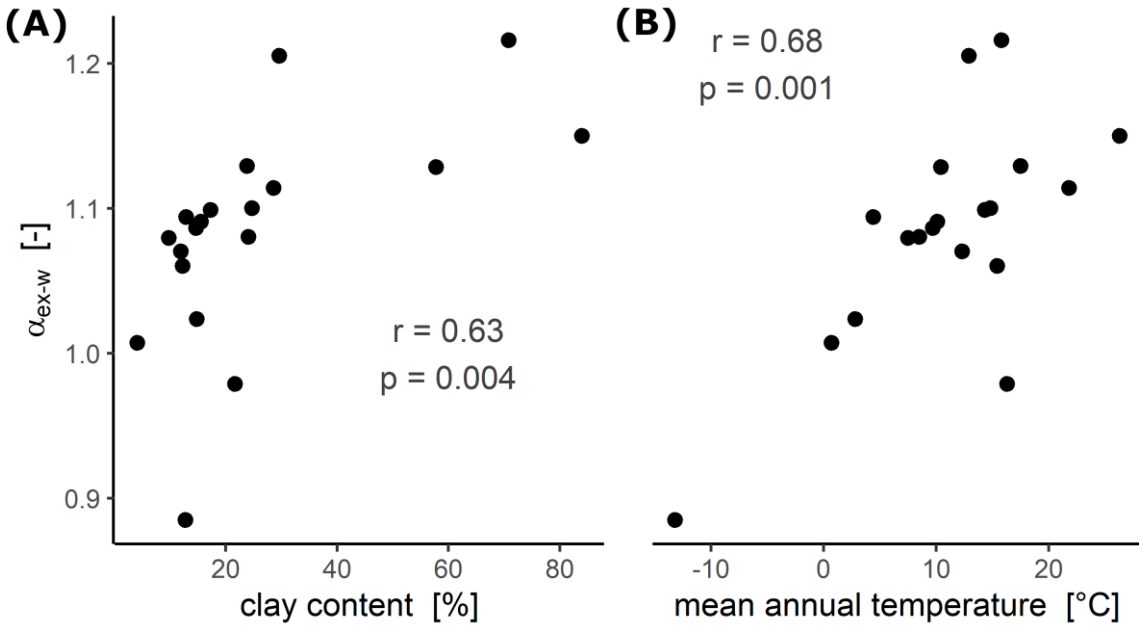

Figure 4.4: Relationship between A, the clay content of bulk soil samples and B, the mean annual temperature at the sampling location and the $\alpha_{ex\text{-}w}$ values of the soil clay fractions.

4.4 Conclusions

Steam equilibration with at least two distinctly different drying conditions can be successfully used to determine the equilibrium fractionation factor between the exchangeable H pool of the clay minerals and soil clay fractions and the H of the steam ($\alpha_{ex\text{-}w}$), although partly only with a considerable error. This error, however, includes both the determination error and the heterogeneity in mineralogical composition between aliquots of the same sample and thus also reflects a natural variation. The determined $\alpha_{ex\text{-}w}$ values were similar to the widely assumed values of 1.00–1.08 in the

literature supporting that the adoption of one of these values in steam equilibration approaches is appropriate. For soil clay fractions and soil clay minerals 1.080 is a suitable average estimate of $\alpha_{ex\text{-}w}$. However, the previously reported correlations between δ^2H values of local precipitation and δ^2H_n values of clay minerals, soil clay fractions and bulk soils can be influenced by the mineral-specific $\alpha_{ex\text{-}w}$ values, if steam equilibration is used to determine the δ^2H_n values.

We did not detect a significant effect of the classical clay separation treatment, including removal of Fe oxides and carbonates, reduction in SOM and dispersion of the remaining material, on the $\alpha_{ex\text{-}w}$ values of clay minerals.

We found that the $\alpha_{ex\text{-}w}$ values of topsoil clay fractions are influenced by their mineralogical composition as assessed via their CEC and latitudinal and elevational locations. The samples with a low CEC tended to show a lower mean $\alpha_{ex\text{-}w}$ value than those with a high CEC. However, the number of samples with a low CEC was small, so further work is necessary to substantiate this conclusion.

Acknowledgments

The authors thank Nadine Gill for help in the laboratory, Harro Meijer for a working example of the memory correction algorithm, Maria Hoerhold for providing deuterium-depleted water (AWI-TD1), and Stefan Dultz for providing the vermiculite. They thank all providers of soil samples: Lars Kutzbach and Christian Knoblauch (RU-PS2), Christian Siewert (RU-17 and RU-S20), Suzanne Robin Jacobs and Sadadi Ojoatre (KE-20, KE-38 and KE-44), Tobias Wirsing (DE-KA1), and Andre Velescu and Tobias Fabian (EC-BOM and EC-SF1). This work was funded by the Deutsche Forschungsgemeinschaft (DFG, Wi1601/25-1).

4.5 References

1. West JB, Bowen GJ, Dawson TE, Tu KP, (Eds). *Isoscapes*. Netherlands: Springer; 2010. doi:10.1007/978-90-481-3354-3
2. Bauer KK, Vennemann TW. Analytical methods for the measurement of hydrogen isotope composition and water content in clay minerals by TC/EA. *Chem Geol*. 2014;363:229-240. doi:10.1016/j.chemgeo.2013.10.039

3. Gilg HA, Girard JP, Sheppard SMF. Conventional and Less Conventional Techniques for Hydrogen and Oxygen Isotope Analysis of Clays, Associated Minerals and Pore Waters in Sediments and Soils. In: *Handbook of Stable Isotope Analytical Techniques. Volume 1*. Elsevier; 2004:38-61. doi:10.1016/B978-044451114-0/50004-1

4. Kanik NJ, Longstaffe FJ, Kuligiewicz A, Derkowski A. Systematics of smectite hydrogen-isotope composition: Structural hydrogen versus adsorbed water. *Appl Clay Sci*. 2022;216:106338. doi:10.1016/j.clay.2021.106338

5. VanDeVelde JH, Bowen GJ. Effects of chemical pretreatments on the hydrogen isotope composition of 2:1 clay minerals: Clay mineral isotope treatment effects. *Rapid Commun Mass Spectrom*. 2013;27(10):1143-1148. doi:10.1002/rcm.6554

6. Schimmelmann A. Determination of the concentration and stable isotopic composition of nonexchangeable hydrogen in organic matter. *Anal Chem*. 1991;63(21):2456-2459. doi:10.1021/ac00021a013

7. Hobson KA, Atwell L, Wassenaar LI. Influence of drinking water and diet on the stable-hydrogen isotope ratios of animal tissues. *Proc Natl Acad Sci*. 1999;96(14):8003-8006. doi:10.1073/pnas.96.14.8003

8. Ruppenthal M, Oelmann Y, Wilcke W. Isotope ratios of nonexchangeable hydrogen in soils from different climate zones. *Geoderma*. 2010;155(3-4):231-241. doi:10.1016/j.geoderma.2009.12.005

9. Ruppenthal M, Oelmann Y, Wilcke W. Optimized demineralization technique for the measurement of stable isotope ratios of nonexchangeable H in soil organic matter. *Environ Sci Technol*. 2013;47(2):949-957. doi:10.1021/es303448g

10. Ruppenthal M, Oelmann Y, del Valle HF, Wilcke W. Stable isotope ratios of nonexchangeable hydrogen in organic matter of soils and plants along a 2100-km climosequence in Argentina: New insights into soil organic matter sources and transformations? *Geochim Cosmochim Acta*. 2015;152:54-71. doi:10.1016/j.gca.2014.12.024

11. Sauer PE, Schimmelmann A, Sessions AL, Topalov K. Simplified batch equilibration for D/H determination of non-exchangeable hydrogen in solid organic material. *Rapid Commun Mass Spectrom*. 2009;23(7):949-956. doi:10.1002/rcm.3954

12. Soto DX, Koehler G, Wassenaar LI, Hobson KA. Re-evaluation of the hydrogen stable isotopic composition of keratin calibration standards for wildlife and forensic science applications. *Rapid Commun Mass Spectrom*. 2017;31(14):1193-1203. doi:10.1002/rcm.7893

13. Wassenaar LI, Hobson KA. Improved method for determining the stable-hydrogen isotopic composition (δD) of complex organic materials of environmental interest. *Environ Sci Technol*. 2000;34(11):2354-2360. doi:10.1021/es990804i

14. Wassenaar LI, Hobson KA. Comparative equilibration and online technique for determination of non-exchangeable hydrogen of keratins for use in animal migration studies. *Isotopes Environ Health Stud*. 2003;39(3):211-217. doi:10.1080/1025601031000096781

15. Schimmelmann A, Lewan MD, Wintsch RP. D/H isotope ratios of kerogen, bitumen, oil, and water in hydrous pyrolysis of source rocks containing kerogen types I, II, IIS, and III. *Geochim Cosmochim Acta*. 1999;63(22):3751-3766. doi:10.1016/S0016-7037(99)00221-5

16. Filot MS, Leuenberger M, Pazdur A, Boettger T. Rapid online equilibration method to determine the D/H ratios of non-exchangeable hydrogen in cellulose. *Rapid Commun Mass Spectrom*. 2006;20(22):3337-3344. doi:10.1002/rcm.2743

17. Chesson LA, Podlesak DW, Cerling TE, Ehleringer JR. Evaluating uncertainty in the calculation of non-exchangeable hydrogen fractions within organic materials. *Rapid Commun Mass Spectrom*. 2009;23(9):1275-1280. doi:10.1002/rcm.4000

18. Grinsted MJ, Wilson AT. Hydrogen isotopic chemistry of cellulose and other organic material of geochemical interest. *N Z J Sci*. 1979;22(3):281-287.

19. Feng X, Krishnamurthy RV, Epstein S. Determination of D/H ratios of nonexchangeable hydrogen in cellulose: A method based on the cellulose-water exchange reaction. *Geochim Cosmochim Acta*. 1993;57(17):4249-4256. doi:10.1016/0016-7037(93)90320-V

20. Bowen GJ, Chesson L, Nielson K, Cerling TE, Ehleringer JR. Treatment methods for the determination of δ^2H and $\delta^{18}O$ of hair keratin by continuous-flow isotope-ratio mass spectrometry. *Rapid Commun Mass Spectrom*. 2005;19(17):2371-2378. doi:10.1002/rcm.2069

21. Qi H, Coplen TB. Investigation of preparation techniques for δ^2H analysis of keratin materials and a proposed analytical protocol. *Rapid Commun Mass Spectrom*. 2011;25(15):2209-2222. doi:10.1002/rcm.5095

22. Hsieh JC, Yapp CJ. Hydrogen-isotope exchange in halloysite: Insight from room-temperature experiments. *Clays Clay Miner*. 1999;47(6):811-816. doi:10.1346/CCMN.1999.0470617

23. Merseburger S, Kessler A, Oelmann Y, Wilcke W. Non-exchangeable stable hydrogen isotope ratios in clay minerals and soil clay fractions: A method test. *Eur J Soil Sci*. 2022;73(4):e13289. doi:10.1111/ejss.13289

24. Merseburger S, Kessler A, Ojoatre S, Berthold C, Oelmann Y, Wilcke W. Global distribution of nonexchangeable stable hydrogen isotope ratios of topsoil clay fractions. *Geochim Cosmochim Acta*. 2023; 347:72-87. doi:10.1016/j.gca.2023.02.007

25. Kessler A, Merseburger S, Kappler A, Wilcke W, Oelmann Y. Incorporation of ambient water-H into the C-bonded H pool of bacteria during substrate-specific metabolism. *ACS Earth Space Chem*. Published online 2022;6(9):2180-2189. doi:10.1021/acsearthspacechem.2c00085

26. Sessions AL, Hayes JM. Calculation of hydrogen isotopic fractionations in biogeochemical systems. *Geochim Cosmochim Acta*. 2005;69(3):593-597. doi:10.1016/j.gca.2004.08.005

27. Ruppenthal M. *Stable Isotope Ratios of Nonexchangeable Hydrogen in Bulk Organic Matter as Novel Biogeochemical Tracer*. PhD Thesis. University of Tübingen; 2014.

28. Savin SM, Epstein S. The oxygen and hydrogen isotope geochemistry of clay minerals. *Geochim Cosmochim Acta*. 1970;34(1):25-42. doi:10.1016/0016-7037(70)90149-3

29. Ito A, Wagai R. Global distribution of clay-size minerals on land surface for biogeochemical and climatological studies. *Sci Data*. 2017;4:sdata2017103, 170103. doi:10.1038/sdata.2017.103

30. Journet E, Balkanski Y, Harrison S. A new data set of soil mineralogy for dust-cycle modeling. *Atmospheric Chem Phys Discuss*. 2013;13. doi:10.5194/acpd-13-23943-2013

31. FAO. Harmonized World Soil Database: Topsoil CEC (clay), Version 1.1. Published online 2009. Accessed January 31, 2022. https://data.apps.fao.org/map/catalog/srv/eng/catalog.search#/metadata/2427214a-42dc-4862-b58a-00b73cbc7a6f

32. Velde B, Meunier A. *The Origin of Clay Minerals in Soils and Weathered Rocks*. Springer Berlin Heidelberg; 2008. doi:10.1007/978-3-540-75634-7

33. Hyeong K, Capuano RM. Hydrogen isotope fractionation factor for mixed-layer illite/smectite at 60° to 150°C: new data from the northeast Texas Gulf Coast 1. *Geochim Cosmochim Acta*. 2004;68(7):1529-1543. doi:10.1016/j.gca.2003.10.002

34. Marumo K, Nagasawa K, Kuroda Y. Mineralogy and hydrogen isotope geochemistry of clay minerals in the Ohnuma geothermal area, Northeastern Japan. *Earth Planet Sci Lett*. 1980;47(2):255-262. doi:10.1016/0012-821X(80)90041-2

35. Sheppard SMF, Gilg HA. Stable isotope geochemistry of clay minerals. *Clay Miner*. 1996;31(1):1-24.

36. Cornell RM, Schwertmann U. *The Iron Oxides: Structure, Properties, Reactions, Occurrences, and Uses*. 2nd, completely rev. and extended ed ed. Wiley-VCH; 2003.

37. Marumo K, Longstaffe FJ, Matsubaya O. Stable isotope geochemistry of clay minerals from fossil and active hydrothermal systems, southwestern Hokkaido, Japan. *Geochim Cosmochim Acta*. 1995;59(12):2545-2559. doi:10.1016/0016-7037(95)00149-2

38. Liu KK, Epstein S. The hydrogen isotope fractionation between kaolinite and water. *Chem Geol*. 1984;46(4):335-350. doi:10.1016/0009-2541(84)90176-1

39. Lawrence JR. *O^{18}/O^{16} and D/H Ratios of Soils, Weathering Zones and Clay Deposits*. PhD Thesis. California Institute of Technology; 1970. Accessed August 1, 2019. http://resolver.caltech.edu/CaltechETD:etd-01132004-094857

40. Gilg HA, Sheppard SMF. Hydrogen isotope fractionation between kaolinite and water revisited. *Geochim Cosmochim Acta*. 1996;60(3):529-533. doi:10.1016/0016-7037(95)00417-3

41. Méheut M, Lazzeri M, Balan E, Mauri F. First-principles calculation of H/D isotopic fractionation between hydrous minerals and water. *Geochim Cosmochim Acta*. 2010;74(14):3874-3882. doi:10.1016/j.gca.2010.04.020

42. Dogan M, Dogan AU, Yesilyurt FI, Alaygut D, Buckner I, Wurster DE. Baseline studies of the Clay Minerals Society special clays: specific surface area by the Brunauer Emmett Teller (BET) method. *Clays Clay Miner*. 2007;55(5):534-541. doi:10.1346/CCMN.2007.0550508

43. Dogan AU, Dogan M, Onal M, Sarikaya Y, Aburub A, Wurster DE. Baseline studies of the Clay Minerals Society source clays: specific surface area by the Brunauer Emmett Teller (BET) method. *Clays Clay Miner*. 2006;54(1):62-66. doi:10.1346/CCMN.2006.0540108

44. Mermut AR, Angel, Cano F. Baseline studies of the clay minerals society source clays: Chemical analyses of major elements. *Clays Clay Miner*. Published online 2001:381-386. doi:10.1346/CCMN.2001.0490504

45. Guggenheim S, Van Groos AK. Baseline studies of the clay minerals society source clays: thermal analysis. *Clays Clay Miner*. 2001;49(5):433-443. doi:10.1346/CCMN.2001.0490509

46. Kogel JE, Lewis SA. Baseline studies of the clay minerals society source clays: Chemical analysis by inductively coupled plasma-mass spectroscopy (ICP-MS). *Clays Clay Miner*. 2001;49(5):387-392. doi:10.1346/CCMN.2001.0490505

47. Chipera SJ, Bish DL. Baseline Studies of the Clay Minerals Society Source Clays: Powder X-Ray Diffraction Analyses. *Clays Clay Miner*. 2001;49(5):398-409. doi:10.1346/CCMN.2001.0490507

48. Borden D, Giese RF. Baseline studies of the clay minerals society source clays: cation exchange capacity measurements by the ammonia-electrode method. *Clays Clay Miner*. 2001;49(5):444-445. doi:10.1346/CCMN.2001.0490510

49. Hower J, Mowatt TC. The mineralogy of illites and mixed-layer illite/montmorillonites. *Am Mineral*. 1966;51(5-6):825-854. doi:10.1346/CCMN.1999.0470617

50. Dultz S, Riebe B, Bunnenberg C. Temperature effects on iodine adsorption on organo-clay minerals: II. Structural effects. *Appl Clay Sci*. 2005;28(1):17-30. doi:10.1016/j.clay.2004.01.005

51. Bors J, Gorny A, Dultz S. Iodide, caesium and strontium adsorption by organophilic vermiculite. *Clay Miner*. 1997;32(1):21-28. doi:10.1180/claymin.1997.032.1.04

52. Steudel A, Weidler PG, Schuhmann R, Emmerich K. Cation exchange reactions of vermiculite with Cu-triethylenetetramine as affected by mechanical and chemical pretreatment. *Clays Clay Miner*. 2009;57(4):486-493. doi:10.1346/CCMN.2009.0570409

53. Steudel A. *Selection Strategy and Modification of Layer Silicates for Technical Applications*. Univ.-Verlag Karlsruhe; 2008. Accessed March 6, 2017. https://doi.org/10.5445/IR/1000010008

54. Qi H, Coplen TB, Gehre M, et al. New biotite and muscovite isotopic reference materials, USGS57 and USGS58, for δ^2H measurements–A replacement for NBS 30. *Chem Geol*. 2017;467:89-99. doi:10.1016/j.chemgeo.2017.07.027

55. Fabian T, Velescu A, Wilcke W. Soil development on heterogeneous parent material under tropical montane forest in South Ecuador. *Tabebuia Bull*. 2019;Issue 6:7. doi:10.5678/lcrs/pak823-825.cit.1399

56. Fabian T, Velescu A, Harteif K, Wilcke W. Soil properties of the cloud forest in Cajanuma and of the pastures along an elevation gradient from 1000 to 3000 m a.s.l. *Tabebuia Bull*. 2020;Issue 7. doi:10.5678/LCRS/FOR2730.CIT.1817

57. Wilcke W, Yasin S, Abramowski U, Valarezo C, Zech W. Nutrient storage and turnover in organic layers under tropical montane rain forest in Ecuador. *Eur J Soil Sci*. 2002;53(1):15-27. doi:10.1046/j.1365-2389.2002.00411.x

58. Schrumpf M, Guggenberger G, Valarezo C, Zech W. Tropical montane rain forest soils : Development and nutrient Status along an altitudinal gradient in the South Ecuadorian Andes. *Erde*. 2001;132(1):43-59.

59. Ojoatre S. *Deforestation and Recovery of the Tropical Montane Forests of East Africa*. PhD Thesis. Lancaster University; 2022. Accessed May 18, 2022. http://www.research.lancs.ac.uk/portal/services/downloadRegister/356576715/2021OjoatrePhD.pdf

60. Messmer ST, Elsenbeer H, Wilcke W. High exchangeable calcium concentrations in soils on Barro Colorado Island, Panama. *Geoderma*. 2014;217–218:212-224. doi:10.1016/j.geoderma.2013.10.021

61. Messmer ST. *Biotic and Abiotic Drivers of the Base Metal Cycling in a Tropical Lowland Rain Forest in Panama*. PhD Thesis. Univerity of Bern; 2014.

62. Siewert C. *Investigation of the thermal and biological stability of soil organic matter: Untersuchungen zur thermischen und biologischen Stabilität der organischen Bodensubstanz*. Shaker; 2001.

63. Siewert C. Rapid Screening of Soil Properties using Thermogravimetry. *Soil Sci Soc Am J*. 2004;68(5):1656. doi:10.2136/sssaj2004.1656

64. Knoblauch C, Beer C, Schuett A, et al. Carbon dioxide and methane release following abrupt thaw of pleistocene permafrost deposits in Arctic Siberia. *J Geophys Res Biogeosciences*. 2021;126(11):e2021JG006543. doi:10.1029/2021JG006543

65. Lobe I. *Untersuchungen zur Schwermetallbelastung von Böden der Nord-Slowakei*. Diploma thesis. University Bayreuth; 1997.

66. Lobe I, Wilcke W, Kobža J, Zech W. Heavy metal contamination of soils in Northern Slovakia. *Z Für Pflanzenernähr Bodenkd*. 1998;161(5):541-546. doi:10.1002/jpln.1998.3581610507

67. Bandowe BAM, Shukurov N, Kersten M, Wilcke W. Polycyclic aromatic hydrocarbons (PAHs) and their oxygen-containing derivatives (OPAHs) in soils from the Angren industrial area, Uzbekistan. *Environ Pollut*. 2010;158(9):2888-2899. doi:10.1016/j.envpol.2010.06.012

68. Shukurov N, Pen-Mouratov S, Steinberger Y, Kersten M. Soil biogeochemical properties of Angren industrial area, Uzbekistan. *J Soils Sediments*. 2009;9(3):206-215. doi:10.1007/s11368-009-0079-8

69. Mehra OP, Jackson ML. Iron oxide removal from soils and clays by a dithionite-citrate system buffered with sodium bicarbonate. In: *Proceedings 7th Nat. Conf. Clays*. Vol 5. ; 1960:317-327. Accessed July 29, 2014. http://www.cabdirect.org/abstracts/19601901561.html

70. DIN ISO 11277. *Bodenbeschaffenheit - Bestimmung Der Partikelgrößenverteilung in Mineralböden. Verfahren Mittels Siebung Und Sedimentation*. Beuth Verlag; 2002. Accessed March 9, 2017. https://doi.org/10.31030/9283499

71. Abbott A. DIY Glove Bag. aprilabbott. Published November 11, 2019. Accessed February 22, 2021. https://aprilabbott.wordpress.com/2019/11/11/diy-glove-bag/

72. Wassenaar LI, Hobson KA, Sisti L. An online temperature-controlled vacuum-equilibration preparation system for the measurement of δ^2H values of non-exchangeable-H and of $\delta^{18}O$ values in organic materials by isotope-ratio mass spectrometry. *Rapid Commun Mass Spectrom*. 2015;29(5):397-407. doi:10.1002/rcm.7118

73. Polyakov VB, Horita J, Cole DR. Pressure effects on the reduced partition function ratio for hydrogen isotopes in water. *Geochim Cosmochim Acta*. 2006;70(8):1904-1913. doi:10.1016/j.gca.2006.01.010

74. Horita J, Wesolowski DJ. Liquid-vapor fractionation of oxygen and hydrogen isotopes of water from the freezing to the critical temperature. *Geochim Cosmochim Acta*. 1994;58(16):3425-3437. doi:10.1016/0016-7037(94)90096-5

75. Guidotti S, Jansen HG, Aerts-Bijma AT, Verstappen-Dumoulin BM a. A, van Dijk G, Meijer H a. J. Doubly Labelled Water analysis: Preparation, memory correction, calibration and quality assurance for delta δ^2H and $\delta^{18}O$ measurements over four orders of magnitudes. *Rapid Commun Mass Spectrom*. 2013;27(9):1055-1066. doi:10.1002/rcm.6540

76. Ammann L, Bergaya F, Lagaly G. Determination of the cation exchange capacity of clays with copper complexes revisited. *Clay Miner*. 2005;40(4):441-453. doi:10.1180/0009855054040182

77. Meier LP, Kahr G. Determination of the Cation Exchange Capacity (CEC) of Clay Minerals Using the Complexes of Copper(II) Ion with Triethylenetetramine and Tetraethylenepentamine. *Clays Clay Miner*. 1999;47(3):386-388. doi:10.1346/CCMN.1999.0470315

78. Soil Survey Staff. *Keys to Soil Taxonomy*. Vol 12th edition. United States Department of Agriculture, Natural Resources Conservation Service; 2014.

79. Bergaya F, Lagaly G, Vayer M. Cation and anion exchange. In: *Developments in Clay Science*. Vol 5. Elsevier; 2013:333-359.

80. Paul D, Skrzypek G, Fórizs I. Normalization of measured stable isotopic compositions to isotope reference scales – a review. *Rapid Commun Mass Spectrom*. 2007;21(18):3006-3014. doi:10.1002/rcm.3185

81. R Core Team. *R: A Language and Environment for Statistical Computing*.; 2022. https://www.R-project.org/

82. Wickham H, Averick M, Bryan J, et al. Welcome to the tidyverse. *J Open Source Softw*. 2019;4(43):1686. doi:10.21105/joss.01686

83. Fick SE, Hijmans RJ. WorldClim 2: new 1-km spatial resolution climate surfaces for global land areas. *Int J Climatol*. 2017;37(12):4302-4315. doi:10.1002/joc.5086

84. Trabucco A, Zomer R. Global Aridity Index and Potential Evapotranspiration (ET0) Climate Database v2. Published online 2019:1705236666 Bytes. doi:10.6084/M9.FIGSHARE.7504448.V3

85. Bowen GJ, Revenaugh J. Interpolating the isotopic composition of modern meteoric precipitation: isotopic composition of modern precipitation. *Water Resour Res*. 2003;39(10):1299-1312. doi:10.1029/2003WR002086

86. Bowen GJ. WaterIsotopes.org. The Online Isotopes in Precipitation Calculator, version 3.1. Published 2022. Accessed April 28, 2021. http://wateriso.utah.edu/waterisotopes/pages/data_access/oipc.html

87. Bigeleisen J. Chemistry of Isotopes: Isotope chemistry has opened new areas of chemical physics, geochemistry, and molecular biology. *Science*. 1965;147(3657):463-471. doi:10.1126/science.147.3657.463

88. Kosmulski M. The pH dependent surface charging and points of zero charge. IX. Update. *Adv Colloid Interface Sci*. 2021;296:102519. doi:10.1016/j.cis.2021.102519

4.6 Supporting information

4.6.1 Text S1: Alternative calculations

In Eq. 4.S1 $\alpha_{ex\text{-}w}$ was derived in the same way as with Eq. 4.3 but for unstandardized dimensionless isotope ratios (R).

$$\alpha_{ex-w} = \frac{b_{R1}\, m_2 - b_{R2}\, m_1}{b_{R1} - b_{R2}}. \qquad (Eq.\ 4.S1)$$

m_1 and m_2 are the slopes of the two regression lines of the δ^2H values of the samples on the δ^2H values of the used equilibration waters originating from two different drying procedures (Figure 4.1). b_{R1} and b_{R2} are the corresponding intercepts of the two equilibration lines. Another way to derive $\alpha_{ex\text{-}w}$ uses the algebraically calculated intersection point Z as proposed by Schimmelmann[6] but instead of the approximate equation for δ^2H_t, we used our Eq. 4.1, which resulted in Eq. 4.S2.

$$\alpha_{ex-w} = \frac{y+1000}{x+1000} \qquad (Eq.\ 4.S2)$$

where y is the δ^2H_t value of the intersection Z(x,y) of the two regression lines and x is the δ^2H_w value of Z(x,y). We used both alternative calculations as controls of the results obtained with Eq. 4.3 and arrived at the same results.

4.6.2 Text S2: Error propagation

Using Gaussian error propagation for Eq. 4.3, we estimated the standard deviation (SD) of the δ^2H_n values with Eq. 4.S3, neglecting covariance of slope (m) and intercept (b). This equation is only valid for delta values in ‰. Note, that SD equals the standard error of slope and intercept multiplied by square root of the number of included δ^2H_t values.

$$SD_{\alpha_{ex-w}} = \sqrt{\begin{matrix}\left(part_{b_1} \cdot SD_{b_1}\right)^2 + \left(part_{b_2} \cdot SD_{b_2}\right)^2 + \\ \left(part_{m_1} \cdot SD_{m_1}\right)^2 + \left(part_{m_2} \cdot SD_{m_2}\right)^2\end{matrix}} \qquad (Eq.\ 4.S3)$$

"part$_i$" are the partial first derivative of Eq. 4.3 (Eq. 4.S4a-d).

$$part_{m_1} = \frac{(b_1-b_2)(1000m_2-b_2-1000)}{(1000(m_1-m_2)-b_1+b_2)^2} \qquad (Eq.\ 4.S4a)$$

$$part_{m_2} = -\frac{(b_1-b_2)(1000m_1-b_1-1000)}{(1000(m_2-m_1)+b_1-b_2)^2} \qquad (Eq.\ 4.S4b)$$

$$part_{b_1} = \frac{1000{m_2}^2+(-1000m_1-b_2-1000)m_2+(b_2+1000)m_1}{(b_1+1000(m_2-m_1)-b_2)^2} \qquad (Eq.\ 4.S4c)$$

$$part_{b_2} = -\frac{(1000m_1 - b_1 - 1000)(m_2 - m_1)}{(b_2 + 1000(m_1 - m_2) - b_1)^2} \quad (Eq.\ 4.S4d)$$

Using Gaussian error propagation for Eq. 4.2 (without index), we estimated the standard deviation (SD) of the δ^2H_n values with Eq. 4.S5, neglecting covariance of slope (m) and intercept (b), which is only valid for delta values in ‰.

$$SD_{\delta^2 H_n} = \sqrt{\left(\frac{\alpha_{ex-w}}{m - \alpha_{ex-w}} \cdot SD_b\right)^2 + \left(\frac{\alpha_{ex-w} \cdot b}{(m - \alpha_{ex-w})^2} \cdot SD_m\right)^2 + \left(\frac{b \cdot m}{(\alpha_{ex-w} - m)^2} \cdot SD_{\alpha_{ex-w}}\right)^2} \quad (Eq.\ 4.S5)$$

The SD of χ_e was estimated by Gaussian error propagation as done by Ruppenthal et al.[9] (Eq. 4.S6).

$$SD_{\chi_e} = \sqrt{\left(\frac{1}{\alpha_{ex-w}} \cdot SD_m\right)^2 + \left(-\frac{m}{\alpha_{ex-w}^2} \cdot SD_{\alpha_{ex-w}}\right)^2} \quad (Eq.\ 4.S6)$$

We estimated the SD of χ_e only in cases for which a SD of the corresponding $\alpha_{ex\text{-}w}$ value could be calculated (Table 4.1), because otherwise m and $\alpha_{ex\text{-}w}$ would be statistically related.

4.6.3 Text S3: Recommendations for the application of steam equilibration to swellable clay minerals

To cope with samples in which the majority of H is exchangeable, such as the swellable three-layer clay minerals we propose three changes of the steam equilibration apparatus[23] for further technical improvements concerning precision and repeatability:

- A capsule press inside the vacuum vessel can overcome the need for the error-prone handling of the individually modified capsule pressing pliers in the glove bag. A capsules press could be made of embedded stainless steel perforated plates, which are moved against each other with a screw. The displacement closes the rectangular holes under which there is, for example, an 80-hole PTFE capsule holder, with the tin or silver capsules being pressed directly at post-equilibration drying temperature. The screw can be driven by a mechanical feed-through from outside the vacuum chamber with a torque wrench or similar.
- A pressure regulator for the diaphragm pump with weaker ultimate vacuum (or alternatively a single vapor-resistant, oil-free pump with higher ultimate vacuum) could narrow the allowable pressure range for drying after equilibration and improve repeatability. Additionally, the

differences between the slopes of the equilibration lines at weaker and stronger drying could be further increased.

- Larger tubing diameter for a more efficient moisture removal. Instead of Swagelok-Quick-Connectors with a convoluted tubing with a large inner surface, standard solid stainless- steel tubing, e.g., KF16 or with larger diameter can connect the vacuum vessel inside the oven.

Table 4.S1: Resulting equilibration lines of the steam equilibration with weaker, medium and stronger drying intensity are given as slope and intercept with standard deviation.

Type	Sample	Treatment	drying intensity after steam equilibration								
			weaker			medium			stronger		
			slope #	intercept # [‰]	n *	slope #	intercept # [‰]	n *	slope #	intercept # [‰]	n *
clay mineral	Illite (IMt-2)	treated	0.144 ± 0.012	-112.0 ± 2.6	11	n.d.	n.d.	n.d.	0.090 ± 0.009	-123.2 ± 2.0	10
		untreated	0.239 ± 0.017	-96.0 ± 3.9	23	0.167 ± 0.012	-115.0 ± 3.2	23	0.156 ± 0.010	-117.0 ± 2.3	23
	Kaolinite (KGa-2)	treated	0.093 ± 0.003	-53.8 ± 0.7	11	n.d.	n.d.	n.d.	0.082 ± 0.012	-59.1 ± 2.9	10
		untreated	0.102 ± 0.006	-52.1 ± 1.4	21	0.085 ± 0.006	-56.3 ± 1.5	53	0.102 ± 0.010	-55.6 ± 2.3	22
	Mg-mont-morillonite (SCa-3)	treated	0.432 ± 0.026	-46.5 ± 5.5	10	n.d.	n.d.	n.d.	0.246 ± 0.037	-95.5 ± 8.7	11
		untreated	0.808 ± 0.052	16.1 ± 11.3	21	0.627 ± 0.023	-36.7 ± 6.1	58	0.588 ± 0.036	-44.9 ± 7.8	26
	Na-mont-morillonite (SWy-3)	treated	0.177 ± 0.018	-106.9 ± 4.0	18	n.d.	n.d.	n.d.	0.108 ± 0.022	-123.6 ± 4.8	23
		untreated	0.331 ± 0.029	-84.8 ± 6.8	19	0.223 ± 0.018	-103.7 ± 4.7	35	0.239 ± 0.017	-107.0 ± 3.9	18
	Vermiculite	treated	0.466 ± 0.066	-51.8 ± 14.6	23	n.d.	n.d.	n.d.	0.349 ± 0.019	-84.5 ± 4.2	10
		untreated	0.772 ± 0.053	11.3 ± 12.0	24	0.669 ± 0.015	-31.6 ± 4.1	23	0.588 ± 0.023	-49.1 ± 5.1	23
other	Biotite (USGS57)	untreated	0.065 ± 0.011	-89.3 ± 2.5	21	0.041 ± 0.004	-91.1 ± 1.1	23	0.043 ± 0.009	-90.2 ± 1.9	18
	Cellulose		0.296 ± 0.013	6.1 ± 3.0	20	n.d.	n.d.	n.d.	0.248 ± 0.010	-3.0 ± 2.2	20
	Muscovite (USGS58)		0.024 ± 0.008	-31.7 ± 1.7	11	0.008 ± 0.007	-29.9 ± 1.8	26	0.015 ± 0.006	-31.7 ± 1.3	9

Continued on the next page.

Table 4.S1: Continued.

Type	Sample	Treatment	drying intensity after steam equilibration								
			weaker			medium			stronger		
			slope #	intercept # [‰]	n *	slope #	intercept # [‰]	n *	slope #	intercept # [‰]	n *
topsoil clay fraction	AR-10A	treated	0.541 ± 0.031	-32.1 ± 6.4	9	0.399 ± 0.005	-63.8 ± 1.3	7	0.306 ± 0.027	-86.9 ± 6.1	12
	AR-14A		0.569 ± 0.041	-30.5 ± 9.4	23	0.408 ± 0.016	-69.8 ± 4.3	7	0.317 ± 0.040	-84.8 ± 8.1	18
	AR-16A		0.557 ± 0.030	-32.0 ± 6.8	12	0.417 ± 0.010	-75.3 ± 2.8	11	0.357 ± 0.042	-82.9 ± 8.7	7
	AR-17A		0.537 ± 0.025	-39.0 ± 5.4	11	0.425 ± 0.015	-74.3 ± 4.0	17	0.354 ± 0.022	-84.8 ± 5.1	11
	AR-19A		0.483 ± 0.022	-56.8 ± 5.1	12	0.370 ± 0.004	-82.9 ± 1.0	6	0.283 ± 0.032	-102.8 ± 6.9	11
	AR-20C		0.582 ± 0.037	-36.2 ± 8.5	24	0.498 ± 0.009	-66.1 ± 2.4	6	0.385 ± 0.022	-79.8 ± 4.7	16
	AR-2A		0.503 ± 0.034	-26.0 ± 7.8	17	0.429 ± 0.020	-51.7 ± 5.3	6	0.347 ± 0.030	-70.2 ± 6.3	20
	AR-4A		0.607 ± 0.029	-27.3 ± 6.1	11	0.509 ± 0.014	-53.2 ± 3.4	8	0.428 ± 0.024	-63.6 ± 5.2	11
	AR-5C		0.448 ± 0.021	-46.8 ± 4.7	12	0.401 ± 0.011	-70.7 ± 2.9	9	0.340 ± 0.015	-79.8 ± 3.1	10
	DE-KA1		0.415 ± 0.018	-46.4 ± 4.3	19	0.347 ± 0.019	-61.4 ± 4.2	10	0.319 ± 0.021	-72.3 ± 4.7	21
	EC-BOM		0.351 ± 0.011	-33.0 ± 2.5	11	0.301 ± 0.006	-42.4 ± 1.6	9	0.330 ± 0.008	-56.3 ± 2.0	8
	EC-SF1		0.190 ± 0.008	-57.8 ± 1.5	9	0.170 ± 0.006	-58.7 ± 1.4	6	0.160 ± 0.015	-66.7 ± 3.4	11
	KE-20		0.447 ± 0.030	-8.2 ± 6.6	11	0.410 ± 0.008	-24.9 ± 2.0	17	0.379 ± 0.030	-39.0 ± 6.8	11
	KE-38		0.386 ± 0.019	-13.2 ± 4.4	10	0.351 ± 0.011	-28.7 ± 2.9	12	0.340 ± 0.028	-38.4 ± 6.3	12
	KE-44		0.493 ± 0.026	-9.8 ± 5.9	12	0.431 ± 0.005	-31.6 ± 1.3	9	0.388 ± 0.031	-42.6 ± 7.7	9
	PA-A9		0.401 ± 0.014	-35.6 ± 3.5	7	0.283 ± 0.013	-60.8 ± 3.3	9	0.258 ± 0.018	-76.0 ± 3.9	8
	RU-17		0.421 ± 0.028	-49.5 ± 6.1	10	0.329 ± 0.015	-67.9 ± 3.7	13	0.288 ± 0.025	-79.7 ± 6.1	9
	RU-PS2		0.226 ± 0.014	-124.9 ± 2.9	10	0.194 ± 0.002	-134.3 ± 0.6	12	0.178 ± 0.011	-132.0 ± 2.6	11
	RU-S20		0.399 ± 0.022	-75.4 ± 4.7	11	0.315 ± 0.005	-93.0 ± 1.3	9	0.266 ± 0.007	-95.6 ± 1.4	9
	SK-Oso		0.214 ± 0.005	-76.8 ± 1.3	10	0.174 ± 0.009	-83.1 ± 2.1	17	0.159 ± 0.007	-84.2 ± 1.6	11
	TH-M1		0.242 ± 0.020	-58.6 ± 4.1	10	0.189 ± 0.047	-68.5 ± 10.4	11	0.193 ± 0.010	-75.0 ± 2.3	10
	UZ-K1		0.316 ± 0.017	-55.7 ± 3.7	11	0.238 ± 0.017	-78.0 ± 4.5	10	0.200 ± 0.018	-90.9 ± 4.1	12

SD is calculated as product of the standard error and the square root of n.

* n is the number of included individual δ^2H_t measurements

Appendix

The appendix is attached as Secure Digital Memory Card containing the following files as Office Open XML (*.xlsx) and Textfile (*.txt):

- Content (Content.txt)
- All tables of this dissertation (tables_of_dissertation.xlsx)
- All IRMS measurement sequence results in evaluated form (including quality controls, memory corrections, and normalization) as used in this dissertation (used_evaluated_IRMS_sequences.xlsx)
- Summary of δ^2H long term quality evaluation of two international reference materials and one in-house standard (summary_long_term_quality.xlsx)
- Functions for various hydrogen isotope calculations as implemented in R (essential_R_functions.R.txt)
- Calculations to estimate the isotopic shift of δ^2H_n of clay fractions caused by the H of residual SOM for the samples DE-KA1, DE-KA2 and SK-Oso (Estimation_of_isotopic_influence_from_H_of_SOM.xlsx)
- Climate data for all sampling locations, including temperature, precipitation, solar radation, evapotranspiration, aridity and δ^2H of precipitation (climate_data.xlsx)
- Collected measurement results of all topsoil samples, including δ^2H analysis of clay fractions, CEC determination and elemental concentrations (gathered_data_of_topsoil_samples.xlsx)